MITNE-175

NEUTRONIC ANALYSIS OF A PROPOSED PLUTONIUM RECYCLE ASSEMBLY

George M. Solan
David D. Lanning
Bruce F. Momsen
Edward E. Pilat

August 1975

Massachusetts Institute of Technology
Department of Nuclear Engineering

MASSACHUSETTS INSTITUTE OF TECHNOLOGY
DEPARTMENT OF NUCLEAR ENGINEERING
CAMBRIDGE, MASSACHUSETTS 02139

NEUTRONIC ANALYSIS OF A PROPOSED PLUTONIUM RECYCLE ASSEMBLY

by

George M. Solan
David D. Lanning
Bruce F. Momsen*
Edward E. Pilat*

August 1975

Report MITNE-175

---

* Yankee Atomic Electric Company

NEUTRONIC ANALYSIS OF A PROPOSED PLUTONIUM RECYCLE ASSEMBLY

by

George M. Solan
David D. Lanning
Bruce F. Momsen
Edward E. Pilat

ABSTRACT

A method for the neutronic analysis of plutonium recycle assemblies has been developed with emphasis on relative power distribution prediction in the boundary area of vastly different spectral regions. Such regions are those of mixed oxide (PuO_2 in natural UO_2) fuel pins relative to enriched uranium pins, or water regions relative to fuel pin regions.

The basic analytical methods for determination of spectrum averaged constants are given in the following descriptions:

(1) Generalized Mixed Number Density (GMND) group constants (based on Breen's Mixed Number Density Method) are generated by a modified version of the spectrum code LASER, called LASER-M.

(2) THERMOS Corrected LASER-M (TCL) group constants are based on mixed oxide- uranium oxide and water region boundary modeling in one dimensional (slab) geometry with the integral transport code THERMOS.

The LASER-M model, as modified by addition of ENDF/B-II thermal cross sections for the plutonium isotopes, is used to predict the criticality of experimental lattices of UO_2 - 2 w/o PuO_2, and fair agreement is shown. LASER-M unit cell depletion calculations with Yankee Core I data (3.4 w/o U-235) to 40,000 MWD/MT and Saxton Core II data (6.6 w/o PuO_2 in natural UO_2) to 20,000 MWD/MT show good isotopic agreement.

Saxton Critical Reactor Experiment (CRX) lattice cores (19 x 19 rod array) consisting of a single fuel type region (mixed oxide or uranium oxide) or multiregions of both pin types were analyzed for relative power distribution comparisons. Cores with water slot regions were included. LASER-M Normal, LASER-M GMND and TCL two group constants were used with PDQ-7 in the calculations. GMND results were in excellent agreement compared to the good agreement of TCL for these cases of isolated spectral disturbances in an asymptotic core region.

The methods were applied to a proposed plutonium recycle "island design" assembly in which a large control rod water region is in close proximity to a zoned mixed oxide region. The TCL method yielded significantly greater power peaking and mixed oxide region average power owing to the spectral influence of the water region explicitly accounted for in this method. Such a result is consistent with published calculations. It is concluded that infinite lattice spectrum calculations are insufficient to deal with spectrum effects more complex than those in the Saxton CRX experiments.

ACKNOWLEDGEMENTS

The work described in this report has been performed primarily by the principal author, G. M. Solan, who has submitted substantially the same report as partial fulfillment of the requirements for the degrees of Master of Science in Nuclear Engineering and Nuclear Engineer at MIT.

The principal author expresses his sincere gratitude to Professor David Lanning for his patience, advice and guidance throughout the course of this work.

The project was developed in cooperation with the Yankee Atomic Electric Company. The financial support and computer access provided by Yankee is deeply appreciated. Special thanks to Dr. Ed Pilat, whose interest laid the foundation of the project and whose technical guidance was always available.

A very special note of thanks to Bruce Momsen, whose advice and encouragement while completing his thesis work at MIT and supervising the project at Yankee was most deeply appreciated. His many helpful ideas and suggestions were invaluable, from both a technical and personal point of view.

The principal author would like to thank the American Electric Power Service Corporation, which generously provided a fellowship in Power Systems Engineering leading to a masters

degree in nuclear engineering. The principal author's introduction to nuclear engineering as a cooperative student at AEP while attending Cornell University was most instrumental in shaping his interests in the field.

The financial assistance for completion of the principal author's nuclear engineers degree was provided by an AEC traineeship administered by the department of nuclear engineering at MIT.

Thanks to J. Scarborough for his interest in the initial phases of the project while a visiting professor at MIT. Many thanks to Professor Kent Hansen for serving as thesis reader amidst his many responsibilities.

TABLE OF CONTENTS

PAGE

LIST OF FIGURES

LIST OF FIGURES
(Continued)

LIST OF FIGURES
(Continued)

LIST OF FIGURES
(Continued)

LIST OF FIGURES
(Continued)

LIST OF FIGURES
(Continued)

FIGURE PAGE

LIST OF TABLES

LIST OF TABLES
(Continued)

CHAPTER 1

INTRODUCTION

1.1 Plutonium Recycle in Thermal Reactors

The desireability of plutonium recycle in thermal reactors has been documented by the large effort expended in the areas of technical feasibility, environmental impact and the safeguard of nuclear materials and facilities.

For more than a decade, developmental work has proceeded through extensive materials, irradiation and physics tests so that the technical aspects of plutonium recycle have been verified.[1] The extensive study undertaken by the AEC Regulatory Staff entitled "A Generic Environmental Statement on the Use of Recycle Plutonium in Mixed Oxide Fuels in LWRs" (GESMO)[2] concludes that there is sufficient experimental work and demonstration of mixed oxide fuel performance to warrant wide-scale commercial use.

The GESMO report concludes that, concerning the environmental impact of the nuclear fuel cycle (mining, milling, production and use), a recycle mode is preferable to a pure uranium cycle. Radiological impact from the production of nuclear fuel would also be reduced.

Problems associated with protecting plutonium against theft and diversion and nuclear facilities against sabotage are considered manageable by the Regulatory Staff. Such issues, however, are important in influencing the timing and extent of utilization, as is the availability of re-

processing and mixed oxide fuel fabrication facilities.

The economics of plutonium recycle is influenced by a number of factors, foremost of which are U_3O_8 and separative work costs, increases in which are favorable to plutonium utilization. The fabrication penalty associated with mixed oxide fuel is the primary additional cost of use. Based on the Regulatory Staff's projections, the expected cumulative dollar value of plutonium generated by 1985 should reach about 2 billion,[2]

Although the technical and performance issues of plutonium recycle are not of current and immediate interest, their continued study is necessary to provide optimum design and core operational capability. The technical issues of plutonium recycle have been summarized by the Regulatory Staff[3] with emphasis on insuring the same margins of operational safety as found in commercial uranium reactors.

1.2 Plutonium Neutron Physics Analysis: Objectives and Problems

The basic objectives of in-core fuel and poison management are general to the use of plutonium-bearing assemblies. Indeed, plutonium utilization is not new, considering that a typical UO_2 core near the end of an equilibrium cycle (20,000 MWD/MT average exposure) will derive about half of its power from bred-in plutonium isotopes. The fuel management objectives, namely

(1) maintenance of criticality,
(2) avoidance of unsafe or unacceptable operation,
(3) optimum power distribution shaping,
(4) fuel irradiation uniformity,

(5) neutron utilization optimization, and
(6) heat production maximization,

are achieved through the control of design variables such as

(1) fuel types and densities,
(2) fuel pin size,
(3) water to metal ratio (lattice pitch),
(4) fuel pin location, and
(5) burnable poison distribution.

The fuel pin size and lattice pitch have generally been determined by the original core design, one which employed enriched uranium fuel. These parameters are fixed in the recycle assembly design to assure a thermal-hydraulic compatibility with existing uranium assemblies. This is necessary under the anticipated gradual introduction of recycle assemblies during core reloadings. Such compatibility is also desireable for power sharing and reactivity lifetime characteristics. Careful fuel management strategies are necessary to obtain an optimum method of introduction of recycle assemblies.

These objectives require the development of accurate methods for prediction of neutronics properties with knowledge of the areas and extents of calculational uncertainty. Such is required for the establishment of adequate design margins and limits. Neutronic design methods developed for uranium cores require reevaluation of inherent model assumptions which may themselves be inadequate due to the physics of plutonium, which is worthy of review.

Pu-239 is produced from the neutron capture of U-238, mostly due to epithermal neutrons. Succeeding neutron cap-

tures directly yield Pu-240,241 and 242. Pu-239 and 241 are fissile. Pu-239 has a significant resonance about 0.3 ev. Pu-240 is fertile with a large 1.0 ev. resonance. Pu-242 is parasitic.

Plutonium isotopic content, as found in discharged LWR fuel, will change in relative atom percent (a/o) with core residence time and spectrum dependencies. In addition, Pu-241 decays to Am-241, a thermal poison, with a 13-14 year half-life. This is a factor which must be considered when calculating the characteristics of a core with significant down-time.

Table 1.1 shows the disparity between the 2200 m/sec cross section values of the fissile isotopes of the main chain. This creates many of the compatibility problems present when a pin of significant plutonium content is placed next to a uranium pin or in a uranium spectrum region. Similar disparity is present in the infinite medium spectra, a plutonium spectrum being harder (higher average thermal neutron velocity) due to the greater resonance absorption. This unfortunately results is significant sensitivity of a plutonium region to an influx of thermal neutrons from adjacent areas.

Table 1.2 compared plutonium with uranium cores,with emphasis on overall performance and design considerations. The following items[3,4] look at plutonium characteristics as they are related to the practicalities of utilization and neutronics calculation in contrast to a uranium core.

Table 1.1

Thermal (2200 m/sec) Neutron Characteristics of Uranium and Plutonium Fissile Isotopes [5]

Parameter		U-235	Pu-239	Pu-241
Cross Sections (barns)				
Fission	(σ_f)	590	738	1015
Capture	(σ_c)	108	287	382
Capture to fission ratio	($\alpha = \sigma_c/\sigma_f$)	0.18	0.39	0.38
Neutrons per fission	(ν)	2.47	2.91	3.06
Neutrons produced per absorption	($\eta = \nu\sigma_f/\sigma_a$)	2.28	2.09	2.23
Energy (Mev) per fission	($\varkappa$)	194	201	205
Fertile atoms produced per absorption		-	0.28	0.27

Absorption defined as fission plus capture

Spectrum averaged values, as used in reactor physics calculations, may be significantly different due to the hardness of the spectrum in plutonium regions. Especially affected is the plutonium capture to fission ratio.

Table 1.2

Comparison of Uranium and Plutonium

Core Design Characteristics[3,6]

Parameter	Pu Core Change	Reason for Difference
Moderator Temp Coefficient	More Negative ($\approx -.5 \times 10^{-4}/^{o}F$)	Increased Resonance Absorption from non-Fissioning Pu-240, 242
Doppler Coefficient	More Negative ($\approx$ - 10%)	Large Pu-240 Resonances
HZP-HFP Reactivity Swing	Increased ($\approx$ 50%)	Larger Moderator Temperature Coefficient
Control Rod Reactivity Margin	Increased (Spatially dependent, $\leq$ 50%)	Larger Moderator and Doppler Coefficients
Installed BOL Reactivity	Reduced ($\approx$ 5 - 10%)	Reduced Depletion Rate of Reactivity and Reactivity Saturates
Reactivity Worths (Control Rod, Boron, Xe)	Reduced ($\leq$ 30%)	Thermal Flux Reduction
Fission Product Poisoning	Increased	Larger Yields and Increased Resonance Absorption
Local Power Peaking	Increased	Increased water worth

Values typical of LWR's

(1) Radioactivity

Plutonium requires special handling, even with sealed rods, due to its strong alpha emission. The fabrication penalty (very sensitive to fabrication plant throughput) plus the added care of handling is an incentive to load plutonium into as few rods as possible.

(2) Cross Section Differences and Power Peaking

Fissile plutonium thermal cross sections are approximately twice those of uranium in a typical LWR spectrum. The resulting harder spectrum and lower overall thermal flux leads to a greater sensitivity to local moderator concentration and spectrum variations, leading to larger power peaking at fuel type and fuel- water interfaces, termed lattice heterogeneities. Such peaking may be reduced by the incorporation of a smaller amount of plutonium in each of a greater number of rods, although this is contrary to the incentive in (1).

(3) Reactivity Effects

Increased resonance self shielding and the continuous production of fertile isotope Pu-240 result in a slower reactivity depletion than that of an equivalent uranium lattice. The initial cell reactivity is less sensitive to fissile isotopic content. More careful fuel management is required to utilize this added reactivity lifetime within power peaking constraints.

(4) Thermal and Near-Thermal Resonances

Resonance absorption and upscatter create a harder and

complicated flux distribution so that the thermal flux calculational region must be extended above the 1.0 ev Pu-240 resonance region, or otherwise taken into account. Such a treatment is recommended in the Regulatory Staff review of plutonium analysis methods.[3] In addition, the resonance structure contributes to more negative Doppler and moderator temperature coefficients.

(5) Isotopics Complications

Fission product treatment must be more comprehensive due to the spectrum complexity, the greater fission product yields and reaction rate increases. The inaccuracy of the higher isotope cross section data results in an inherent decrease in the accuracy of plutonium fuel isotopic analysis.

(6) Spectrum Complexity and Sensitivity

Plutonium does not exhibit a typical 1/v absorption cross sectional energy dependence in the epithermal region, so that cross section averaging is more spectrum dependent or sensitive than for a uranium core. Resonance absorption at high energies complicates the spectrum calculation.

(7) Energy and Temperature Dependencies

The capture to fission ratio, neutron yields per absorption and plutonium to uranium fission ratios are strongly spectrum and temperature dependent, even in the thermal energy range.

(8) Resonance Interactions

U-238 and Pu-239 resonance overlap must be considered.

(9) Particle Self-Shielding

Mixed oxide particle non-homogeneity can decrease effective fission cross sections and capture to fission ratios. This effect should be minimal, however, for anticipated particle sizes of 20-50 um.

(10) Short Term Transient Parameters

Plutonium fuel has a smaller (about 1/3) delayed neutron fraction and a shorter (about 3/4) prompt neutron lifetime than uranium fuels, resulting in a more rapid increase in power for a specified reactivity change. The energy release of such a transient, however, is dependent upon the negative feedback mechanisms (Doppler and void coefficients) which are greater for plutonium fuel. The result is that care must be taken in the determination of kinetics parameters and the design of control systems, since the core characteristics are sensitive functions of the spatial distribution of plutonium in the core.

(11) Cross Section Data and Calculations

The accuracy of plutonium cross section data, especially of the higher isotopes, is not as good as that of uranium. This, in addition to the increased number of isotopes present, introduces an inherent decrease in the accuracy of plutonium relative to uranium fuel calculations.

(12) Power Measurement Inaccuracies

Normalization of relative powers between uranium and mixed oxide rods via gamma scan measurements has led to experimental errors a few percent larger than would be encountered in all uranium fuel. In the techniques using gross

gamma scan data, the difference in the gamma spectrum and the ratio of gamma decay heat to beta particle decay heat must be known, and this data is subject to greater experimental uncertainty in mixed oxide fuels.

The neutron physics considerations, when taken in conjunction with inherent calculational model assumptions, introduce discrepancies in prediction of lattice physics parameters, which may be conveniently expressed as a bias in k_{eff}, the effective multiplication constant of the system. Liikala, et.al.[7] presents a thorough discussion of the areas of calculational uncertainty and estimated k_{eff} bias, the summary of which is presented in Table 1.3. The values given represent the expected deviations from actual k_{eff} of a cold, clean, near-critical lattice for a reasonable range of lattice pitches when making the designated approximation or assumption, as done in standard physics calculations. Such values are obtained by comparison with an alternate calculation which models more exactly the phenomena in question. Notice that the k_{eff} bias values for plutonium and uranium lattices differ.

One primary area of uncertainty, neutron cross section experimental data, is expanded according to isotope and energy region in Table IX (p. 286) of the Liikala, et.al. article. Further experimental work must proceed here, as well as in the related area of resonance overlap. More discussion of this problem is given in Section 4.1.

Table 1.3

Areas of Calculational Uncertainty for Uranium and Plutonium Oxide Lattice Analysis and Estimated Bias in Calculated k_{eff} (7)

Area and Description of Assumptions	% k_{eff} Bias uranium | plutonium
1. Slowing Down Calculation	
A. Spatial Fast Effect Neglected- flat spatial fast flux assumed, underestimating fast fissioning of U-238	-0.2 to -0.5
B. Resonance Overlap Neglected- reduced effective resonance integrals, primarily due to U-238 and Pu-239 overlap	none | 0.0 to -0.5
2. Thermalization Calculation	
A. Unit Cell Reflecting Boundaries- one dimensional spatial calculation prohibits directional flux gradients, partially rectified by extra regions and "white" boundary conditions (open lattices most affected)	-0.1 to -0.5
B. Energy Detail- standard 30 energy group treatment for uranium lattices not sufficient for representation of Pu-239 thermal resonance	none | 0.1
C. Thermal Group Upper Boundary- significant neutron upscattering into 1.056 ev Pu-240 resonance (tight lattices, large Pu-240 content lattices most affected)	none | 0.0 to -0.7
D. Anisotropy Approximation- effect accounted for by adjustment of scattering matrix elements, significant effect for certain lattices	inconclusive

Table 1.3

(Continued)

Area and Description of Assumptions	% k_{eff} Bias uranium | plutonium
3. Leakage Calculation	
A. Axial Leakage Representation- use of one dimensional radial diffusion theory (measured axial buckling) for a homogeneous cylindrical core; streaming in the fuel and channels neglected	0.25
B. Spatial Detail- number of space points and regions used, especially at the core boundary and reflector	-0.5 | -1.0
C. Energy Detail- Insuffucient representation of fast leakage (large leakage systems most affected)	<-0.5
D. Diffusion Theory Assumption- Directional effects not accounted for (large leakage systems most affected)	inconclusive
4. Assembly Physical Detail	
A. Fuel Homogeneity Assumption- Spatial self shielding of PuO_2 particles produces positive reactivity effect due to Pu-239,240 absorption resonances, negative due to Pu-239 fission rate (particle size and Pu-240 content dependent)	none | 0.1 to 0.7
B. Lattice Hardware-Ignored	<0.2
5. Physical Parameter Uncertainties	
A. Neutron Cross Sections	
i. Experimental Uncertainties (greatest for loose lattices since largest uncertainties are non-thermal)	±0.5- ±1.5 | ±1.0- ±2.0
ii. Cross Section Sets	±0.7 to ±3.8

Table 1.3

(Continued)

Area and Description of Assumptions	% k_{eff} Bias* uranium | plutonium
B. Diffusion Coefficient Definition- model representation of leakage term	±0.5
C. Axial Buckling derived from Reflector Savings- assumed equivalent measurement from exponential and critical cores, radially and axially the same	< 0.1
D. Manufacturer Tolerances	random

* The typical procedure for determination of the values of bias in k effective for each area of calculational uncertainty is use of a more sophisticated (higher order) calculation with respect to that area. A comparison of this calculation's result and that obtained by standard cell and lattice analysis techniques yields % k_{eff} bias.

It is to be recognized that any measure of the accuracy of a series of calculational techniques is a combination of that of the accuracy of basic experimental data and the model assumptions inherent in its handling, which in the case of neutron physics calculations includes spatial and spectral collapsing, weighting and averaging.

1.3 Research Objectives

The analysis of plutonium recycle assemblies requires the development of methods and techniques based on the unique properties of a plutonium fueled system. That is, methods designed for use in analysis of uranium fueled systems may be inadequate from the viewpoint of detail, accuracy or model assumption in any number of areas. Although the neutron analysis aspects of plutonium utilization are theoretically understood, one should not minimize their importance. Experimental and developmental work must proceed at a pace to insure the same operational safety margins afforded uranium cores without unnecessary sacrifice of overall core efficiency.

Our objective in this study is the investigation and use of currently available and modified computational techniques and their applicability in the prediction of mixed oxide lattice neutronics characteristics. Verification of techniques with experimental results is performed by comparison of criticality in cold lattices, isotopics with burnup and relative power distributions. In addition, our methods are utilized in the power distribution calculation of a plutonium recycle assembly

proposed for use in a nuclear power reactor. The result of this calculation is compared to published calculations.

Such a study is independent of those efforts by reactor vendors and groups[8] and, by its nature, not as comprehensive. Independent calculational efforts are warranted, however, by nuclear facility owners and operators in accordance with their responsibility of providing safe, reliable and economic electric power. This is independent of the practical value of dealing with the methodologies, techniques and associated problems of the neutronics of plutonium recycle required for the study of developing methods of analysis.

1.4 Model Verification

1.4.1 Critical Experiment Analysis

Evaluation of k_{eff} for a critical lattice by computational methods using known lattice dimensions, properties and the critical buckling is one means of comparison of either cross section sets with their various spectrum weightings or calculational models. Work previously performed at MIT[9] in verification of cross section set and resonance parameter changes to the spectrum code LASER[10] is continued by analyzing UO_2- 2 w/o PuO_2 Hanford criticals[11] for a variety of lattice pitches of both 8 and 24 a/o Pu-240 content.

1.4.2 Isotopic Comparisons

The changes in isotopic content and the spatial distri-

bution of isotopes within the fuel pin may be calculated with a one-dimensional depletion code such as LASER. Mass spectrometric and radiochemical analysis yields isotopic data which may be obtained at various values of pin burnup. This may be done on a volume averaged basis or at a given radial position by axial microdrillings to obtain a radial distribution of each isotope within the pin. Comparison of data with calculation is informative in comparison of spectrum weighted cross section sets or spectrum and volume averaging models. Yankee Core I (3.40 w/o U-235) pin isotopic data to 40,000 MWD/MT[12,13] and Saxton Core II (6.6 w/o PuO_2) pin isotopic data to 20,000 MWD/MT[14,15] are compared with one dimensional depletion calculations (LASER).

1.4.3 Experimental Power Distribution Comparisons

The ability to calculated relative power distributions is important in both assembly and core analysis. Assembly analysis results in relative power values between lattice pins. The aim is determination of a design which minimizes local power peaking at lattice discontinuities (water regions, control rod areas or boundaries between regions of differing pin types) while maintaining adequate criticality (fissile content) throughout burnup.

Calculated relative power distributions of cold, critical lattices are compared with experimental data from the Saxton Reactor Experiments (CRX), performed as a part of the Saxton Plutonium Program.[16] Various lattice configurations

were used in the experiments, including single region cores (all similar pins), water slot cores (a few pins removed from the lattice) and multiregion cores (a uranium pin region and a plutonium pin region). The cores are small (19 x 19 rod array).Comparisons of the calculated results of relative pin power are made with published calculations[17] in addition to the actual experimental data.

1.4.4 Design Assembly Power Distribution Comparisons

The methodology developed and applied to the experimental cases for power distribution calculation is utilized for a plutonium recycle assembly design proposed for use in a pressurized water reactor. In addition to the practical nature of the calculation, it also serves as a verification of the methods employed by correspondence with published assembly parameter characteristics.

The design case for study is a Combustion Engineering plutonium recycle assembly concept[4] which is presented in Figure 1.1. The assembly is a 14 x 14 pin array. Enriched uranium rods surround islands of mixed oxide rods in an "island" design concept. The objective is minimization of power peaking and better matching of regional (plutonium or uranium) average powers by creation of hard spectrum (fissile plutonium) areas segregated from the effects of the soft spectrum control rod water cells (each four (4) unit cells large). Such an idea is similar to that of varying enrichments within a BWR lattice to prevent excess power peaking near areas of high thermalization, such as the control rod followers.

Figure 1.1 Maine Yankee Assembly Design-
Plutonium Island Concept

14 x 14 array Pitch: 0.580 in.

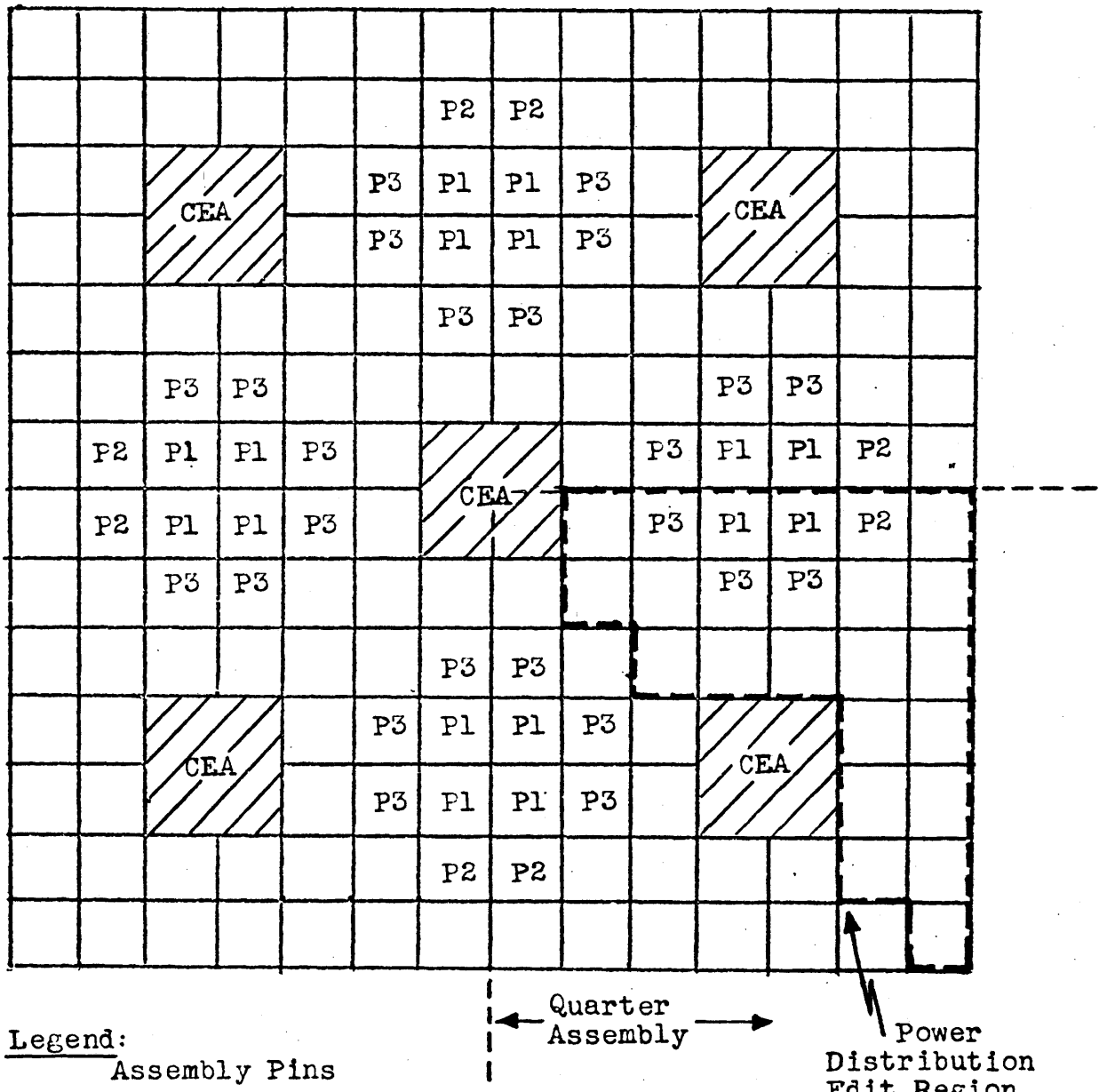

Legend:

Assembly Pins

	3.47 w/o U-235
P1	2.61 w/o Pu
P2	2.39 w/o Pu
P3	2.30 w/o Pu

Plutonium in Natural Uranium

CEA — Control Element Assembly: Control Rod Water Cell

The problems of relative power distribution calculation are similar to those in the experimental cases (Section 1.4.3), namely large water regions and mixed oxide- uranium oxide pin type boundaries. Different, however, is the proximity of one discontinuity to the other, yielding spectrum interactions whose magnitude of influence on relative pin and regional powers must be investigated.

Two significant assembly parameters for design and fuel management purposes are peak to average pin power and regional (fuel type) average powers, both of which are published calculational values for comparison. It is to be stressed that good comparison with calculations does not mean correspondence with actual data nor does closeness of calculations to the overall experimental power distribution assure correct reaction rate or reactivity prediction. Therefore, model benchmarking should include comparisons with all of the significant, obtainable characteristics of a reactor core.

CHAPTER 2

ANALYTICAL METHODS

2.1 Introduction

The basic assumption in most reactor physics calculations in present use is that the space and energy dependences of the neutron flux are separable, so that a spectrum (energy) calculation can be initially performed followed by a separate spatial calculation.

The spectrum calculation is restricted to a particular reactor region, usually a small region of fuel and water called a unit cell and characterized by a given geometry, materials compositions and densities, and temperatures. The results of the calculation are effective, spectrum-averaged few group constants for this unit cell to correctly represent the overall reaction rates in this geometric region.

The spatial calculation uses the effective, spectrum-averaged few group constants in a numerical solution of the spatial flux distribution over a region of the reactor (usually an assembly or the entire core). The resultant flux values enable determination of relative reaction rates and, hence, power production among the various pins and core regions.

2.2 Spectrum Analysis

2.2.1 Introduction

The spectrum calculational procedure is responsible for correctly representing the gross reaction rate characteristics of a small portion of the core. The first stage is knowledge of basic cross section data. Spectrum codes contain cross

section "libraries" or sets which have been reduced from experimental data by flux weighting over an assumed neutron spectrum, which should be chosen as typical of the reactor and reactor region in question. The code further reduces this data by use of the physical properties of the system to calculate a spectrum for averaging. Different techniques are used to obtain this spectrum, based on different assumptions. The theoretical treatment generally differs in the fast (plus epithermal) and the thermal regions. Due to the necessity for the spectral detail of these solutions, the calculations are limited to zero or one spatial dimension.

The standard approach taken in obtaining the fast plus epithermal spectrum (typically above 1 ev) in a unit cell is solution of the Fourier- transformed transport equation using the B-1 or P-1 approximation. One method of spectrum solution in the thermal range is one dimensional integral transport theory, which is discussed in the next section. The following sections deal with unit cell analysis, especially regarding mixed oxide fuels. Finally the Generalized Mixed Number Density Method (GMND) is discussed as a means of obtaining spectrum-averaged constants based on Breen's Mixed Number Density approach.[18]

2.2.1 One Dimensional Integral Transport Theory

One dimensional integral transport theory is a standard method for spectrum code use in the thermal region where group to group scattering is significant. The solution afford-

ed by this method is spatially dependent, so that the energy group structure need consist of about 30-50 groups (up to about 2 ev) instead of the larger number required to correctly represent self- shielding effects in a zero dimensional calculation. The one dimensional integral transport theory equation with isotropic scattering is solved by the computer program THERMOS.[19,20] It is expressed as

$$v(E)N(\underline{r},E) = \int d\underline{r}'\, R(\underline{r},\underline{r}',E) \int_0^\infty dE'\, P(\underline{r}',E,E')N(\underline{r}',E') \tag{2.1}$$

where

$v(E)$	neutron velocity
$N(\underline{r},E)$	density of neutrons in dE about energy E and in $d\underline{r}$ about position $\underline{r}$
$R(\underline{r},\underline{r}',E)$	transport kernel relating flux of neutrons of velocity $v(E)$ about $\underline{r}$ to a unit isotropic source about $\underline{r}'$
$P(\underline{r},E,E')$	probability per second that a neutron of velocity v' will scatter to velocity $v(E)$

with the transport kernel defined as

$$R(\underline{r},\underline{r}',E) = \frac{1}{4\pi(\underline{r}-\underline{r}')^2} \exp\left| \int_{\underline{r}'}^{\underline{r}} ds\, \Sigma_t(\underline{r},E) \right| \tag{2.2}$$

where

$\Sigma_t(\underline{r},E)$	probability per unit length of interaction of neutron in dE about energy E and in $d\underline{r}$ about position $\underline{r}$,

and separation of an epithermal source terms defined by

$$\int_0^{\infty} dE' \, P(\underline{r}',E,E') \, N(\underline{r}',E') =$$

$$S(\underline{r}',E) + \int_0^{E^*} dE' \, P(r',E,E') \, N(\underline{r}',E') \qquad (2.3)$$

where

$S(\underline{r}',E)$ source of neutrons of energy E about position $\underline{r}'$.

In Eq. (2.2), it is evident that the transport kernel is isotropic, as is the birth rate density and the epithermal source, Eqs. (2.1) and (2.3). The scattering matrix in Eq. (2.3) is extended to a thermal cutoff energy E^*, above which a slowing down source is used with an assumed $1/E$ shape dependence. The thermal cutoff should be chosen as the energy above which thermal upscatter is negligible. A more complete discussion of the theory and the numerical techniques of solution is presented in the THERMOS literature cited.

The THERMOS thermal spectrum solution is the foundation of the LASER[10] unit cell depletion code. Another unit cell spectrum code, LEOPARD,[21] is often used for uranium fuel analysis and has been modified for proposed use with plutonium fuels.[15]

Both LASER and LEOPARD employ the program MUFT[22] in the epithermal and fast regions of solution. The essential difference is in the thermal treatment, LASER solving the cylindrical, one dimensional transport equation subject to isotropic scattering to explicitly obtain a thermal energy-

wise spatial flux shape to use for averaging of unit cell constants. LEOPARD, on the other hand, computes a Wigner-Wilkins SOFOCATE[23] spectrum with energy-dependent disadvantage factors determined from a modified form of the Amouyal-Benoist[24] approximation to account for the thermal self-shielding of each group. More extensive code descriptions are given in Chapter 3. The consequences of these different LASER and LEOPARD treatments when applied to mixed oxide fuels is discussed in Section 2.2.3.

2.2.2 Unit Cell Analysis

The core region of neutron spectrum solution and group constant spectrum averaging is termed a unit cell. The unit cell is generally the representation of a cylindrical fuel rod (fuel, gap, clad) and the surrounding square pitch of moderator, which is cylindricized so as to maintain moderator volume (Wigner- Seitz Approximation). The boundary condition for the cell solution should be chosen to match the cell reaction rates of a more sophisticated (e.g. Monte Carlo) calculation. Some form of "white" boundary condition is generally used, incorporating a pure scattering region with a reflecting boundary. Thus, the basic assumption of a zero current boundary condition is inherent in unit cell codes, so that a unit cell is implicitly assumed to reside in an infinite sea of similar cells (i.e., an infinite lattice solution).

Clearly this assumption is invalid for intercell regions

of strong flux gradients. Such a region is between a uranium pin and a water region, in which the spectrum softening of the extra moderator influences the reaction rates in the uranium pin. A similar effect is witnessed between adjacent uranium and plutonium pins. The hard plutonium pin spectrum inflences the uranium pin reaction rates. Such "extended" spectrum effects are discussed in Section 2.3.

The assumption of the separability of space and energy dependencies of the neutron distribution in the core enables one to concentrate initially on the spectrum dependencies by a unit cell calculation. The primary calculation performed is a numerical determination of the flux, $\phi(r_k,E_i)$, for a given number of space and energy intervals to obtain position dependent, group averaged constants, $\bar{\sigma}^j_\alpha(r_k)$, defined as

$$\bar{\sigma}^{\,j}_{\alpha}(r_k) = \frac{\sum_i^I \sigma^{\,j}_{\alpha}(E_i)\ \phi(r_k,E_i)}{\sum_i^I \phi(r_k,E_i)} \qquad (2.4)$$

where

r_k	space position representing region k
E_i	energy representing energy interval ΔE_i
$\sigma^{\,j}_{\alpha}(E_i)$	cross section for reaction α , averaged over ΔE_i by an assumed neutron spectrum, for nuclide j.

The values of $\sigma^j_\alpha(E_i)$ are those present in the cross section library of the code. The position dependent constants in Eq.(2.4) are then volume averaged to obtain cell or region averaged constants, namely

$$\bar{\sigma}^{j}_{\alpha} = \frac{\sum_{k}^{K} \bar{\sigma}^{j}_{\alpha}(r_k) \; V_k}{\sum_{k}^{K} V_k} \qquad (2.5)$$

where

V_k subvolume associated with position r_k ,

and the summation over k extending over the whole unit cell or a specific region, respectively.

Extreme care should be taken in the definition and use of group constants. The definitions should be obtained from the applicable literature. In general, two types of group averaged constants are defined. Their definitions are most conveniently remembered in terms of a reaction rate equation.

One defines cell averaged <u>effective</u> cross sections $\bar{\sigma}^{j}_{\alpha,\text{eff}}$ as those which, in combination with the cell averaged number density of nuclide j, N^{j}_{cell} , the cell volume, V_{cell} , and the cell averaged total group flux, $\bar{\phi}_{\text{cell}}$, yield the correct cell reaction rate for nuclide j in reactions per second, namely R^{j}_{cell} . That is,

$$R^{j}_{\text{cell}} = N^{j}_{\text{cell}} \; \bar{\sigma}^{j}_{\alpha,\text{cell}} \; \bar{\phi}_{\text{cell}} \; V_{\text{cell}} \qquad (2.6.1)$$

where

$$\bar{\phi}_{\text{cell}} = \sum_{k}^{K} \sum_{i}^{I} \phi(r_k, E_i) \qquad (2.7)$$

and the summation over k extends over the whole cell.

Similarly, one defines <u>region averaged</u> cross sections, $\bar{\sigma}^{j}_{\alpha,\text{reg}}$, as those which reproduce the correct regional reaction rates. That is, the regional reaction rate for nuclide

j, R^j_{reg} (in reactions per second), results from a product of the cross section with the region averaged number density, N^j_{reg}, the region volume, V_{reg}, and the region averaged group flux, $\bar{\phi}_{reg}$. That is,

$$R^j_{reg} = N^j_{reg} \bar{\sigma}^j_{\alpha,reg} \bar{\phi}_{reg} V_{reg} \qquad (2.6.2)$$

with $\bar{\phi}_{reg}$ analogous to Eq. (2.7), the summation in Eq. (2.7) over k extending only over the region of interest.

Note that these definitions apply only over a given energy group (few group) defined by the energy limits in (2.4) and (2.6). Similar definitions apply for the transport cross sections, $\bar{\sigma}_{tr}$ or $\bar{\Sigma}_{tr}$, to reproduce the correct cell (or region) leakage rates. Careful definition is required here and with the diffusion coefficient, $\bar{D}$, since the methods of spectrum weighting differ (see Chapter 3 of Reference 25). Similar care is necessary in the use and definition of self-shielding factors to describe spatial flux variations relative to the average flux level in the cell.

The spatial, few group calculation homogenizes a unit cell region to calculate a two (or three) dimensional flux distribution. Thus, such a calculation uses effective group constants from the spectrum code so that, when weighted by the spatial flux variation, relative total cell reaction rates are obtained.

2.2.3 Spectrum Methods with Mixed Oxide Fuels

In Section 2.2.1, the essential difference between the

spectrum codes LEOPARD and LASER was discussed, namely their thermal spectrum treatment. The advantage of LASER, a result of its explicit spatial calculation of the neutron number density for each energy group, is magnified in the calculation of mixed oxide fuel unit cell parameters due to the excessive resonances and group dependent self-shielding present.

Celnik, et.al.[26] discusses and compares calculational methods for mixed oxide fuels and concludes the following concerning LEOPARD and LASER:

(1) Criticality Prediction (k_{eff})

The LEOPARD thermal treatment using cell homogenization and disadvantage factors is inadequate, especially in the calculation of flux depressions associated with the plutonium resonances (particularly for loose lattices). The LASER thermal calculation can account for this. LASER criticality predictions, therefore, are better over a range of lattice pitches.

(2) Thermal Spectrum Calculations

The Nelkin thermalization model[27] for bound element neutron scattering,used in LASER, is preferable to the Wigner- Wilkins spectrum in LEOPARD. The use of an upper bound of 1.855 ev for the thermal treatment in LASER is preferable due to its inclusion of the large 1.0 ev Pu-240 resonance.

(3) Isotopic Distribution with Burnup

The spatial distribution of xenon, samarium and the plutonium isotopes with burnup is significant, so that LASER is prefered due to the spatial nature of its calculation.

(4) Reactivity Depletion (k_∞)

LASER and LEOPARD reactivity depletion results for mixed oxide fuel are in good agreement with expected values, though it is clear that LEOPARD correspondence is due to a cancellation of the spatial and spectral model inaccuracies.

It is to be noted that modifications to LEOPARD have been made by a number of workers[15,28] for increased compatibility with plutonium fuels by overcoming some of these shortcomings.

2.2.3 The Generalized Mixed Number Density (GMND) Method

The Generalized Mixed Number Density method was developed by Mertens[25] at MIT as an extension of Breen's Mixed Number Density (MND) theory.[18] The modifications necessary to obtain GMND group constants from the modified version of LASER, called LASER-M, were made by Momsen.[9] More complete discussion of the theory in this section is presented in these and other references.[29]

Breen notes that the use of regionwise thermal constants with flux and current continuity results in a discontinuity of activation at boundaries of vastly different spectra, such as that between a mixed oxide pin and a uranium pin, or a fuel pin and a large water region. Use of a boundary condition of neutron activation, rather than flux, continuity over an energy interval results in a change in the definition of the one group constants. Conservation of activation, namely

$$\int \sigma(E)\ \phi(E)\ dE \qquad (2.8)$$

where

$\sigma(E)$	energy dependent cross section
$\phi(E)$	energy dependent neutron flux

is equivalent, for a 1/v absorber, to a conservation of neutron number density, since

$$\int \sigma(E)\ \phi(E)\ dE \simeq \int \frac{1}{v(E)}\ \phi(E)\ dE = \int N(E)\ dE = \overline{N} \qquad (2.9)$$

where

$v(E)$	neutron velocity
$N(E)$	energy dependent neutron number density

One may rewrite the standard one group diffusion equation,

$$-\nabla\cdot\overline{D}\ \nabla\overline{\phi} + \overline{\Sigma}_a\overline{\phi} = S \qquad (2.10)$$

in terms of neutron number density, namely

$$-\nabla\cdot\overline{Dv}\ \nabla\overline{N} + \overline{\Sigma_a v}\ \overline{N} = S \qquad (2.11)$$

where the bars denote spectrum averaging and where

$D(E)$	diffusion coefficient
$\Sigma_a(E)$	macroscopic absorption cross section
S	source term for the group

Instead of input of $\overline{D}$ and $\overline{\Sigma}_a$ as spectrum averaged constants from a spectrum code for solution of the spatial equation, Eq. (2.10), for $\overline{\phi}$, solution of the mathematically equivalent equation, Eq. (2.11) for $\overline{N}$ requires values of $\overline{\Sigma_a v}$ and $\overline{Dv}$, namely

$$\overline{\Sigma_a v} = \frac{\int \Sigma_a(E)\ \phi(E)\ dE}{\int \frac{1}{v(E)}\ \phi(E)\ dE} = \frac{\overline{\Sigma}_a}{\left(\overline{\frac{1}{v}}\right)} \qquad (2.12)$$

and

$$\overline{Dv} = \frac{\int D(E)\ \nabla\phi(\underline{r},E)\ dE}{\int \frac{1}{v(E)}\ \nabla\phi(\underline{r},E)\ dE} = \frac{\overline{D}_{grad}}{\left(\overline{\frac{1}{v}}\right)_{grad}} \qquad (2.13)$$

where Eq. (2.13) defines the values of $\overline{D}_{grad}$ and $\left(\overline{\frac{1}{v}}\right)_{grad}$, the averages over a gradient spectrum.

The essential differences in the activation continuity group constants are the weighting of D(E) by a gradient spectrum instead of the normal unit cell spectrum and the change of $\overline{\Sigma}_a$ by $\left(\overline{\frac{1}{v}}\right)$, a relative enhancement for spectrum hardness over normal diffusion theory values.

Experiment and higher order calculations show that activation shapes are best matched when the gradient spectrum is Maxwellian (i.e. softer than the normal cell spectrum). Thus, the spectrum averaging in Eq. (2.12) is done over the normal unit cell spectrum, while that in Eq. (2.13) is done over a Maxwellian spectrum. This is the basis of MND thermal cross sections in LEOPARD, the spectrum in Eq. (2.12) from SOFOCATE and that in Eq. (2.13) Maxwellian.

The basis of GMND theory also recognizes this spectrum difference, using normal unit cell spectrum averaging in Eq. (2.12) while, using the features of a spatial calculation such as that in LASER, mathematically approximating the gradient spectrum in Eq. (2.13). Thus, the thermal group equation

for solution becomes

$$- \nabla \cdot \bar{D}_{GMND} \nabla \bar{N} + \bar{\Sigma}_{a,GMND} \bar{N} = S \qquad (2.14)$$

where

$$\bar{\Sigma}_{a,GMND} = \frac{\bar{\Sigma}_a}{\overline{\left(\frac{1}{v}\right)}} \qquad (2.15)$$

and

$$\bar{D}_{GMND} = \frac{\bar{D}_{grad}}{\overline{\left(\frac{1}{v}\right)}_{grad}} \qquad (2.16)$$

The values of these terms are obtained from a LASER spectrum code calculation. $\bar{\Sigma}_a$ is the normal spectrum averaged constant. $\overline{\left(\frac{1}{v}\right)}$ is equal to $\frac{1}{\bar{v}_{cell}}$, where $\bar{v}_{cell}$ is the cell averaged neutron velocity for the thermal group. $\bar{D}_{grad}$ is approximated as the normal spectrum averaged $\bar{D}$, since the difference is apparently not significant[25]. $\overline{\left(\frac{1}{v}\right)}_{grad}$ is approximated as

$$\overline{\left(\frac{1}{v}\right)}_{grad} = \frac{1}{\bar{v}_{grad}} \simeq \frac{\Delta \bar{N}}{\Delta \bar{\phi}} = \frac{\bar{N}(r_1) - \bar{N}(r_2)}{\bar{\phi}(r_1) - \bar{\phi}(r_2)} \qquad (2.17)$$

where r_1 and r_2 are positions in the moderator, far from and near to the fuel pin, respectively.

Thus may we define LASER-M GMND thermal group constants relative to normal LASER-M constants as

$$\bar{\Sigma}_{\alpha,\,GMND} = (\bar{\Sigma}_\alpha)(\bar{v}_{cell}) \qquad (2.18)$$

and

$$\bar{D}_{GMND} = (\bar{D})(\bar{v}_{grad}) \qquad (2.19)$$

for reaction α. Similar definitions apply to the microscopic

parameters. The modification of LASER to form LASER-M, as described in Section 3.2, includes the calculation of GMND values. The constants for the fast and epithermal groups are unchanged from the normal group constants.

It is instructive to attempt to predict the changes in relative power distribution in a diffusion theory calculation that would result from the use of GMND, relative to normal, group constants, especially near water slots or uranium-plutonium pin boundaries. For a water slot, $\bar{\nu}_{cell}$ (water slot) < $\bar{\nu}_{cell}$ (uranium pin cell), so that from Eq. (2.18), the reaction rates of pins surrounding the water will be enhanced so as to increase the local power peaking. For uranium- plutonium pin boundaries, $\bar{\nu}_{cell}$ (uranium pin cell) < $\bar{\nu}_{cell}$ (plutonium pin cell), so as to enhance the plutonium reaction rates relative to the uranium reaction rates in contrast to the normal group constants. For most pin cells, $\bar{\nu}_{cell} > \bar{\nu}_{grad}$, so that the importance of pin leakage is diminished relative to absorption, though for assembly and core calculations, the leakage term in Eq. (2.14) is small.

Mertens shows that for uranium- plutonium pin type boundaries and interior water slots, GMND cross sections show reasonable agreement, in a power distribution sense, with more rigorous calculations. Comparisons with experimental power distributions in Chapter 6 demonstrate the improvement in power distribution prediction of GMND values over normal spectrum averaged constants for these lattice discontinuities.

There are two basic shortcomings of the general MND

method[29]. Use of a Maxwellian diffusion length is incorrect for regions near lumped absorbers. The GMND method, with its implicit use of the spectrum spatial characteristics, does not suffer from this shortcoming. Secondly, both methods fundamentally assume activation by a 1/v absorber. This is generally not the case for mostly plutonium systems in which the thermal region extends into resonance energies. Nevertheless, the success of MND and GMND use in regions of spectrum discontinuities warrants its use in this study for comparison of results with those obtained from normal spectrum averaged methods.

2.3 Extended Spectrum Effects

The inherent zero current boundary condition present in unit cell codes, as discussed in Section 2.2.2, assumes that a unit cell resides in an infinite lattice of similar cells. The separability of the spectral from spatial effects may no longer be so simply handled for many mixed oxide cases due to the sensitivity of the plutonium thermal reaction rates to spectral softening. Not only is the spectrum calculation influenced, but the diffusion theory assumption of small flux gradients, inherent in spatial,few group calculations, may be invalidated.

The truly correct method of approach to a complicated spatial- spectral problem is explicit representation of the geometry and energy dependencies, which, due to the complexity and the limitations of computer storage, requires a Monte

Carlo solution. Expense makes this prohibitive. A practical way is introduction of more spatial effects in the spectrum calculation, namely an accounting for the pin's local environment. This may be accomplished by use of an "extra" region to model cell boundary influences or calculation of a spectrum covering a region larger than a unit cell.

Chapter 5 discusses a method developed to account for such adjacent pin spectral effects by obtaining correction factors for the infinite lattice LASER-M group constants. The factors apply to the thermal group constants and are based on a spatially extended thermal calculation using THERMOS. Whereas the spectral detail in this calculation is good, the one dimensional limitation in THERMOS requires development of an equivalence relationship between unit cells and the slab regions used to represent them in modeling a row of unit cells. Spatial detail is sacrificed so as to include an extended spectrum region.

An opposite approach is sacrifice of spectral detail while maintaining the correct geometry surrounding the unit cell. Some similar type of correction factors might thus be obtained. The complicated geometry would require a collision probability model with, perhaps, two dimensional transport theory, as has been proposed for the preliminary specifications of a recycle computational package[8]. Here it is necessary to evaluate the effects of group collapsing and the limited geometry extent.

The method developed in Chapter 5 results in the deter-

mination of THERMOS corrected LASER-M (TCL) thermal group constants for use in few group diffusion theory power distribution calculations. Comparisons with experimental data (Chapter 6) and published calculations for a proposed recycle assembly (Chapter 7) are made using Normal, GMND and TCL thermal group constants in diffusion theory calculations.

2.4 Spatial Analysis by Few Group Diffusion Theory

The general approach for the solution of the spatial relative power distribution in a reactor is few group diffusion theory. The cases for study are two dimensional pinwise relative power distributions, the x-y lattice represented by a two dimensional array of mesh points. The homogenization of the fuel pin and square pitch of surrounding moderator is performed by the spectrum code which supplies group averaged constants for that particular unit cell region. The spatial pointwise flux solution enables a determination of spatial, flux averaged, pointwise values (e.g. reaction rates, power) which are then volume averaged to obtain cell averaged values.

The computer program PDQ-7[30], as described in Section 3.1.3, is used to perform a numerical, few group solution of the flux and power distribution over the spatial mesh. The code requires as input few group, spectrum averaged values of $\overline{D}$ (or $\overline{\Sigma}_{tr}$), $\overline{\Sigma}_a$, $\overline{\Sigma}_r$, $\overline{\nu\Sigma}_f$, and $\overline{\kappa\Sigma}_f$ for the particular regions of the mesh layout, where g is the group designation, the macroscopic removal,($\overline{\Sigma}_r$), pertains only to the next

highest (lowest energy) group, and κ is energy per fission in units of watt-seconds per fission. LASER-M supplies such values for input. A group independent buckling value is used to represent the axial leakage in the two dimensional problem. Boundary values are, optionally, zero flux (used for full core and reflector calculations) or zero current (assembly calculations).

The few group calculations generally use two groups. This is deemed acceptable for plutonium pin calculations due to the high thermal cutoff (1.855 ev) of the LASER-M spectrum calculation for inclusion of the major resonance structures of the plutonium system. Hellens[4] indicates that, for calculations of average plutonium pin power in an island design, the diffusion theory group number influence is small (on the order of 2%) relative to the inclusion of transport (S_n calculational) effects (on the order of 7%).

The accuracy of diffusion theory results is limited by its applicability, in a theoretical sense, to the given situation. Although mixed oxide- uranium oxide fuel type boundaries and water slot- fuel boundaries do not fulfill the diffusion theory criteria of the absence of strong flux gradients, these transport effects can be accounted for by the spatial nature of the extended spectrum calculation. That is, diffusion theory results can be made to agree with higher order calculations through appropriate adjustments in the few group constants.

CHAPTER 3

ANALYTICAL TOOLS

3.1 General Description

The sequence of calculational steps towards obtaining relative power distribution values is, in this study, employment of a LASER version, LASER-M, to obtain few group, cell averaged effective constants for use in a PDQ diffusion theory calculation. THERMOS is the foundation of the thermal LASER calculation, namely one dimensional transport theory. In addition, separate THERMOS slab calculations are performed to obtain thermal group correction factors to the LASER-M thermal constants, as discussed in Chapter 5.

3.1.1 THERMOS

The computer code THERMOS[19,20] is used to compute the scalar thermal neutron flux as a function of position by numerical solution of the integral transport equation subject to isotropic scattering (see Eqs.(2.1)-(2.3)). One dimensional slab or cylindrical geometry transport kernels are available. The code has been written for use with any thermal scattering kernel (e.g. free gas, Brown-St.John, Nelkin, etc.)as computed by a separate program, called GAKER[20]. The program LIBP[20] prepares the cross section library tape for THERMOS, with each isotope represented by an absorption (and, optionally, fission and scattering) cross section set, generally in 30 to 50 energy groups in the thermal range. The geometric transport

kernels are built-in, and the solution proceeds through use of Gauss iteration, renormalization, over-relaxation and extrapolation methods.

The geometric representation in one dimension utilizes a given number of space points, any consecutive group of which determines a subvolume, with which can be associated given concentrations of available nuclides and a thermal neutron source. The source is input as an epithermal scattering cross section (barns) and a nuclide source concentration (atoms per barn-cm), the product of which has the units of cm^{-1}, or a macroscopic removal cross section ($\overline{\Sigma}_r$). The source flux shape may be specified as $(1/E)^q$, where q is a variable. Flux averaged and volume averaged values of $\overline{\Sigma}_a$, $\overline{\Sigma}_f$, $\overline{\nu\Sigma}_f$, $\overline{\Sigma}_s$, $\overline{D}$ and $\overline{\Sigma}_{tr}$ may be obtained over the desired subvolumes as well as a designated number of energy groups. The group constants for each isotope are also obtainable. Boundary conditions are, optionally, vacuum or reflecting.

The THERMOS version used in this study was made available by the Yankee Atomic Electric Company[31] . The version uses a 30 energy group structure up to 1.855 ev (equal to the LASER thermal cutoff). The maximum number of space points is 25, an improvement over the Argonne version[20] .

The cross section master library for the Yankee THERMOS contains ENDF/B-II (Evaluated Nuclear Data File)[32] thermal cross sections, similar to those incorporated into LASER-M for the plutonium isotopes by Momsen[9], discussed in Section 3.2. The Nelkin scattering kernel representation for hydrogen is available for a series of temperature values. Honeck's

correction for anisotropic scattering[33] has been incorporated in the P_0 scattering matrix for hydrogen by Yankee Atomic. That is, the P_1 scattering kernel is taken into account by summation of P_1 group in-scattering and subtraction from the given P_0 diagonal term. The numerical instability caused by this correction was removed by elimination of overrelaxation and extrapolation in the iterative solution process.

For the aid of those wishing to use THERMOS at MIT, Appendix B gives helpful notes.

3.1.2 LASER

The multigroup energy program LASER[10] is based on a modified version of the slowing-down program MUFT[22] and the thermalization transport theory code THERMOS. It calculates the neutron flux spectrum of an individual cell in a uniform lattice using a three region model (fuel, clad, moderator) in cylindrical geometry with a built-in, surrounding, white scattering ring. A burnup calculation is optional, as is a correction for non-linear effects in the system of burnup equations. Due to the spatial nature of the THERMOS calculation, the distribution of burnup and isotopics as a function of radius in the fuel rod is explicitly calculated. Buckling and criticality poison searches are optional.

The MUFT calculation provides a solution in the epithermal (1.855 ev to 5.53 kev) and fast (5.53 kev to 10 Mev) energy ranges. The solution is that of the Fourier-transformed transport equation using the consistent B-1 approximation

with the Greuling-Goertzel slowing down approximation in an infinite, homogeneous medium. The finite geometry is simulated by a leakage term. Shielding or "L" factors are applied to the resonance cross sections of U-238 to account for spatial self-shielding, Dancoff and Doppler effects as calculated by Strawbridge[34] with a correlation making use of Hellestrand[35] data. A 50 energy group structure is used from 1.855 ev to 10 Mev. The MUFT calculation provides the isotropic source to the thermal group, which is assumed spatially flat with an asymptotic 1/E shape dependence.

The THERMOS solution in the thermal range (under 1.855 ev), as described in Sections 2.2.1 and 3.1.1, is a solution of the integral transport equation subject to isotropic scattering using a cylindrical transport kernel. The range is divided into 35 energy groups, chosen specifically to accurately represent the 0.3 ev Pu-239 and 1.0 ev Pu-240 resonances. One may choose between a free gas (Wigner-Wilkins) or Nelkin scattering kernel for light water. The Pu-239 and Pu-240 resonances are Doppler broadened in terms of a line shape function.

The burnup calculation, due to the explicit spatial flux solution, may be performed with relatively large time steps. The fission products are separated into Xe-135, Sm-149 and a lumped pseudo fission product (one fission product produced per fission event) whose cross section is input as a polynomial with burnup. The user also specifies the spatial de-

pendence of the U-238 epithermal capture.

Further discussion of LASER is presented in the references[9,10,36].

2.1.3 PDQ-7

The PDQ-7[30,37,38] program calculates a discrete numerical solution to the few group, time independent neutron diffusion equation for a heterogeneous reactor in one, two or three dimensions. Downscatter is permitted to only the next lowest energy group, though two overlapping thermal groups may be used to describe a microscopic cross section as a linear combination of two spectrum averaged values. Flux and volume weighted values of region-dependent parameters and regionwise and/or pointwise flux and power distribution output edits are available. The possible geometries for variable mesh layout are rectangular, spherical (1D), cylindrical (1D, 2D) and hexagonal (2D,3D). Boundary conditions may be zero flux, zero current or rotationally symmetric.

Depletion calculations are performed, either pointwise or block, by the HARMONY part of the PDQ/HARMONY package[39].

The version of PDQ operable at MIT is similar to the version of PDQ-7 revised by the Aerojet Nuclear Corporation[38].

3.2 The Modification of LASER: LASER-M

3.2.1 General

The modifications to the standard Argonne version of

LASER by Rim[40] and, primarily, Momsen[9] are described briefly in Sections 3.2.2 and 3.2.3, and encompass thermal cross section and thermal resonance parameter changes. Output additions, discussed in Section 3.2.4, were made to increase the compatibility with input requirements of diffusion theory codes and enable convenient use of GMND cross sections (Section 2.2.4).

3.2.2 Cross Sections

Two major revisions were made to the LASER thermal library. Rim normalized the U-235 cross section values to the 2200 m/sec parameters of Sher, et.al.[41] Momsen added ENDF/B-II thermal cross sections for Pu-239, 240, 241 and 242. The weighting function for the processing of these cross sections was 1/E, joined to a Maxwellian distribution. The applicable references contain further information.

Uotinen, et.al.[42] and Liikala, et.al.[7] discuss the details of cross section sets and the influences on calculational results. The following general points are significant:

(1) The cross sections contributing to the largest uncertainties in k_{eff} (see Table 1.3) are the non-thermal data for U-238 and Pu-239, the former due to its especially high concentration and resonance structure.

(2) There is a serious unresolved discrepancy in the U-238 measurement of the infinite dilute resonance integral versus the calculation of such using the detailed, energy-dependent cross section data. This itself is a

contribution of about 1% $\Delta k/k$ in k_{eff} calculational uncertainty.

(3) The expected calculational uncertainties due to cross sections are significant (UO_2 lattices: ±1.5 to ±0.5%, PuO_2-UO_2 lattices: ±2 to ±1% $\Delta k/k$ in k_{eff}). The larger uncertainties apply to tight lattices, due to (1).

Concerning the thermal cross sections of plutonium, the following comments are pertinent:

(1) All of the thermal cross sections for the plutonium isotopes of ENDF/B-II and ENDF/B-III are the same, except for those of Pu-242. The correction to the Pu-242 thermal cross section, as noted by Uotinen, et.al. (p. 127) should be made to LASER-M.

(2) Recent data discussed by Uotinen, et.al. point to areas of investigation and possible revision to ENDF/B values, especially concerning

- The capture to fission ratio (α) of Pu-239 from 0.5 to 1.0 ev
- Discrepancies in the 2200 m/sec values of Pu-240 capture
- Neutron yield per absorption (η) energy dependency of Pu-241

Further developments in the evaluation of plutonium cross sections for thermal reactor applications should be followed.

3.2.3 Resonance Parameters

Rim included data in LASER to evaluate the line shape

function of the 0.3 ev Pu-239 resonance and the virtual level to account for Doppler broadening. Momsen changed the thermal resonance parameters for the 1.0 ev Pu-240 resonance to ENDF/B-II values obtained by calculations using a 1/E weighting joined to a U-235 fission spectrum.

Areas of possible improvement to ENDF/B-II values due to new and conflicting data are discussed by Uotinen, et.al., and include:

(1) The resonance capture integral above 0.5 ev for Pu-239

(2) The neutron width (Γ_n) of the Pu-240 1.0 ev resonance

(3) Resonance parameters of Pu-242 less than 150 ev

The problem of the neglect of resonance overlap in general, and specifically between U-238 and Pu-239, is serious in its influence on calculated k_{eff} (see Table 1.3) for a typical mixed oxide lattice. Results of work by Hellens[43] indicate a -0.1 to -0.4% $\Delta k/k$ effect for the 8 a/o Pu-240 criticals of UO_2- 2 w/o PuO_2 (discussed in Section 4.1). The solution to this situation is a reevaluation of the "L" factor procedure used in LASER (Section 3.1.2) and corrections by correlations which would account for the plutonium isotopic content. Hellens[4] refers to work by Borressen and Goldstein which uses an equivalence relation for the resonance integrals of Pu-239 and Pu-240. Such investigations and their possible inclusion within the LASER methodology should be followed.

3.2.4 Output Additions

The primary incentives for the output edit modifications

undertaken by Momsen[9] were to increase compatibility of the code with diffusion theory code input requirements, to include a calculation of GMND macroscopic and microscopic thermal group constants (Section 2.2.4) and to reduce the voluminous LASER output. The computer listing of changed subroutines is present in Appendix E of Reference 9.

The changes incorporated in LASER-M are:

(1) Calculation of an approximate microscopic transport cross section (all groups) and an approximate microscopic removal cross section (non-thermal groups) based on a hydrogen-only scattering assumption

(2) Calculation of a thermal diffusion coefficient averaged only over the moderator region

(3) Calculation of fast and epithermal spectrum averaged values of energy per fission ($\bar{\kappa}$) for macroscopic and microscopic parameters, plus neutrons per fission ($\bar{\nu}$)

(4) Calculation of an approximate neutron velocity averaged over a gradient spectrum ($\bar{v}_{grad}$) by use of Eq. (2.17) or

$$\bar{v}_{grad} = \frac{\bar{\phi}(r_1) - \bar{\phi}(r_2)}{\bar{N}(r_1) - \bar{N}(r_2)} \qquad (3.1)$$

where the bars are thermal group spectrum averages of neutron flux ($\bar{\phi}$) and neutron number density ($\bar{N}$). Points r_1 and r_2 are spatial points number 11 (point number 12 is the outer edge of the moderator region) and 7 (adjacent to the fuel pin in the moderator), respectively, in the LASER-M terminology.

(5) Calculation of GMND thermal group constants (Eqs. (2.18) and (2.19)) using values of $\bar{v}_{grad}$ and $\bar{v}_{cell}$ (cell averaged thermal group velocity) as calculated by LASER-M

(6) Calculation of cell volume fractions and a cell averaged equivalent thermal microscopic cross section for oxygen

(7) Output edit flexibility and a condensed output edit for microscopic cross sections

CHAPTER 4

UNIT CELL MODEL VERIFICATION:

CRITICAL EXPERIMENT ANALYSIS AND ISOTOPIC COMPARISONS

4.1 Plutonium Critical Experiment Analysis

4.1.1 Introduction

Critical experiment analysis is performed in order to assess the accuracy of the calculational model. Critical experiment calculations using LASER-M are performed to verify the accuracy of the present model, as contrasted to the normal LASER. This is not a comparison of the cross section sets and resonance parameters, per se.

The technique used for the critical analyses was an experimental determination of the buckling (from reflector savings measurements) of close-to-critical configurations. This experimental value is input to LASER-M as the geometric buckling (leakage term) and the materials buckling is not searched, so that the geometric buckling is also used in the calculation of the fast and thermal spectrum. The value of k_{eff} derived from a two group (fast plus epithermal, (1) and thermal, (2)) representation, as in LASER, is

$$k_{eff} = k_{eff,1} + k_{eff,2}$$

$$= \frac{\overline{\nu\Sigma}_{f1}}{\overline{\Sigma}_{a1} + \overline{\Sigma}_{r1} + \overline{D}_1 B_g^2} + \frac{\overline{\Sigma}_{r1}\,\overline{\nu\Sigma}_{f2}}{(\overline{\Sigma}_{a1} + \overline{\Sigma}_{r1} + \overline{D}_1 B_g^2)(\overline{\Sigma}_{a2} + \overline{D}_2 B_g^2)} \qquad (4.1)$$

where

$\overline{\Sigma}_{\alpha i}$ — macroscopic, multigroup spectrum averaged cross section for energy group i and reaction α

$\overline{D}_i$ — diffusion coefficient for energy group i

$\overline{B}_g$ — group independent geometric buckling term

and the calculated value of k_{eff} should equal 1.0 for the critical lattices modeled. As mentioned above, the buckling values are approximations derived from reflector savings. The typical accuracy of such measurements is sufficient so that an error as large as 10% in the axial reflector savings influences k_{eff} by less than 0.001 $\Delta k/k$ [11].

Criticals analysis with the comparison of the calculated group constants is one way of investigating the sensitivity of the LASER calculation to cross section set and resonance parameter changes. Use of a series of lattice pitches for such calculations and observation of the resultant trends in k_{eff} can give insight regarding the source of discrepancies, usually related to a model assumption inaccuracy. The actual choice of cross section sets themselves is quite another matter, not dealt with in this study.

Isotopic distribution within the fuel pin as a function of burnup provides the second important source of model and cross section set experimental feedback, as discussed in Sections 4.2 and 4.3.

4.1.2 Previous Work

The present critical analyses are performed parallel to

those of Momsen[9] with LASER-M. Momsen's calculations utilized data from UO_2- 1.5 w/o PuO_2 criticals performed as part of the Hanford experiments at Battelle[11,44] and UO_2- 6.6 w/o PuO_2 criticals performed at the Westinghouse Reactor Evaluation Center (WREC)[26]. The standard options used in the LASER-M analysis were:

(1) Measured experimental bucklings used as the geometric (input) buckling

(2) Materials buckling not searched

(3) Nelkin scattering kernel used (see Section 2.2.3)

(4) U-238 L factor searched, remaining isotopic L factors set equal to 1.0

(5) Inputs for fuel, moderator and resonance effective temperatures were values from the experimental (cold) condition

The LASER-M values of k_{eff} were compared with those obtained by Westinghouse with a revised version of LEOPARD[45,46]. Both these comparisons and those performed by Celnik, et.al.[26] illustrate the superior ability of the LASER code to account for the spatial flux dependence and self shielding within the pin by the more accurate k_{eff} prediction over a wider range of lattice pitches. In addition, the LASER-M version gave better values of k_{eff}, with better or equivalent spreads in k_{eff} over lattice pitch. Table 4.1 is a correction[47] for the Hanford (1.5 w/o PuO_2) experiment calculation of Momsen and shows excellent agreement. It should be noted that these criticals were primarily Pu-239 in plutonium content (about 90 a/o).

Table 4.1

RESULTS OF CALCULATIONS ON THE HANFORD (1.5 w/o PuO_2) EXPERIMENTS

(Experimental K_{eff} = 1.00000 in all cases)

Pitch (inches)	$k_{effective}$		
	LASER-M*	LASER**	LEOPARD**
0.55	0.997598	1.00666	1.01652
0.60	1.00048	1.01123	1.02397
0.71	1.00349	1.01761	1.03144
Δk_{eff}***	0.00589	0.01095	0.01492
Average Error	0.212 %	1.183 %	2.398 %

* This table replaces Table 4.3 (p. 73) of Momsen[9]. The LASER-M values have been recalculated based on a pure Zr number density of 0.04312 atoms/barn-cm. An erroneous value had been used in the previous calculations (Reference 47).

** Westinghouse calculations, Reference 45

*** Spread in k_{eff} for the three lattice pitches

Mertens[25] performed a LASER calculation for the Hanford UO_2-2 w/o PuO_2 criticals[11,48] and the results were in agreement with calculations of Celnik, et.al.[26].

4.1.3 Hanford 2 w/o PuO_2 Criticals: Description

Critical experiments were performed at the Battelle Northwest Laboratory for a variety of hexagonal lattice pitches of 2 w/o PuO_2 rods (plutonium in natural uranium). Another important parameter varied was plutonium isotopic fraction, with trials designated as 8, 16 and 24 a/o Pu-240. The higher isotope content rods are more typical of first generation (and more especially equilibrium) recycle plutonium isotopics.

The physical characteristics of the six (6) cases of critical lattices investigated are contained in Table 4.2. They are hexagonal pitches of 0.80, 0.93 and 1.05 inches for both 8 and 24 a/o Pu-240. The pin fuel contents in the references do not match (Reference 11, p. 263, Figure 10 and Reference 26, p. 18, Table 4), although the effect of such differences is minor as evidenced by the overall similarity in the value of group constants and self shielding factors between the LASER-M and Celnik, et.al. calculations.

The experimental buckling values, as given in the references, also do not match to within experimental error. This may be explained, however, by the different reflector conditions and different dates of experimental analysis (the latter influences Pu-241 content due to decay to Am-241) for these ex-

Table 4.2

Fuel Rod Specifications

UO_2- 2w/o PuO_2 Hanford Criticals

Fuel Rod Dimensions(in):

Fuel diameter	0.505
Rod diameter	0.565
Clad Thickness	0.030
Active Length	36.00

Fuel Loadings:

Fuel density (gm/cm^3)	9.54
PuO_2(2w/o of mixture) (gm/rod)	22.56
Total mixture, PuO_2 plus natural UO_2, (gm/rod)	1128.0

Cladding: Zr-2, seal welded end plugs

Isotopics:	Nominal 8% Pu-240 @ 22°C	Nominal 24% Pu-240 @ 24°C
atom %		
Pu-239	91.615	71.762
Pu-240	7.654	23.503
Pu-241	0.701	4.080
Pu-242	0.031	0.656

Hexagonal Pitch (in)	0.80	0.93	1.05
H/Pu atom ratio	238	391	554
H_2O/Rod volume	1.211	1.987	2.808
Experimental Buckling (m^{-2})	RESULTS		
8a/o Pu-240	93.7±0.3	103.3±0.3	101.3±0.5
24a/o Pu-240	63.1±0.2	79.4±0.2	77.6±0.3

periments using the same fuel rods. No Am-241 decay correction factor is used. Based on the dates in the appendix of Reference 11 and the microscopic fission cross section of Pu-241 from the LASER-M calculations, however, the lost Pu-241 can account for 0.001 $\Delta k/k$ in k_{eff} for certain trials (see Table 4.3).

3.1.4 Calculational Results and Comparisons

The Hanford 2 w/o PuO_2 results, as calculated with LASER-M, are given in Table 4.3, as are the results of similar calculations for these experiments. The LASER-M computer input listings for these trials are given in Appendix A. The LASER (Sher,Wescott Thermal) results refer to the standard LASER version calculations, from Reference 26. All the LASER version results are spectrum calculations, compared to the higher order calculational results given using BRT (Battelle Revised THERMOS), the slowing down program HRG3 (similar to MUFT[22]) and the one dimensional diffusion theory code HFN, from Reference 7. The higher order calculations were performed for the two sets of cross sections given, BNWML (Battelle Northwest Master Library)[49] and ENDF/B-II, used for both the fast and thermal groups.

It is evident that the results of the higher order calculations exhibit much smaller spreads in k_{eff} with lattice pitch and less obvious a trend. The difference between these results (different cross section sets) was attributable to the non-thermal parameters, primarily the larger epithermal spec-

Table 4.3 Comparison of Calculated Values of k Effective

2 w/o PuO_2 Hanford Criticals

Atom % Pu-240	Hexagonal Pitch (inches)	Spectrum Calculations		Spectrum plus Diffusion Theory Calculations HRG3,BRT,HFN	
		LASER Sher,Wescott Thermal	LASER-M ENDF/B II Thermal	BNWML Thermal,Fast	ENDF/B-II Thermal,Fast
8	0.80	0.998	0.984	0.992	0.963
	0.93	-	1.015	0.998	-
	1.05	1.018	1.022	0.991	0.978
24	0.80	-	1.003*	0.994	0.968
	0.93	-	1.008	0.996	-
	1.05	1.019	1.013*	0.998	0.986

* The decay of Pu-241 to Am-241 from the time of isotopic separation to that of the experimental work represents a loss of fissile content and a gain in thermal poison absorption. A simple calculation accounting for only the loss of fissile content can be made by use of the effective fission cross section of Pu-241 from LASER-M and its contribution in the equation for k_{eff}. Such a calculation shows that these values of k_{eff} should be reduced by 0.001.

trum averaged U-238 values of ENDF/B-II relative to BNWML[7].

The comparison between the LASER version spectrum results given centers around the differences in the LASER thermal cross section sets. Notice that the LASER-M ENDF/B-II values spread is larger for the 8 a/o Pu-240 cases, which is undesireable, although the values for the 24 a/o Pu-240 cases are quite acceptable. Table 4.4 shows, in general, the major differences exist in $k_{eff,2}$, the thermal contribution to k_{eff} (see Eq. (4.1)). Both $k_{eff,1}$ and the fast plus epithermal group constants (given in Reference 26 for the Sher, Wescott trials) are in excellent agreement. Investigation of the microscopic effective thermal constants reveals for the two cross section sets that:

(1) Significantly larger Pu-240 absorption is present with the ENDF/B-II set, from +4.8% (tight lattice) to +5.7% (loose lattice) relative to the Sher, Wescott set.

(2) Slight (<1%) deviations exist in ENDF/B-II relative to the Sher, Wescott group constants, namely

U-235 absorption	+0.2% to +0.5%
Pu-239 absorption	-0.6%
Pu-239 fission	+0.2%

The increased sensitivity of the $k_{eff,2}$ values to lattice pitch is due to item (1), the effect more pronounced in the tight lattice where Pu-240 resonance absorption is a large fraction of the thermal group absorption, and hence depressing $k_{eff,2}$. The $k_{eff,2}$ value for the largest pitch, however, is slightly greater for the ENDF/B-II case. This is due to the

Table 4.4

Comparison of Calculated Values

of k_{eff}-2 w/o PuO_2 Hanford Criticals for

Different LASER Thermal C/S Sets

Atom % Pu-240	Hexagonal Pitch (inches)	Thermal C/S Set	$k_{eff,1}$	+ $k_{eff,2}$	= k_{eff}
8	0.80	Sher,Wescott	0.170	0.828	0.998
		ENDF/B-II	0.168	0.816	0.984
	0.93	Sher,Wescott	-	-	-
		ENDF/B-II	0.114	0.901	1.015
	1.05	Sher,Wescott	0.0860	0.932	1.018
		ENDF/B-II	0.0864	0.936	1.022
24	0.80	Sher,Wescott	-	-	-
		ENDF/B-II	0.170	0.833	1.003
	0.93	Sher,Wescott	-	-	-
		ENDF/B-II	0.113	0.896	1.008
	1.05	Sher,Wescott	0.0855	0.933	1.019
		ENDF/B-II	0.0854	0.927	1.013

Sher,Wescott values are from UNC-5168 [26]

ENDF/B-II C/S (thermal) for Pu isotopes and Sher [41] normalized U-235 C/S for values calculated by LASER-M in this study

larger U-235 absorption cross section and the heavier fuel loadings in the LASER-M calculations (about 1%) due to the aforementioned reference value differences.*

The increased sensitivity to lattice pitch is not favorable, but the categorical preference of one cross section set is not possible since some additional sensitivity is expected from the increased Pu-240 absorption alone (given the modeling problems associated with this isotope). In addition, there is good agreement for the 24 a/o Pu-240 values due specifically to the increased Pu-240 absorption in the ENDF/B-II calculations, which depresses $k_{eff,2}$ even for highly thermalized lattices where the Sher,Wescott values are at their worst. This is more in agreement with the excellent results of the previous criticals analysis by Momsen.

The overall comparison of cross section sets by criticals in this study shows only fair to good agreement, with comparable deficiencies in each set. More careful determinations of model versus cross section deficiencies should be made with higher order calculations, in addition to the use of isotopic comparisons for these and future cross section modifications.

4.2 Isotopic Comparison with Yankee Core I Depletion

4.2.1 Introduction

As discussed in Section 1.4.2, a unit cell depletion of

*In addition, it should be noted that the value of 1.144×10^{20} atoms U-235/cc in Reference 26, Table 7, p. 22 does not correspond to a natural uranium composition based on the given value of 2.048×10^{22} atoms U-238/cc.

LASER-M supplies changes in isotopic content and distribution with burnup for comparison with mass spectrometric and radiochemical analyses of spent fuel. Yankee Core I data for a batch core of 3.4 w/o U-235 was modeled to allow for comparison with isotopic data obtained from fuel rods located in the center of assemblies, away from water slots(i.e., in an asymptotic spectrum region). The analysis was carried out for selected rods which achieved burnups of 40,000 MWD/MT, and therefore were pins with large plutonium content. Comparisons were made with main chain isotopes with burnup (U-235, 236, Pu-239, 240, 241 and 242).

4.2.2 Operational and Data Description

The primary source of power history data and the results of isotopic analyses are given in WCAP 6086[12]. In accordance with the Yankee Core Evaluation Program (EYC), three phases of experimental investigation included:

I Removal of 56 rods from 14 Core I assemblies

II Removal of 7 rods from a Core I and II assembly

III Removal of 8 rods from a Core I, II and IV assembly

Data from each phase is presented in the references. Phases I and II of the program used Cs-137 and Sr-90 as burnup indicators. Phase III and later extensions used Cs-137 and a heavy element (HE) method, with Nd-148 used as an indicator for resolving discrepancies. Additional Yankee samples, using Cs-137 as an indicator, were analyzed at Pacific Northwest Laboratories and the results are described as the BNWL-1122[50]

data.

Further references discussing the data and comparison calculations include WCAP 6077[13], YAEC 1060[51], YAEC 1053[52] and, specifically concerning LASER, WCAP 6069[36].

4.2.3 Unit Cell Modeling

4.2.3.1 Input Parameters

The basic input parameters for the LASER-M depletion and their sources are given in Table 4.5. The actual computer input listing for LASER-M is given in Appendix A. Specific input details include the following. Hot pellet and clad dimensions were used and the clad and gap region homogenized, as necessary in LASER. No moderator boron was present in the reactor, although the extra region absorption was approximated by an addition of boron to the moderator, as obtained by comparison of the 2200 m/sec cross section values of B-10 and stainless steel. This is necessary due to the lack of an extra region modelling capability in LASER. The Nelkin thermal scattering kernel was used and the resonance self-shielding L factor was searched at the various time steps, although the change with burnup was not large, as noticed by Poncelet[36]. An L factor of unity was judged acceptable for the remaining isotopes.

LASER also requires as input a spatial distribution of the U-238 resonance capture, and this was obtained from Reference 36. Non-linear effects in the burnup calculation were neglected (an option in LASER), since Poncelet showed that

Table 4.5

Yankee 3.4w/o U-235 Depletion Data (YAEC-1053)(52) (WCAP-6069)(36)

Hot Dimensions (cm)

Pellet radius	0.3750
Clad inner radius (SS-348)	0.3801
Clad outer radius	0.4337
Moderator outer radius	0.6098

Volume Fractions (hot)

Pellet (UO_2)		1.000
Clad	Stainless Steel(348)	0.918
	Void	0.082
Moderator		
	H_2O, 514°F,2100 psia	1.000
Extra Region		
Volume fraction in supercell		0.0680
	H_2O, 514°F,2100 psia	0.4611
	SS-348	0.0982
	Zr-2	0.4327
	Void	0.0080

(Extra region data used to obtain moderator boron value -- to account for added cell absorption)

wppm Boron to account for extra region absorption	135.7
Unit cell area (cm^2)	1.168

Loadings

U-235 (kg/core)	712
U-236 (kg/core)	4
U-238 (kg/core)	20222
atoms/b-cm U in fuel (WCAP 6069)	0.022400
MTU/cm(x10^6) (WCAP 6069)	3.912
Power level (w/cm)	73.308
Buckling (cm^{-2})	0.0007
Temperature (°F) Resonance Effective	1305

Time steps (hrs)	Xenon	100
	Samarium	400
	Normal	2000

for Yankee fuel up to 25,000 MWD/MT, this effect is only about a 3% adjustment in burnup. The materials buckling in this problem was not searched, since, as discussed by Momsen[9], it has little effect on the calculation. The standard THERMOS iteration in LASER was chosen without extrapolation, since extrapolation failed to provide a converged solution.

As discussed by Momsen[9], the LASER variable for the effective fuel temperature (to Doppler broaden the U-238 resonances) may be defined as that temperature which gives the correct experimental power defect of reactivity from hot standby to full power conditions. When viewed thusly, from an isotopics point of view, one would expect excess Pu-239 accumulation due to the fact that resonance absorption was the parameter chosen to accomodate a reactivity match[51]. It is true, however, that the majority of the additional absorption will be of this type. Alternately, the effective temperature may be viewed as that temperature above the average fuel temperature which takes into account the hardening of the materials velocity spectrum from a Maxwellian as a result of neutron absorption[29]. This more physical argument makes clear that the spectrum hardening effect is real, although its magnitude may not be as great as that calculated from the power defect consideration. In spite of the definitional uncertainties, a value of 1305°F was used to Doppler broaden the U-238 and Pu-240 resonances, equal to that calculated for YAEC 1053 and WCAP 6077. This is the power defect calculated value. The average fuel temperature was 1100°F.

4.2.3.2 Fission Product Treatment

As mentioned in Section 3.1.2, the fission product treatment in LASER is separated into an explicit Xe-135 and Sm-149 representation, with all other fission products represented by one pseudo fission product. A single pseudo fission product atom is assumed to be produced per fission event. The cross sections for this lumped fission product are input to LASER as a polynomial in burnup, expressed as

$$\sigma_{a_o}^{th} = a_o + a_1 B + a_2 B^2 + a_3 B^3 \qquad (0 < E < 1.855ev)$$

$$\sigma_a^{epi} = b_o + b_1 B + b_2 B^2 + b_3 B^3 \qquad (1.855ev < E < 5530ev)$$

$$\sigma_a^{fast} = 0 \qquad (E > 5530ev) \qquad (4.1\text{-}4.3)$$

where B is burnup in MWD/MT. $\sigma_{a_o}^{th}$ is the 2200 m/sec value of an assumed 1/v cross section (in barns) and σ_a^{epi} is assumed constant with energy. The coefficients a_i and b_i are the input values.

Calculation of such equivalent fission product cross sections is performed by a separate code, such as CINDER[53]. CINDER utilizes a chosen coupling of fission product nuclide chains by radioactive decay and neutron absorption along with an assumed flux history to yield effective, lumped fission product cross sections with burnup. The epithermal cross section in Eq. (4.2) is often expressed as a resonance integral (RI) versus burnup. The epithermal cross section and resonance integral are proportional to each other, the constant of proportionality being the lethargy width Δu (i.e., $\sigma_{epi}=RI/\Delta u$). The results of a CINDER calculation are expressed as a polyno-

mial by a fitting procedure. It is important that the fit be of relatively greater accuracy at higher burnups. (Poncelet[36] gives the fission product fractional absorption rate for Yankee fuel as about 2% at 5000 MWD/MT, and increasing to about 9% at 25,000 MWD/MT in Figure 4.5 of the reference.)

Published CINDER calculations[54] for a 0.37 inch pellet diameter UO_2 fuel pin lattice, similar to the Yankee fuel, are available for σ_o(2200 m/sec) and the resonance integral (RI). Figures 4.1 and 4.2 show the variation of σ_o(2200 m/sec) with water to metal ratio (W/U) and w/o U-235, respectively. Linear interpolation for the applicable W/U (=2.7) on Figure 4.1 for the 4 w/o U-235 fuel and the slight displacement of this curve due to the enrichment effect of Figure 4.2 results in an estimated σ_o(2200 m/sec) curve in Figure 4.3 for the Yankee fuel. Similar interpolation with W/U was made for the slight resonance integral dependence of these calculations, as given in Figure 4.4. Figure 4.5 presents this curve. The resonance integral is relatively insensitive to fuel enrichment (this is basically a U-238 effect).

Figures 4.3 and 4.5 display the interpolated curves as well as the polynomial fits of the curves deemed acceptable to represent them due to their correspondence at the higher burnup ranges. These fits yield the following equations* in burnup (B, in MWD/MT) for the respective values (in barns)

$$\sigma_o(2200 \text{ m/sec}) = 1.4862(2) - 6.0009(-3)\ B + 2.6701(-7)\ B^2 - 4.9216(-12)\ B^3$$

* $1.4864(2) = 1.4864 \times 10^2$

Figure 4.1 Thermal Microscopic Fission Product Cross Section for UO_2 Fuel as a Function of Burnup for Various Water to Metal Ratios

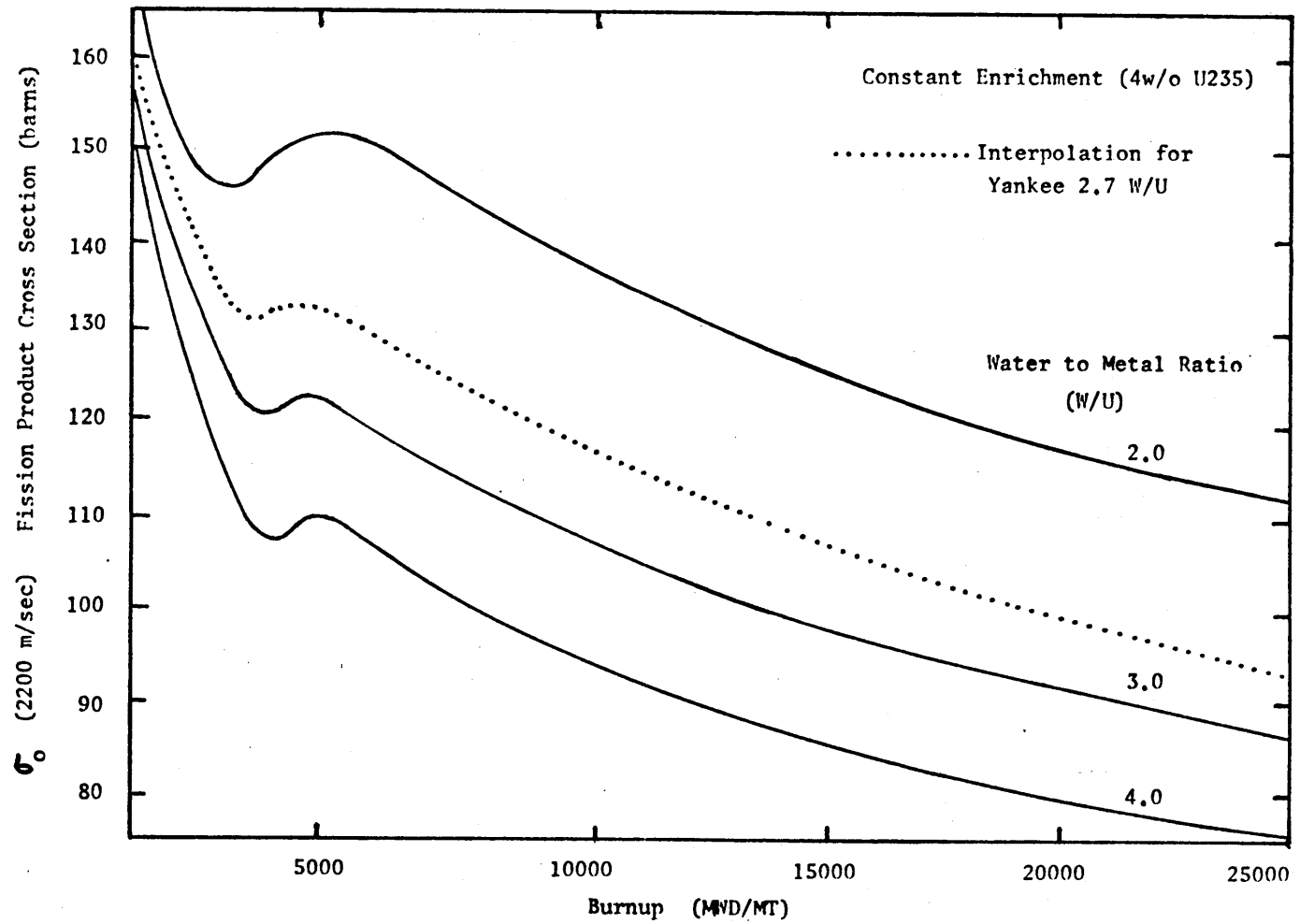

Figure 4.2 Thermal Microscopic Fission Product Cross Section for UO_2 Fuel as a Function of Burnup for Various Enrichments of U-235

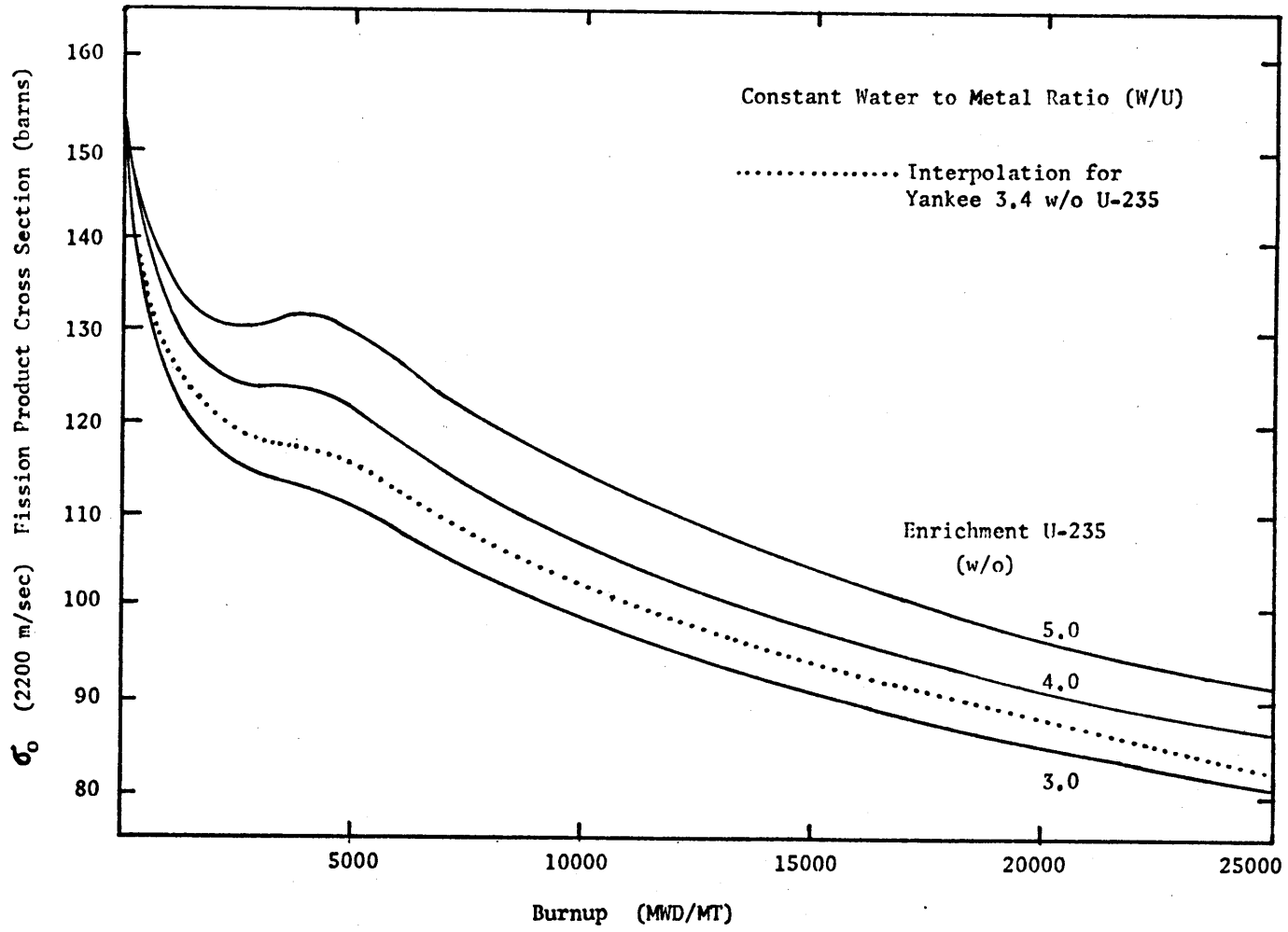

Figure 4.3 Yankee Thermal Microscopic Fission Product Cross Section as a Fuction of Burnup and Third Order Polynomial Fit for use in LASER-M

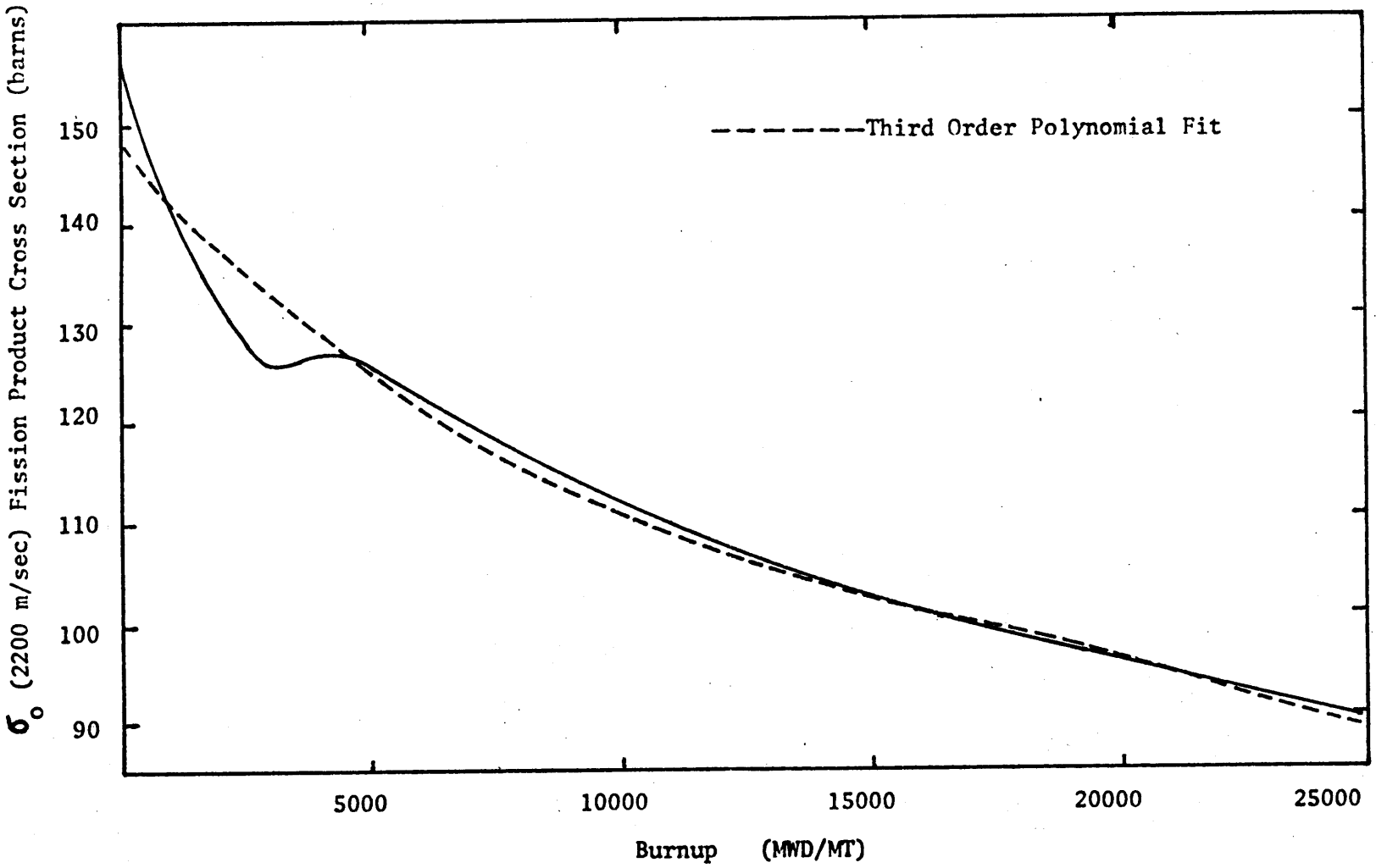

Figure 4.4 Fission Product Resonance Integral (RI) for UO_2 Fuel as a Function of Burnup for Various Water to Metal Ratios

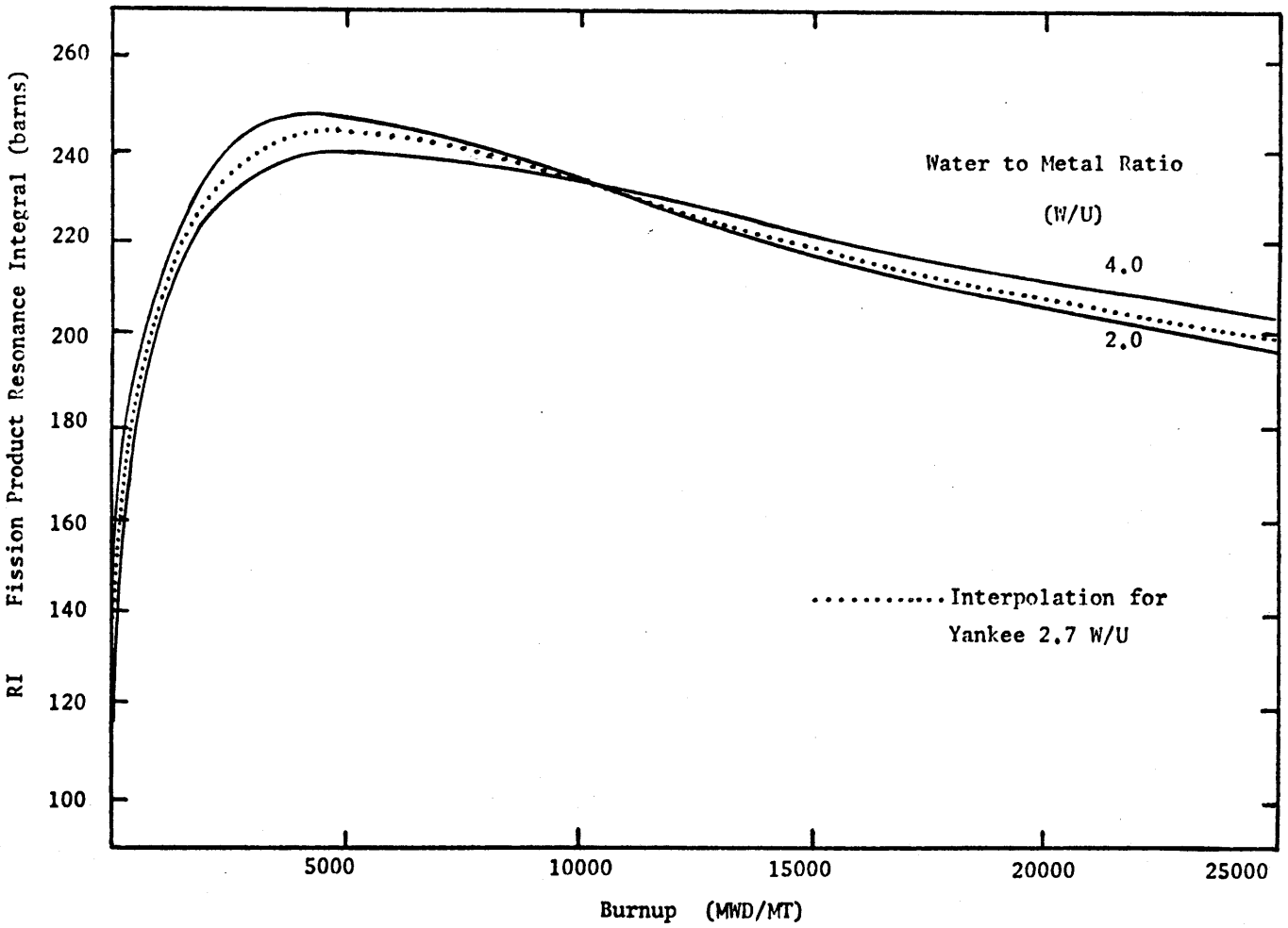

Figure 4.5 Yankee Fission Product Resonance Integral as a Function of Burnup and Third Order Polynomial Fit for use in LASER-M

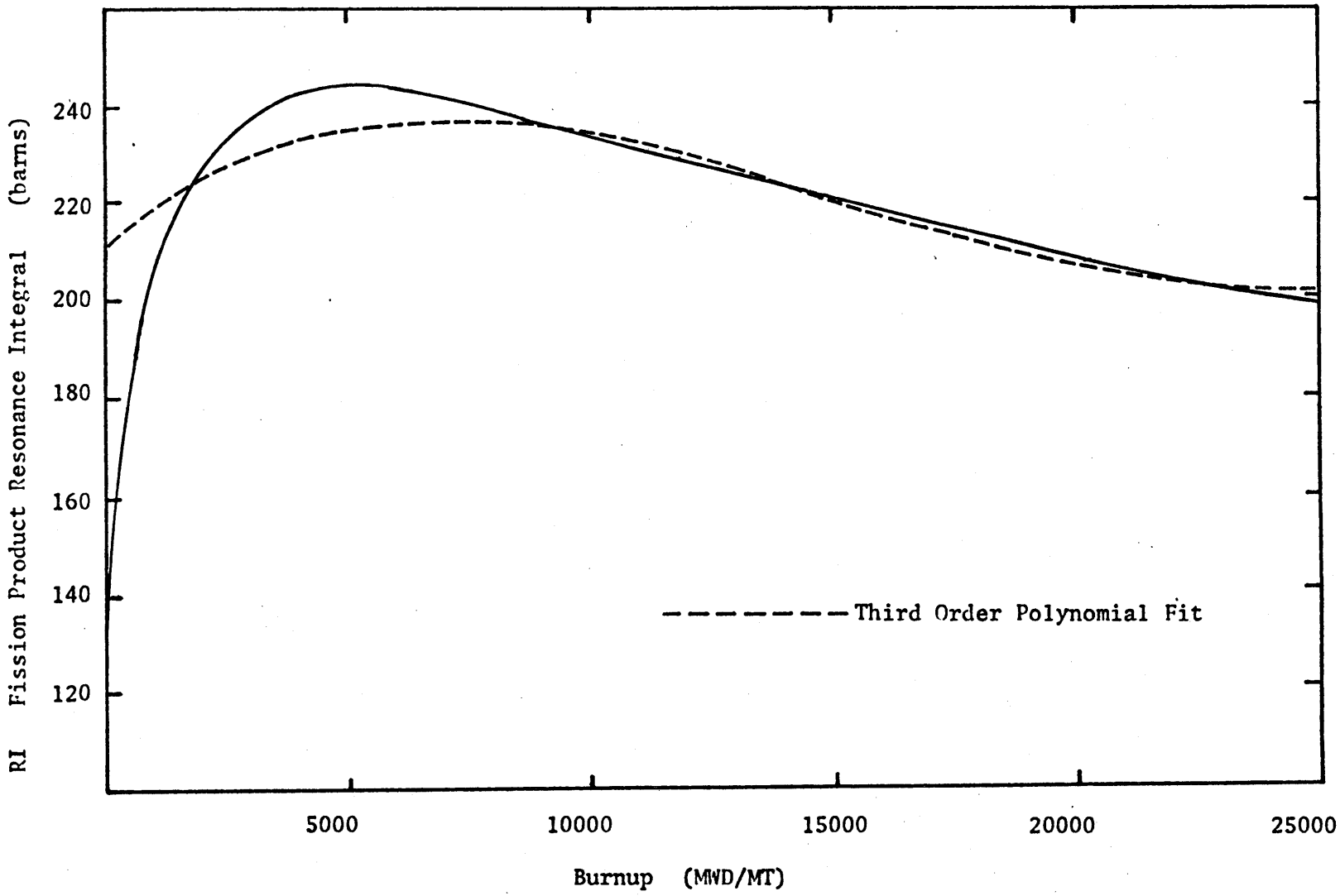

$$RI(5530ev - 0.625ev) = 2.1167(2) + 8.0523(-3)\ B - 7.3569(-7)\ B^2 + 1.5975(-11)\ B^3 \qquad (4.4\text{-}4.5)$$

The coefficients of $\sigma_o(2200\ m/sec)$ in Eq. (4.4) correspond directly to those required in Eq. (4.1). Modifications must be made to the resonance integral, first to transform it to an epithermal cross section and finally to the correct energy interval of Eq. (4.2) (i.e., 5530 ev to 1.855 ev). Transformation to an epithermal cross section is made by knowing that a value of 34 barns corresponds to a resonance integral of 390 barns[54]. Thus,

$$\sigma_a^{epi'} = 1.8453(1) + 7.0200(-4)B - 6.4137(-8)B^2 + 1.3927(-12)B^3 \qquad (4.6)$$

where the prime refers to the 5530 ev to 0.625 ev energy range of the value.

The energy interval transformation is based on maintaining the total fission product absorption (under 5530 ev) value independent of cutoff. Since the thermal part of the absorption is assumed 1/v and the epithermal absorption energy independent, total absorption is equated for the primed (0.625 ev thermal cutoff) and unprimed (1.855 ev thermal cutoff) cases as

$$\sigma_{a_o} \frac{v_o}{\bar{v}} \frac{\bar{\phi}_{th}}{\bar{\phi}_{th+epi}} + \sigma_a^{epi} \frac{\bar{\phi}_{epi}}{\bar{\phi}_{th+epi}} = \sigma_{a_o} \frac{v_o}{\bar{v}'} \frac{\bar{\phi}'_{th}}{\bar{\phi}'_{th+epi}} + \sigma_a^{epi'} \frac{\bar{\phi}'_{epi}}{\bar{\phi}'_{th+epi}} \qquad (4.7)$$

where

σ_{a_o}	2200 m/sec absorption
v_o	2200 m/sec
$\bar{v}$	cell averaged neutron velocity
$\bar{\phi}_{th}$	cell averaged total thermal flux
$\bar{\phi}_{epi}$	cell averaged total epithermal flux
$\bar{\phi}_{th+epi}$	cell averaged flux to 5530 ev
σ_a^{epi}	epithermal absorption cross section

The values of σ_{a_o} and $\sigma_a^{epi'}$ are known as a function of burnup from Eqs.(4.4) and (4.6), respectively. The cell averaged flux ratios and neutron velocities were taken from identical beginning of life LEOPARD (primed) and LASER (unprimed) cell calculations.(The epithermal flux in LEOPARD from 5530 ev to 0.625 ev is designated as $\bar{\phi}^{3/3}$, the third fast group.) Thus, the only unknown is the desired σ_a^{epi}, which, along with σ_{a_o} for use in LASER-M in Eqs. (4.1) to (4.3), is

$$\sigma_{a_o} = 1.4864(2) - 6.0009(-3)B + 2.6701(-7)B^2 - 4.9216(-12)B^3$$

$$\sigma_a^{epi} = 1.8815(1) + 7.7706(-4)B - 7.0995(-8)B^2 + 1.5416(-12)B^3$$

(4.8-4.9)

Momsen[9] verifies this method by comparison of LEOPARD and LASER depletions and notes their equivalent fractional fission product absorption. Note that for the Yankee LASER-M depletion, pseudo fission product capture was 6% of the total cell captures at 20,000 MWD/MT and 7% at 25,000 MWD/MT.

4.2.4 Calculational Results and Comparisons

A comparison of LASER-M isotopic calculations and associated isotopic data from all three phases of the EYC Program (including the BNWL 1122 data) for the main chain isotopes (U-235, U-236, Pu-239, Pu-240, Pu-241, and Pu-242) as functions of burnup are presented in Figures 4.6 to 4.11. The uncertainty in the measured values, according to YAEC 1053, is 2 to 5%. There are some conspicuous uncertainties in the trends, namely the nine (9) WCAP 6086 points below the majority for Pu-239 (Figure 4.8), which are the same points above the majority for Pu-240 (Figure 4.9). These are values from perturbed spectrum regions and are included for completeness.

Excellent agreement between the LASER-M calculated and measured values is shown in Figures 4.6 to 4.8 for U-235, U-236 and Pu-239. The Pu-240 (Figure 4.9) and Pu-241 (Figure 4.10) calculations predict slightly low and high values, respectively, with burnup, although the values are within the estimated uncertainty in measurement. The Pu-242 calculational prediction (Figure 4.11) is low, probably due to the cross section error discussed in Section 3.2.2. In conclusion, the isotopic agreement is good.

Similar calculations of the Yankee depletion are given by Poncelet (WCAP 6069) and Cacciapouti, McCoy (YAEC 1053). The latter were performed with the LOCALUX code[55], which adds to the basic LASER an extra region capability and built-in fission product treatment. The LOCALUX results were essentially equivalent to those of LASER-M, except for the Pu-240

Figure 4.6 Yankee Core I Spent Fuel- U-235 Atom Percent as a Function of Burnup

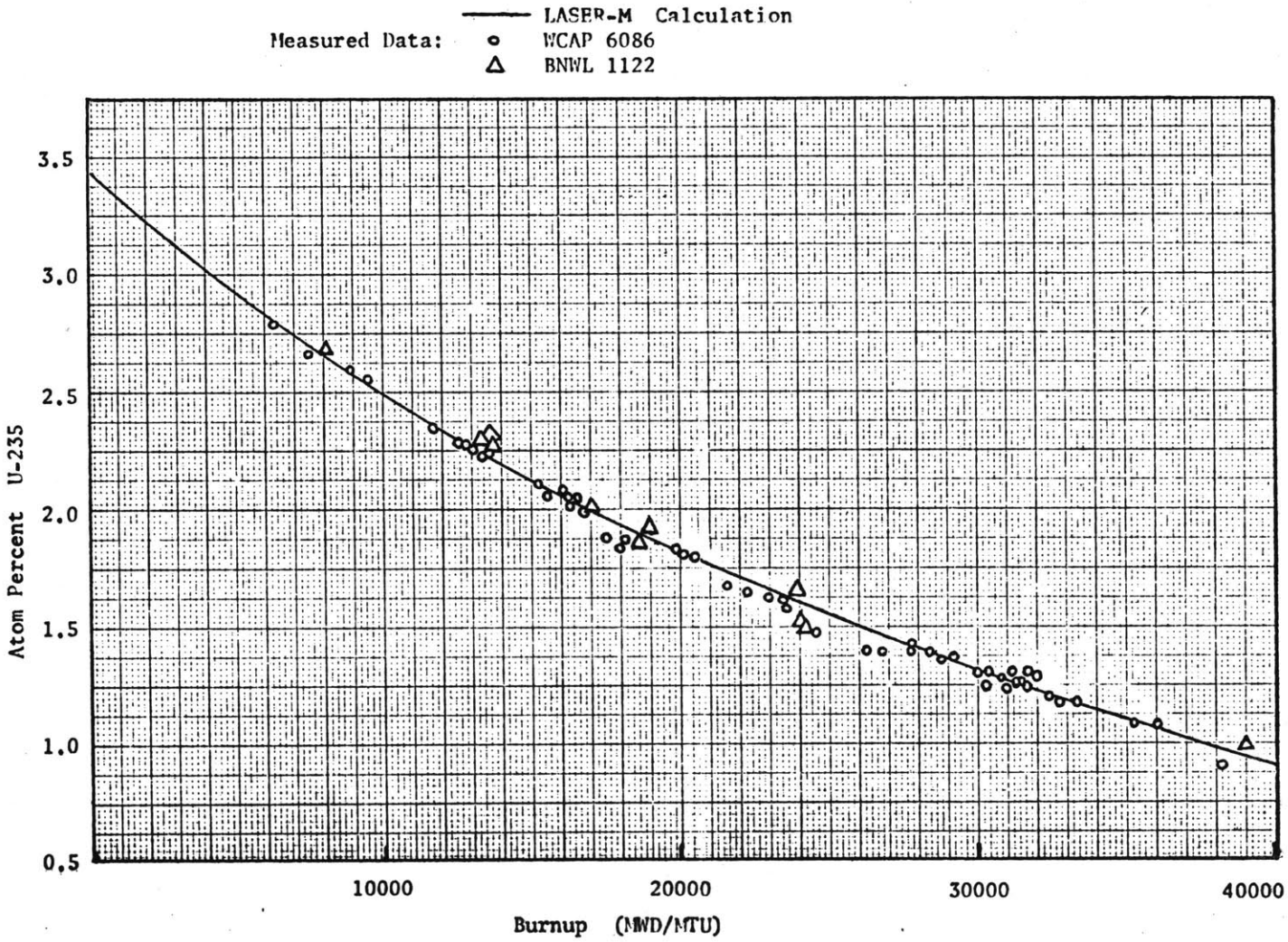

Figure 4.7 Yankee Core I Spent Fuel- U-236 Atom Percent as a Function of Burnup

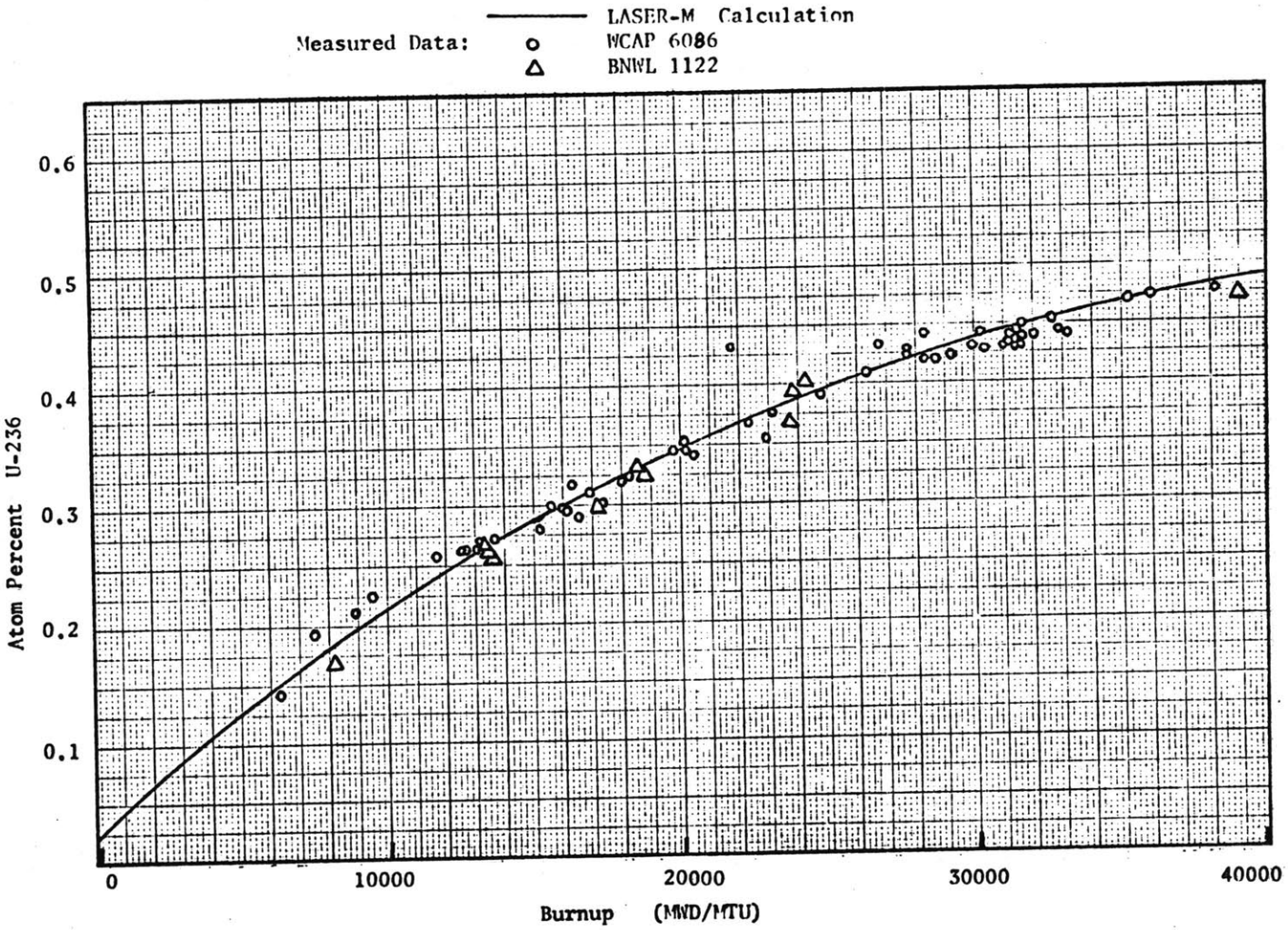

Figure 4.8 Yankee Core I Spent Fuel- Pu-239 Atom Percent as a Function of Burnup

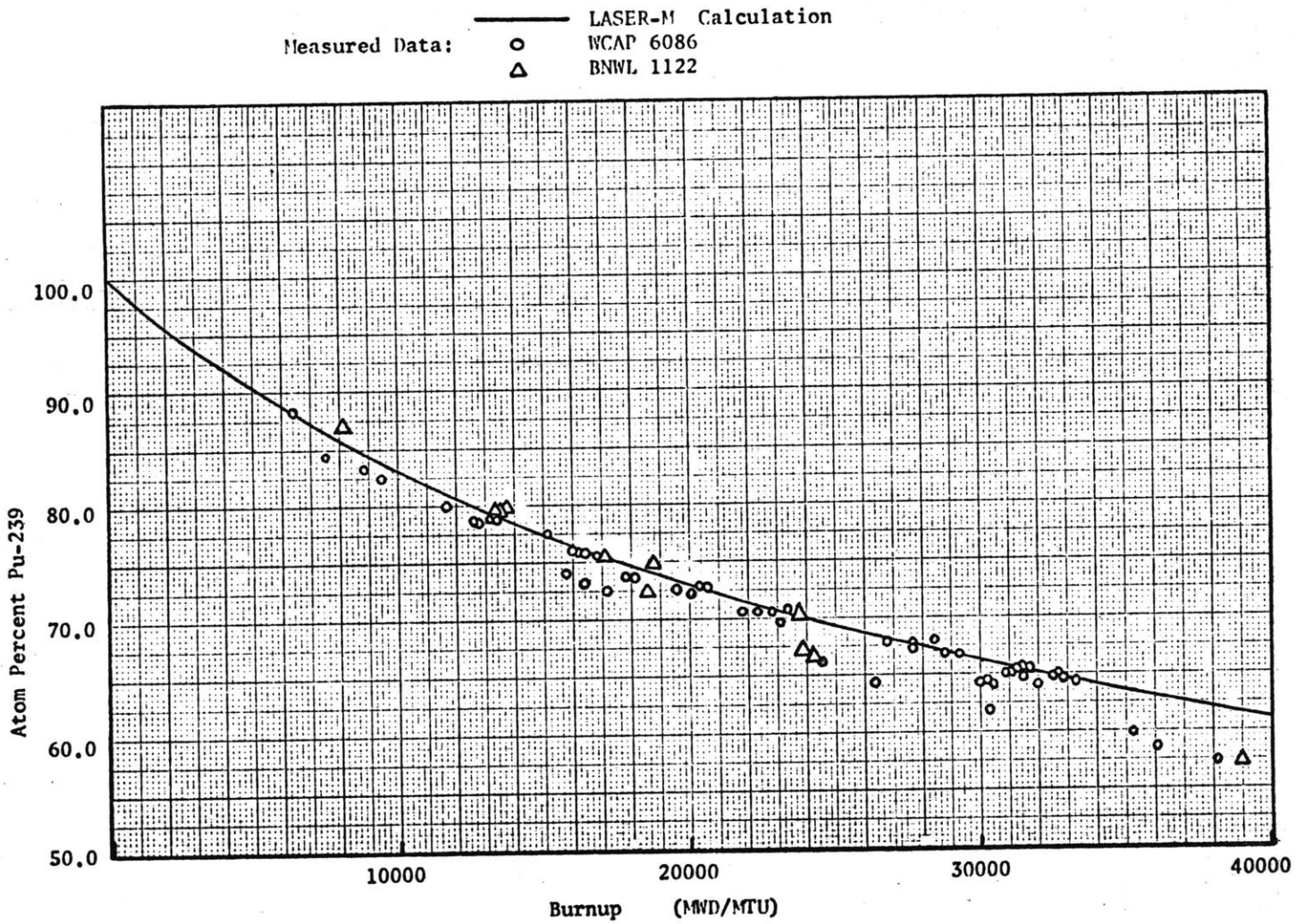

Figure 4.9 Yankee Core I Spent Fuel- Pu-240 Atom Percent as a Function of Burnup

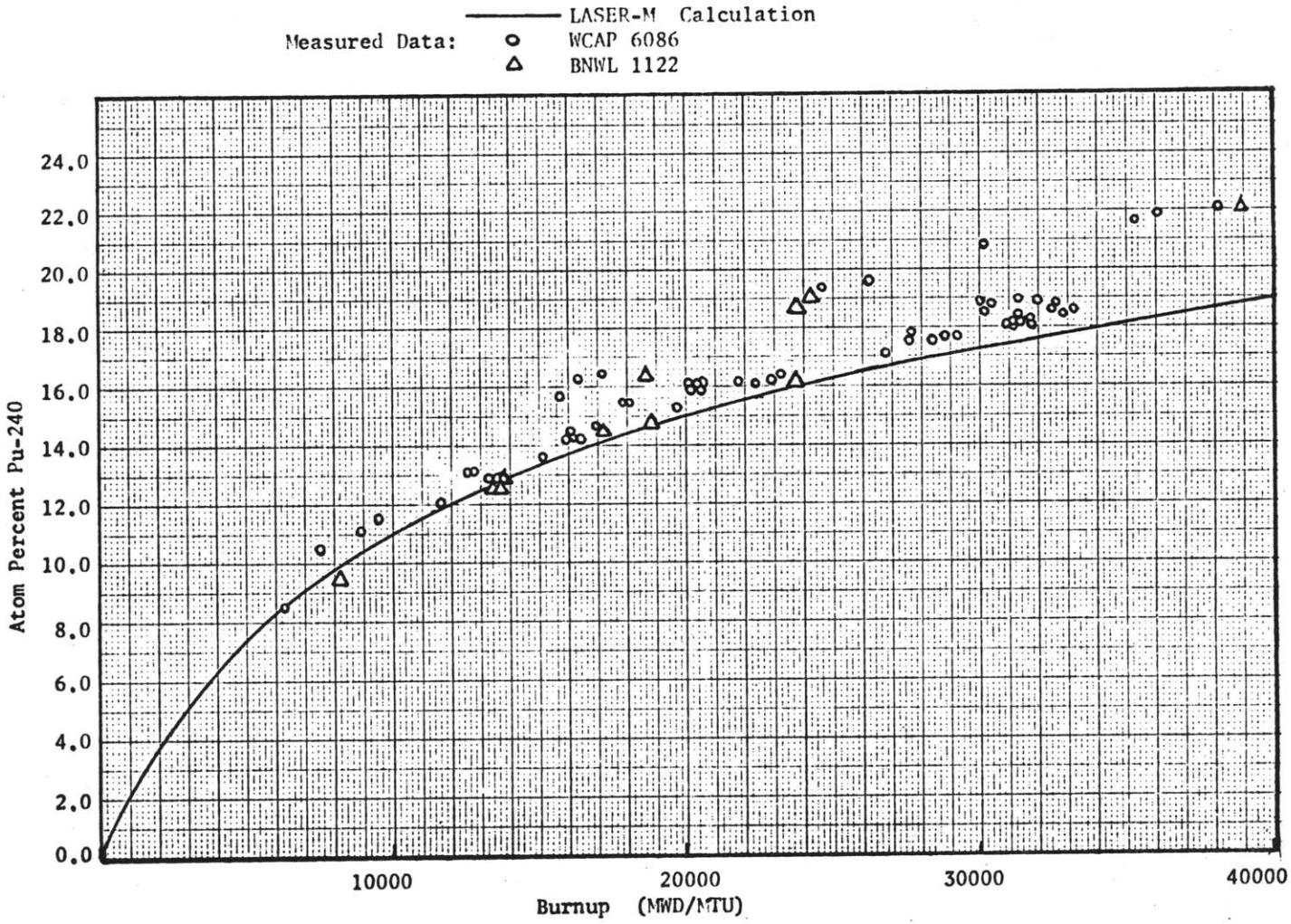

Figure 4.10 Yankee Core I Spent Fuel- Pu-241 Atom Percent as a Function of Burnup

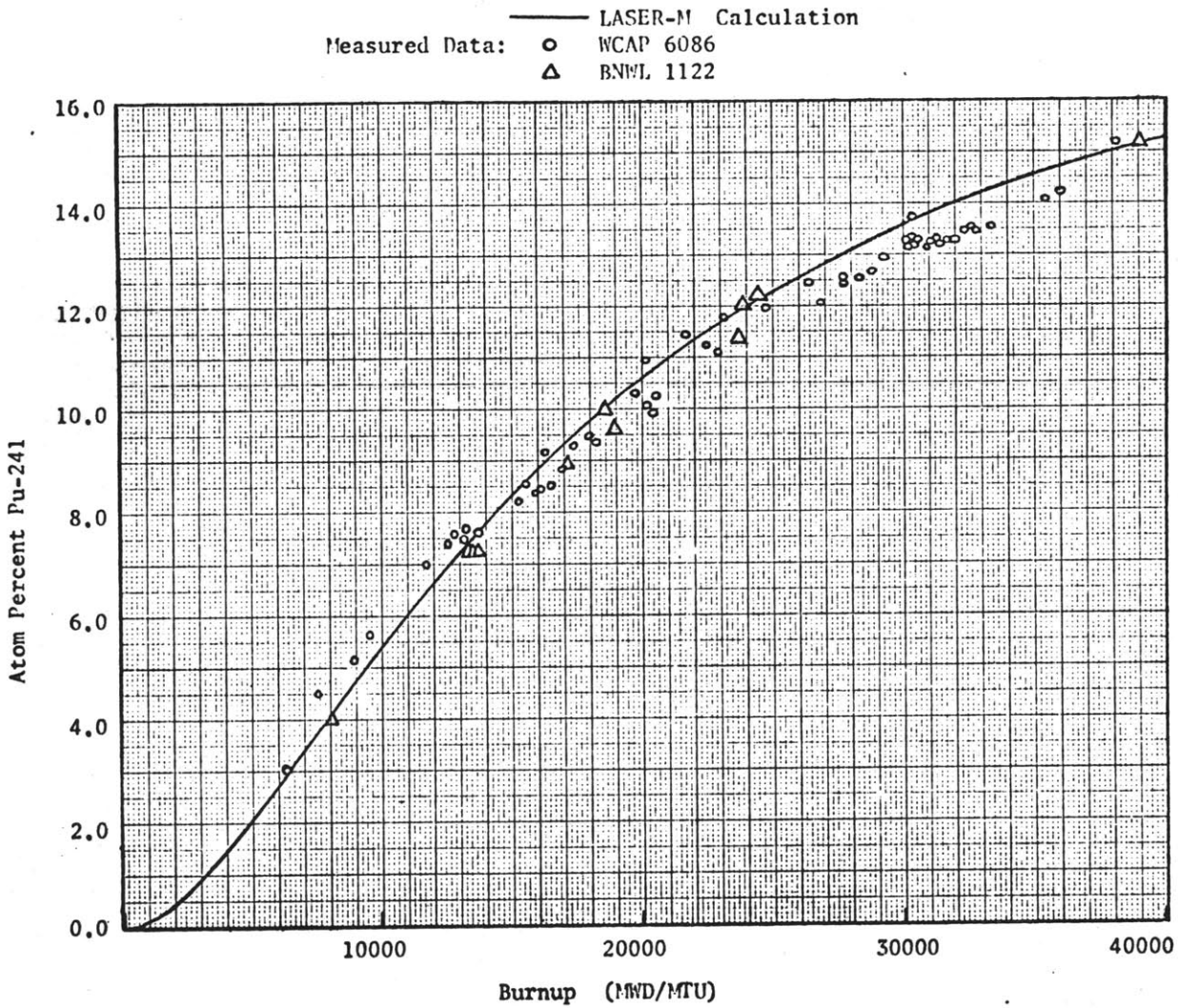

Figure 4.11 Yankee Core I Spent Fuel- Pu-242 Atom Percent as a Function of Burnup

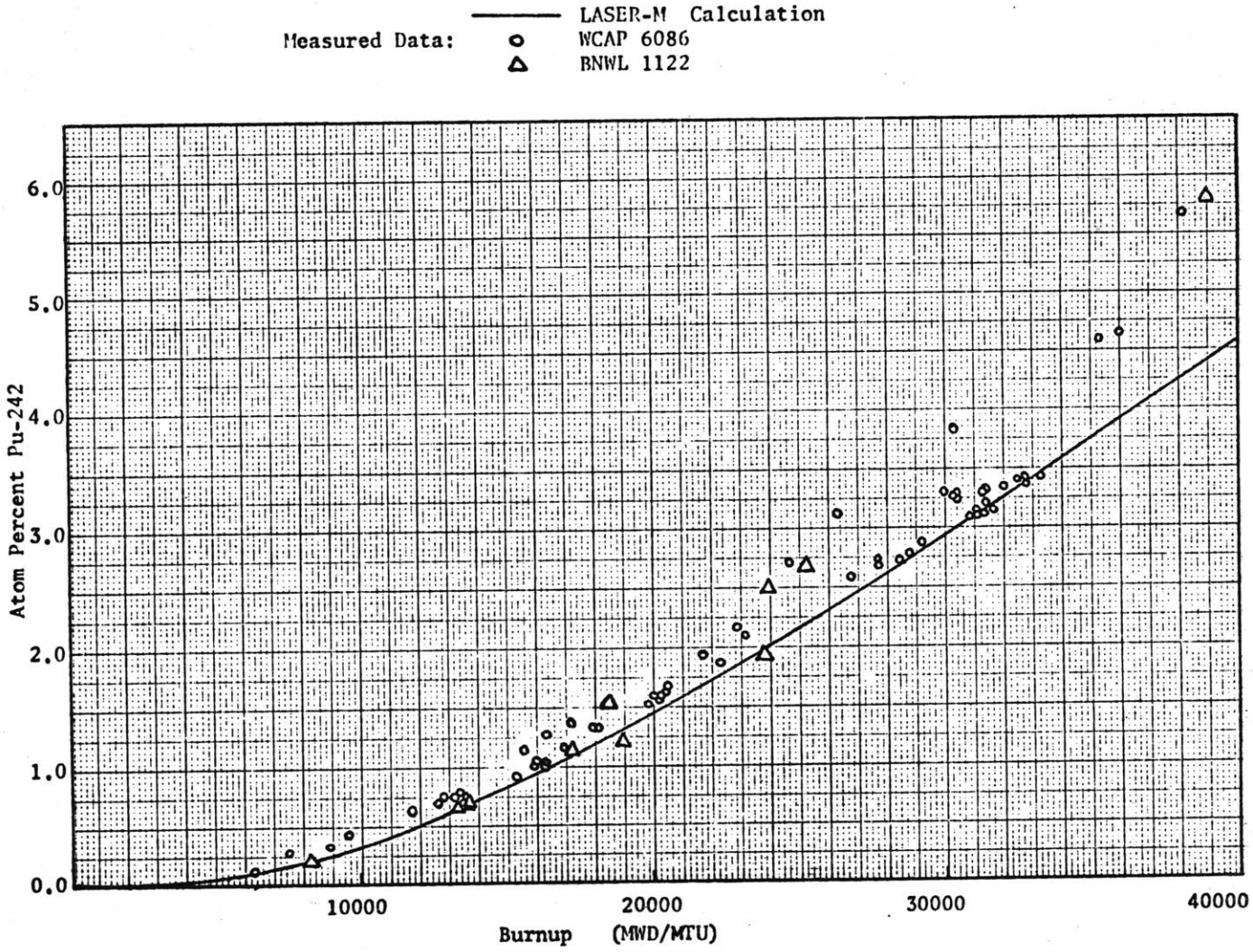

underprediction. The Pu-240 underprediction and the Pu-241 overprediction indicate a trend of calculated excess Pu-240 cell absorption.

As an indication of the differences in effective cell thermal absorption and fission cross sections as calculated based on different cross section sets, Figure 4.12 presents the Poncelet LASER calculated values and those of LASER-M with burnup. The larger Pu-240 LASER-M value at high burnups is noticable. The beginning of life value, however, is less. The Pu-241 LASER-M fission cross section is also greater. The remaining values are equivalent.

In conclusion, the overall calculational prediction by LASER-M of experimental Yankee main chain isotopic content is good, equivalent to the accuracy of alternate calculations.

4.3 Isotopic Comparison with Saxton Core II Depletion

4.3.1 Introduction

Saxton Core II mass spectrometric and radiochemical analysis results for UO_2- 6.6 w/o PuO_2 mixed oxide fuel rods irradiated to a maximum rod averaged burnup of 20,000 MWD/MT can be used for comparison with unit cell LASER-M depletion calculations, similar to those for Yankee Core I. Pelletized fuel results for samples from the asymptotic core region have been used for the comparison described below. Comparisons were made with main chain isotopes (U-235, U-236, Pu-239, Pu-240, Pu-241 and Pu-242) on a pin radially averaged basis as well as for an actual radial distribution within the pellet, as obtained

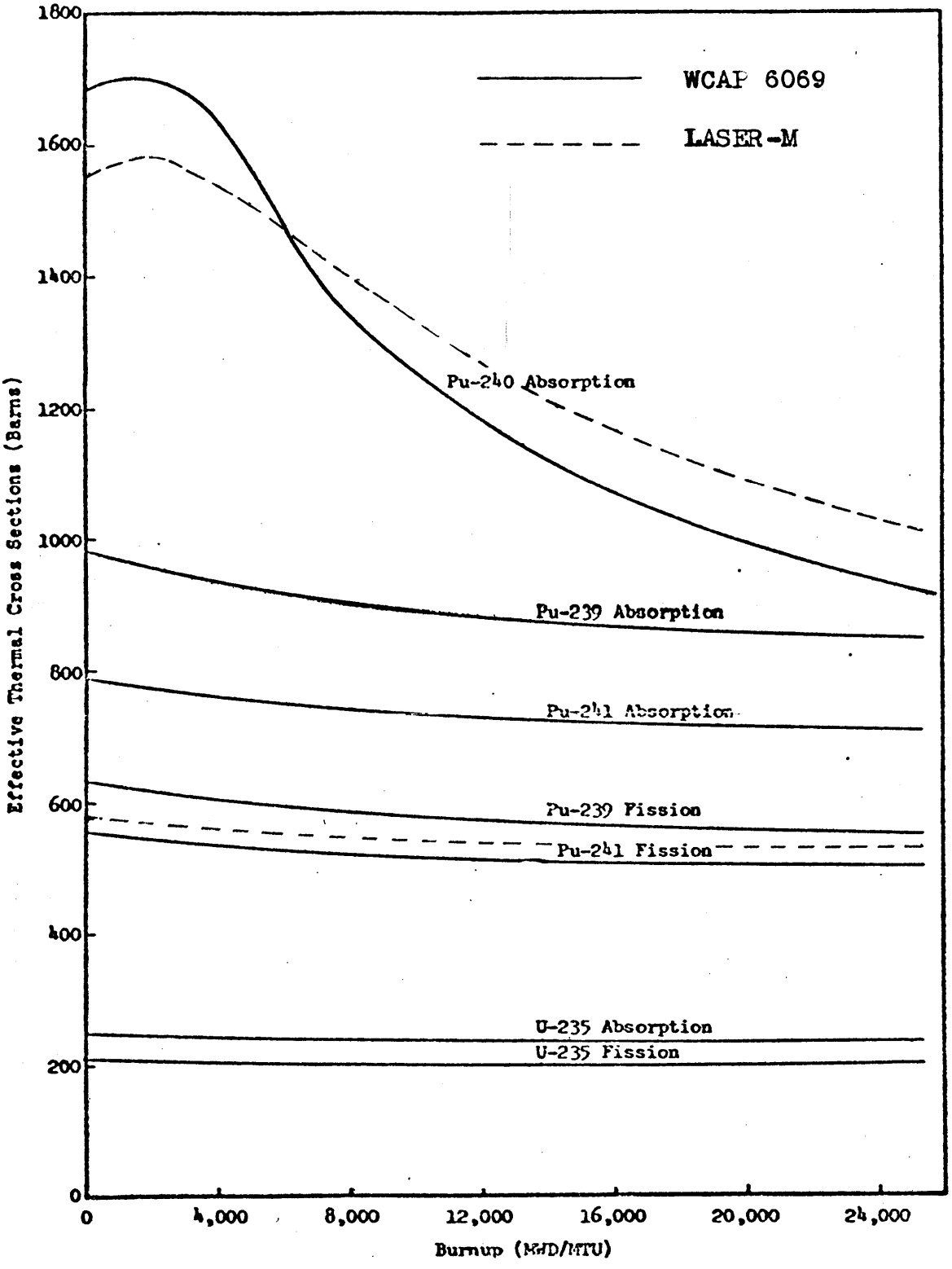

Figure 4.12 Yankee Core I Depletion Analysis
Effective Thermal Cross Sections as a
Function of Burnup

experimentally from axial microdrillings.

4.3.2 Operational and Data Description

The primary source of isotopic analysis and power history data is WCAP 3385-56(2)[15]. Nineteen (19) zircaloy-clad rods containing both pelletized and vibratory compacted PuO_2-UO_2 fuel were removed from the central region of Saxton Core II. The rods of interest for the study are five (5) axial samples from three (3) different rods (Rods RI, JF and MY) for radially averaged isotopic data and one axial sample used for microdrilling (Rod RI), all in the asymptotic spectrum region.

For each sample, burnup accumulation determination was performed by two methods, the heavy element (HE) method, based on the conservation of heavy nuclei, and the Nd method, based on the buildup of fission product Nd-148.

The irradiation history is complicated by the fact that, of the total elapsed time of 996 days of the life of Core II, the core was at zero power for 533 days. This period cannot be ignored in the irradiation history due to the decay of Pu-241 to Am-241 with a halflife of about 14 years. Accurate representation of the irradiation history is also necessary for calculation of short lived isotopes and precursors (e.g., Pu-236, Pu-238 and Cm-242).

4.3.3 Unit Cell Modeling

4.3.3.1 Input Parameters

The basic input parameters for the LASER-M depletion and

and their sources are given in Table 4.6. The LASER-M computer input listing is given in Appendix A.

Specific input details include the following. Cold temperature dimensions were used, since the difference due to thermal expansion was not considered significant. The clad and gap region was homogenized, as necessitated by LASER. Power level and temperatures varied with power history (see Table G-1 of the reference) and the values input represent averages used by Westinghouse for similar (LEOPARD) calculations. Following the exact power history with LASER is awkward and requires program termination and continuation for each power level or temperature change.

Concerning the calculations outlined in Table 4.6, the LASER burnup input requirement of (watts/gm)(or(watts/cm) and (MTM/cm)) is given as a non-zero power time average, using the accumulated MWD/MT value for the core. Isotopic concentrations in the fuel are expressed relative to U-238 in the reference, thus, a value of atoms U-238/ b-cm was calculated based on a theoretical density of 10.96 g/cc for UO_2. The value of H_2O atoms/b-cm was calculated using the water to oxide ratio. No moderator boron was present in the reactor.

The Nelkin scattering treatment was used, as recommended in Section 2.2.3 for mixed oxide fuels. The resonance self shielding L factor for U-238 was searched at the various time steps, although the change was not great with burnup (0.7478 to 0.7487 from 0 to 20,000 MWD/MT). An L factor of 1.0 was used for the remaining isotopes, under the assumption that the high

Table 4.6

Saxton 6.6 w/o PuO_2 Depletion
Core II Data and Calculations
(WCAP 3385-56(2))[15]

		Page of Reference
Cold Dimensions (in.)		
Fuel Radius	0.16870	Table G-2, p.G-3
Clad inner radius	0.17225	
Clad outer radius	0.19550	
Pitch	0.0580	
Temperature (°F)		
Fuel average	1290	Table G-2, p.G-3
Clad	638	
Moderator	530	
Resonance effective	1032	
Isotopic Atom Densities (relative to U-238)		
U-235	0.00734	Table 7-2, p. 7-4
U-238	1.00000	
Pu-239	0.0625	
Pu-240	0.00594	
Pu-241	0.000605	
Pu-242	0.0000521	
Total (plus Th,Pa,etc.)	1.0765	

Calculations:

Power density: LASER requires input of (watts/cm) and (MTM/cm). Their quotient is the only important variable, so that only (watts/gm) is needed.

Using values of: 20,014 MWD/MT total
10,468 non-zero power hours

Obtain: 45.886 watts/gm — Table G-1, p. G-2

U-238 atoms/b-cm:

Using values: 0.02442 atoms U/b-cm — Theoretical value based on 10.96 g/cm^3
94% theoretical density — Table G-2, p. G-3
0.2664 fuel hot volume fraction — Table G-2, p. G-3
0.2658 fuel cold volume fraction (above)
1.0765 atoms metal/U-238 atom (above)

Obtain: 0.021273 atoms U-238/ b-cm

Table 4.6
(Continued)

Page of Reference

Calculations: (continued)

H_2O atoms/b-cm:

Using: 0.2664 fuel hot volume fraction
0.64496 moderator hot volume fraction
Table G-2, p.G-3
1.860 water/oxide ratio (hot)
Table G-2, p.G-3

Obtain: 0.025691 atoms/b-cm

Additional Data: (Table G-2, p.G-3)

Geometric Buckling ($cm^{-2}x10^2$)	0.498
Initial U-238 L factor (L factor will be searched)	0.74436
No Pu-240 L factor will be used (L_{240} equal to 1.0)	

Time Steps:

Xenon (hrs)	50
Samarium (hrs)	200
Normal (hrs)	1000

(Equivalent of 12 time steps to 20,000 MWD/MT)

A 2000 hr time step run was made to determine the extent of the differences in results

(1.855 ev) thermal energy treatment accounts for most of the resonance shielding (especially in Pu-240). The spatial distribution of U-238 captures was the same as that used in the Yankee depletion (Section 4.2.3.1). The materials buckling, as input, was not searched and the standard THERMOS iteration technique was used without extrapolation, as suggested for mixed oxide fuels.

The depletion time step duration (non Xe and Sm) was 1000 hours, which is comparable to a Yankee time step (2000 hours) in that about 12 time steps are required to attain 20,000 MWD/MT. Another calculation was performed with 2000 hour time steps (6 time steps to 20,000 MWD/MT) to assess the effect of less frequent flux shape renormalization. The good LASER spatial detail makes this feasible.

Non-linear effect consideration in the burnup equations, as an option in LASER, was not used. The need for such a calculation may result from the spectrum hardening accumulated during the given time step. This hardness influences the cell fission to absorption ratio and, based on this, a simple hand calculation using the LASER-M depletion results was performed in order to assess what effective correction can be made to each burnup step.

A burnup correction (ΔB) for a given burnup step was made as follows:

(1) The accumulated cell fissions and absorptions output by LASER-M was used to calculate a fission to absorption ratio during each burnup step.

(2) A corrected fission to absorption ratio for each burnup

step was calculated as the average of that calculated in item (1), characteristic of the initial flux shape of the burnup step, and that calculated for the next burnup step, characteristic of the final flux shape of the burnup step.

(3) The ratio of the values calculated in item (2) to item (1) (which is less than 1.0 due to the increasing number of absorptions per fission) was used as a factor to correct the burnup step value.

Following this procedure for the LASER-M depletion, the total accumulated corrected burnup was less than 2% different than that calculated for either of the time step cases. Thus, nonlinear effects in the burnup equations need not be accounted for on a practical basis for this unit cell.

The resonance effective temperature in Table 4.6 (from Westinghouse calculations) was used to Doppler broaden the U-238 and Pu-240 resonances in LASER-M.

4.3.3.2 Fission Product Treatment

The determination of a pseudo lumped fission product cross section as a function of burnup for the Saxton Core II fuel was made in a manner analogous to the procedure followed for the Yankee fuel in Section 4.2.3.2. Coefficients in the third order polynomial equations with burnup, Eqs. (4.1) to (4.3), were obtained using a least squares fitting procedure.

The Westinghouse calculated (WCAP 3385-12[56]) values of the thermal lumped fission product cross section, σ_{a_0}(2200 m/sec)

and the resonance lumped fission product cross section, $\sigma_a^{epi'}$, as functions of burnup are given in Figures 4.13 and 4.14, respectively. The prime on the epithermal (resonance) value denotes the energy interval 5530 ev- 0.625 ev. The associated polynomial fits, chosen as a result of their good correspondence to the actual calculation at high burnup, are shown in the figures and given below* , corresponding to Eqs. (4.4) and (4.6) of the Yankee fuel, with B in MWD/MT.

$$\sigma_{a_o}(2200 \text{ meters/second}) = 2.7370(2) - 1.3414(-2)B + 5.0359(-7)B^2 - 9.6941(-12)B^3$$

$$\sigma_a^{epi'}(5530 \text{ ev} - 0.625 \text{ ev}) = 2.4440(1) + 1.3421(-3)B - 1.0472(-7)B^2 + 2.2727(-12)B^3$$

(4.10-4.11)

Transformation to the LASER epithermal energy cutoff value is necessary for Eq. (4.11), as for the Yankee equation of Section 4.2.3.2. The transformation effected by the conservation of absorption argument, Eq. (4.7), is again used. Input values for the cell fluxes and velocities are obtained from a beginning of life LASER calculation and published LEOPARD values (Reference 17, Table E-2, p. E-11). The result of this calculation is input values of the coefficients for σ_a^{epi} for the LASER epithermal region (5530 ev- 1.855 ev). The LASER-M microscopic lumped fission product cross sections for the Saxton fuel, with B in MWD/MT, are thus

* $2.7370(2) = 2.7370 \times 10^2$

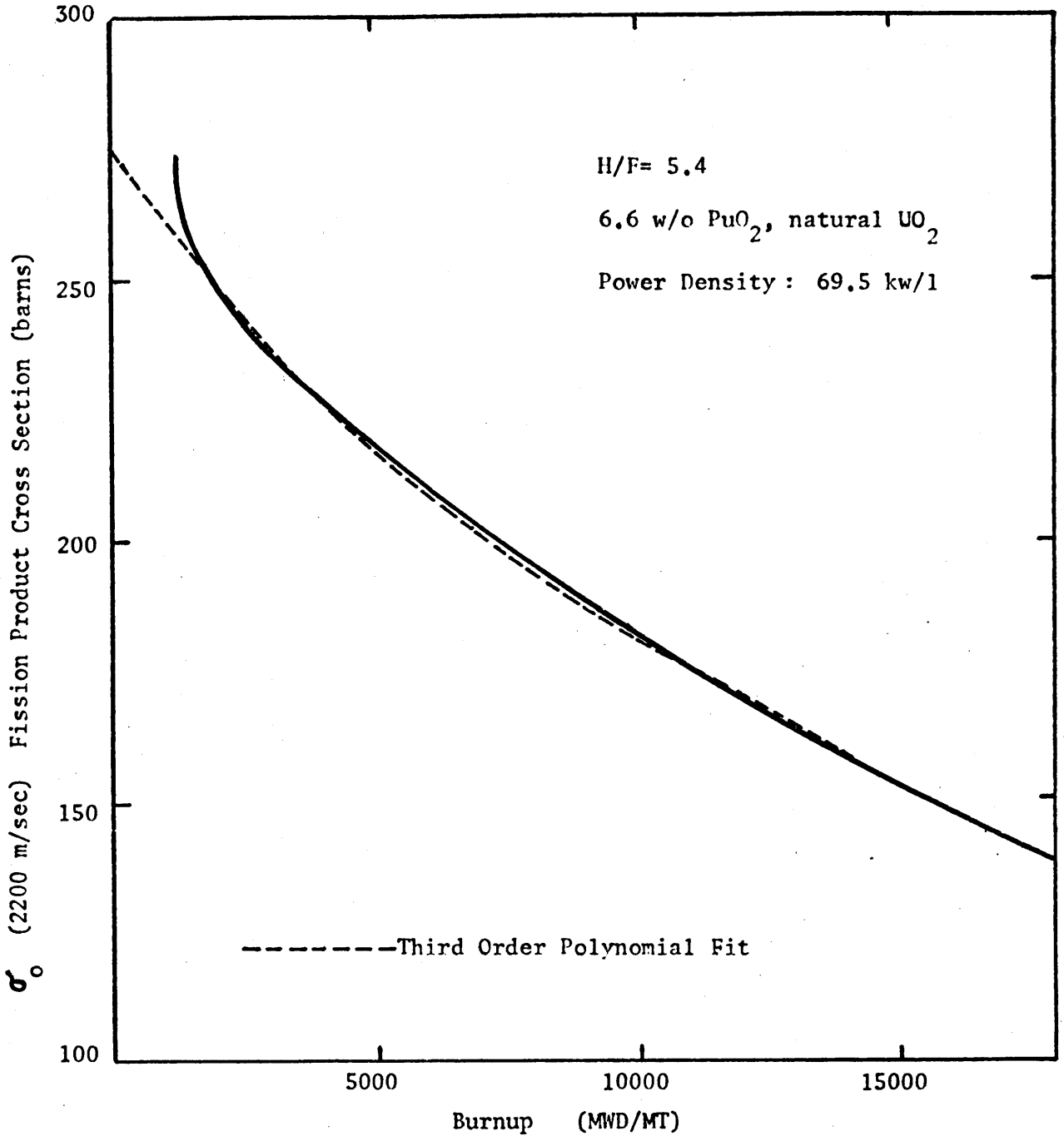

Figure 4.13 Saxton PuO_2-UO_2 Fuel Thermal Microscopic Fission Product Cross Section as a Function of Burnup and Third Order Polynomial Fit for use in LASER-M

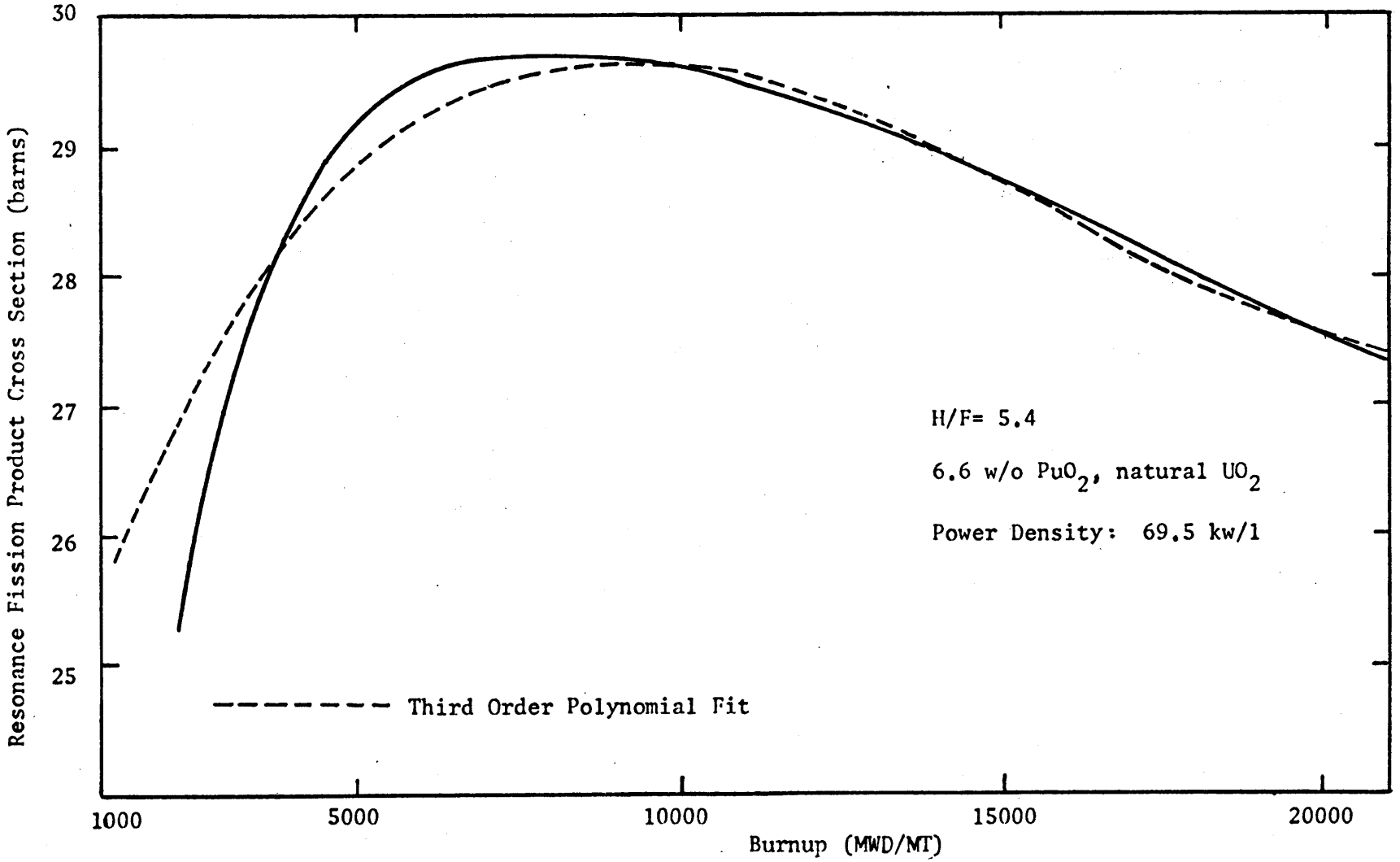

Figure 4.14 Saxton PuO_2-UO_2 Fuel Resonance Fission Product Cross Section as a Function of Burnup and Third Order Polynomial Fit for use in LASER-M

$$\sigma_{a_0} = 2.7370(2) - 1.3414(-2)B + 5.0359(-7)B^2 - 9.6941(-12)B^3$$

$$\sigma_a^{epi} = 1.9026(1) + 1.4903(-3)B + 1.1628(-7)B^2 + 2.5236(-12)B^3$$

(4.12-4.13)

Note that the lumped fission product cell capture rate resulting from the LASER-M calculation was 4% of the total at approximately 20,000 MWD/MT, a few percent less than the 6% for the Yankee 3.4 w/o U-235 pin at the same burnup.

4.3.4 Calculational Results and Comparisons

The LASER-M calculated and experimental values of atom percents with burnup for U-235, U-236, Pu-239, Pu-240, Pu-241 and Pu-242 are presented in Figures 4.15 to 4.17. These values are cell (i.e., radially) averaged values. Neither the actual numerical values with burnup nor the rod identifications of each point are given in the reference report, although it is given that the pellet data for each point is from asymptotic spectrum region rods (RI, JF, MY). These results are discussed in conjunction with the discussion of Table 4.7, since the trends are similar.

For the sake of comparison, two distributions with burnup for Pu-241 atom percent are depicted in Figure 4.17, one in which the LASER-M values correspond to a constant (non-zero power time averaged) power density and the other the corrected values which result from inclusion of the zero power time period decay to Am-241. Appendix C contains the details of this cor-

Figure 4.15 Saxton Core II Mixed Oxide Fuel- U-235 and U-236 Atom Percent as a Function of Burnup

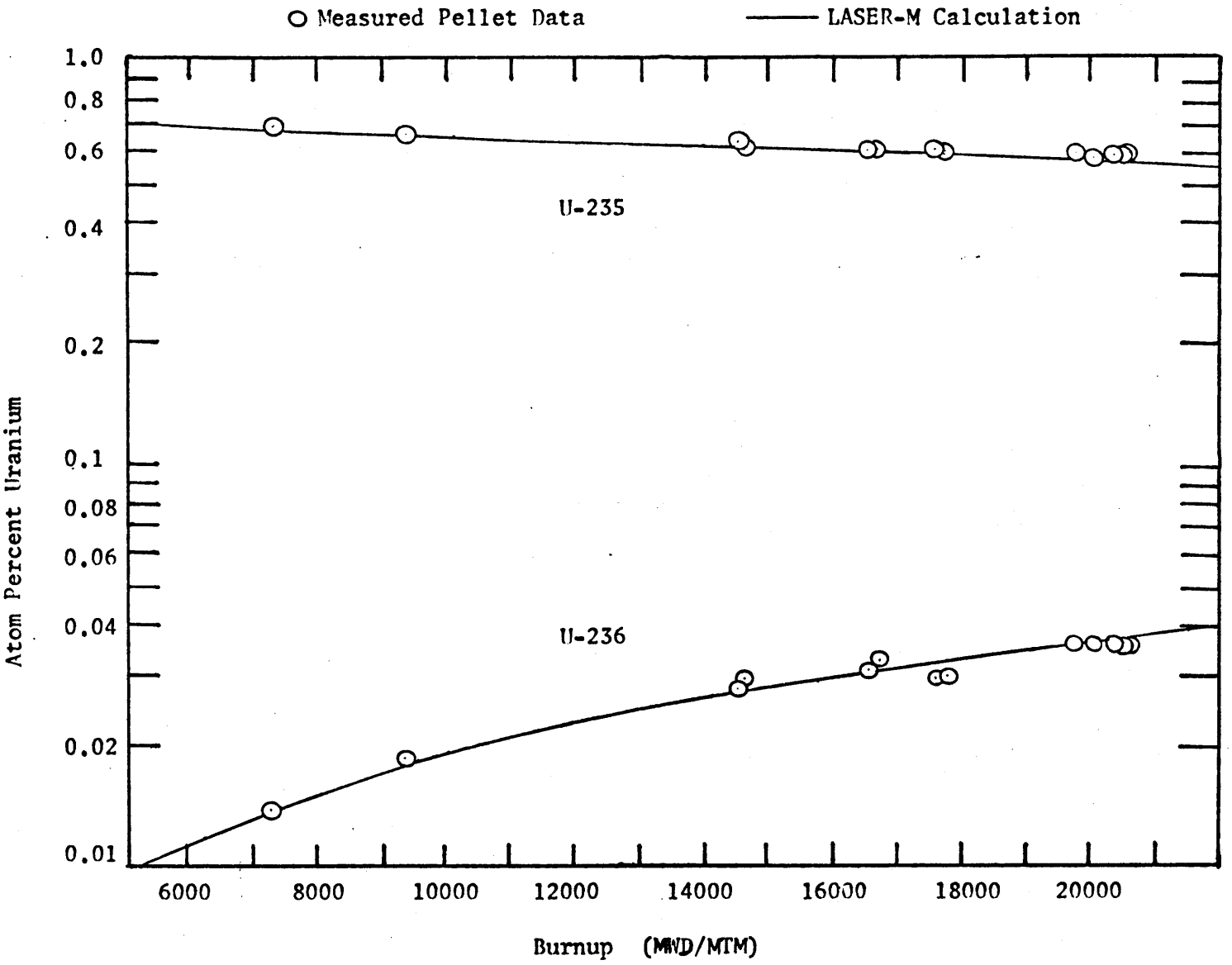

Figure 4.16 Saxton Core II Mixed Oxide Fuel- Pu-239 and Pu-240 Atom Percent as a Function of Burnup

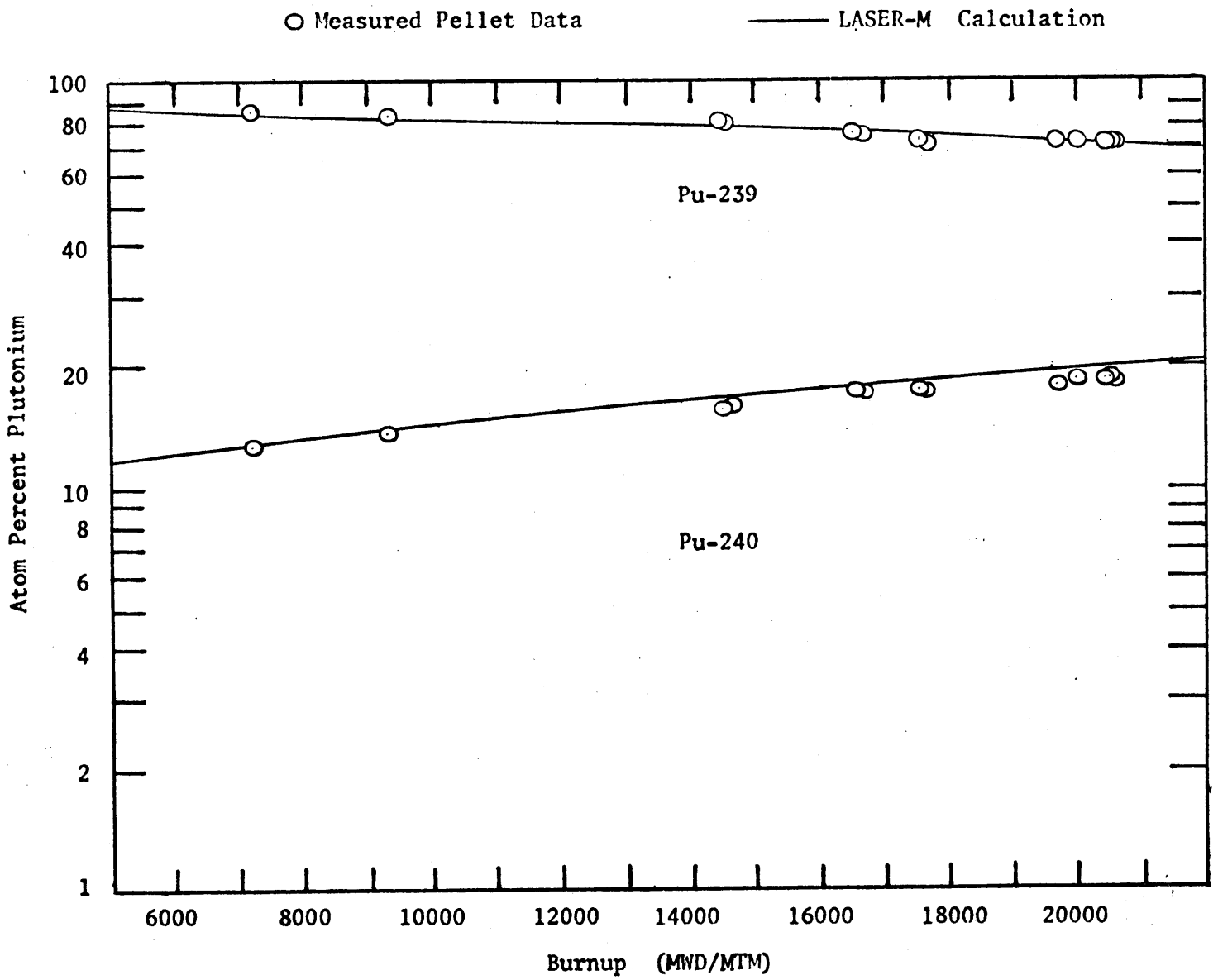

Figure 4.17 Saxton Core II Mixed Oxide Fuel- Pu-241 and Pu-242 Atom Percent as a Function of Burnup

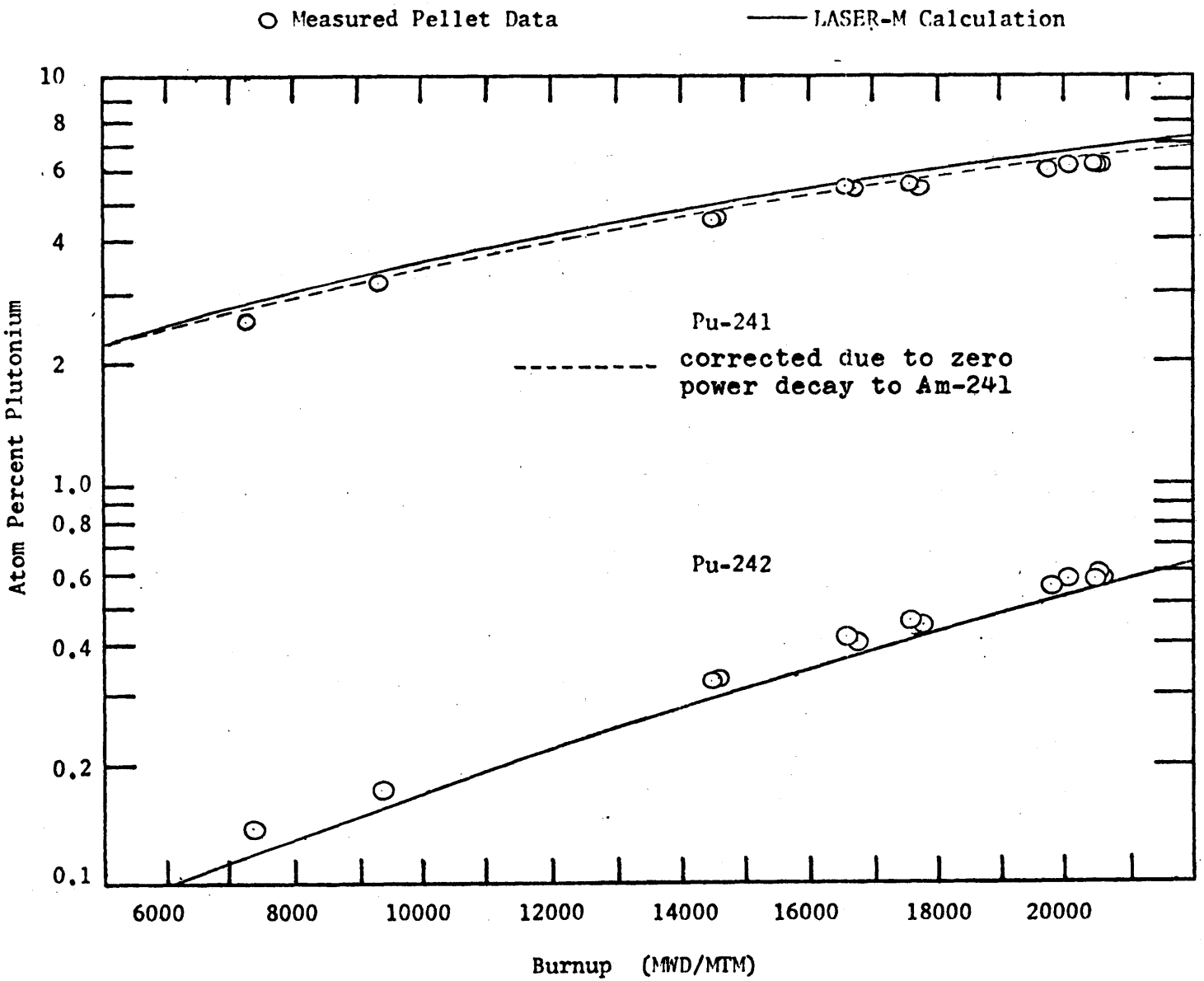

rection calculation. Note that the influence is significant (8.8% in Pu-241 atom percent at end of life).

The trend in plutonium to uranium mass ratio (Pu/U) with burnup is given in Figure 4.18. It should be noted that the analysis of archive samples shows that the analysis input values for these and the Westinghouse calculations were low by 1.82% in Pu/U, so that the underprediction in Figure 4.18 is not as serious as depicted.

The actual numerical values for the average of the five radial samples of atom percent content at approximately 20,000 MWD/MT are given in Table 4.7, presumably from the five data points in Figures 4.15 to 4.18 shown near this burnup value. LASER-M results are given for both the 6 and 12 time step depletions, interpolated linearly to a burnup of 20,481 MWD/MT, which is an average of that determined from the samples using both indicator methods.

The percent deviation of the LASER-M results from experimental, in Table 4.7, is

$$\text{Percent Deviation } (\%) = \frac{(\text{a/o LASER-M}) - (\text{a/o EXP})}{(\text{a/o EXP})} \times 100 \qquad (4.14)$$

for each time step case and each isotope. The trends shown in Figures 4.15 to 4.17 are depicted in the table, namely LASER-M predictions which are within experimental error for U-235 and U-236, less than 1.5% low for Pu-239, 2.4% high for Pu-240, about 1% high for Pu-241 and 4% for Pu-242. The experimental 2σ values for the experimental data are taken

Figure 4.18

Saxton Core II Mixed Oxide Fuel- Plutonium to Uranium (Pu/U) Mass Ratio as a Function of Burnup

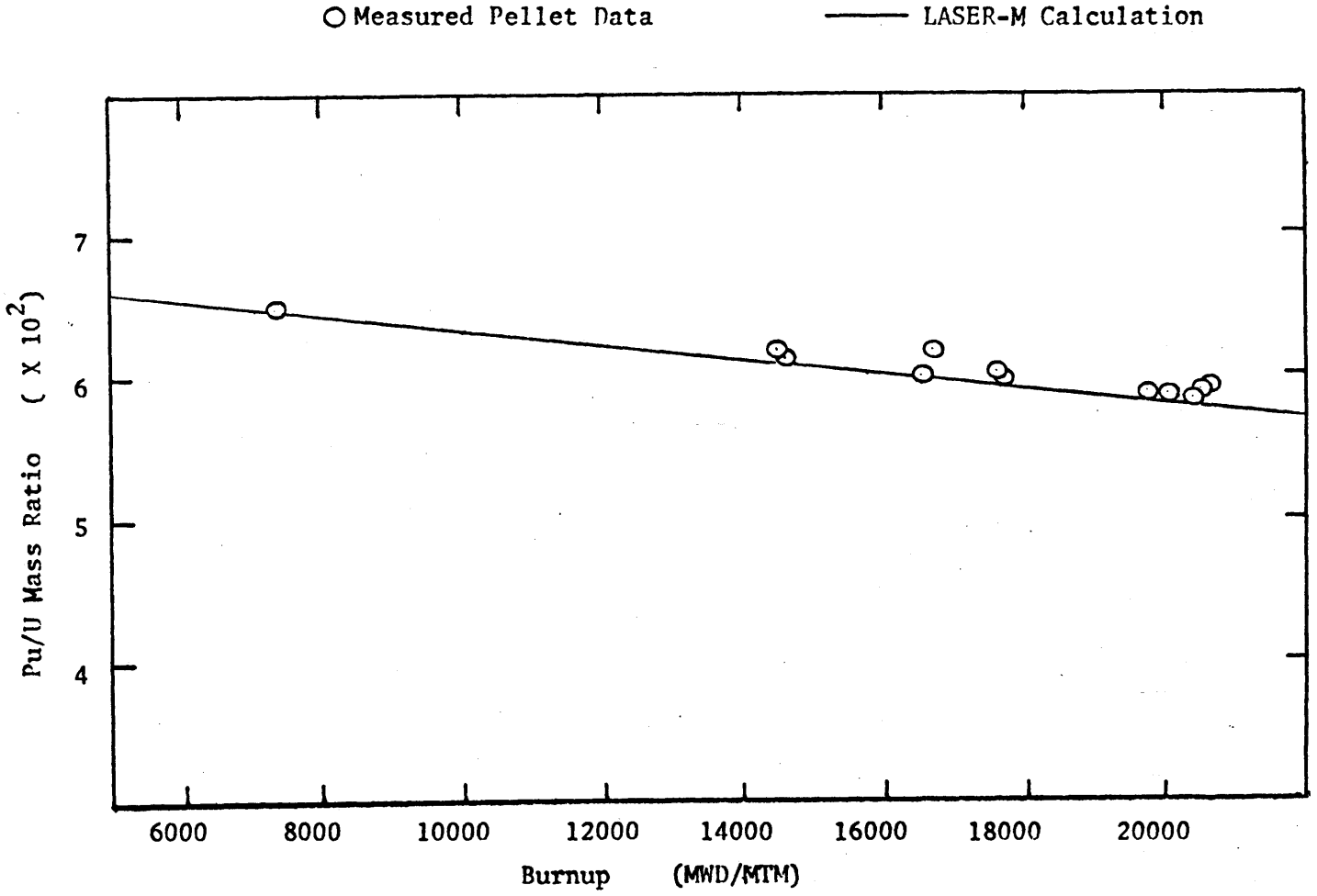

Table 4.7

Saxton Isotopic Data

and Comparison with LASER-M Calculation

(WCAP 3385-56(2) Appendix A)

Fuel Isotopics in Asymptotic Spectrum:
5 Rod Position Average, burnup determined by two methods- heavy element (HE) and Nd-148 (ND) methods

	Rod Number	Zone	Burnup (MWD/MT) HE Method	ND Method	% Difference $\frac{(HE-ND)}{ND} \times 100$
1.	RI	4	20,195	19,673	2.65
2.	RI	6	21,057	20,451	2.96
3.	RI	8	21,170	20,557	2.98
4.	JF	7	20,645	20,109	2.67
5.	MY	6	20,737	20,226	2.53
		Average	20,481		2.76%

Isotope	Experiment: 5 Rod Average a/o @ 20,481 MWD/MT	Calculated: Atom Percent LASER-M Results at 20,481 MWD/MT 6 Time Steps of 2000 hrs.	12 Time Steps of 1000 hrs.	Experimental 2σ (%)
U-235	0.5744	0.5723 ** (-0.37%)	0.5706 (-0.66%)	0.9%
U-236	0.0358	0.0374 (4.47%)	0.0358 (5.31%)	5.6%
Pu-239	73.94	73.24 (-0.95%)	72.94 (-1.35%)	0.03%
Pu-240	19.15	19.31 (0.84%)	19.61 (2.40%)	0.2%
Pu-241 *	6.23	6.31 (1.28%)	6.30 (1.12%)	0.3%
Pu-242	0.575	0.545 (-5.22%)	0.552 (-4.00%)	0.9%
Pu/U Mass Ratio $\times 10^2$	5.98	5.79 (-3.18%)	5.77 (-3.51%)	0.7%

(Based on Isotopics from Archive Samples, the initial value of Pu/U was low by 1.82% (p. 7-2))

LASER-M results linearly interpolated between values of 20,075 and 23,898 MWD/MT for 6 time step case and 19,597 and 21,509 MWD/MT for 12 time step case.

* Corrected for decay to Am-241 during zero power time periods and core EOL to isotopics analysis time period (see Appendix C)

** Percent difference defined in Eq. 4.14

from the reference and indicate, evidently, error in the radiochemical and mass spectrometer procedure. Certainly they are not large enough to describe the spread in the five data point values as shown in the figures (about 2-5%), which leads to the conclusion that the LASER-M isotopic prediction is good to excellent.

It is interesting to note that the results of the six (6) time step depletion are quite equivalent to those of the twelve (12) time step case. This is a virtue of the LASER spatial flux shape detail. An additional factor is the small change with burnup of $\bar{v}_{grad}$, the velocity averaged over the gradient spectrum, as discussed in Sections 2.2.3 and 3.1.2. The change in this quantity can be seen as a measure of the change in the thermal flux gradient. Thus, a small change over a burnup period indicates that the recalculation of the spatial dependence of the spectrum is not significant. The fact that the Saxton pin was plutonium-bearing, and therefore did have a high value of $\bar{v}_{grad}$ initially results in a change with burnup (up to 20,000 MWD/MT) of only 0.6%, a reduction due to the overall plutonium depletion. The Yankee uranium pin (Section 4.2), in comparison, witnessed a 14.5% increase in the same quantity due to the spectrum hardening caused by the plutonium buildup. Thus, a similar lengthening of the burnup step in the Yankee pin case might not be feasible.

Although the change in the spatial dependence of the spectrum with burnup is thus seen to be greater for the Yankee uranium pin, the overall spectrum change in the cell in the

thermal range, as indicated by the change in $\bar{v}_{cell}$ (cell averaged thermal velocity), is slightly greater for the Saxton plutonium pin. Whereas the Yankee pin undergoes a 2.7% spectrum hardening (increase in $\bar{v}_{cell}$), the Saxton pin's spectrum is softened (decrease in $\bar{v}_{cell}$) by 3.5% through 20,000 MWD/MT.

Calculations similar to those of the Saxton Core II depletion, namely pin averaged radial sample isotopic content with burnup, were performed by Westinghouse, the results of which are given in the reference report. The Westinghouse proprietary methods for unit cell calculation are based on the LEOPARD[21] code with a higher isotope calculation (HIC)[57] among the modifications listed in Figure 4.19 for plutonium analysis capability. Table 4.8 shows the LEOPARD-HIC results and the deviations from experimental for both pelletized and vibrationally compacted fuels at about 20,000 MWD/MT for an asymptotic spectrum region of Saxton Core II. The pellet results are very similar to the LASER-M results of Table 4.7.in magnitude of deviation, both analyses yielding good to excellent results.

The fuel pin radial dependence of the isotopes U-235, U-236, U-238, Pu-239, Pu-240, Pu-241, and Pu-242, as determined from experiment and the LASER-M calculation (the latter for five spatial points within the fuel) are shown in Figures 4.20 to 4.26. These results are from the LASER-M 12 time step case and are linearly interpolated between 19,597 and 21,509 MWD/MT to correspond to approximately 20,553 MWD/MT, within the estimated burnup of the experimental values. The actual

Figure 4.19

Westinghouse

Pu METHODS SUMMARY

Pu Cross Sections	ENDF/B Libraries
Pu 240 Resonance	
Self-Shielding	Analytic RI Correlation Similar to U-238
Upscattering	Included in RI Correlation
Resonance Overlap	Neglected
T_{eff}	
U-238	MONTE-CARLO - Empirically Adjusted for Burnup
Pu-240	Similar to U-238 with Concentration Variations Considered
Higher Isotope Chains	• Linearized Chains • Matrix Exponential
Control Rods	Multi-Energy Transport Approximation
Spatial Depletion	X-Y Two-Group Diffusion with Pointwise Feedback

Table 4.8

Westinghouse
LEOPARD-HIC Calculated Results Comparison

SAXTON CORE II
MAIN CHAIN U ISOTOPES

Parameter	Measurement Relative Uncertainty Percent	Percent Difference* Between Calculation and Measurement	
		Pellet	Vipac
U-234 Concentration	29.4	2.9	6.1
U-235 Concentration	0.9	- 0.8	0.2
U-236 Concentration	5.6	5.2	5.3
U-238 Concentration	0.01	0.00	0.00
Pu-238 Concentration	2.3	- 24.6	-23.9
Pu-239 Concentration	0.03	0.86	- 1.18
Pu-240 Concentration	0.2	2.2	3.3
Pu-241 Concentration	0.3	3.6	3.4
Pu-242 Concentration	0.9	0.4	0.9
Pu-239/U-238 Atom Ratio	0.7	- 4.8	-4.9
Pu/U Mass Ratio	0.7	- 3.9	-3.9

Taken from WCAP 3385-56(2), Table 8-1, p. 8-3

* $\frac{\text{Calculated - Measured}}{\text{Measured}}$ x 100 at about 20,000 MWD/MT

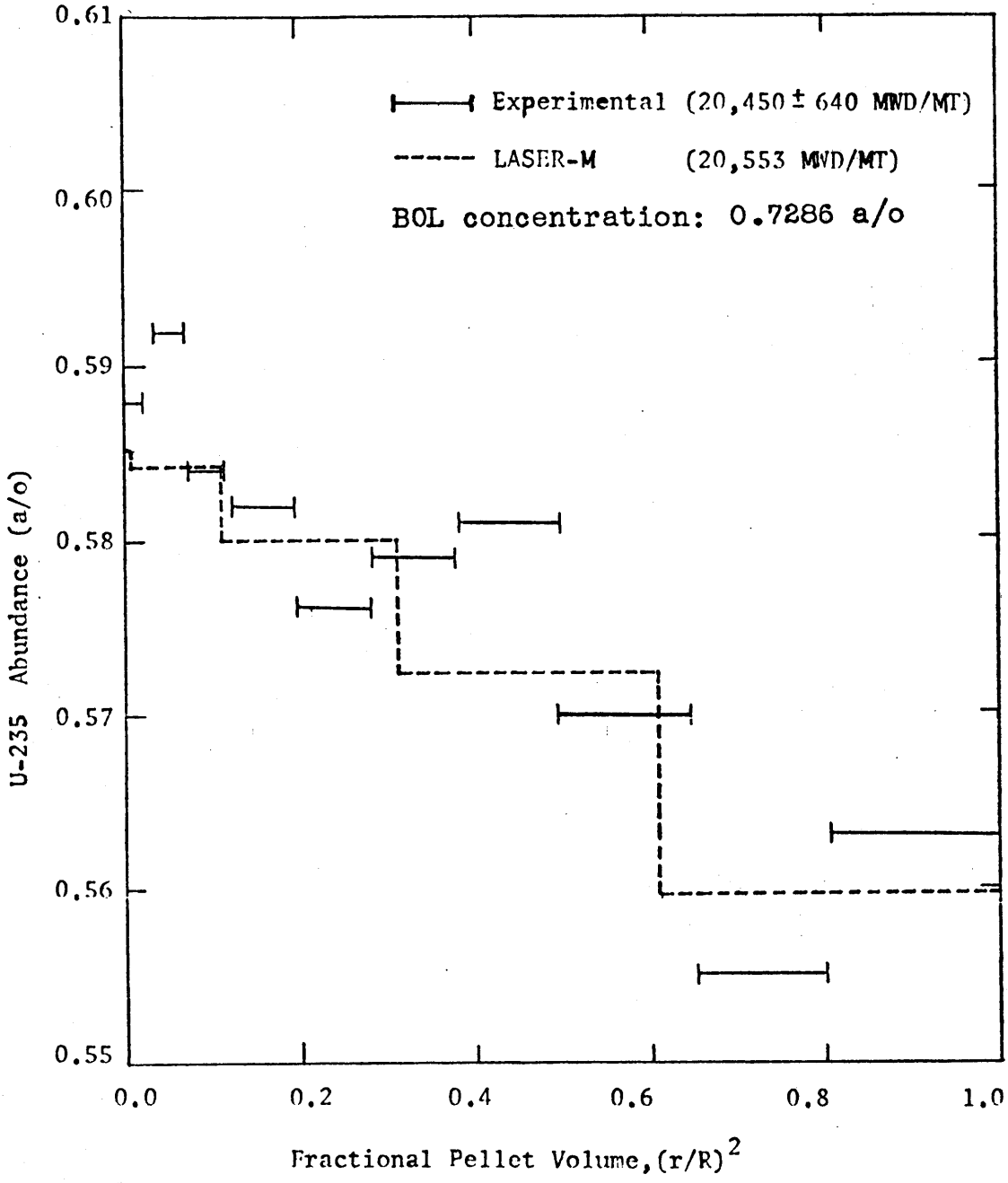

Figure 4.20 Saxton Core II Mixed Oxide Pin- Calculated versus Experimental Radial Distribution of U-235 (Asymptotic Spectrum) Rod RI, Zone 7

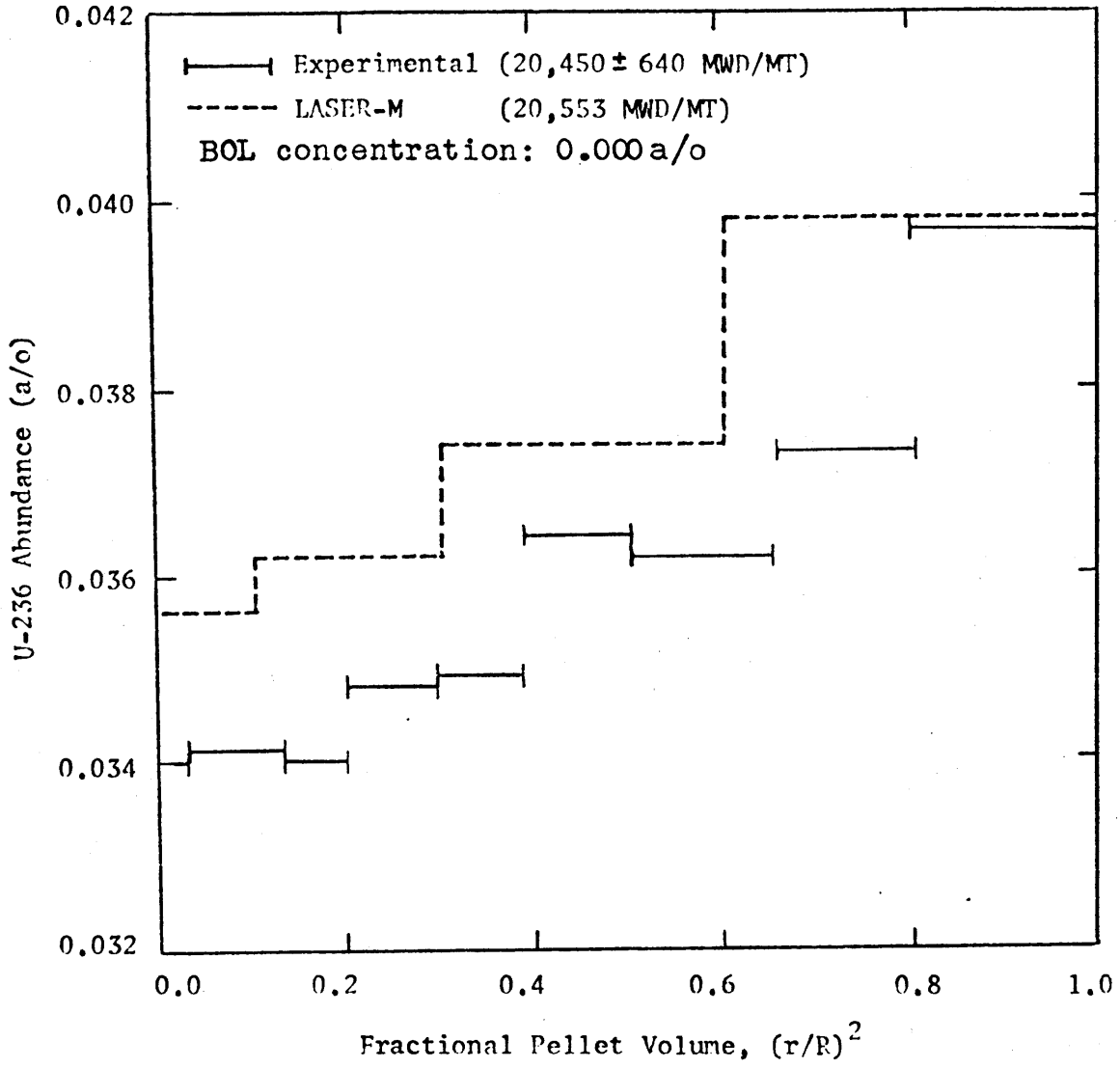

Figure 4.21 Saxton Core II Mixed Oxide Pin- Calculated versus Experimental Radial Distribution of U-236 (Asymptotic Spectrum) Rod RI, Zone 7

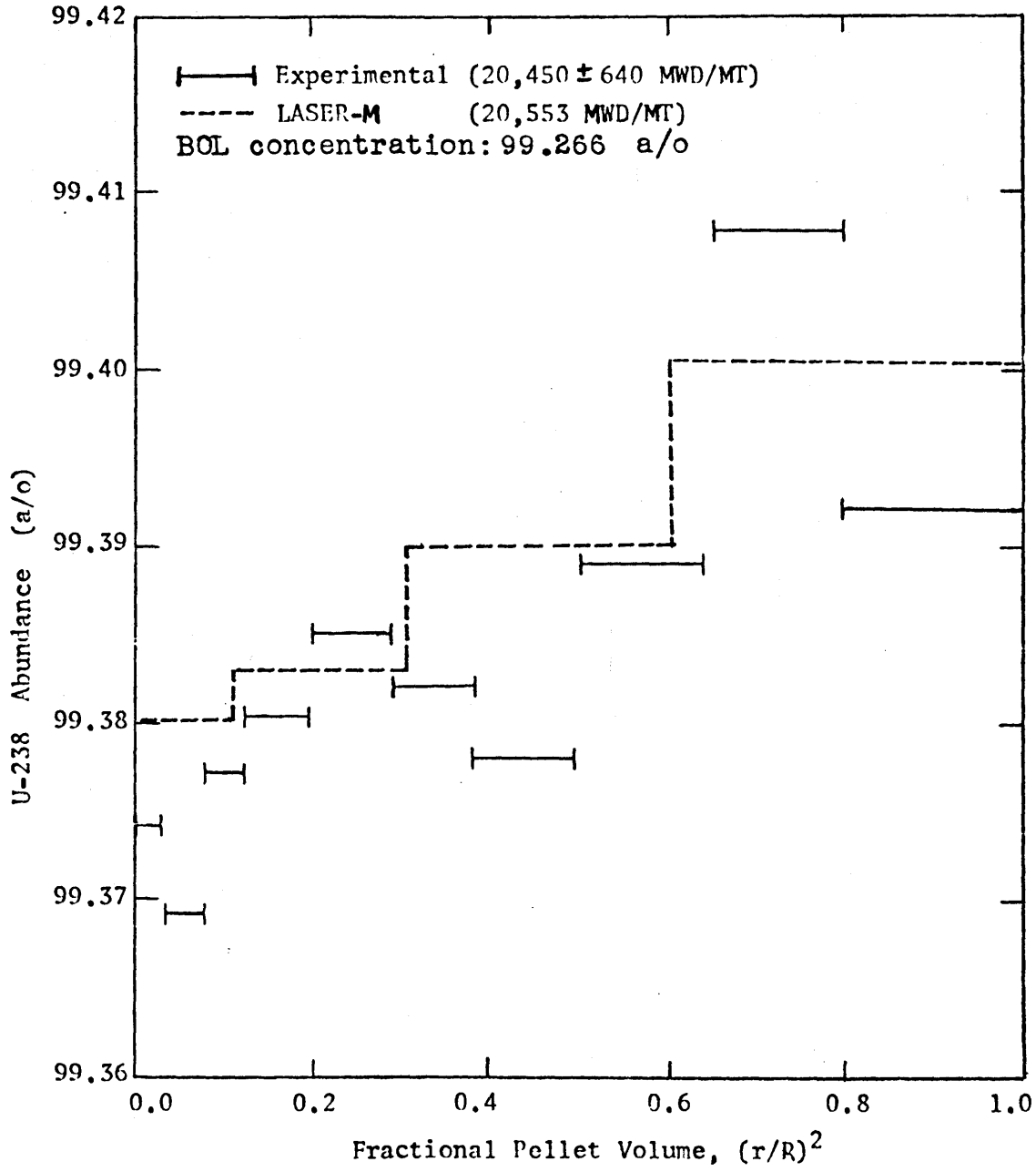

Figure 4.22 Saxton Core II Mixed Oxide Pin- Calculated versus Experimental Radial Distribution of U-238 (Asymptotic Spectrum) Rod RI, Zone 7

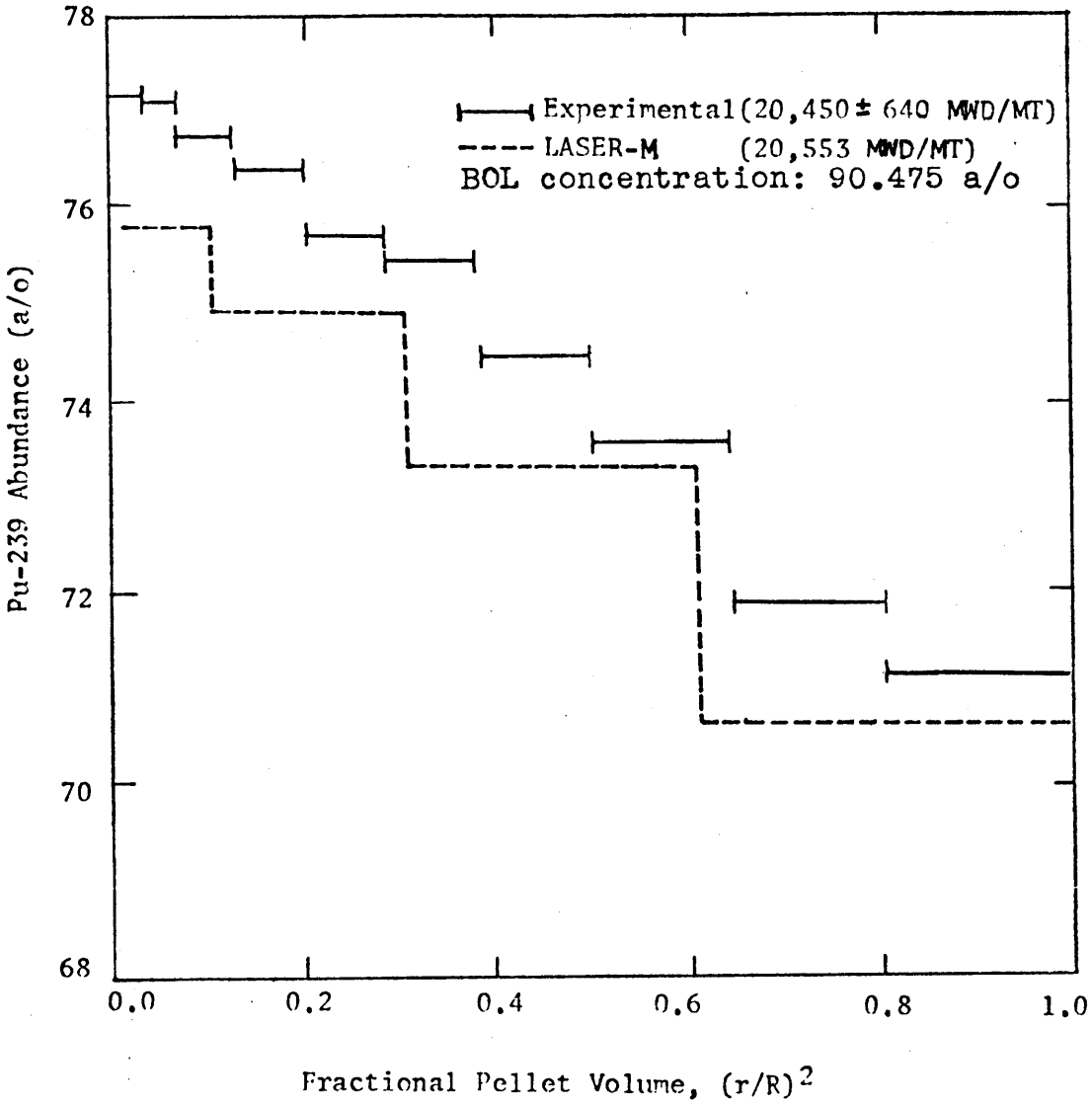

Figure 4.23 Saxton Core II Mixed Oxide Pin- Calculated versus Experimental Radial Distribution of Pu-239 (Asymptotic Spectrum) Rod RI, Zone 7

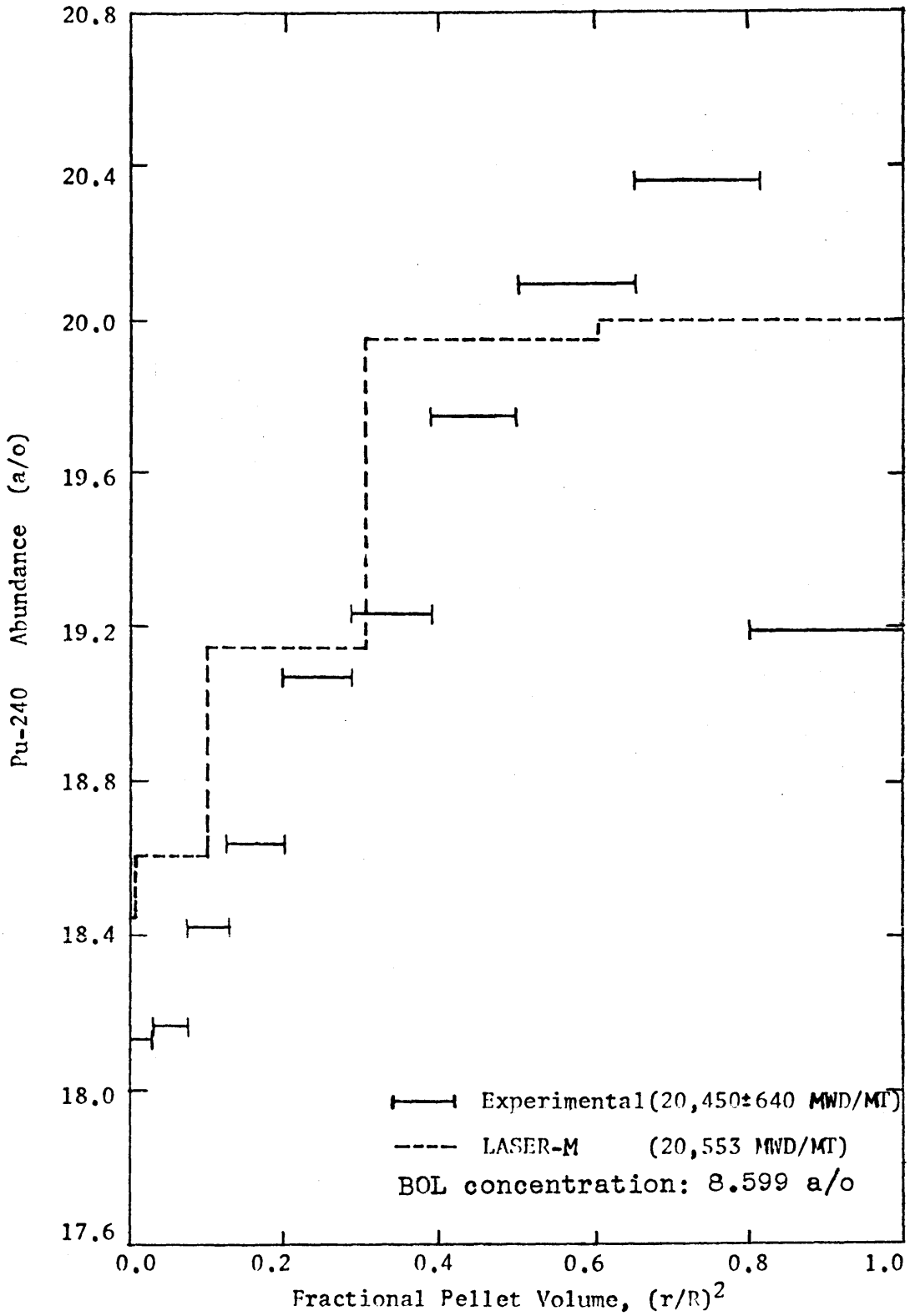

Figure 4.24 Saxton Core II Mixed Oxide Pin- Calculated versus Experimental Radial Distribution of Pu-240 (Asymptotic Spectrum) Rod RI, Zone 7

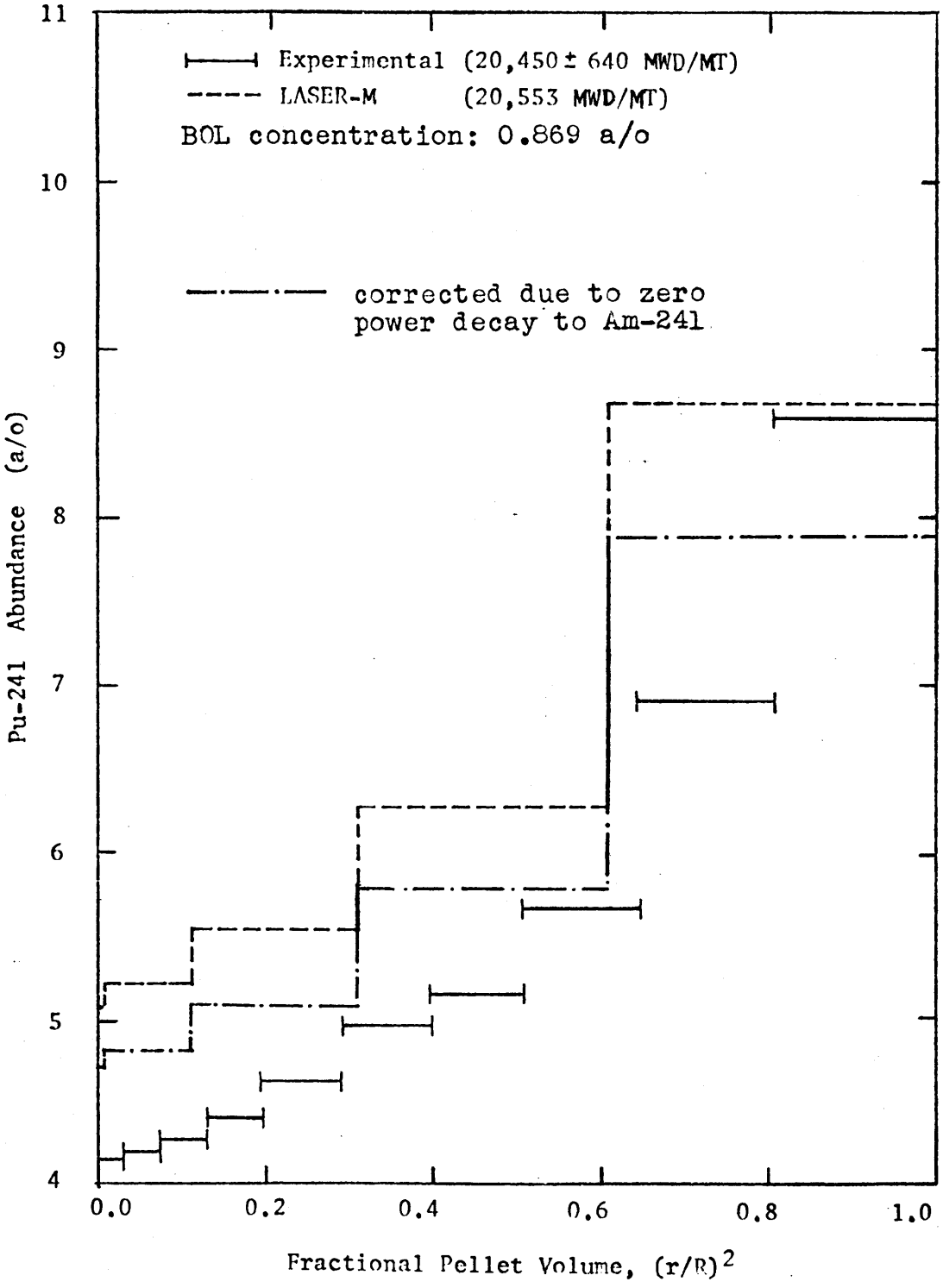

Figure 4.25 Saxton Core II Mixed Oxide Pin- Calculated versus Experimental Radial Distribution of Pu-241 (Asymptotic Spectrum) Rod RI, Zone 7

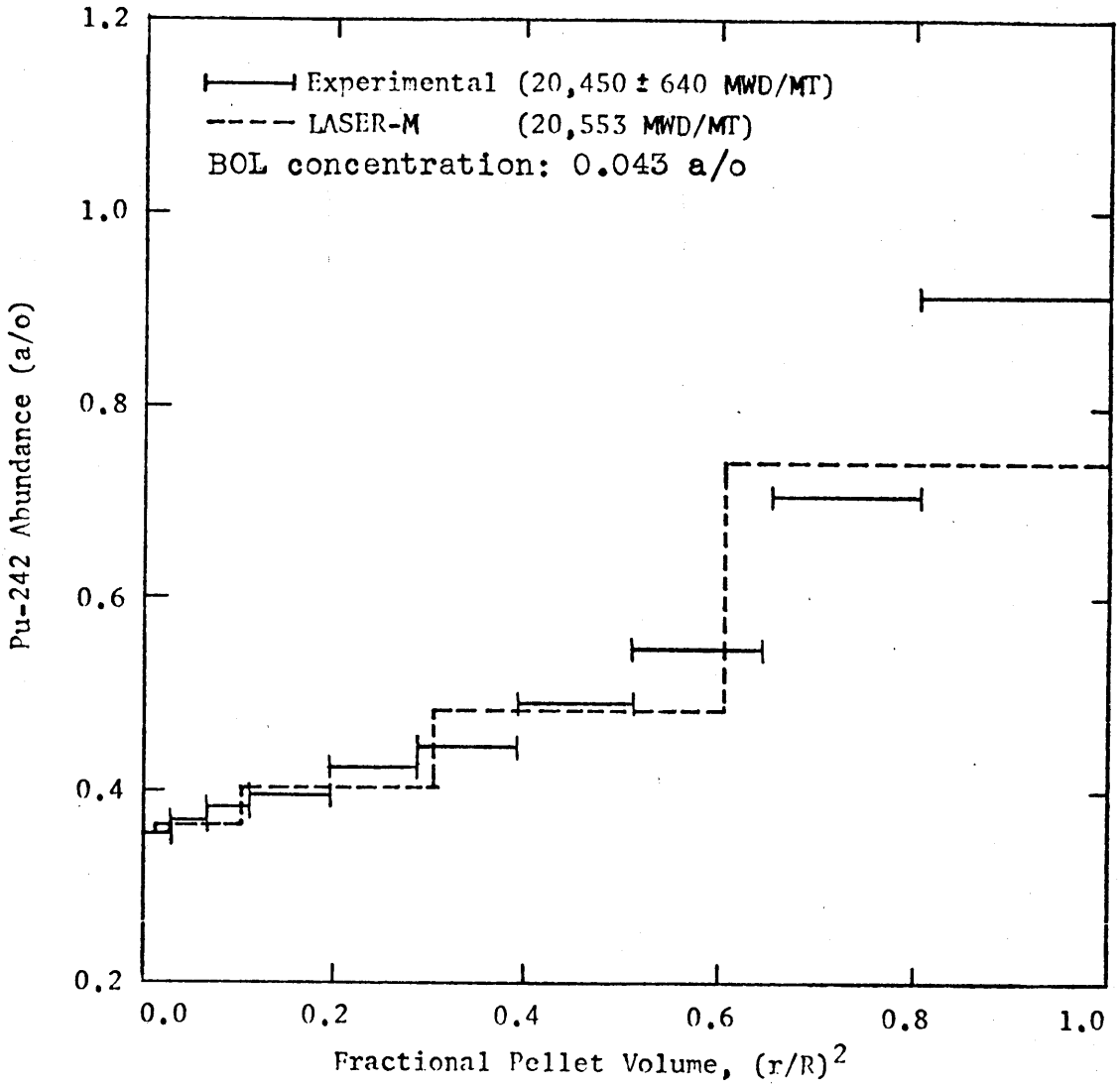

Figure 4.26 Saxton Core II Mixed Oxide Pin- Calculated versus Experimental Radial Distribution of Pu-242 (Asymptotic Spectrum) Rod RI, Zone 7

experimental data is from Rod RI at Axial Zone 7 (in an asymptotic region near mid-core). Thus, the experimental values are from only one sample, so that in concluding whether the calculational predictions are, on the average, high or low for a given isotope, one should more reliably refer to the five rod, radially averaged data of Table 4.7. The importance of the radial distributions is the LASER-M prediction of the correct pin isotopic distribution shape. The experimental errors for these cases are not given in the reference, although by comparison with the radially averaged data, it is small relative to the actual data value spread between samples in the pin.

The U-235 distribution in Figure 4.20 shows good prediction of the experimental shape. The rapid surface depletion is due to both the surface flux depression in the fuel as well as the softer surface spectrum. The increase at the very surface is likely a migration effect, not accounted for in LASER-M.

The U-236 distribution in Figure 4.21 predicts a good distribution shape (neglecting the surface effect inherited from the U-235), however, the calculated average value is high, as was the calculated value for the radial samples relative to the five sample average in Table 4.7. The result, however, is within experimental error, which is large for this isotope. Notice that the Yankee prediction (Figure 4.7) was better.

The U-238 distribution in Figure 4.22 and the Pu-239

distribution in Figure 4.23 are strongly influenced by the LASER-M input value of the spatial distribution of U-238 captures from Poncelet[36]. The shape prediction is relatively good, though slightly fewer captures at the pellet center, relative to the average, are predicted than are found experimentally. This indicates that the Poncelet data is relatively good for plutonium fuel use. The low average level of the Pu-239 distribution prediction is largely accounted for by the error of low input Pu/U mass ratio as discovered by archive sample analysis. The Pu-239 distribution follows the general trend of the U-235 distribution for the same reasons, though the gradient is more pronounced due to the large resonance self shielding of the 0.3 ev resonance.

The Pu-240 distribution in Figure 4.24 is fairly well predicted. The steep gradient due to the Pu-239 captures is slightly underpredicted, as is the surface depression. This depression results from the Pu-240 spatial self shielding as it becomes more important with surface buildup of the isotope. This distribution is highly burnup dependent and its good prediction is necessary for such important calculations as that of the Doppler coefficient for the core.

The Pu-241 distribution in Figure 4.25 is good in light of the Am-241 decay correction of the average value (Appendix C), while the underprediction of the gradient itself is inherited from Pu-240. The Pu-242 prediction in Figure 4.26 is also good.

In summary, the overall LASER-M isotopics calculation

of the Saxton Core II depletion are quite acceptable and LASER-M can thus be expected to give reasonable results for core analysis of isotopics in asymptotic plutonium pin regions.

The weaknesses of the code with respect to plutonium analysis capability should be investigated as to their influence on calculational results. The important areas of study which can improve the LASER-M model for plutonium analysis are:

(1) Improved resonance integral correlations and models for Pu-239, Pu-240 and U-238

(2) Better and more comprehensive higher isotope calculational capability

The input data may be improved for such calculations, especially with regard to:

(1) Plutonium pin spatial epithermal capture distributions (Monte Carlo calculation)

(2) Resonance temperature determination

CHAPTER 5

MODELING OF EXTENDED SPECTRUM EFFECTS: THERMOS CORRECTED LASER-M (TCL) THERMAL GROUP CONSTANTS

5.1 Introduction

As discussed in Section 2.3, the extended spectrum effects of adjacent pins can have significant influence on the determination of effective group constants resulting from a spectrum calculation. This is a consequence of both the violation of the inherent zero current boundary condition unit cell assumption and the sensitivity of a hard spectrum pin (like plutonium) to spectral softening effects. The result is the inability to predict relative reaction rates among pins or assemblies in a spatial calculation using these constants,obtained from a normal unit cell calculation. This is observable through relative power distribution calculation comparisons with experimental data or higher order calculations.

This chapter is an attempt to develop a method to account for the local environment of an individual pin and the consequences on its thermal spectrum and calculated thermal group constants. The method is based on the one dimensional transport theory code THERMOS (discussed in Section 3.1.1), which uses the same type of thermal spectrum solution as does LASER-M. A THERMOS spatially extended (i.e., more than one unit cell) calculation provides correction factors to the LASER-M uniform lattice (i.e., isolated unit cell in an infinite sea of such cells) thermal group constants to create THERMOS Corrected LASER-

M (TCL) thermal group constants.

5.2 The Choice of a Slab Equivalence Model

The one dimensional nature of the THERMOS solution makes necessary the choice of either concentric cylinders or adjacent slabs to model both an individual pin cell and its surrounding environment. The virtue of a cylindrical model lies in its correct geometric representation of the unit cell region and, therefore, good unit cell flux shape representation. Its weakness, however, is the environmental equivalence modeling which necessarily must be performed on some homogenized, concentric volume averaged basis to provide "rings" of surrounding region material. This is problematic in that the spatial nature of the environment is necessarily lost, and this alone can be significant. For instance, the spectral disturbance created on a uranium pin spectrum by a water slot to one side and a plutonium pin to the other cannot sufficiently be represented by homogenization of these two regions uniformly around the unit cell, since a geometric separation of the water and plutonium regions is essential in establishing which spectrum effect is dominant as a uranium cell spectrum influence. More reasonable, in this instance, might be two separate calculations of these two region influences. In either case, however it is not clear that the effect of any volume averaged environment surrounding the unit cell will correspond to the very directional disturbances of the lattice.

In order to avoid some of the aforementioned problems,

a slab approach was chosen. The most undesireable feature of this method is loss of the unit cell fuel pin geometry, which is discussed below . In such a model, three adjacent slabs, a fuel slab boardered by two moderator slabs, represents the unit cell region. The method of such a "representation" will be discussed.

The loss of the correct fuel pin geometry is mitigated by the following:

(1) The unit cell equivalence concept, presented in the next section, which adjusts the slab thicknesses to obtain a cell-averaged parameter equivalence.

(2) The use of the THERMOS slab results as correction terms for the LASER-M thermal cell constants. One thus expects to retain the benefits of the correct cylindrical geometry flux averaging and Doppler broadening afforded by the LASER-M unit cell code.

(3) The establishment of correction terms on a relative change basis, namely use of the ratio of values from two slab calculations. One thus expects to overcome the geometric influence on the spectral averaging.

The advantages of a slab model consist of the following:

(1) The discrete use of fuel and moderator slabs as adjacent environmental influences on either side of a unit cell equivalent slab introduces a geometric effect in the calculation.

(2) There is a definite equivalence between two individual

unit cells in a calculation when they are positioned adjacently and represented as slabs. There is created a symmetry of spectral influence, each on the other (i.e., there is no distinction between the primary unit cell region representation and the "environmental" one).

(3) Slab modeling may generally extend over a large enough number of unit cells (namely, a row of unit cells in a lattice) so that boundary conditions of zero current may be truly applicable.

5.3 Unit Cell Equivalence: Individual Cell Slab

The choice of a slab model requires a method of establishing criteria for some type of spectral equivalent to the normal cylindrical unit cell. Figure 5.1-(A) indicates a reasonable slab form, namely a fuel (plus homogenized clad and gap) region of half-thickness, t, surrounded by two moderator regions of thickness T. The equivalence model involves defining t and T for the slab cell based on a correspondence with cylindrical unit cell characteristics.

The first condition to expect the slab cell model to fulfill, from a spectrum sensitivity argument, is conservation of the unit cell fuel to water ratio, an analog of the Wigner-Seitz approximation. Namely, for a fuel pin with radius R_{f+c} (including clad and gap) in a lattice of pitch P (see Figure 5.1-(A)), the ratio (t/T) is fixed, for a given lattice, by

$$\left(\frac{t}{T}\right) = \frac{\pi R_{f+c}^2}{P^2 - \pi R_{f+c}^2} \qquad (5.1)$$

Through incorporation of the correct fuel to water volume ratio, it is expected that the major determinant of the spectral description of the unit cell is included. There is a remaining degree of freedom, however, and this is used to obtain an overall thermal spectrum fuel to moderator flux sharing equivalence to the cylindrical unit cell. That is, using the LASER-M cylindrical unit cell values of average thermal flux in the fuel plus clad regions, $\bar{\phi}_{f+c}$, and the cell averaged thermal flux, $\bar{\phi}_{cell}$, the half- thickness of the fuel slab is adjusted (T obeying Eq. (5.1) for the given value of t) in the THERMOS slab representation until the calculated THERMOS result obeys

$$\left.\frac{\bar{\phi}_{f+c}}{\bar{\phi}_{cell}}\right|_{\text{LASER-M}} = \left.\frac{\bar{\phi}_{f+c}}{\bar{\phi}_{cell}}\right|_{\text{THERMOS SLAB}} \tag{5.2}$$

In a practical sense, this final restriction is a correction for the large geometry differences between the two models. The adjustment of t is best expressed as an adjustment of the dimensionless parameter (t/R_{f+c}), the ratio of the two geometric characteristics of the fuel region in the models.

The term <u>individual cell slab</u> is defined as that slab representation of moderator-fuel-moderator, with zero current boundary conditions, which corresponds to an individual cylindrical unit cell representation by the equivalences of Eqs. (5.1) and (5.2).

Certainly the choice of these equivalences as those important characteristics for conservation in modeling is debate-

Figure 5.1 THERMOS Individual Cell Slabs and Cell Row Multislabs to represent Unit Cells and Cell Rows

(A) THERMOS Individual Cell Slab

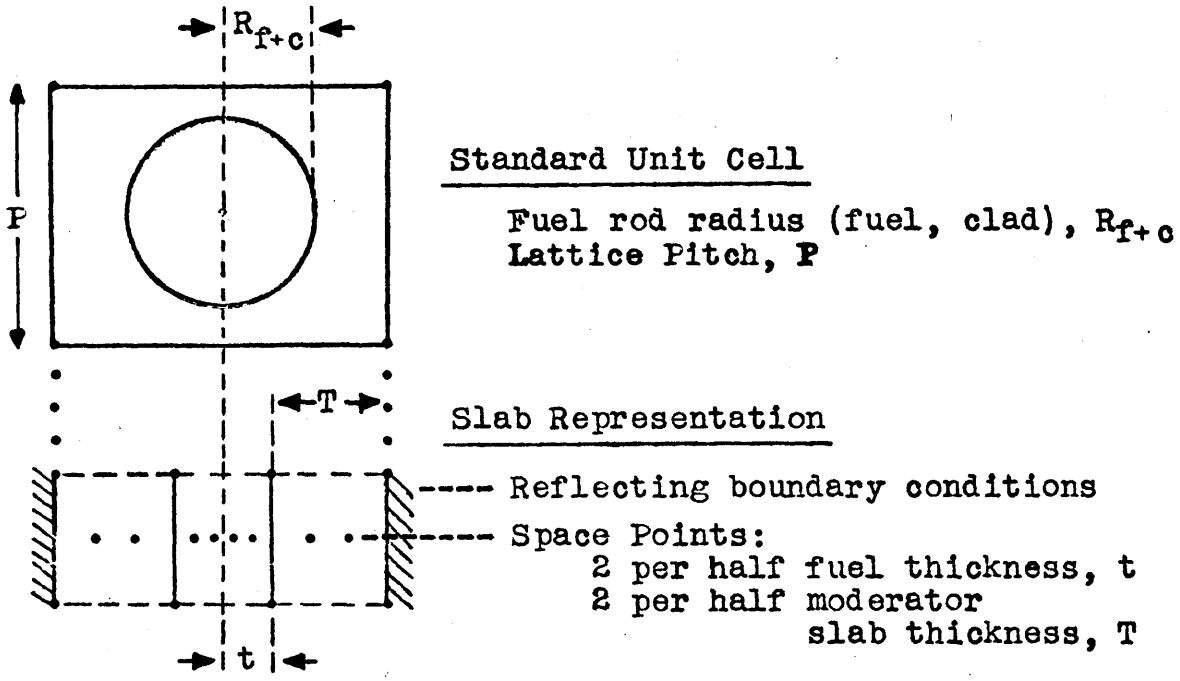

(B) THERMOS Cell Row Multislab

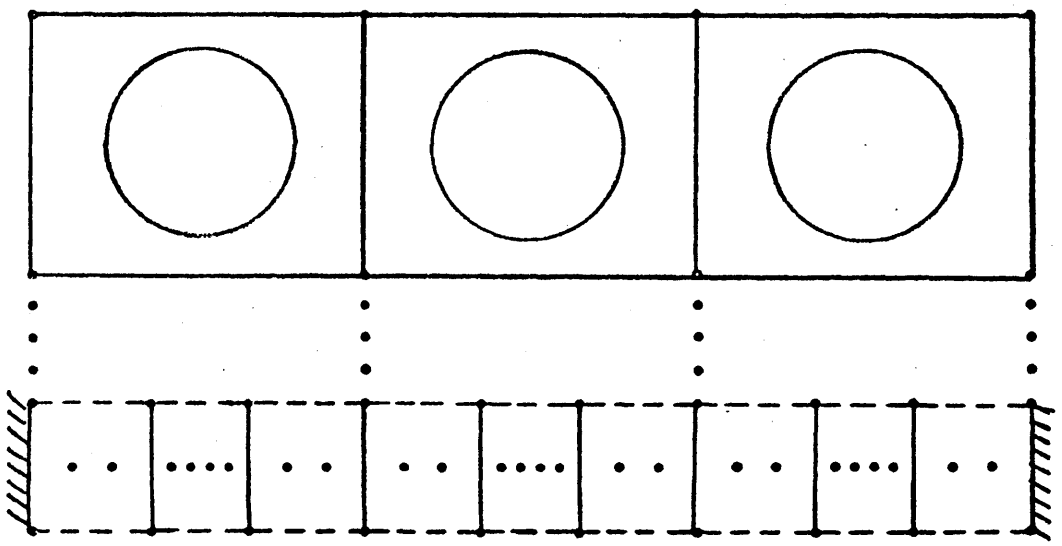

able. The matter, however, is subject to test by comparison of the results of the slab analysis with those of the LASER-M calculations. The most acceptable equivalence of models would be equality of cell averaged microscopic constants, although this is asking much of the model. What is hoped for is a spectral equivalence, most observable from an equivalence of fractional isotopic absorption, especially from spectrum sensitive isotopes such as Pu-240.

The following individual cell slab modeling decisions for this study result from space point and region number limitations, respectively, of the THERMOS code:

(1) Eight (8) space points are assigned to an individual slab cell region, four (4) each to the fuel and moderator (see Figure 5.1).

(2) The fuel, clad and gap is homogenized for the pin.

The thermal neutron source input term to THERMOS, as discussed in Section 3.1.1, is expressable as $\bar{\Sigma}_r$, the macroscopic removal cross section for the fast plus epithermal group. This is obtainable, for the individual cell slab, from the LASER-M unit cell calculation corresponding to that unit cell type. The source is placed in the moderator.

5.4 Cell Row Equivalence: Cell Row Multislabs

The environmental influences on the individual unit cell spectrum are considered by an extension of the region of zero current boundary condition calculation to include a number of adjacent unit cell regions. In the slab model representation,

a series of adjacent individual cell slabs (Figure 5.1-(B)) serves this function, as representative of a row of unit cells with zero current boundary conditions. Such a configuration of individual cell slab regions is termed a cell row multislab.

Each fuel region in the cell row multislab model is chosen to be of equal thickness, as is each moderator region. This is a fuel and moderator equivalence of volume from one unit cell region to the next. Since there are different fuel types in a typical cell row multislab, however, and their chosen thicknesses for representation of an individual cell slab by Eq. (5.2) means these thicknesses are not necessarily equal, there is difficulty in defining the fuel thickness for the cell row multislab.

The solution lies in the method in which the results of the slab calculations are used. Environmental influences are expressable as a percent change in the given individual cell slab region parameter in the cell row multislab calculation relative to the individual cell slab calculation. For example, for a THERMOS microscopic effective cross section, $\bar{\sigma}_\alpha^{\,j}$ (see Section 2.2.2), one obtains the value $\bar{\sigma}_\alpha^{\,j,ind}$ from the individual cell slab calculation and $\bar{\sigma}_\alpha^{\,j,mult}$ from the corresponding unit cell region from the cell row multislab calculation. Effectively, the difference between these values is the result of the environment modeled in the cell row multislab. This expression of difference is

$$(\%\bar{\sigma}_\alpha^{\,j})_x = \frac{\bar{\sigma}_\alpha^{\,j,mult} - \bar{\sigma}_\alpha^{\,j,ind}}{\bar{\sigma}_\alpha^{\,j,ind}} \times 100 \qquad (5.3)$$

and is applicable to a given unit cell region in the environment modeled by the given cell row multislab along, say, the x direction in the lattice. Since Eq. (5.3) is applicable to one unit cell type, the half fuel thickness t is taken as applicable by Eqs. (5.1) and (5.2) to that unit cell (or individual cell slab). The other adjacent fuel and moderator regions in the cell row multislab thus will not necessarily correspond to their characteristic values of t and T, however, this effect is small due to the small change in these variables with unit cell type.

Thus, $(\%\bar{\sigma}_\alpha^j)_x$ in Eq. (5.3) is a percent correction term to account for the spectral environment modeling of the x direction cell row. Expression as a percent change is mitigation of the geometric simplicity of the model.

The source term used in the cell row multislab calculation may conveniently be a volume averaged source from those fueled unit cells in the cell row. This is equivalent to a spatially flat epithermal flux assumption for the moderator regions.

5.5 Corrections to Infinite Lattice Unit Cell Thermal Constants: TCL Thermal Constants

The value of $(\% \bar{\sigma}_\alpha^j)_x$ is a correction term due to the x direction cell row environment of the unit cell. By recognizing that another correction term $(\% \bar{\sigma}_\alpha^j)_y$ is calculable from a transverse cell row environment calculation, it is reasonable to adjust the standard LASER-M infinite lattice group constants, $\bar{\sigma}_\alpha^{j,\ \text{LASER-M}}$, to display the characteristics of some sort of

"averaged" environment, namely

$$\bar{\sigma}_\alpha^{j,TCL} = C\ \bar{\sigma}_\alpha^{j,LASER\text{-}M} \tag{5.4}$$

where

$$C = 1 + 1/2\left(\frac{(\%\bar{\sigma}_\alpha^{j})_x + (\%\bar{\sigma}_\alpha^{j})_y}{100}\right) \tag{5.5}$$

and $\bar{\sigma}_\alpha^{j,TCL}$ is the THERMOS corrected (or environmentally corrected) LASER-M thermal group constant.

The simple average of Eq. (5.5) ignores influences from diagonal pins on the unit cell spectrum, which might cause slight error in the case of strong spectral influences, such as water slot regions. The modeling of a water slot is simple in this slab approach- a pin-wide water slot, for instance, simply requires insertion of a slab of moderator of thickness 2(t + T), where the values of t and T are determined by the adjacent fuel pin unit cells (see Figure 5.1).

Thus, creation of TCL effective thermal group constants for unit cell areas requires the calculation, for each region type boundary, of a series of at most two (x and y direction) cell row multislab calculations and one individual cell slab calculation per pin, given the LASER-M normal group constants and the correct estimated values of fuel and moderator thicknesses. In practice, one cell row multislab calculation generally serves a series of unit cells, so that this procedure is quite inexpensive. The result of the calculations is determination of Eqs. (5.4) and (5.5), namely values of $\bar{\sigma}_\alpha^{j,TCL}$ (or $\bar{\Sigma}_\alpha^{j,TCL}$) for each specific unit cell area for use as the

thermal group regionwise input values for two or three dimensional power distribution (spatial) few group calculations.

5.6 Verification and Application

The TCL spectrum correction method is applied, in the remaining chapters, to a variety of experimental and design power distribution cases which are complicated in a spectrum interference sense. Three separate methods are used in all the power distribution cases, all derivatives of the LASER-M unit cell calculation, namely Normal (spectrum averaged), GMND (see Section 2.2.4) and TCL calculated two group constants. These constants are input values to the PDQ-7 (see Section 3.1.3) diffusion theory spatial calculation to obtain two dimensional relative power distributions for the various lattice cases.

Chapter 6 details the experimental power distribution calculations of the Saxton Critical Reactor Experiment (CRX) configurations, as mentioned in Section 1.4.3. Chapter 7 applies these methods to a plutonium island design assembly for comparison with published calculations, as briefly discussed in Section 1.4.4.

CHAPTER 6

MODEL VERIFICATION:

SAXTON CRITICAL REACTOR EXPERIMENT (CRX) POWER DISTRIBUTION CALCULATIONS

6.1 Introduction

The Saxton Critical Reactor Experiments (CRX) were performed with single region and multiple region lattices of enriched UO_2 and mixed oxide (PuO_2-UO_2) fuel rods, the same rods eventually installed in the Saxton Partial Plutonium Core (and used in the isotopics studies, whose results are discussed in Section 4.3). The purpose of the experiments, which dealt primarily with pin relative power distribution and criticality measurements for cold lattices, was verification of the Saxton Partial Plutonium Core design methods.

The extensive scope of the studies and the results are contained in WCAP 3385-54[16]. The analytical modeling of these lattice configurations by Westinghouse design methods and the calculated results, including relative power distribution calculations, are given in WCAP 3385-51[17].

The core configurations studied in the present work were unborated 19 x 19 pin lattices, near critical and well reflected. The purpose of this work is evaluation of the analytical methods of relative power distribution established, especially the use of THERMOS Corrected LASER-M (TCL) thermal group constants in a few group diffusion theory calculation, as developed in Chapter 5, as an alternative to the standard use of Normal or GMND LASER-M group constants. Comparison is

with the experimental results and the published Westinghouse calculational technique results.

6.2 Experiment Description

6.2.1 Core and Fuel Specifications and Experimental Methods

The reference reports contain the complete experimental plan and analysis. The following discussion deals only with the experimental aspects of those trials applicable to this study.

The basic Saxton Critical Reactor Facility, a 19 x 19 pin array lattice, is illustrated in Figure 6.1. (Another series of experiments were performed with a 27 x 27 pin array, but these were not as extensive.) The series of trials chosen for analysis were of 0.56 inch square lattice pitch. The active core fuel height is 36.6 inches, which in addition to the small lattice size, indicates that this is an extremely small, high leakage core. The experiments were analyzed cold (about 20°C) and near critical, with the reactor control maintained by water height adjustment. Besides providing control, water height adjustment was the primary method of criticality comparison for different configurations by knowledge of the experimentally determined differential moderator worth.

The rod types used in the core configurations were enriched UO_2 (5.742 w/o U-235) and mixed oxide (6.6 w/o PuO_2 in natural UO_2) pins. The plutonium content was 81 w/o fissile, so that the mixed oxide rod fissile content was 6.03

Figure 6.1 Saxton Critical Reactor Facility
19 x 19 Pin Array Core

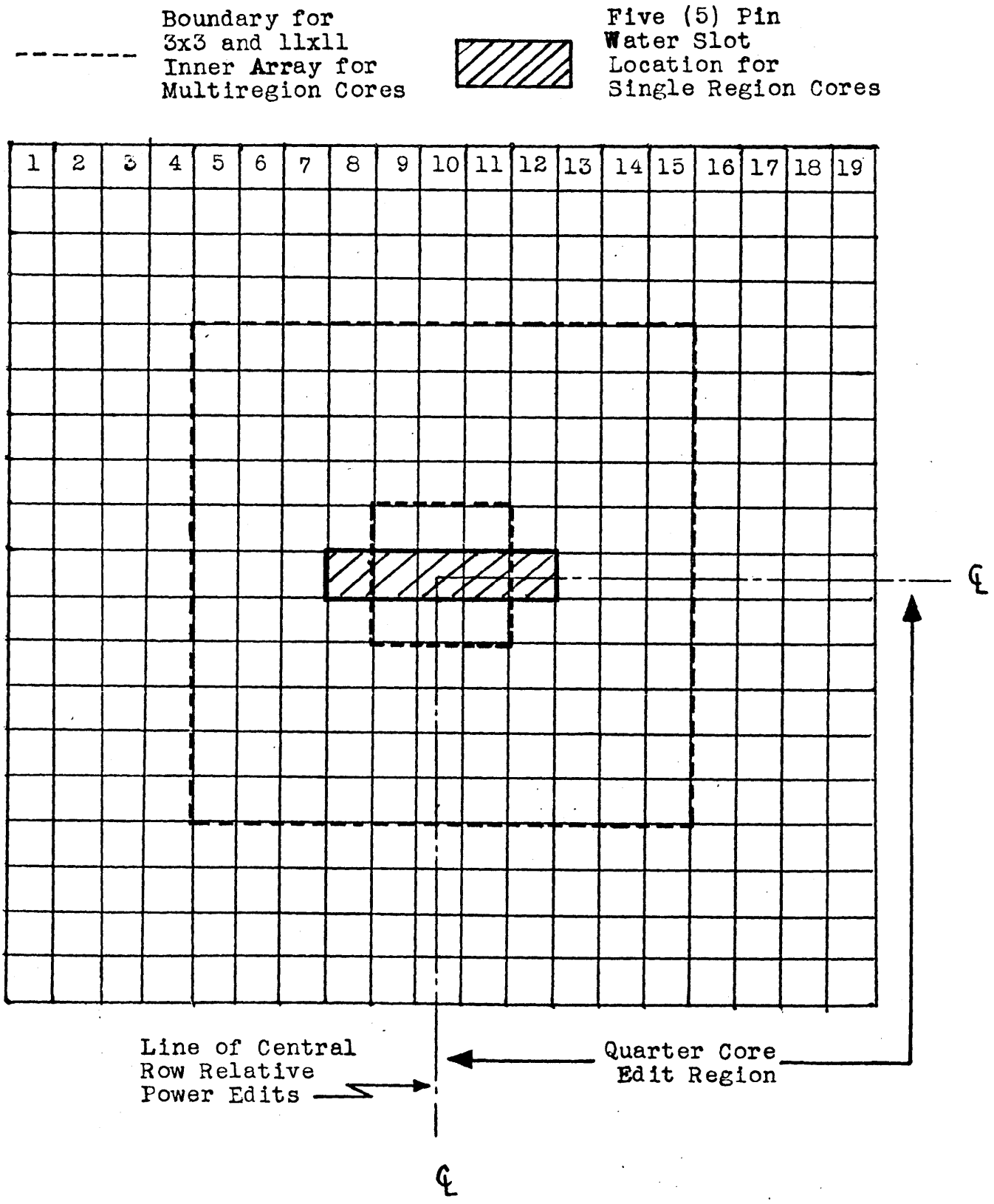

w/o (fissile). The fuel rod specifications are detailed in Table 6.1.

The primary parameters experimentally determined from the core configurations which are of interest to this study are:

(1) Buckling measurements (axially and radially) and reflector savings measurements for single region cores

(2) Pin relative power distribution measurements for single and multiregion (i.e., both fuel pin type) cores, measurements taken at the core midplane

(3) Power peaking effects near moderator (water) slots for single region cores

(4) Reactivity worths of water slots and multiregion core configurations relative to the single region cores

The experimental determination of the relative power between different pin types in a multiregion core presents a discrepancy in the average relative value determined, depending upon the experimental method used, as mentioned in Section 1.2. The standard method of single fuel type core relative power distribution determination is fuel rod activation. The relative power is established by knowledge of the fission product gamma activity, corrected for fission product decay. This technique is not applicable to cores containing different types of fissile material due to the differences in spectra, decay characteristics and fission product yields. As a result, the following two methods were developed and

Table 6.2

Fuel Rod Specifications

Saxton CRX Facility

(Ref. 16, Appendix A, Attachment A, p.42)

Pelletized Fuel Characteristics	PuO_2-UO_2 6.6w/o PuO_2	UO_2 5.742w/o U-235
Dimensions (inches)		
Pellet diameter	0.3374	0.357
Clad outer diameter	0.391	0.391
Clad inner diameter	0.3445	0.361
Rod fuel length	36.6	36.6
Theoretical density(g/cm^3)	11.46	10.96
Percent theoretical density	94	93
Loadings (g/rod)		
PuO_2-UO_2 / UO_2	546.576	604.250
PuO_2	36.074	-
Pu	31.815	-
U-235	(natural UO_2)	30.578
Pu-239	28.789	-
Pu-240	2.727	-
Pu-241	0.283	-
Pu-242	0.013	-

used in the multiregion Saxton CRX core relative power distribution determinations:

(1) Foil Method

This procedure utilizes fission product analysis with an isotope for which the fission product yield is fairly well known for each fissile material. The fission yield of Ba-140 enables determination of a number of fissions that occur in the rod, given the La-140 (daughter of Ba-140) activity decay characteristics. Relative power is then obtained from use with the experimental energy per fission values for each isotope.

(2) Thermal Method

This procedure relies upon a direct measurement of fission power through the use of heating rates. Thermally insulated rods were used to experimentally measure, for each fuel rod type, the temperature changes at the rod surface by thermocouples attached to the clad. After shutdown, these same rods were gamma scanned. The result of these two measurements is a time dependent conversion factor for converting pin gamma decay ratios to thermal power ratios.

The discrepancy between the relative pin power measurements by use of the two methods is that, for a reference uranium pin, the thermal method yields average plutonium pin powers generally 5% greater than the foil method. The Saxton report WCAP 3385-51, Appendix C, discusses the foil method procedure and assigns an accuracy of $\pm 2.5\%$ to the measurement of a given pin power relative to the reference pin power. This

error is primarily the result of spectrum shifts on the power sharing factors. Appendix D of the reference details the thermal method procedure and the associated accuracy is given as several percent.

Notice that these values are not only much larger than the experimental error for pin relative power distribution values of single region cores, which for the Saxton experiments is ± 1.4% (= 2σ), but the methods discrepancy introduces an additional concern. For the purpose of these experiments, Westinghouse concludes:

> It is noted that the two techniques yield results that are within the accuracy of the two experiments, but are consistently different. It is felt that the major part of the difference is in the calorimetric technique, since spectroscopic analysis of these fuel rods were performed with fairly good results.
>
> (WCAP 3385-51, Appendix C, p. 11)

The results of the Westinghouse analysis provide correspondence with the foil method experimental results. This is in no way a grounds for preference of an experimental method. Further resolution of the discrepancy is required to optimize plutonium use in thermal reactors. For the present purposes, both experimental results are reported and a preference made only on the basis of further experimental work.

6.2.2 Loading Configurations and Comparison with LWR Cores

The core loading configurations chosen for this analysis emphasize relative (fuel type) region power sharing and water slot power peaking problems. Such cores contain areas of spec-

tral complexity, as discussed in Chapter 5.

The following core arrangements are presented for analysis using the given UO_2 and PuO_2-UO_2 pins in a 19 x 19 lattice array:

(1) Reference UO_2 core

(2) Reference PuO_2-UO_2 core

(3) UO_2 core with central water slot created by removal of five (5) fuel rods from a cell row

(4) PuO_2-UO_2 core with central water slot created by removal of five (5) fuel rods from a cell row

(5) Multiregion core with an 11 x 11 inner lattice of PuO_2-UO_2 rods surrounded by UO_2 rods

(6) Multiregion core with a 3 x 3 inner lattice of PuO_2-UO_2 rods surrounded by UO_2 rods

The illustration of these core regions is given in Figure 6.1. The lattice pitch is 0.56 inches.

The characteristics of such cores are similar to those of a commercial LWR with respect to fuel type, cladding and lattice pitch. Areas of interfaces between different fuel types are of concern in LWRs for plutonium recycle design applications. Water slot region peaking is also important, applicable to control rod regions.

The significant differences, from a neutronics analysis point of view, between these experimental cores and commercial LWRs, and the consequences for methods application and verification are:

(1) The fissile loading of the experimental pins is greater

than that planned for commercial LWR use. The result is an accentuation of power peaking and thermal flux depression within the rod. Similarly, problems in the analysis of these effects will be magnified.

(2) The lower temperature of the experimental core yields a softer spectrum, due primarily to the added moderation, Although accentuation of pin averaged power results, the Doppler broadening predictions, such as for Pu-240 (in addition to U-238), are not adequately tested.

(3) The small size of the experimental core results in a significant flux and relative power variation within the lattice (a peak power pin to minimum power pin relative power ratio of about 2.0). Core configuration effects must be recognized and analyzed superimposed on this large gradient. This is quite different from the standard LWR situation, which for most regions consists of flat power (zero current boundary condition) areas. There is a problem in obtaining the standard experimental core power distribution shape (especially near the core boundary) independent of the configuration, under the model assumptions of two group diffusion theory and a group-independent leakage representation in the spatial calcuation. These assumptions are more applicable, however, to the LWR applications anticipated.

(4) The spectral disturbances in these core configurations are isolated in a sense that a single water slot or mixed oxide fuel region is placed within an asymptotic core region. The plutonium island design assembly of Figure 1.1 is a much

more complicated spectral overlap problem due to the adjacent positioning of a water region and a uranium-mixed oxide pin type boundary, in addition to the variation of plutonium content (zoning) within the plutonium region.

6.3 Spectrum Analysis: LASER-M Infinite Lattice Group Constants

The calculation of few group, unit cell constants, as discussed in Section 2.2.2, is provided by the spectrum code LASER-M in this study. These are infinite medium (i.e., uniform lattice of similar pins) results due to the white boundary condition implicit in the calculation. The constants are termed LASER-M Normal, corresponding to cell spectrum averaged effective values, or LASER-M GMND, also cell spectrum averaged effective values, but derived from the theory presented in Section 2.2.4 and its application in Section 3.2.4.

6.3.1 Input Description

The parameters necessary for LASER-M fueled unit cell input are obtainable, for the most part, from the fuel specifications of Table 6.1. The actual computer input listings for the unit cell types are given in Appendix A.

Specific input details include the following. Cold lattice dimensions were applicable due to the core analysis conditions. Gap and clad homogenization, as necessitated by LASER-M, was performed. No moderator boron was present. The only significant active core structural material was a thin (0.25 inch) center core guide plate (lying across the core), which was

neglected in the calculations. The moderator unit cell region volume corresponded to that in a normal square pitch around the fuel pin. The average fuel and resonance temperatures were chosen as 16°C for all cases, although the actual experimental temperatures varied from 15.4°C to 21.2°C. The error introduced is not significant, since the temperature coefficient of reactivity for these cores is approximately 10^{-5}/°C.

Fuel region number densities were calculated using average rod loadings distributed within the fuel volume (neglecting axial gaps) within the pin and theoretical atoms per gram values of the individual oxides.

The LASER-M options chosen include the following. The materials buckling was searched and this, therefore, was used for the fast spectrum calculation. The Nelkin thermalization treatment was used. The U-238 L factor was searched, the values for the other nuclides set equal to 1.0. The epithermal U-238 spatial capture distribution was again obtained from Poncelet[36]. The standard THERMOS iteration technique was used without extrapolation.

LASER-M group constants for the spectrum in the water regions (e.g., the core reflector boundary and water slots created by rod removals) must be calculated by a LASER-M run in which a small (less than 0.1 cm in radius) fuel region of dilute U-235 concentration provides a neutron source. The clad region is also made extremely small, although this region can be used to represent the correct volume fraction of structural material present in the specific water region. This

calculation, therefore, assumes "soft spectrum" water. Momsen[9] verifies the results of this procedure by comparison LEOPARD unfueled cell calculations.

6.3.2 Unit Cell Comparison

The macroscopic group constants obtained from the LASER-M calculations for the two fuel cell types (5.742 w/o U-235 and 6.6 w/o PuO_2) and the water cell region are presented in Table 6.2. These are effective cell constants, used for representation of the entire cell reaction rate, the microscopic components of which are defined by Eq. (2.5). The macroscopic effective constants are expressable in terms of the microscopic values, $\bar{\sigma}^{j}_{\alpha,eff}$, of Eq. (2.5) as

$$\bar{\Sigma}_{\alpha,eff} = \sum_j N^j_{cell} \bar{\sigma}^{j}_{\alpha,eff} \qquad (6.1)$$

where N^j_{cell} is the cell averaged number density of nuclide j and $\bar{\Sigma}_{\alpha,eff}$ the macroscopic effective constant for reaction α for the given energy group.

The values given are effective two group (fast plus epithermal and thermal) constants, with the thermal cutoff at 1.855 ev, which are deemed acceptable for power distribution calculations by the arguments of Section 2.4. The macroscopic removal cross section, as defined in the LASER manual, is derived from a neutron conservation argument, relating the total thermal reaction rate to the total fast (plus epithermal) flux.

The fast plus epithermal constants are defined as equal

Table 6.2

Macroscopic Group Constants

from LASER-M

Saxton CRX

Pin Type	Energy Group	Group Parameters: Diffusion (cm)	Absorption $(cm)^{-1}$	Removal $(cm)^{-1}$	NuFission $(cm)^{-1}$	KFission (watt-sec/cm)x10^{12}	Thermal Average Velocity (units of 2200 m/second): $\bar{v}$ cell	$\bar{v}$ gradient
6.6 w/o PuO_2	Fast + Epi	1.2125	0.011958	0.023685	0.012402	0.14473	1.9917	1.3581
	Thermal-Normal	0.28986	0.22575	-	0.37463	4.4244		
	-GMND	0.39365	0.44962	-	0.74616	8.8121		
5.742 w/o U-235	Fast + Epi	1.1722	0.010964	0.024687	0.009521	0.12252	1.7986	1.0803
	Thermal-Normal	0.28762	0.13903	-	0.23758	3.1975		
	-GMND	0.31071	0.25006	-	0.42732	5.7187		
Water Cold No B	Fast + Epi	1.2605	0.00066850	0.048688	-	-	1.1747	1.1507
	Thermal-Normal	0.16067	0.016880	-	-	-		
	-GMND	0.18487	0.022178	-	-	-		

in the Normal and GMND representations. GMND thermal constants, in units of (cm^{-1} x 2200 m/sec) are defined by Eqs. (2.18) and (2.19) with $\bar{v}_{grad}$, the cell velocity averaged over the gradient spectrum, approximated by Eq. (3.1).

Notice for the normal thermal constants of the two fuel pin types the large values of the absorption and fission constants for the plutonium pin relative to the uranium pin, despite the relatively small difference in fissile content (6.03 versus 5.742 w/o). This difference would be even more pronounced were the plutonium pin calculation to include some spectrum softening, more closely modeling its placement in a uranium spectrum region. Notice that the GMND representation, in weighting the reaction constants by $\bar{v}_{cell}$, increases the relative plutonium to uranium thermal pin absorption. The water region GMND absorption, similarly, is significantly depressed relative to the pin absorptions due to its very thermalized (i.e., low $\bar{v}_{cell}$) nature.

It should be recognized that the value of $\bar{v}_{grad}$ output by LASER-M for the water cell calculation (containing an extremely small amount of fuel to provide a neutron source) is quite unstable. That is, due to the cell's practically flat thermal flux and uniform neutron density, Eq. (3.1) is almost indeterminate. As a result, the calculation of $\bar{v}_{grad}$ should more rightly use, for points r_1 and r_2 in Eq. (3.1), a point in the water region and a point in the moderator region of an adjacent cell, respectively, with the appropriate normalization. This would correspond more to the idea of

a gradient for the region. In practice, however, the leakage term is sufficiently small so that no appreciable change is noticed in the pin relative power distribution. Changes in the water cell region effective absorption, however, can have a significant influence.

The calculated LASER-M Normal and GMND two group constants are the basis of the Saxton relative power distribution calculations presented in Section 6.5, along with the calculated TCL group constants, derived from the methods of Chapter 5 and discussed in the next section.

6.4 Extended Spectrum Effects: TCL Thermal Constants

The guidelines for calculation of TCL thermal group constants are presented in Chapter 5. Defined there are individual cell slabs and cell row multislabs as the THERMOS model slab analogs of unit cells and cell rows, respectively, by use of a thermal spectrum equivalence condition. THERMOS modeling is required for those lattice areas which are anticipated to experience local spectrum disturbances in the asymptotic core region which are significantly different from those characteristic of the given infinite medium unit cell. For the Saxton CRX experiments analyzed, such areas may be categorized as:

(1) Uranium- mixed oxide pin type (region) boundary

(2) Water slot- uranium pin region boundary

(3) Water slot- plutonium pin region boundary

6.4.1 Input Description

As mentioned in Section 5.3 and depicted in Figure 5.1, the geometric THERMOS slab representation of an individual cell slab contains a four space point fuel region surrounded by two space point moderator regions. The characteristic dimensions of the geometry of the individual cell slab, the fuel slab half thickness, t, and the moderator slab thickness, T, are adjusted to correspond to conditions (Eqs. (5.1) and (5.2)) of a fuel to moderator volume and thermal averaged fuel to cell flux ratio equivalence to the corresponding LASER-M unit cell parameters.The THERMOS problem is solved with zero current boundary conditions. The individual cell slab calculations for the Saxton CRX facility correspond to the two pin cell types of Table 6.2, enriched uranium and mixed oxide. The primary data for the input values to the THERMOS calculation is obtainable from the LASER-M input data of Section 6.3. The actual THERMOS input listings for the individual cell slabs,as well as the cell row multislabs, are given in Appendix A.

The cell row multislab calculations performed for the spectral problem areas identified are depicted in Figure 6.2, namely the mixed oxide (pin type) boundary and the water slot, the latter for both uranium and mixed oxide pin cores. The unit cell areas are symbolized as either "U" or "P" for uranium or plutonium pin, and numerically according to position with respect to the spectrum discontinuities. The symbols U1 and P1 correspond to the standard infinite lattice pin types

Figure 6.2 Saxton CRX Multiregion and Water Slot Cores Modeling of Mixed Oxide Boundary and Water Slot by THERMOS Multislabs

A. THERMOS Multislab Mixed Oxide Boundary

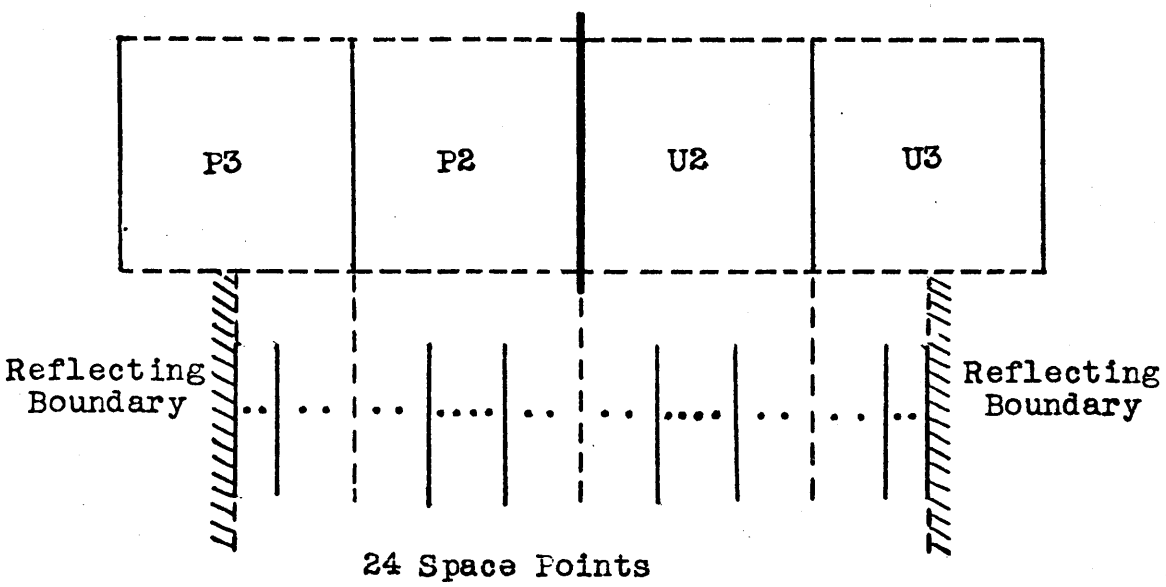

B. THERMOS Multislab Water Slot (Slot is one unit cell wide)

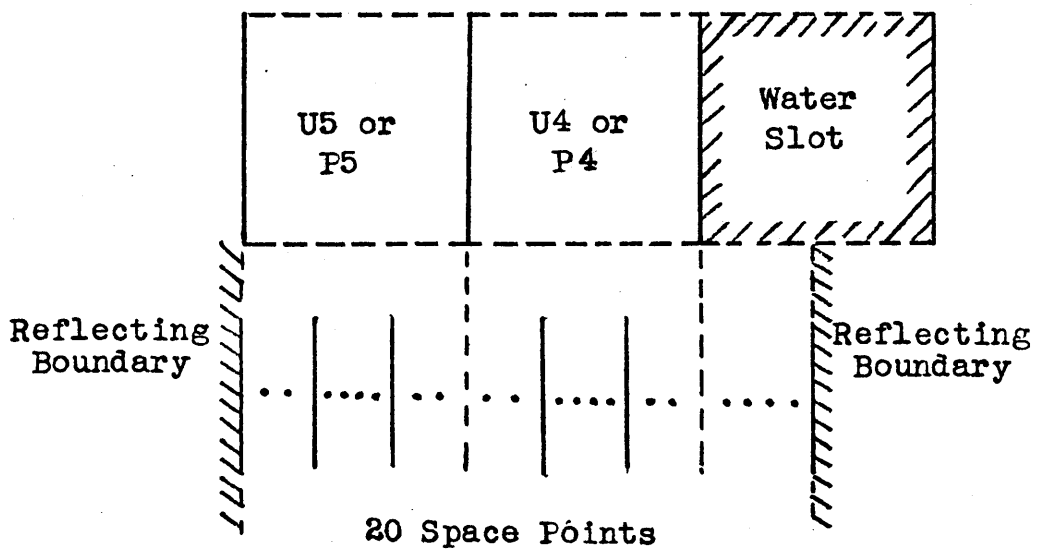

in which no THERMOS spectrum correction is necessary.

The mixed oxide boundary modeling incorporates one and one half unit cell regions to each side of the physical boundary, as dictated by the code dimensional limitations. The reflecting boundary conditions are not strictly applicable, but are estimations not significantly in error due to the fact that the boundaries are primarily in infinite medium(all one pin type) regions. The water slot modeling includes half the one-cell-wide water slot and two adjacent unit cell regions. The reflecting boundary condition at the water slot is applicable due to the problem symmetry, while that far from the slot is approximate, as in the mixed oxide boundary case. These regions are depicted in Figure 6.2.

The epithermal neutron source term placed in the moderator for the mixed oxide boundary cell row multislab is proportional to the average value of $\overline{\Sigma}_r$, the macroscopic removal terms, for the two pin types (Table 6.2). Thus, the source is homogenized in the moderator region for this case where the source terms are similar in magnitude. The source for the water slot cell row multislab, however, is in the moderator but kept regionally distinct between the fuel moderator regions and the water slot itself. This is a result of the vast thermal neutron water region epithermal removal, which makes homogenization inapplicable. The epithermal flux distribution for the calculations is designated as $1/E$.

The fuel regions are homogenized fuel, clad and gap. The number densities correspond to those of the LASER-M unit cell input, changed to this volume- homogenized basis. The

moderator density also corresponds to the LASER-M value. The THERMOS energy averages correspond to the 1.855 ev LASER-M cutoff value. The standard THERMOS iteration is used without extrapolation.

The pin designations used in Figure 6.2 are more meaningful when it is made evident which pins they represent in the experimental lattices. This is accomplished for the quarter core configurations in Figures 6.3 to 6.5. Figures 6.3 and 6.4 show the 3 x 3 and 11 x 11 inner plutonium region cores, respectively. Figure 6.5 shows the water slot core with UO_2 pins (mixed oxide case analogous). The pin designations correspond to those in Figure 6.2. These are the lattice cells whose group constants are to be adjusted by the TCL method according to Eqs. (5.4) and (5.5) prior to use in the PDQ power distribution calculation.

The designation U4 is applied to the uranium pin boardering on the water slot, as modeled. It is seen that the designation U4 is also given to pins on the core boundary. The modeling of these boundary pins is not correct, since the boundary condition (zero current) is wrong. A separate THERMOS calculation for these pins should be performed, but was not since careful calculation of these pin powers was not necessary for our purposes. The use of group constants equal to those used for the water slot pin at least introduces some core boundary peaking. Similarly, the pin at the water slot corner is designated as U5 in order to introduce some of the slot effect. These estimated corrections are secondary to

Figure 6.3 Saxton CRX Multiregion (3x3 Inner) Core Pin Designation for TCL-PDQ Calculation

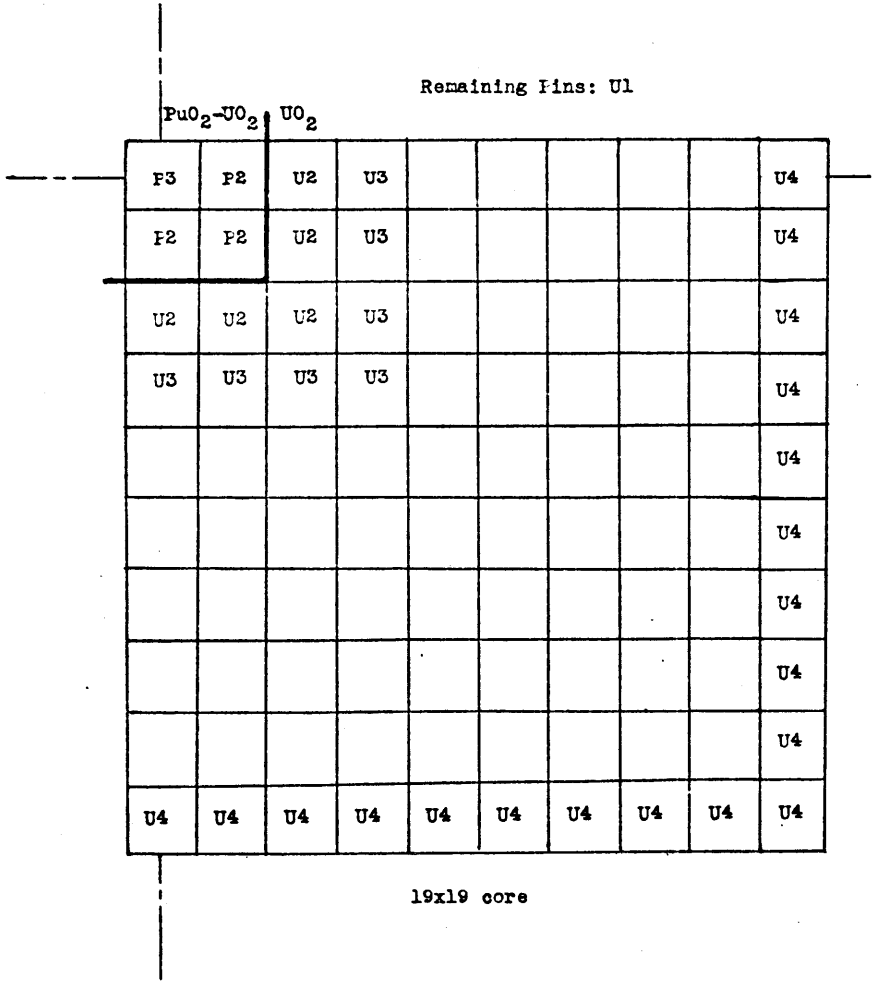

Figure 6.4 Saxton CRX Multiregion (11x11 Inner) Core Pin Designation for TCL-PDQ Calculation

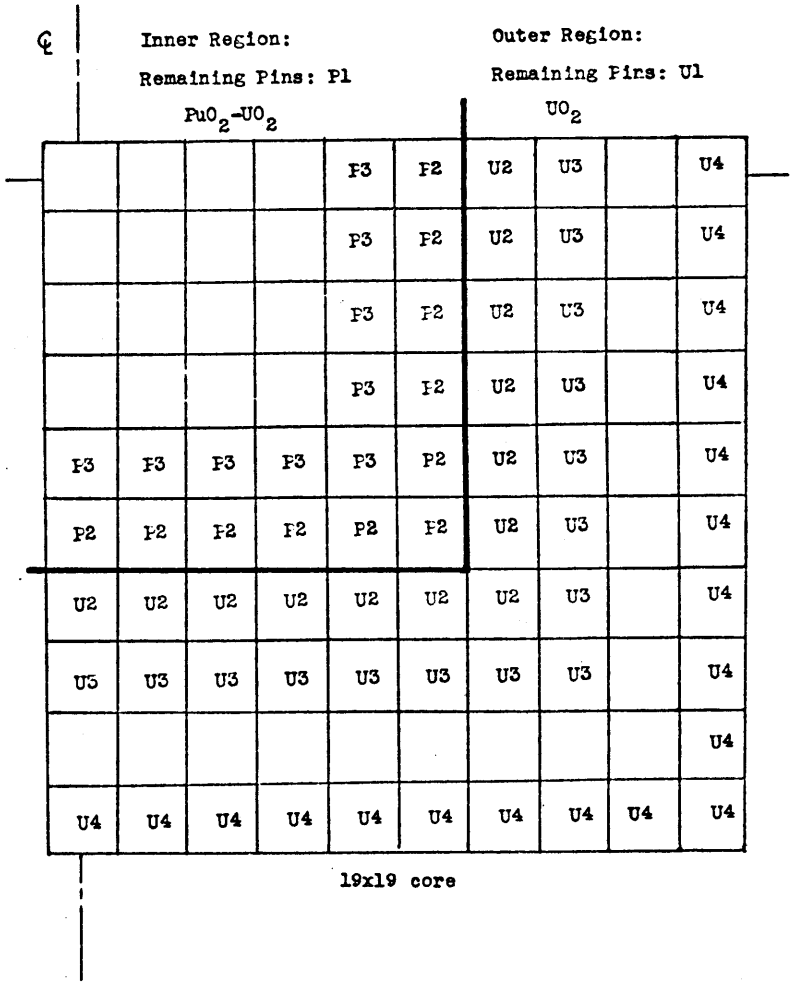

Figure 6.5 Saxton CRX Water Slot (5 Rod) UO_2 Core (19x19)

Pin Designation for TCL-PDQ Calculation

Remaining Pins: U1

℄

℄

Water Slot			U4	U5					U4
U4	U4	U4	U5						U4
U5	U5	U5							U4
									U4
									U4
									U4
									U4
									U4
									U4
U4	U4	U4	U4	U4	U4	U4	U4	U4	U4

Pin Designations for PuO_2-UO_2 Core are analogous

effects of interest at the lattice discontinuities.

6.4.2 Individual Cell Slabs

According to Section 5.3, the individual cell slab model for each Saxton pin type must obey Eqs. (5.1) and (5.2), the latter in comparison with the corresponding unit cell LASER-M results. The value of (t/T) for the slab is defined by Eq. (5.1). The change in the cell thermal flux ratio given by Eq. (5.2) is not strongly sensitive to changes in (t/R_{f+c}), the fuel (plus clad) region half slab thickness to the actual pin radius. As a result, the flux ratio is used as a variable with which to linearly interpolate the correct value of fuel half thickness, t.

Table 6.3 outlines this interpolation procedure, namely for each pin cell,

(1) Two THERMOS individual cell slab cases are calculated with the ratio (t/T) always conserving fuel to moderator volume (Eq. (5.1)) but with t or (t/R_{f+c}) variable, t equal to the values t_1 and t_2, chosen arbitrarily.

(2) The actual unit cell LASER-M ratio of fuel (plus clad) average thermal flux to total cell thermal flux is obtained, as is the same ratio from the calculations in item (1).

(3) Linearly interpolating between (t_1/R_{f+c}) and (t_2/R_{f+c}) to obtain the flux ratio equality (Eq. (5.2)) yields a a cell "Equivalent t/R_{f+c}" for the individual cell slab.

The equivalence of the individual cell slab to the unit

Table 6.3 Determination of THERMOS Individual Slab Fuel and Clad Thickness (t) Equivalent to LASER-M Cylindrical Cell-

Saxton Pins

(t/T)=(fuel plus clad thickness/moderator thickness)= 0.38288 (preserve water to metal ratio)

(t/R_{f+c})=(fuel plus clad thickness/pin outer radius) will be taken as that ratio at which the fuel plus clad to total cell thermal flux ratio is equal to that of the LASER-M cylindrical unit cell. (linear interpolation used)

Pin Type	Fuel plus clad thermal flux/ Total cell thermal flux			Equivalent
	LASER-M	(t_1/R_{f+c})=0.431	(t_2/R_{f+c})=0.863	(t/R_{f+c})
6.6 w/o PuO_2-UO_2	0.7922	0.8033	0.6359	0.460
5.742 w/o U-235	0.8924	0.8915	0.7742	0.429

The values of (t/R_{f+c}) will be those used in the THERMOS multislab for determination of deviation of thermal constants from the THERMOS individual slabs to account for the spectral effect of the cell row by use of TCL (THERMOS corrected LASER-M) constants.

cell, in a spectrum sense, is examinable by relative reaction rate comparison. Table 6.4 shows the fractional isotopic thermal absorptions of the cell slab calculations performed in item (1) for the two values (t_1/R_{f+c}) and (t_2/R_{f+c}), as well as their interpolation to the Equivalent t/R_{f+c}. The relative absorptions are quite comparable to those in the analogous LASER-M calculation. (The percent differences are simply the differences between the two percent absorption values for the Equivalent t/R_{f+c} and LASER-M cases.) The most spectrum sensitive isotope, as is evident from the change in value with change in t, Pu-240, is also reasonably well represented in a cell fractional absorption sense. The good fractional absorption equivalence is justification of Eqs. (5.1) and (5.2) as criteria for equivalence modeling, as required to use the individual cell slabs as indicators of the spectrum environment effects.

6.4.3 Cell Row Multislabs

According to Section 5.4, the cell row multislab modeling of the cell row environment is used to obtain the induced changes in the group parameters by calculation of the percent changes (relative to the individual cell slab values) of the given cell constants. Namely, calculated values of Eq. (5.3) are obtained to express the spectrum influence of the cell row grouping on the individual cell slab parameters. Since effective macroscopic parameters are of interest in the power distribution calculations, the calculation of $(\% \bar{\Sigma}_\alpha)_x$ is performed similar to Eq. (5.3) by use of the macroscopic constants.

Table 6.4 Comparison of Fractional Isotopic Thermal Absorption- LASER-M Normal C/S versus THERMOS Individual Slab C/S for various values of Fuel plus Clad Thickness (t) - Saxton Pins

Pin Type	Isotope	Percent of Cell Total Thermal Absorption				
		$(t_1/R_{f+c})=0.431$	$(t_2/R_{f+c})=0.863$	Interpolated (t/R_{f+c})	LASER-M	Difference (%)
6.6w/o PuO_2-UO_2	U-235	3.6	4.1	3.6	3.8	-0.2
	U-238	2.4	2.6	2.4	2.4	0.0
	Pu-239	80.7	81.9	80.8	80.2	0.6
	Pu-240	10.6	8.8	10.5	9.1	1.4
	Pu-241	0.08	0.08	0.08	0.08	0.0
	Pu-242	0.006	0.006	0.006	0.009	-0.003
	etc.	2.0	1.7	2.0	3.7	-1.7
5.742w/o UO_2	U-235	86.0	86.3	86.0	82.3	3.7
	U-238	6.3	6.3	6.3	5.9	0.4
	etc.	7.7	7.5	7.7	11.9	-4.2

$(\%\,\bar{\Sigma}_\alpha)_x$, according to Section 5.4, is calculated for a unit cell region using parameters from the cell multislab calculation of fuel slab half thickness corresponding to that calculated (Table 6.3) for the individual cell slab. Again a linear interpolation procedure is used to obtain this percent correction term for a given unit cell region, namely

(1) Two THERMOS cell row multislab cases are calculated for each cell row with the ratio (t/T) always given by Eq. (5.1), but with (t/R_{f+c}) variable, t equal to values t_1 and t_2.

(2) $(\%\,\bar{\Sigma}_\alpha)_x$ of a given unit cell region is calculated (similar to Eq. (5.3)) for values of t equal to t_1 and t_2, using the cell row multislab calculations of item (1) and the individual cell slab calculations (Table 6.3) corresponding also to thicknesses t_1 and t_2.

(3) The $(\%\,\bar{\Sigma}_\alpha)_x$ applicable as a TCL thermal group constant correction term for a given unit cell region is that linearly interpolated between those calculated in item (2) for the given "Equivalent t/R_{f+c}" value of the individual cell slab in Table 6.3.

This procedure is demonstrated in Figure 6.6 for the cell row groupings and unit cell region designations of Figure 6.2. The figures show the variation of $(\%\bar{\Sigma}_a)_x$, the relative change in the macroscopic effective thermal absorption of the given unit cell region, as a function of multislab fuel slab thickness, expressed as (t/R_{f+c}). Take, for instance, unit cell region P8, modeling a plutonium pin adjacent to a uranium

Figure 6.6 Variation of THERMOS Multislab Thermal C/S as a Function of Slab Thickness
Saxton Pins

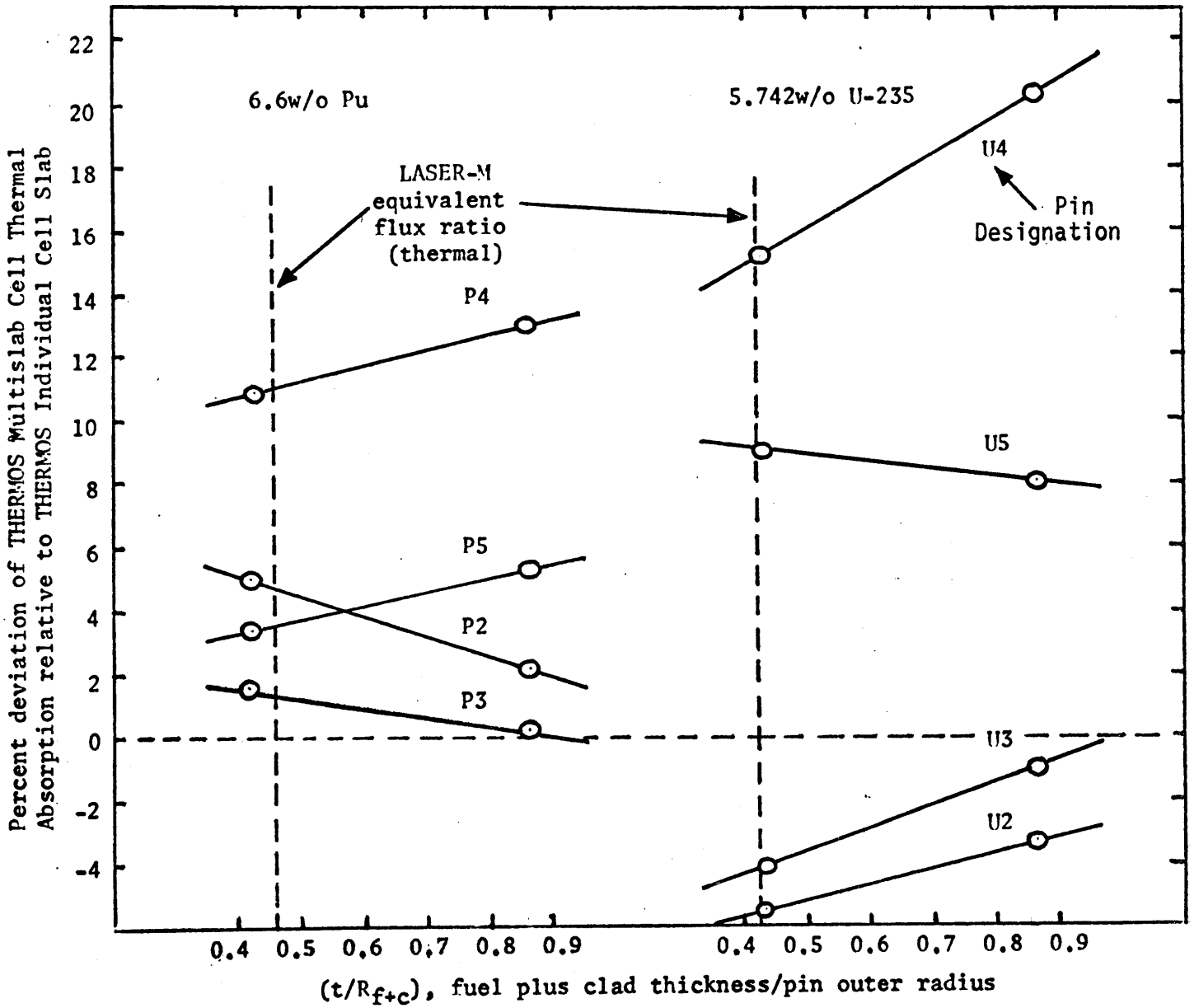

pin. Figure 6.6 shows that the effective macroscopic thermal absorption constant for this multislab unit cell region is more than 5% greater than that of the individual cell slab for a "thin" fuel ($t_1/R_{f+c} = 0.431$) calculation and about 2% greater for a "thick" fuel ($t_2/R_{f+c} = 0.863$) calculation. Linearly interpolating, one obtains for the unit cell equivalent t/R_{f+c} (labeled LASER-M equivalent flux ratio (thermal)) for a plutonium pin a TCL correction factor of about 5% for the cell row influence.

One notices from Figure 6.6 that the thermal absorption values due to the cell row spectrum influences are significant, especially for the water slot pins (U4,U5,P4 and P5). The variations are not too strongly dependent upon (t/R_{f+c}), indicating that the linear interpolation methods of this section and Section 6.4.2 are sufficient.

The values of $(\%\overline{\Sigma}_a)_x$ (from Figure 6.6) and $(\%\overline{\nu\Sigma}_f)_x$, as interpolated to the correct equivalent thickness for the given cell, are displayed in Figure 6.7, these being the TCL correction terms. Notice the significant increases due to the water slot thermalization, even distant from the water itself. These values are probably overestimates due to the assumed reflecting boundary at the end locations. A more extensive calculation (spatially) could resolve the question. Notice also the spectral softening of the mixed oxide region (higher values) and spectrum hardening of the uranium regions (lower values).

6.4.4 TCL Thermal Group Constants

In accordance with the discussion of Section 5.5, the val-

Figure 6.7 Variation of THERMOS Cell Row Thermal Constants- Saxton CRX Multiregion and Water Slot Cores

A. Mixed Oxide Boundary:

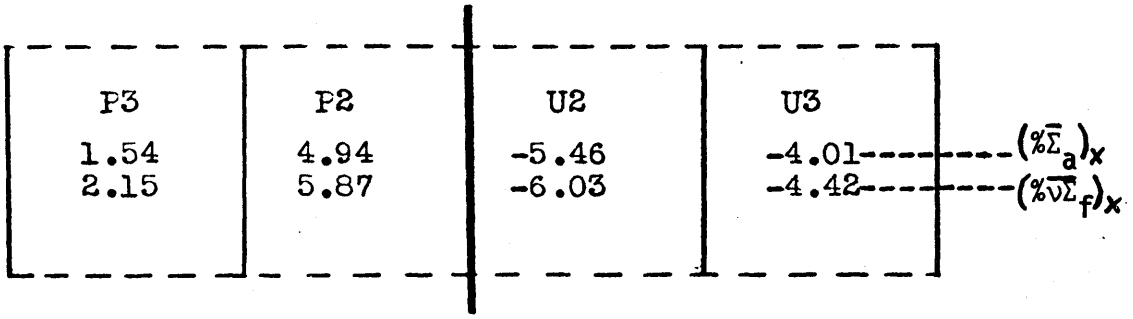

(Variation relative to Individual Cell Slab Constants)

B. Water Slots:

Uranium Core

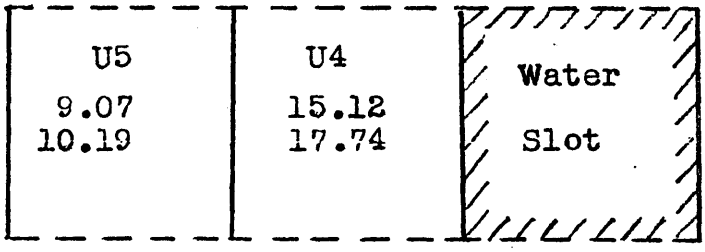

Mixed Oxide Core

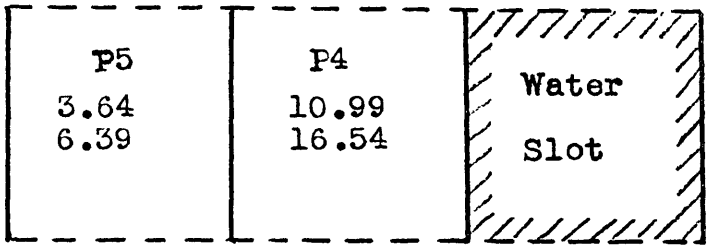

ues of $(\%\overline{\Sigma}_\alpha)_x$ are correction terms to the x direction cell row environments of the unit cell regions. Notice that the cells transverse to those of Figure 6.2 for all the core configurations are of the same cell type, so that they are non-influential in a spectral sense. That is, the transverse factors, $(\%\overline{\Sigma}_\alpha)_y$, are zero. So, the two dimensionally "averaged" environment correction factor becomes, analogous to Eq. (5.5),

$$C = 1 + 1/2 \left(\frac{(\% \overline{\Sigma}_\alpha)_x}{100} \right) \tag{6.2}$$

to define the TCL macroscopic thermal group constant as

$$\overline{\Sigma}_\alpha^{TCL} = C \quad \overline{\Sigma}_\alpha^{LASER\text{-}M} \tag{6.3}$$

The LASER-M Normal macroscopic group constants are used in Eq. (6.3) in this study. An alternate approach would be use of the GMND constants, which is valid from the continuity of activation argument of Section 2.2.3. The rationale accepted in this study, however, is that of assessment of the methods (GMND and TCL) as independent means of solution to the spectral complexity problem.

The possible application of the TCL method to the GMND constants, if performed, should be based on consistent use of GMND values throughout the THERMOS slab calculations. That is, the correction factor in Eq. (6.2) should contain the percent change in $\overline{\Sigma}_\alpha^{GMND}$ (i.e., $(\overline{\Sigma}_\alpha^{Normal} \overline{\nu}_{cell})$) in the multislab calculation relative to the individual cell slab calculation.

Application of Eq.(6.3) is made for $\overline{\Sigma}_a$, $\overline{\nu\Sigma}_f$, and $\overline{\kappa\Sigma}_f$ (see Section 3.1.3) of the appropriate cell regions in the core

configuration (Figures 6.3 to 6.5). The values of $\bar{D}$ (or $\bar{\Sigma}_{tr}$) representative of the LASER-M unit cell (normal constants) are retained for each region. Similar TCL factors would be calculable for $\bar{D}$, however, the THERMOS version available did not provide a spectrum averaged diffusion coefficient. Inclusion of this effect can be observable, although not as significant as the adjustments in the cell reaction rates.

The group constants for the water regions are taken equal to the LASER-M Normal constants. This characterizes the water as a well thermalized region. There is good reason, however, to apply a similar correction term to the water cell constants, indicative of the water region environment. Indeed, the macroscopic absorption for the THERMOS water region in the plutonium pin environment was 4% less than that of the water region among uranium pins. This difference would be of more significance if more absorption (i.e., significant boron content) were present in the water region.

6.5 Spatial Analysis by Few Group Diffusion Theory: PDQ-7 Relative Power Distribution Calculations

The Saxton CRX core configurations (Figures 6.3 to 6.5) are analyzed for two dimensional pin relative power values by the spatial diffusion theory code PDQ-7 (see Section 3.1.3). Three separate methods were used to provide group averaged, two group effective region constants for these calculations. They are designated as LASER-M Normal, LASER-M GMND and TCL group constants, as obtained in Sections 6.3 and 6.4. The

methods are compared primarily on their ability to predict power peaking at uranium- mixed oxide pin type boundaries and at pins adjacent to water slots, the types of discontinuities intentionally incorporated in these lattices.

6.5.1 Input Description

A general description of the spatial diffusion theory code PDQ-7 is given in Section 3.1.3. The calculations performed were two dimensional relative power distributions. That is, values are obtained for each unit cell region to express the power production in that pin relative to the average power production. Two group effective constants represent the relative reaction probabilities (per unit volume) in each region.

The following points summarize the input details of the calculations. The PDQ-7 computer input listings are given in Appendix A.

(1) Macroscopic, effective two group constants were used.

(2) A unit cell region was modeled pointwise as a 2 x 2 spatial mesh region. This is a standard procedure for pinwise diffusion theory calculations. An extra mesh point representation is at times used in strong flux gradient areas (e.g., Westinghouse calculations for the Saxton cores, Section 6.5.3). This is anticipated to be unnecessary as a result of the careful spectral- spatial treatment, especially in the TCL method. It is also hoped to be avoided due to input complications and computer storage limitations in large problems.

(3) The core axial leakage is represented by an axial buckling term which was input as the experimental value (0.00113 cm^{-2}) for both single region core types. This value is assumed both group and region independent in the input. This is a poor assumption for this small a core and introduces problems in the power distribution correspondence with experiment at the core boundary regions. This problem does not affect the methods comparison since the lattice discontinuities of primary interest are centrally located in the core.

(4) Core boundary reflection is modeled by about twenty (20) pitch lengths of moderator containing five (5) spatial points. The core calculation requires a zero flux boundary condition. The moderator for reflection represents the amount through which the fast (two group) flux would be approximately 3% of its value right at the core boundary. This value was calculated via the fast age approximation and exponential flux shape using the LASER-M unit cell fast age value. Correct core boundary modeling is important to the relative power distribution calculation.

(5) Quarter core symmetry exists in all of the core configurations presented, so that this is the core portion modeled with reflecting boundary conditions at the core centerlines and zero flux boundary conditions at the edge of the core boundary moderator.

6.5.2 Comparison of Results

Calculated results from the PDQ calculations using LASER-M

Normal, LASER-M GMND and TCL group constants are compared on a pin relative power basis with the experimental values. The experimental data was taken in terms of pin power relative to a reference pin (a pin designated with a power of 1.000) and the calculated values are expressed in the same way.

The percent deviation of a calculated pin power value from the experimental value is expressed as

$$\text{Percent (\%) Deviation} = \frac{\text{Calculated} - \text{Experimental}}{\text{Experimental}} \times 100 \qquad (6.4)$$

The average pin error, in percent, for a series of pin values is the average of the absolute values of the individual pin deviations.

The Saxton CRX configurations are classified according to single region cores, water slot cores and multiregion cores. The comparison is presented for different groupings of pins, namely the central cell row (also termed a flat core traverse), which follows the path from the core boundary to the center along the core centerline, or selected pins from the full quarter core region (see Figure 6.1).

6.5.2.1 Single Region Cores

The single region cores are full uranium or mixed oxide pin cores. These are the reference cores upon which to base the effect of discontinuities introduced in succeeding configurations.

The UO_2 core central cell row relative pin power values

are compared to the Normal and GMND group constants results in Figure 6.8. It should be recognized that, due to the lack of spectrum discontinuities, TCL and Normal group constants are equal, except for the boundary pins. This makes a slight difference in the Rod Number 3 pin relative power value, but essentially the TCL and Normal results are equal.

The trend of deviation resulting from the inadequacy in the modeling of these cores is shown in the figure and discussed in Sections 6.2.2 and 6.5.1. That is, the general flux curvature across the core is underestimated, so that the percent deviations grow positive (assumed zero at the core center) as one travels from the core center region (Rod Number 8) towards the core boundary. (The data from the reference has been renormalized to Rod Number 8 to demonstrate this effect. Such renormalization has been performed for other selected configurations.)

The average pin error is roughly twice the experimental (2σ) error, but good enough for the core central region pins to allow adequate methods comparison. The GMND results, in this case, are slightly better than the Normal (or TCL) results.

The analogous figure for the PuO_2-UO_2 core is given in Figure 4.9. Here the flux curvature is only slightly underestimated and the results are very good. Figures 6.10 to 6.12 show the quarter core configurations of the same calculations, normalized to a different pin, for the three methods. The renormalization makes the underestimation more evident. The results are good and the GMND method is slightly better by the average pin error criteria.

Figure 6.8

Saxton CRX Reference UO_2 Core
Central Row Relative Power
Distribution Comparison

Experimental Values compared to LASER-M, PDQ calculations using Normal or GMND values of Two Group Constants

Reference:

WCAP 3385-54, Appendix A,
Table IV, p.7
Estimated values (Est) from
Appendix A, Figure 4,
p. 11 (read from graph)

Average Pin Error:

Normal C/S: 2.88%

GMND C/S: 2.32%

Experimental Accuracy:

±1.4% (=2σ)

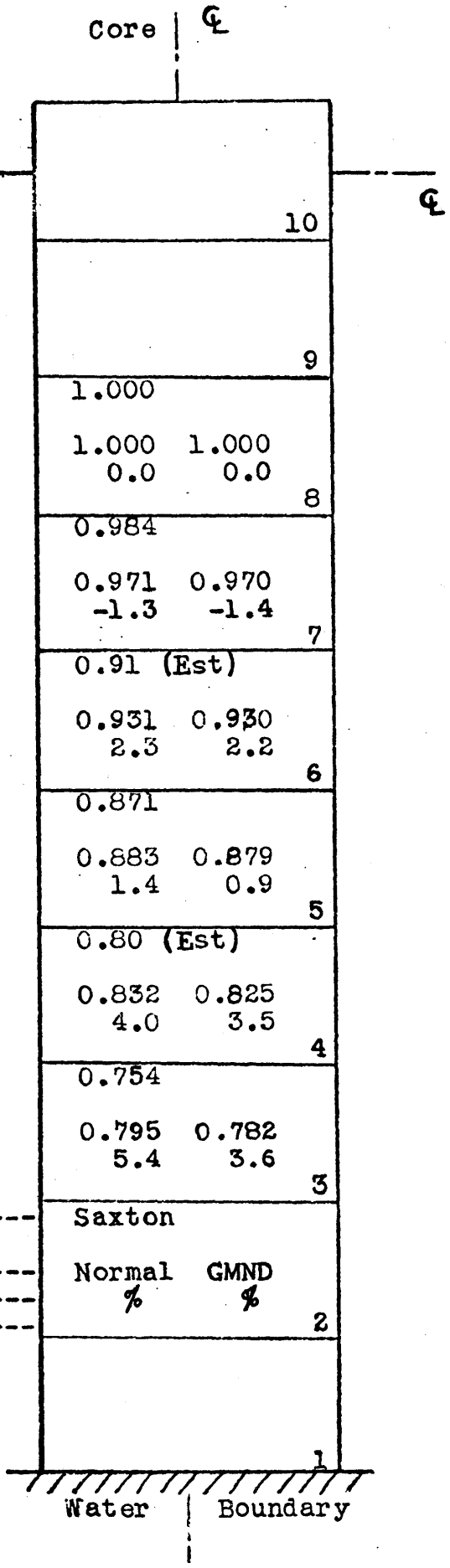

Relative Power:
(Referenced to Pin 8)
Experimental----------
Calculated using given
Two Group Constants----------
Deviation from Experimental----
Rod Number from Boundary-------

Figure 6.9

Saxton CRX Reference PuO_2-UO_2 Core Central Row Relative Power Distribution Comparison

Experimental values compared to LASER-M, PDQ calculations using Normal or GMND values of Two Group Constants

Reference:

WCAP 3385-54, Appendix A, Table IV, p. 7

Average Pin Error:

Normal C/S: 1.72%

GMND C/S: 1.45%

Experimental Accuracy:

±1.4% (=2σ)

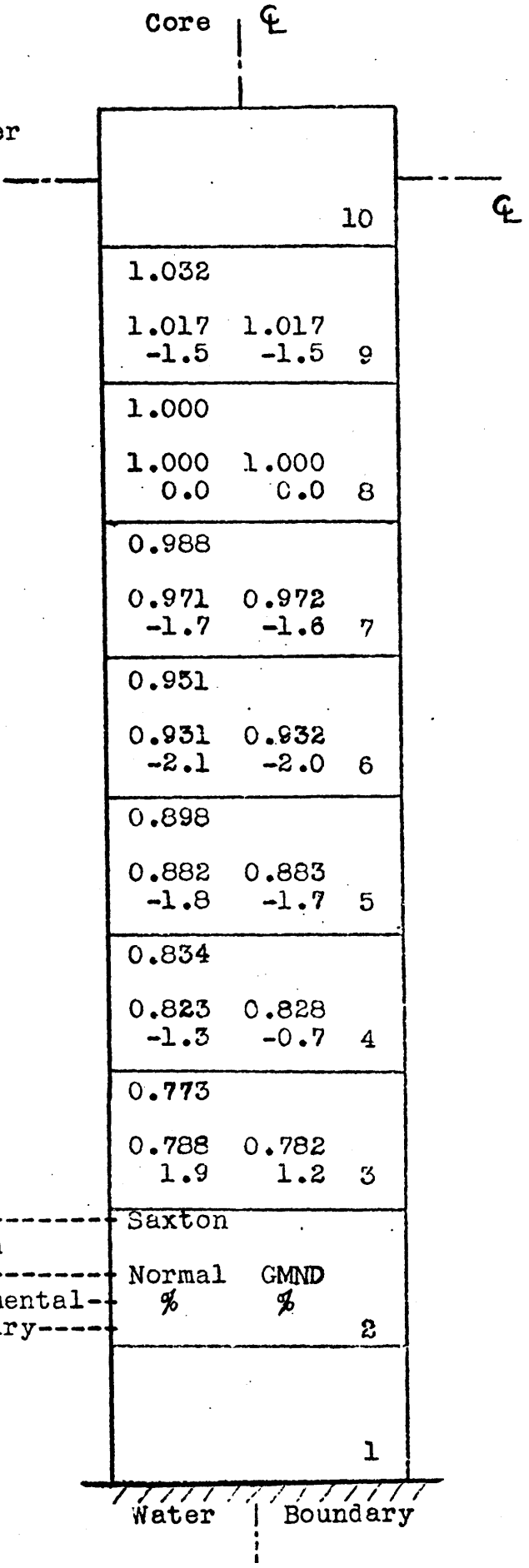

Relative Power:
(Referenced to Pin 8)
Experimental
Calculated using given Two Group Constants
Deviation from Experimental
Rod Number from Boundary

Figure 6.10 Saxton CRX Reference PuO_2-UO_2 Core Relative Power Distribution Comparison- Normal C/S

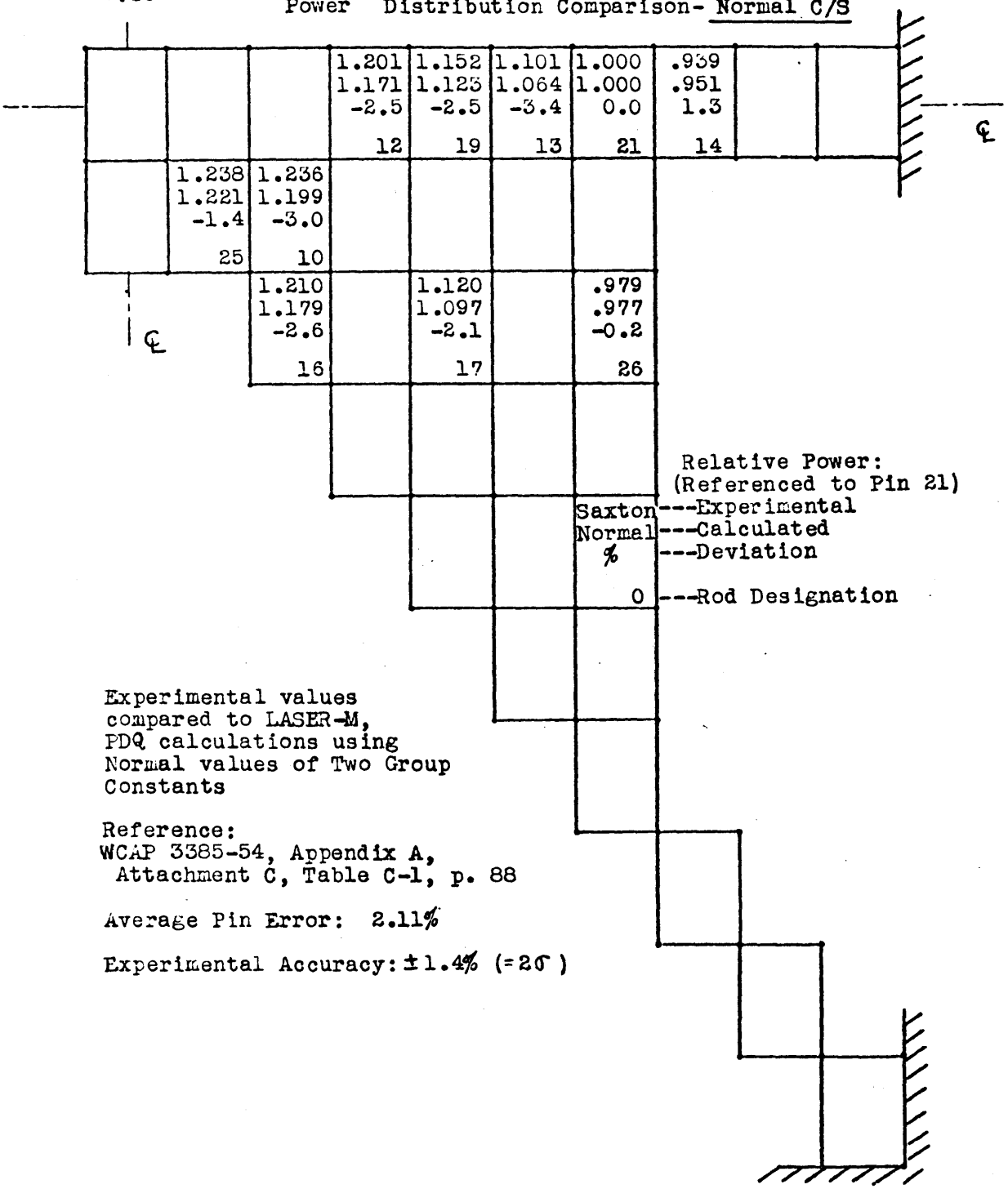

Experimental values compared to LASER-M, PDQ calculations using Normal values of Two Group Constants

Reference:
WCAP 3385-54, Appendix A, Attachment C, Table C-1, p. 88

Average Pin Error: 2.11%

Experimental Accuracy: ±1.4% (=2σ)

Figure 6.11 Saxton CRX Reference PuO_2-UO_2 Core Relative Power Distribution Comparison- GMND C/S

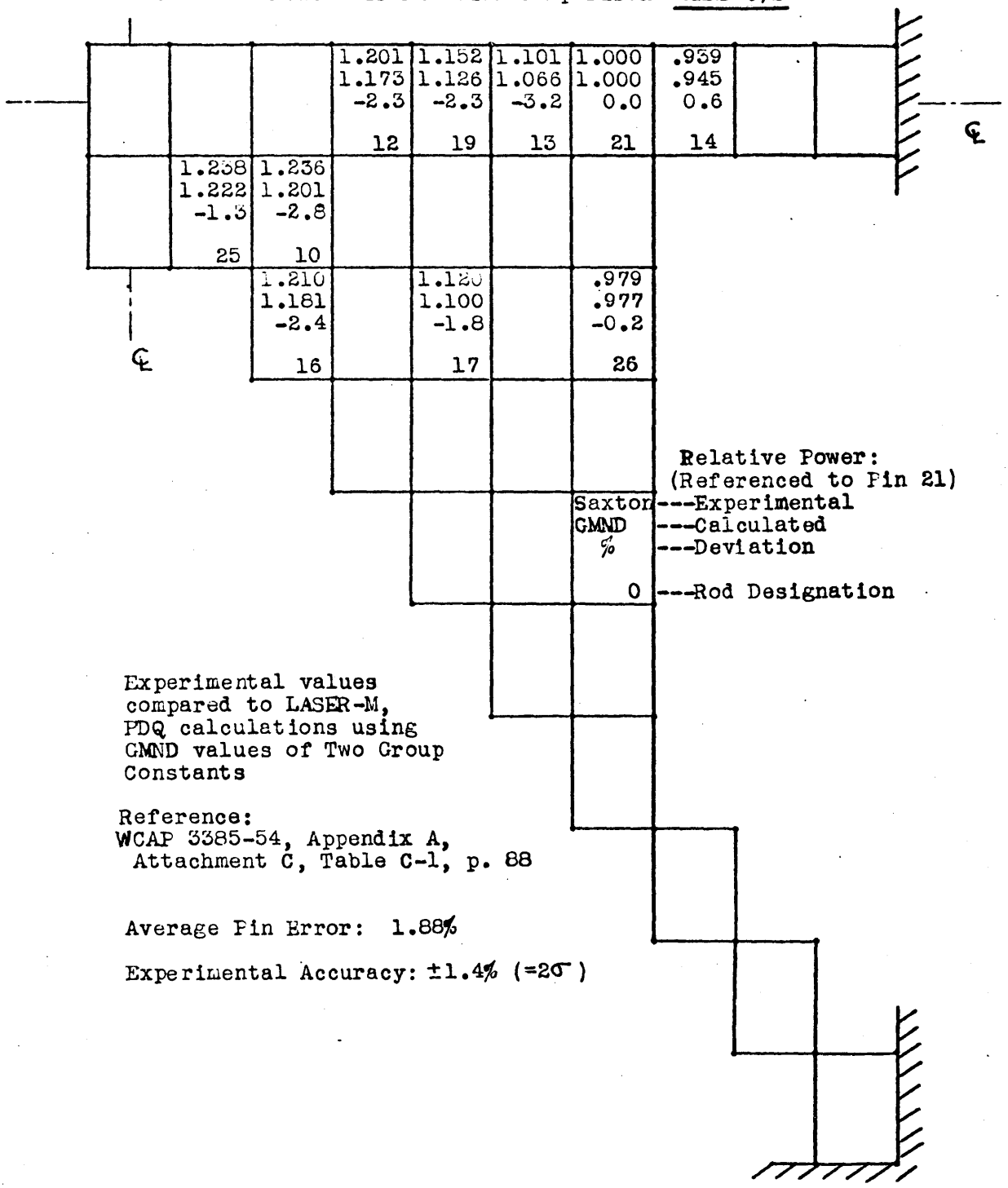

Figure 6.12 Saxton CRX Reference PuO_2-UO_2 Core Relative Power Distribution Comparison- TCL C/S

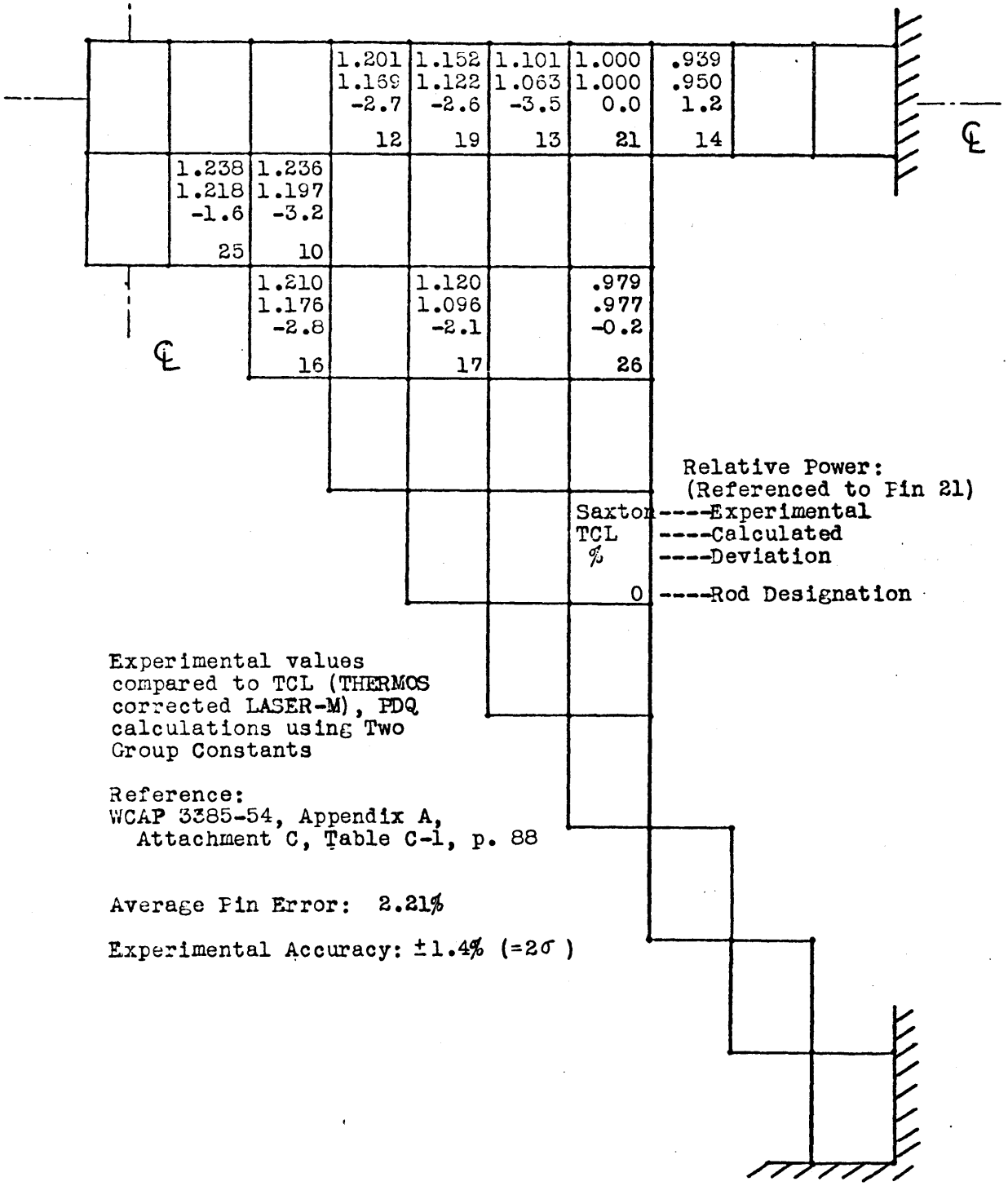

Experimental values compared to TCL (THERMOS corrected LASER-M), PDQ calculations using Two Group Constants

Reference:
WCAP 3385-54, Appendix A, Attachment C, Table C-1, p. 88

Average Pin Error: 2.21%

Experimental Accuracy: ±1.4% (=2σ)

The single region core results are sufficiently good to allow for comparisons of the calculational methods on the basis of their ability to predict relative powers in spectrum disturbance regions (near midcore).

6.5.2.2 Water Slot Cores

Single region cores are transformed to water slot cores by the removal of five (5) central rods, as illustrated in Figure 6.1. Figure 6.13 gives the central cell row calculated results for the UO_2 core, for the cell row perpendicular to the water slot.

It is evident here that the GMND and TCL methods can adequately handle the slot power peaking. The Normal constants poorly underpredict the adjacent pin slot power. The GMND method results are the most acceptable, although the TCL results are better than is apparent from the percent deviation at the adjacent pin to the slot. This is due to the normally expected low values of this pin power from the overall core flux curvature underprediction discovered in the single region core calculations (Figure 6.8). Another interesting observation is that of the TCL method overprediction at Rod Number 8 and underprediction at Rod Number 7. Such might have been averted were the TCL method applied more than a two fuel pin distance from the water slot (Figure 6.2). This should be evident from the sufficiently large spectrum influence on this second pin in Figure 6.7, indicating that the effect on the third pin would not be negligible. Both the GMND and TCL results, however, are

Figure 6.13

Saxton CRX UO_2 Core with 5 Rod Central Water Slot- Row Relative Power Distribution Comparison

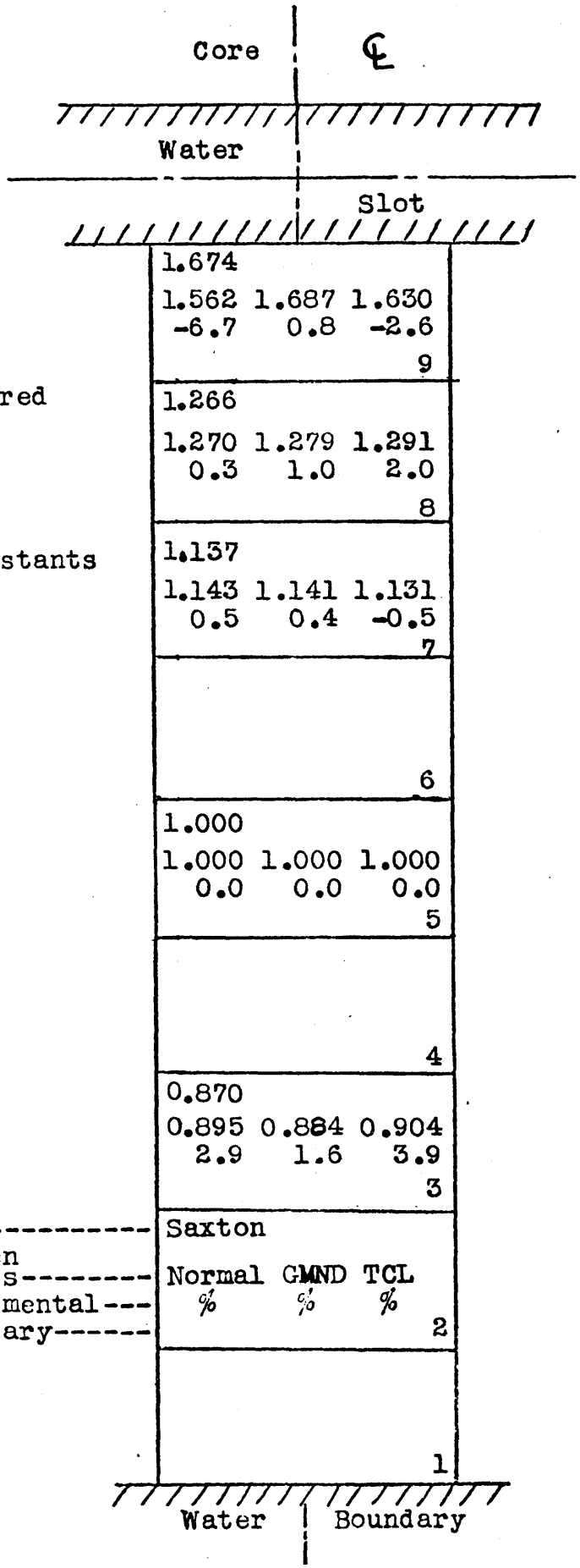

Experimental values compared to:
- LASER-M Normal
- LASER-M GMND
- TCL (THERMOS corrected LASER- M)

values of Two Group Constants for PDQ calculation.

Reference:
WCAP 3385-54, Appendix A, Table IV, p. 7

Average Pin Error:

LASER-M Normal:	2.60%
LASER-M GMND:	0.95%
TCL:	2.20%

Experimental Accuracy:

$\pm 1.4\%$ ($=2\sigma$)

Relative Power:
(Referenced to Pin 5)
- Experimental
- Calculated using given Two Group Constants
- Deviation from Experimental
- Rod Number from Boundary

acceptable for this UO_2 core water slot power peaking case.

The central cell row water slot calculated results for the PuO_2-UO_2 core are shown in Figure 6.14. Figures 6.15 to 6.17 are the full quarter core resultsfor the three calculational methods. Again it is clear that the Normal constants cannot sufficiently reproduce the correct slot adjacent pin peaking. Both the GMND and TCL model results are very good, considering the core flux curvature problem. The problem is most pronounced in the quarter core figures due to the reference pin position. It is evident that the water spectrum effect does not propogate as far in the mixed oxide lattice as it does in the uranium one, as seen from the change in the group constants of the pin furthest from the slot in Figure 6.7. In the mixed oxide case, therefore, a two unit cell plus water slot TCL multislab model appears to be sufficient.

In conclusion, the water slot power peaking predictive abilities of the GMND and TCL methods (with PDQ-7) for these cases are good (TCL) to very good (GMND). The Normal group constants are unacceptable, grossly underpredicting the water effect.

6.5.2.3 Multiregion Cores

The multiregion cores consist of uranium pins with inner regions of mixed oxide pins in either an 11 x 11 or 3 x 3 centrally located array, as depicted in Figures 6.1, 6.3, and 6.4.

The experimental analysis is complicated by the use of two separate techniques which yield consistently dissimilar

Figure 6.14

Saxton CRX PuO_2-UO_2 Core with 5 Rod Central Water Slot- Row Relative Power Distribution Comparison

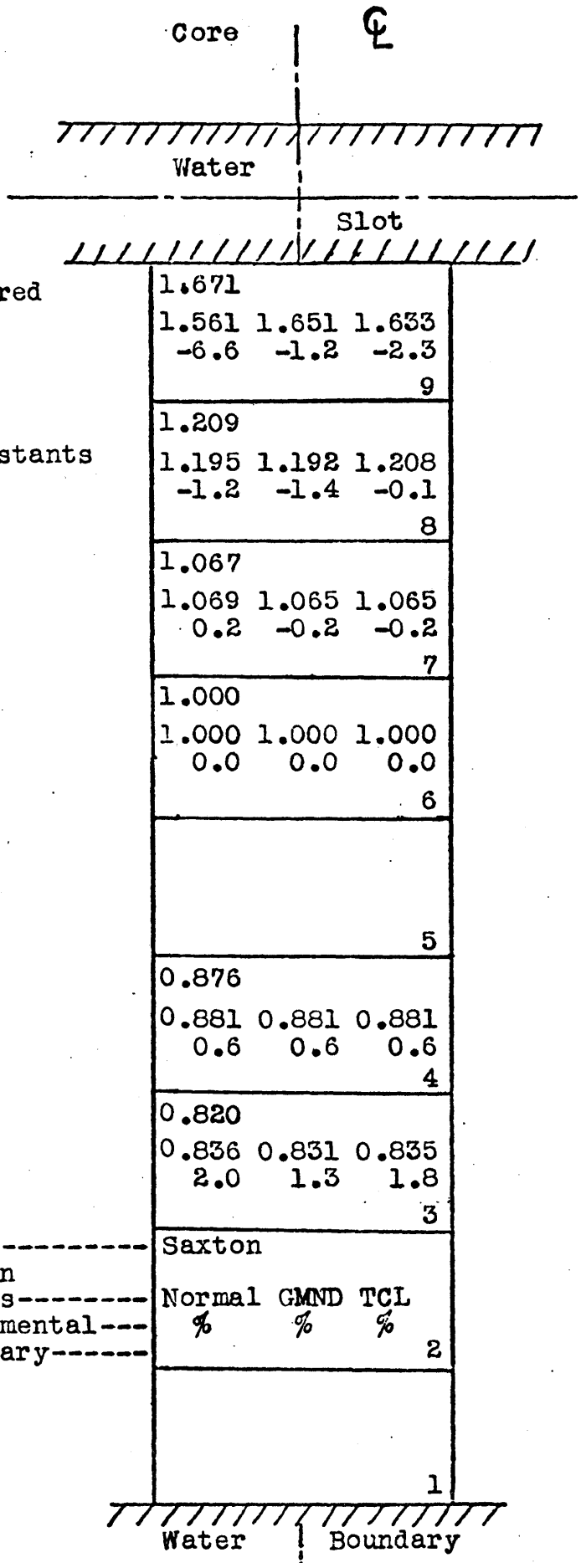

Experimental values compared to:
- LASER-M Normal
- LASER-M GMND
- TCL(THERMOS corrected LASER-M)

values of Two Group Constants for PDQ calculation.

Reference:
WCAP 3385-54, Appendix A, Table IV, p. 7

Average Pin Error:

LASER-M Normal:	2.12%
LASER-M GMND:	0.94%
TCL:	1.00%

Experimental Accuracy:

$\pm 1.4\%$ ($=2\sigma$)

Relative Power:
(Referenced to Pin 6)
- Experimental----------
- Calculated using given Two Group Constants--------
- Deviation from Experimental---
- Rod Number from Boundary------

Figure 6.15 Saxton CRX PuO_2-UO_2 Core with 5 Rod Central Water Slot Relative Power Distribution Comparison- Normal C/S

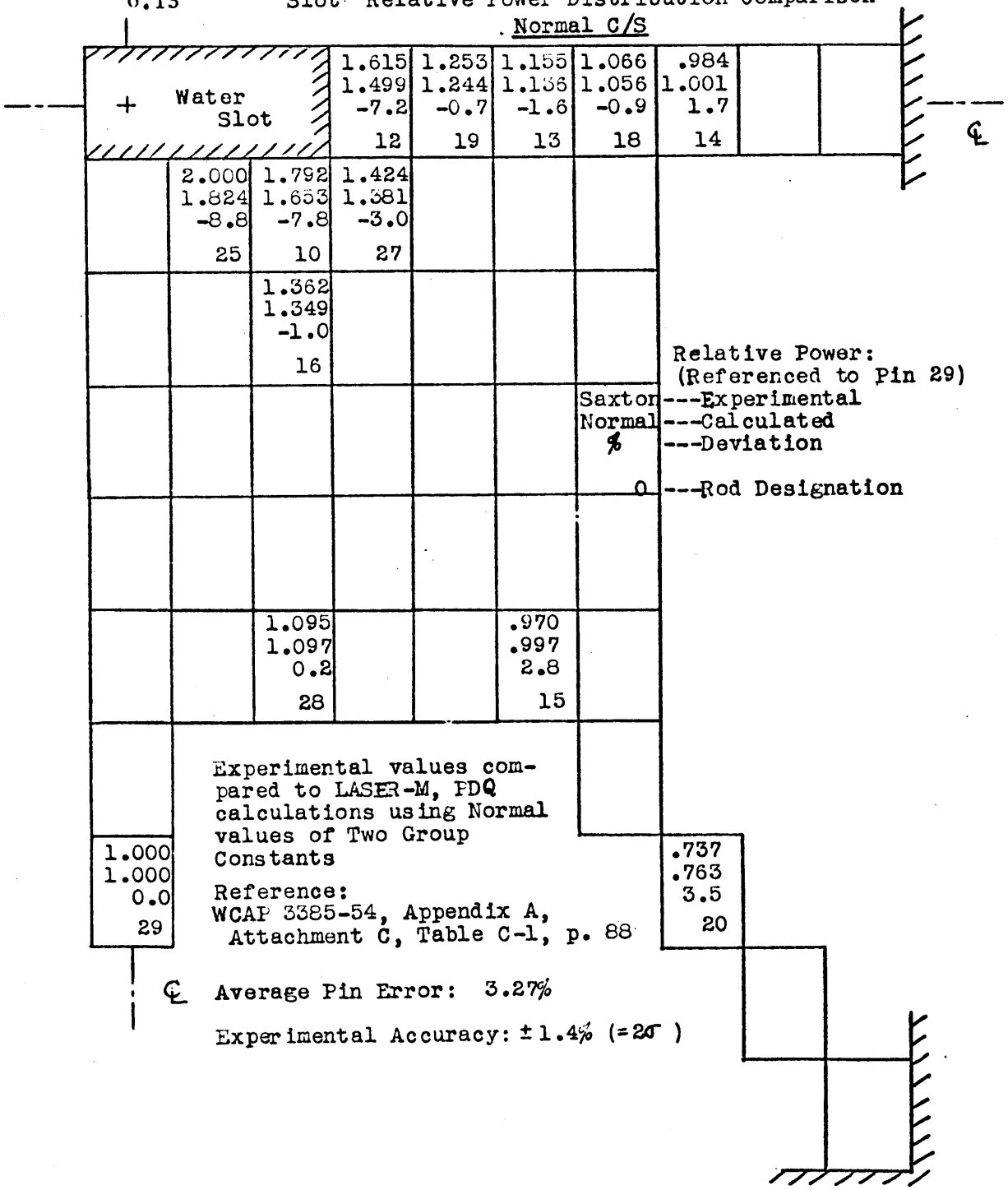

Figure 6.16 Saxton CRX PuO_2-UO_2 Core with 5 Rod Central Water Slot Relative Power Distribution Comparison- GMND C/S

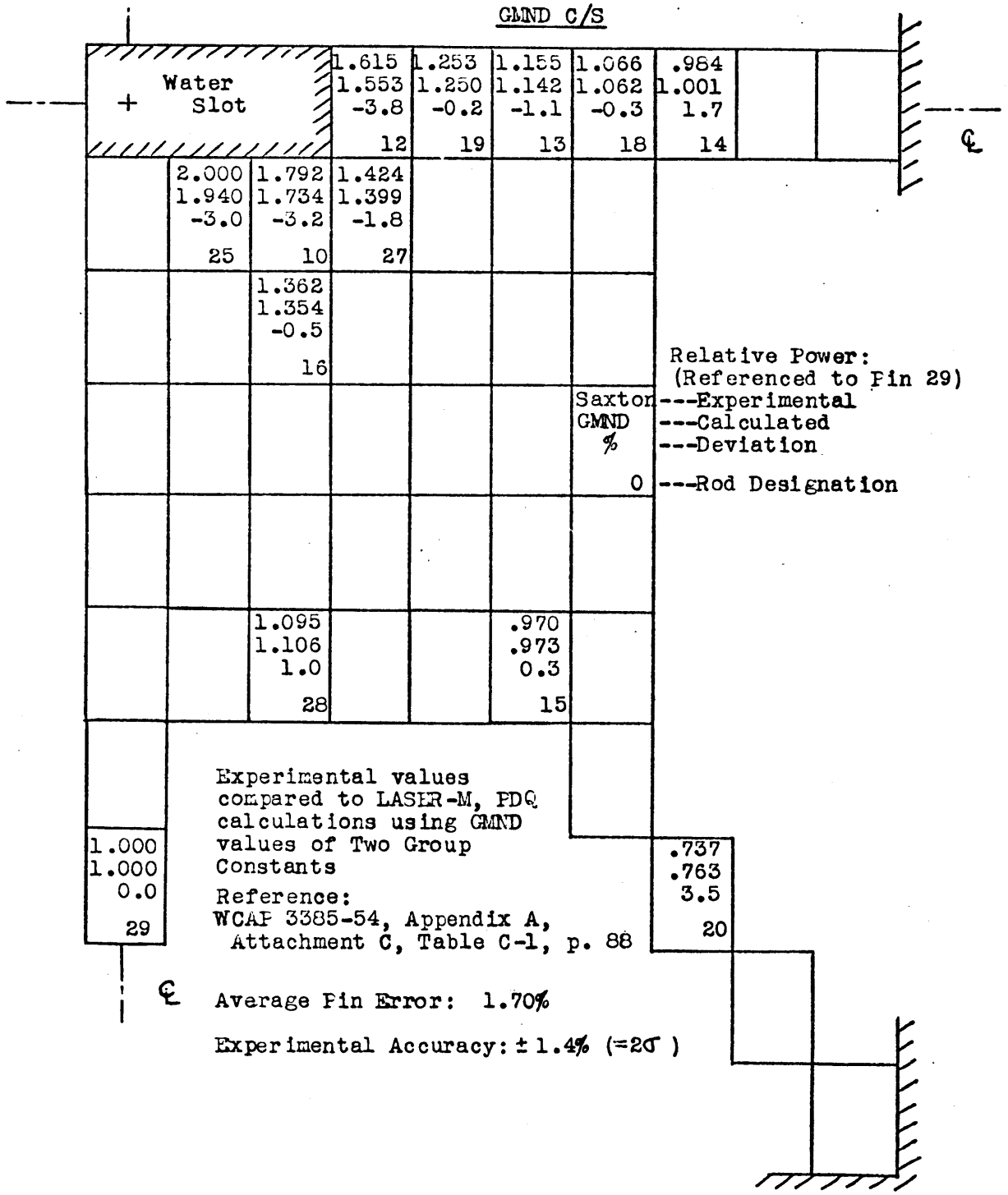

Figure 6.17 Saxton CRX PuO_2-UO_2 Core with 5 Rod Central Water Slot Relative Power Distribution Comparison- TCL C/S

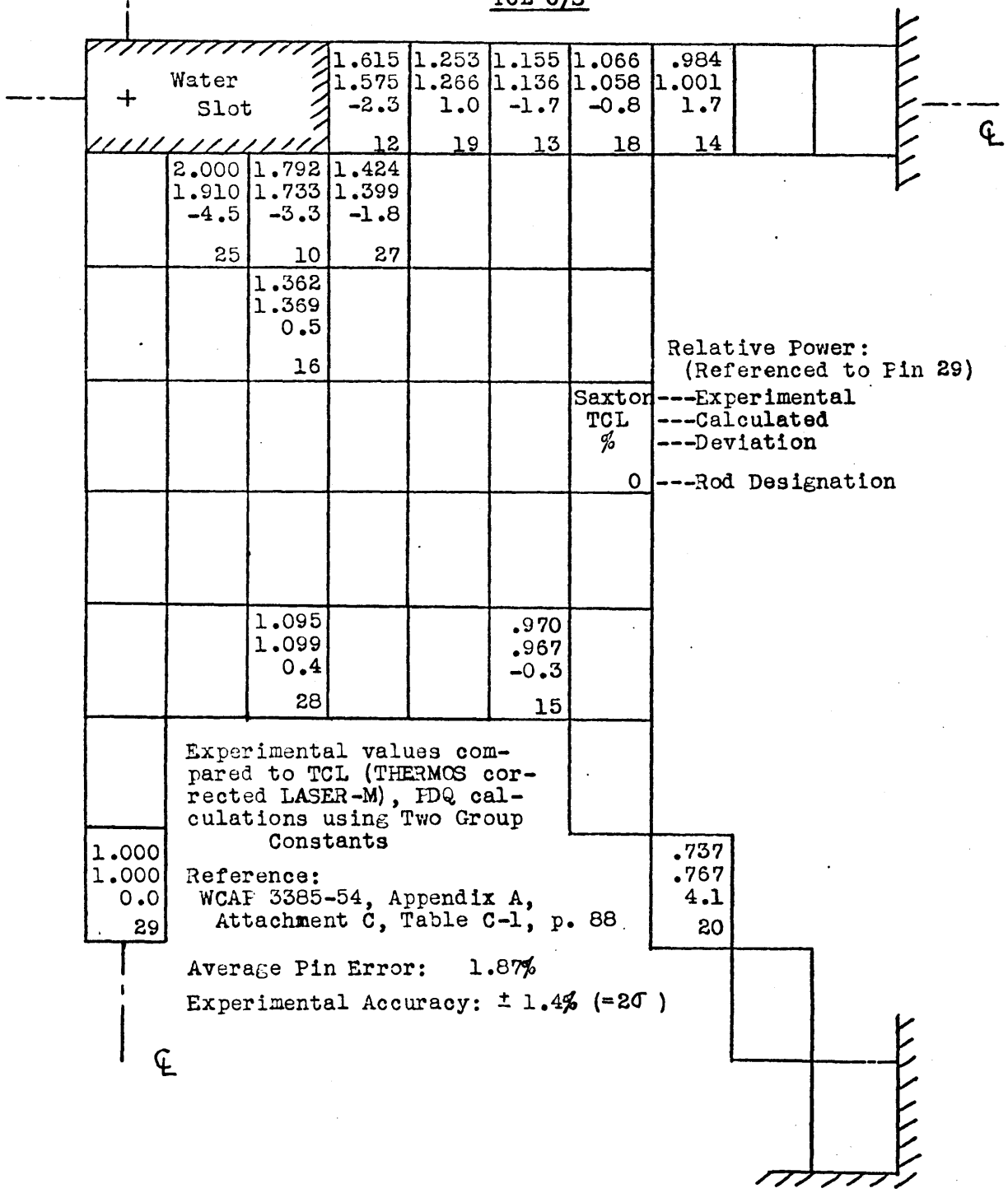

results. The methods are the foil and thermal methods, as discussed in Section 6.2.1. The thermal method, it is recalled, measures higher average plutonium pin powers (about 5%) relative to the foil method. Therefore, correspondence of calculations must be discussed relative to a given method.

The 11 x 11 inner mixed oxide region quarter core power distributions by the foil method for the three analysis methods are given in Figures 6.18 to 6.20. As previously seen, the core boundary pins are in poor agreement, especially near the core corner, for each method of analysis. The primary pins of interest, near the pin type region boundary, are in good agreement with the foil experimental results for all methods of analysis. Notice that the mixed oxide boundary pin peaking is most accentuated by the TCL method, followed by the GMND method and finally the Normal method. In this sense, the TCL method is the most conservative.

The thermal experimental results for this same 11 x 11 mixed oxide region configuration and the comparison with the analytical methods results are given in Figures 6.21 to 6.23. Since the reference pin is in the mixed oxide region, each mixed oxide pin relative power value is equal to the foil method result. The thermal method uranium pin values, however, are demonstrably lower than the foil method values (from a plutonium (mixed oxide) reference pin). It is noticed that the good analysis correspondence with the foil experimental data means a poor correspondence (overprediction) of uranium pin powers relative to the thermal method experimental data

Figure 6.18 Saxton CRX Multiregion (11 x 11 Inner) Core Relative Power Distribution Comparison-Normal C/S,Foil Method

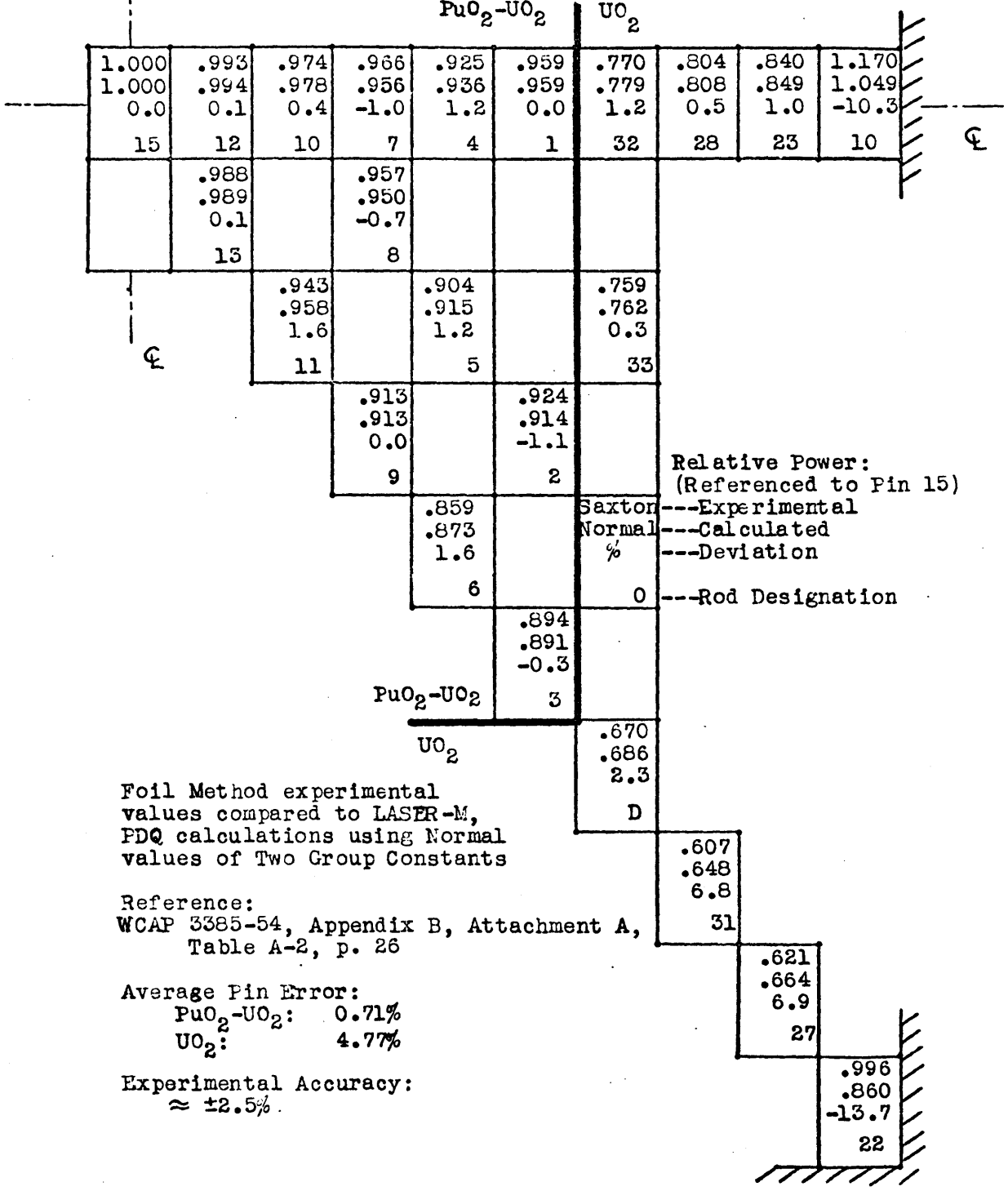

Foil Method experimental values compared to LASER-M, PDQ calculations using Normal values of Two Group Constants

Reference:
WCAP 3385-54, Appendix B, Attachment A, Table A-2, p. 26

Average Pin Error:
PuO_2-UO_2: 0.71%
UO_2: 4.77%

Experimental Accuracy:
≈ ±2.5%.

Figure 6.19 Saxton CRX Multiregion (11 x 11 Inner) Core Relative Power Distribution Comparison- GMND C/S, Foil Method

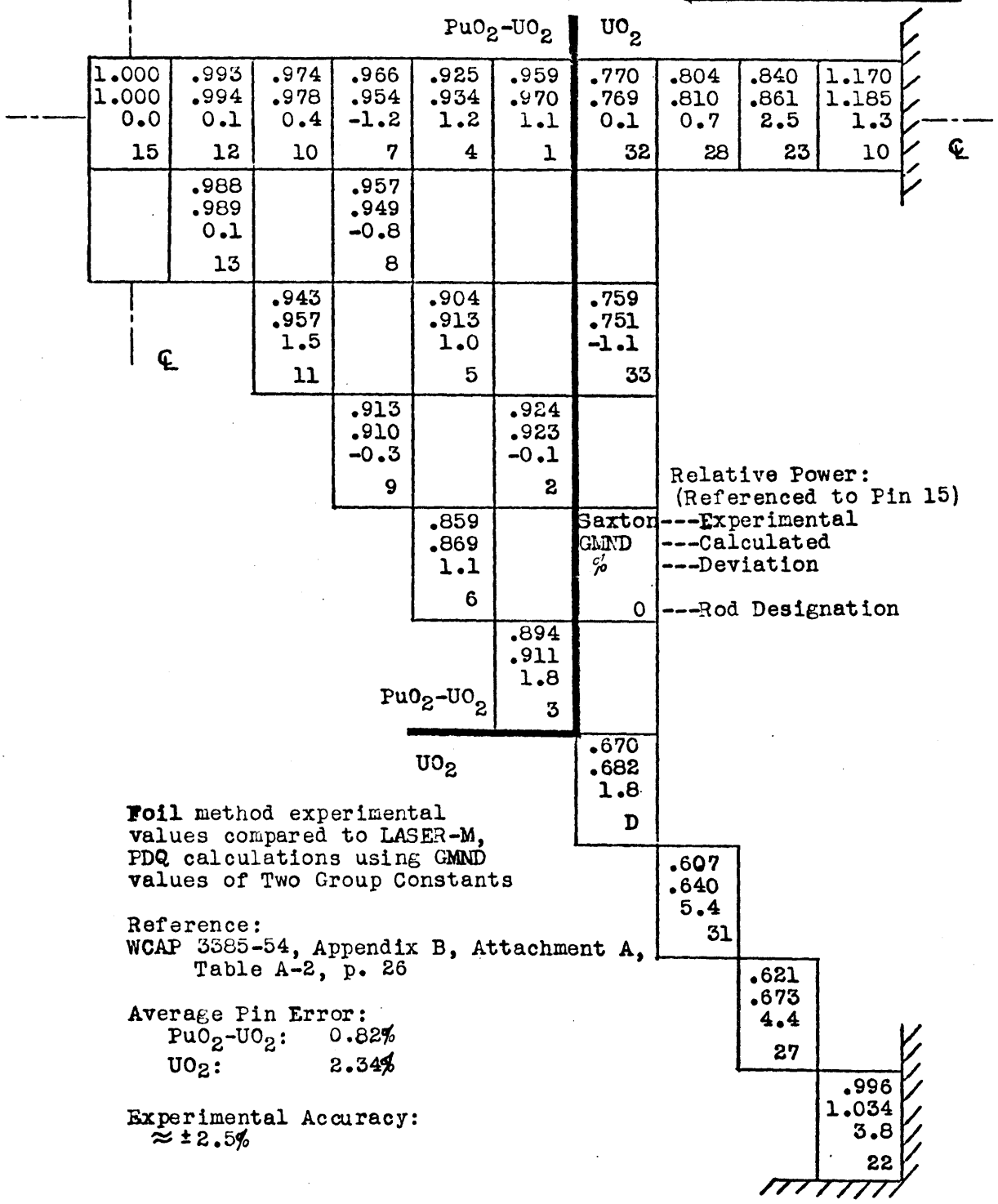

Foil method experimental values compared to LASER-M, PDQ calculations using GMND values of Two Group Constants

Reference:
WCAP 3385-54, Appendix B, Attachment A, Table A-2, p. 26

Average Pin Error:
PuO_2-UO_2: 0.82%
UO_2: 2.34%

Experimental Accuracy:
$\approx \pm 2.5\%$

Figure 6.20 Saxton CRX Multiregion (11x11 Inner) Core Relative Power Distribution Comparison- TCL C/S, Foil Method

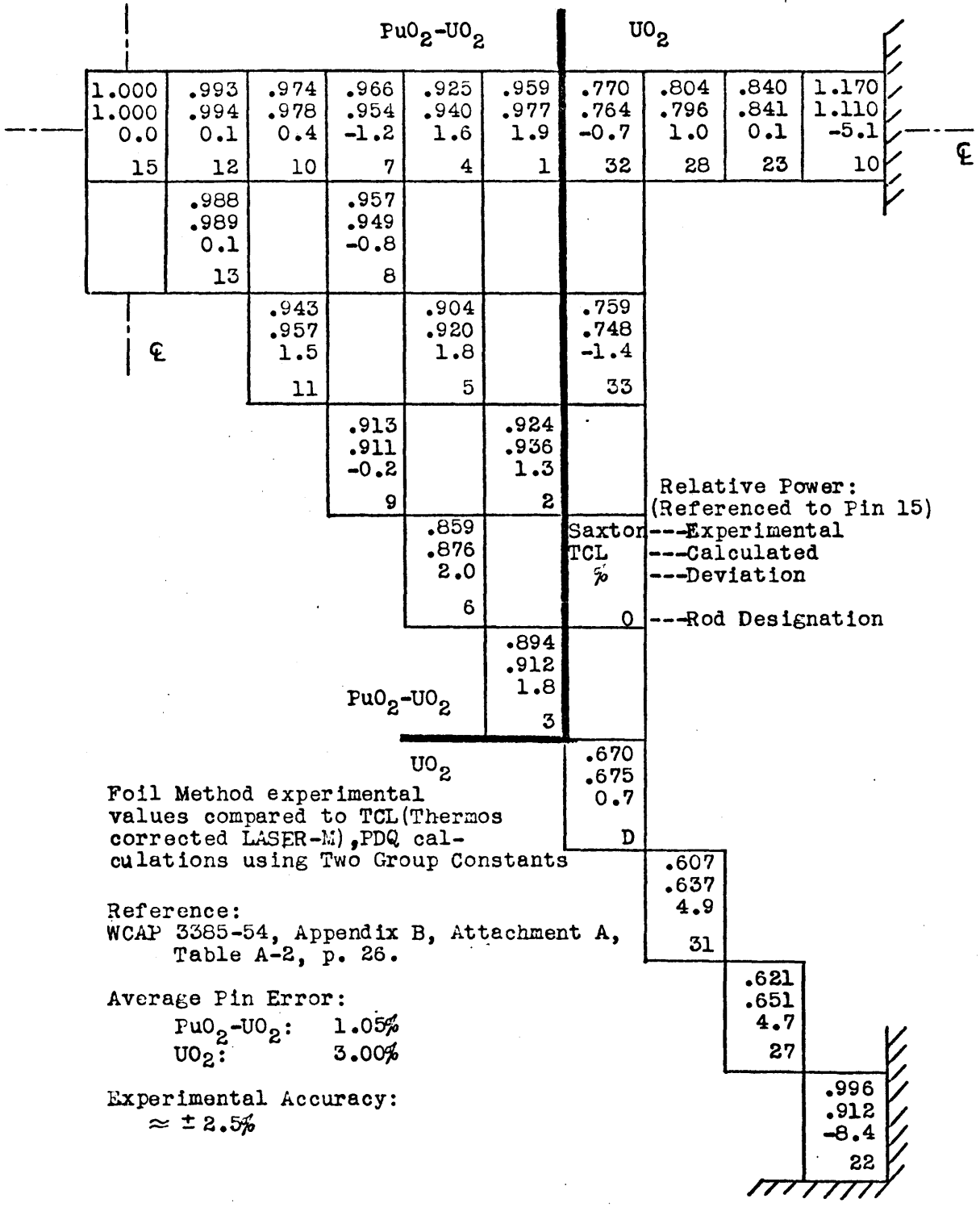

Foil Method experimental values compared to TCL(Thermos corrected LASER-M),PDQ calculations using Two Group Constants

Reference:
WCAP 3385-54, Appendix B, Attachment A, Table A-2, p. 26.

Average Pin Error:
PuO_2-UO_2: 1.05%
UO_2: 3.00%

Experimental Accuracy:
$\approx \pm 2.5\%$

Figure 6.21 Saxton CRX Multiregion (11 x 11 Inner) Core Relative Power Distribution Comparison-Normal C/S, Thermal Method

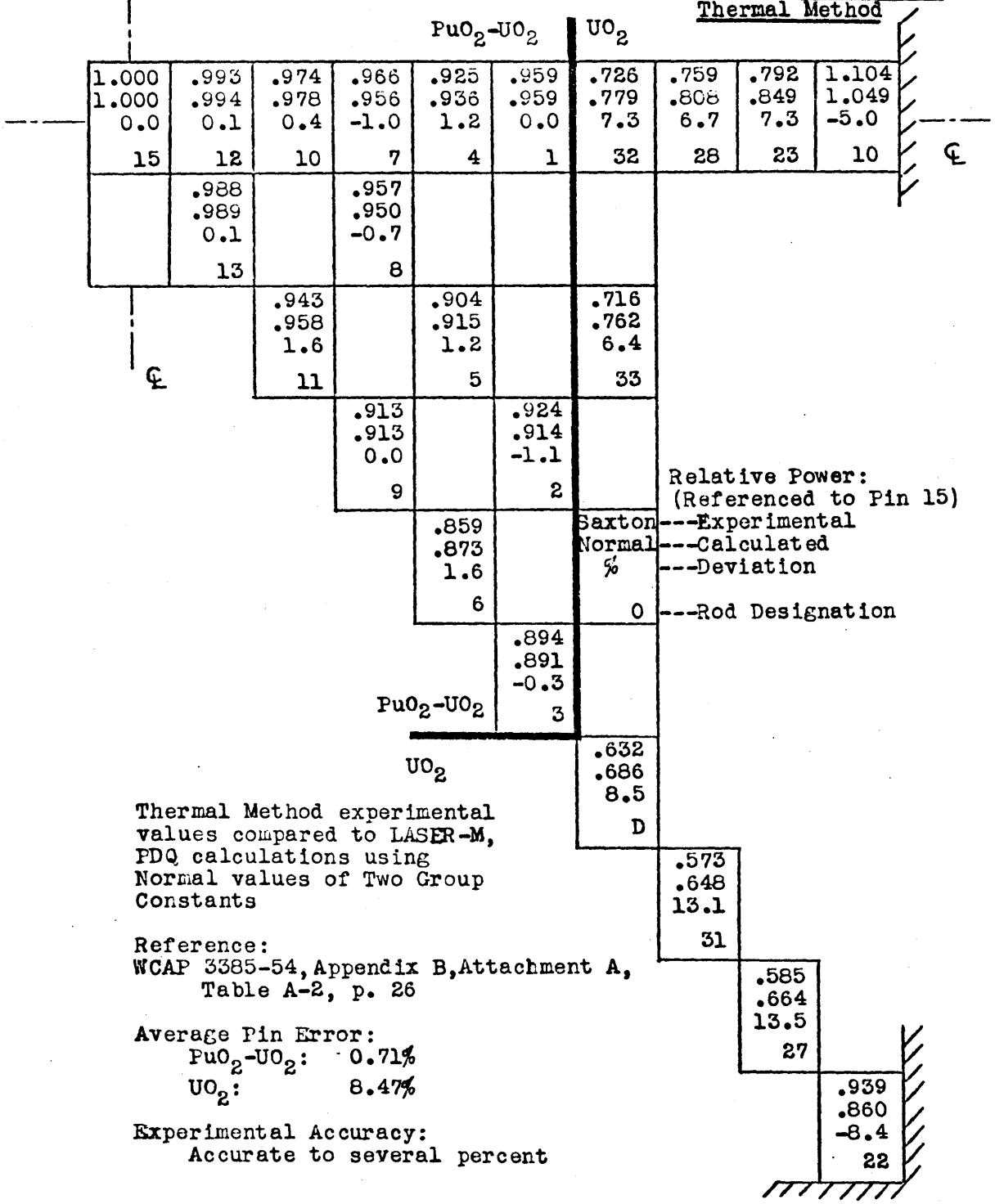

Thermal Method experimental values compared to LASER-M, PDQ calculations using Normal values of Two Group Constants

Reference:
WCAP 3385-54, Appendix B, Attachment A, Table A-2, p. 26

Average Pin Error:
PuO_2-UO_2: 0.71%
UO_2: 8.47%

Experimental Accuracy:
Accurate to several percent

Figure 6.22 Saxton CRX Multiregion (11 x 11 Inner) Core Relative Power Distribution Comparison- GMND C/S, Thermal Method

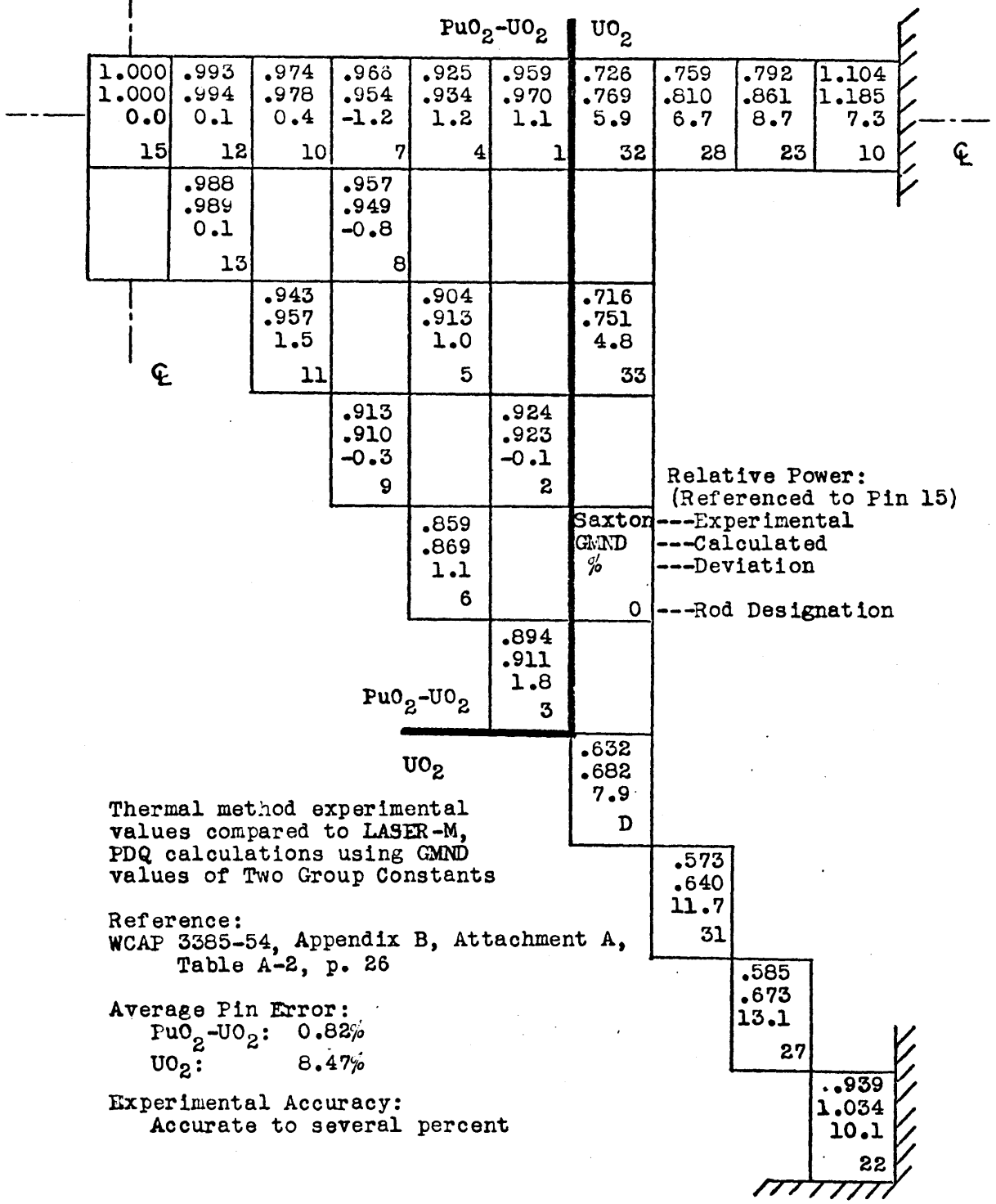

Thermal method experimental values compared to LASER-M, PDQ calculations using GMND values of Two Group Constants

Reference:
WCAP 3385-54, Appendix B, Attachment A, Table A-2, p. 26

Average Pin Error:
PuO_2-UO_2: 0.82%
UO_2: 8.47%

Experimental Accuracy:
Accurate to several percent

Figure 6.23 Saxton CRX Multiregion (11x11Inner) Core Relative Power Distribution Comparison- TCL C/S, Thermal Method

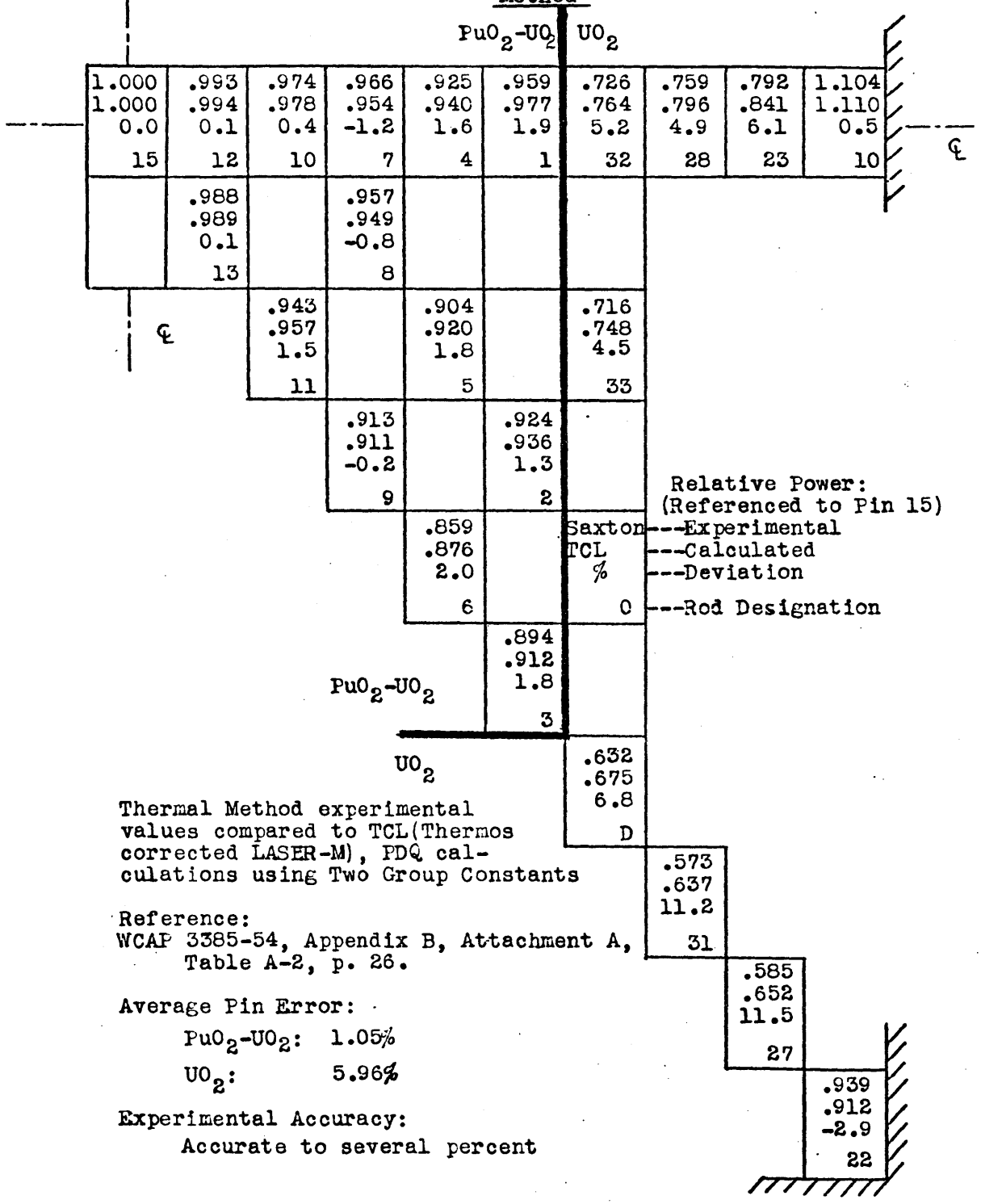

Thermal Method experimental values compared to TCL(Thermos corrected LASER-M), PDQ calculations using Two Group Constants

Reference:
WCAP 3385-54, Appendix B, Attachment A, Table A-2, p. 26.

Average Pin Error:

PuO_2-UO_2: 1.05%

UO_2: 5.96%

Experimental Accuracy:
Accurate to several percent

for each of the analysis techniques.

The 3 x 3 inner mixed oxide region quarter core power distributions by the foil method are compared with the analytical results in Figures 6.24 to 6.26. The Normal and GMND values correspond rather well, with a tendency to overpredict mixed-oxide region power and peaking. For the TCL method, the overprediction is appreciable, so that the correspondence with the foil method data is only fair. The same trend in mixed oxide region power and peaking is evident (from Normal, to GMND, to TCL) with change in method of analysis.

The same 3 x 3 inner mixed oxide region arrangement is given in Figures 6.27 to 6.29, with the thermal method experimental results the reference values for the comparison. Since the reference pin is a uranium pin, the thermal method values are higher in the mixed oxide region and equal in the uranium region relative to the foil values. The higher relative mixed oxide region powers result in good correspondence for the TCL values and underprediction for the Normal and GMND methods given the thermal method results. Thus, for the 3 x 3 inner mixed oxide region core, the TCL analysis results are "between" the two experimental methods' results for mixed oxide relative power.

In conclusion, the multiregion core calculations demonstrated that the LASER-M Normal, LASER-M GMND and TCL analysis methods (with PDQ-7) result in agreement in relative pin power with the foil experimental method results. With progression from the Normal, to GMND, to TCL methods, there was witnessed predictions of increasing mixed oxide pin average power and

Figure 6.24 Saxton CRX Multiregion (3x3 Inner) Core Relative Power Distribution Comparison-Normal C/S, Foil Method

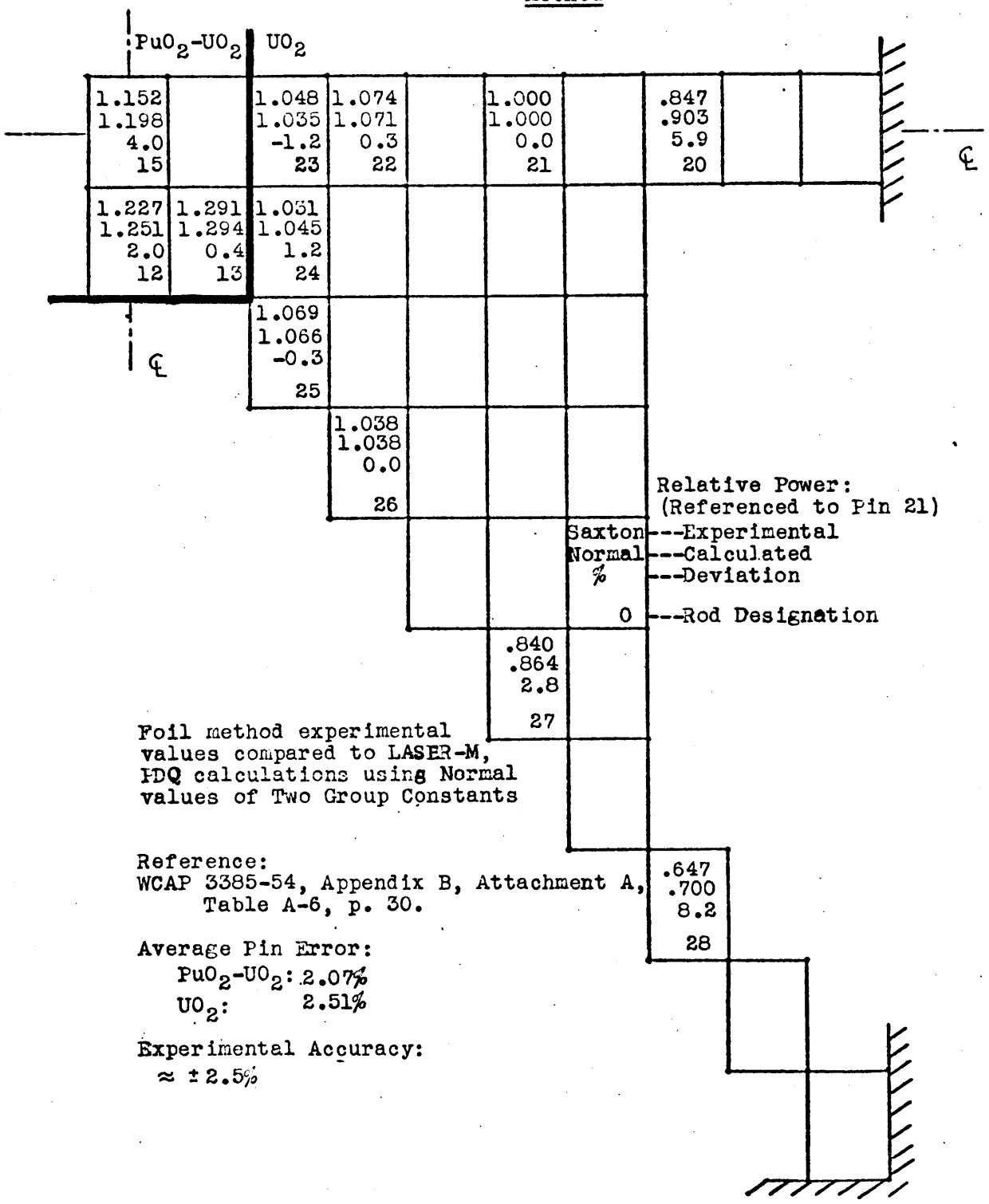

Figure 6.25 Saxton CRX Multiregion (3x3 Inner) Core Relative Power Distribution Comparison-GMND C/S, Foil Method

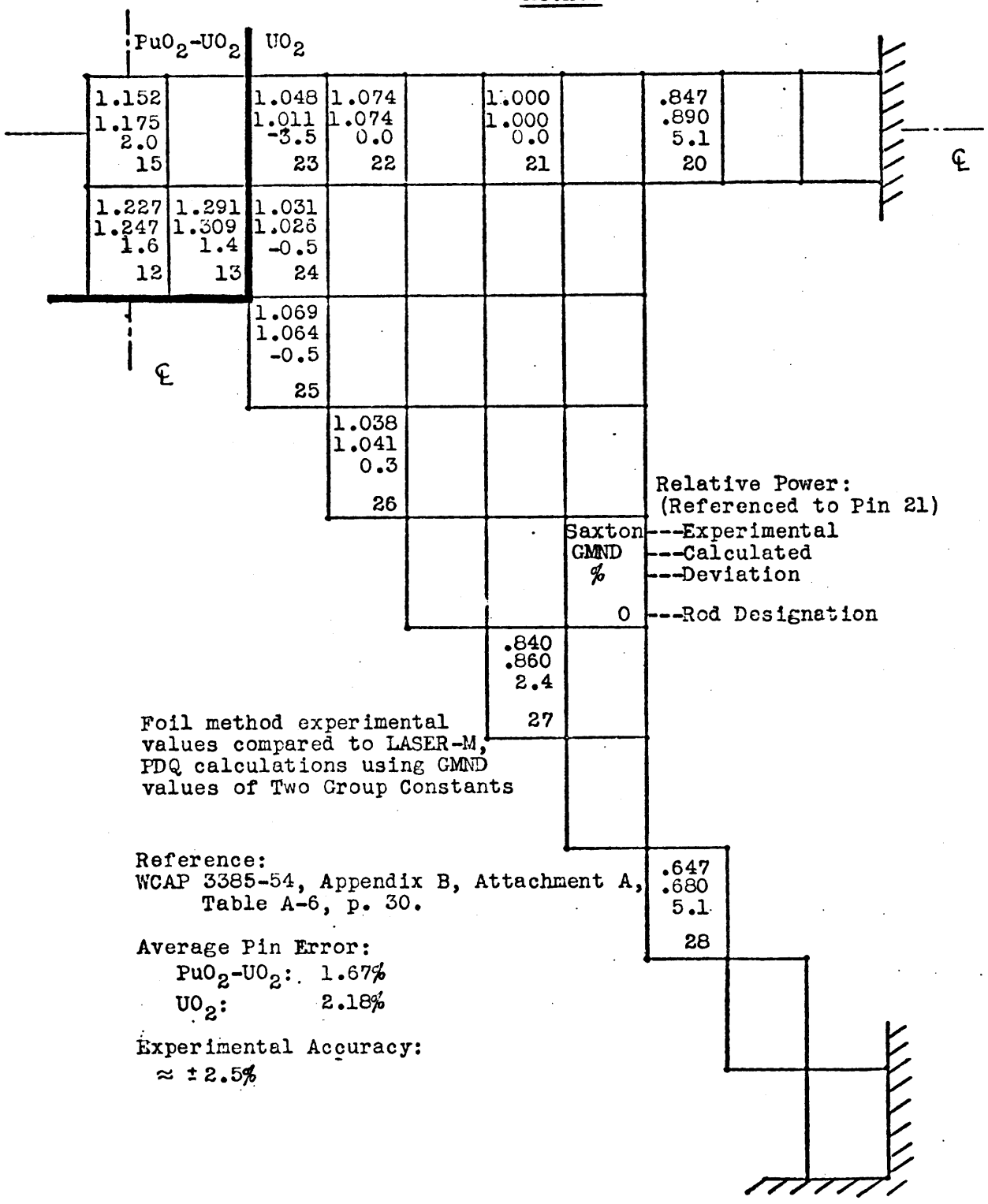

Foil method experimental values compared to LASER-M, PDQ calculations using GMND values of Two Group Constants

Reference:
WCAP 3385-54, Appendix B, Attachment A, Table A-6, p. 30.

Average Pin Error:
PuO_2-UO_2: 1.67%
UO_2: 2.18%

Experimental Accuracy:
$\approx \pm 2.5\%$

Figure 6.26 Saxton CRX Multiregion (3x3 Inner) Core Relative Power Distribution Comparison- TCL C/S, Foil Method

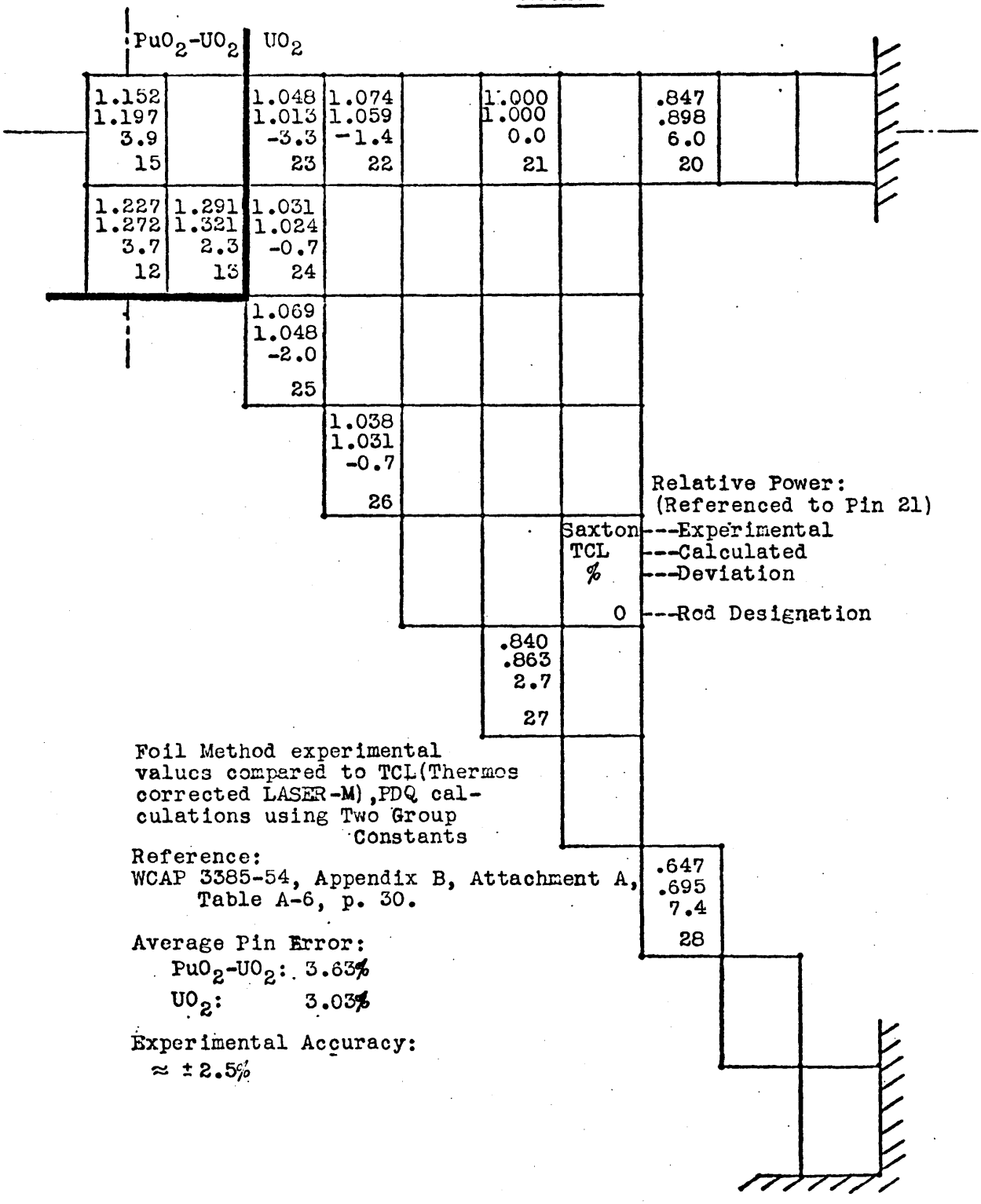

Figure 6.27 Saxton CRX Multiregion (3 x 3 Inner) Core Relative Power Distribution Comparison-Normal C/S, Thermal Method

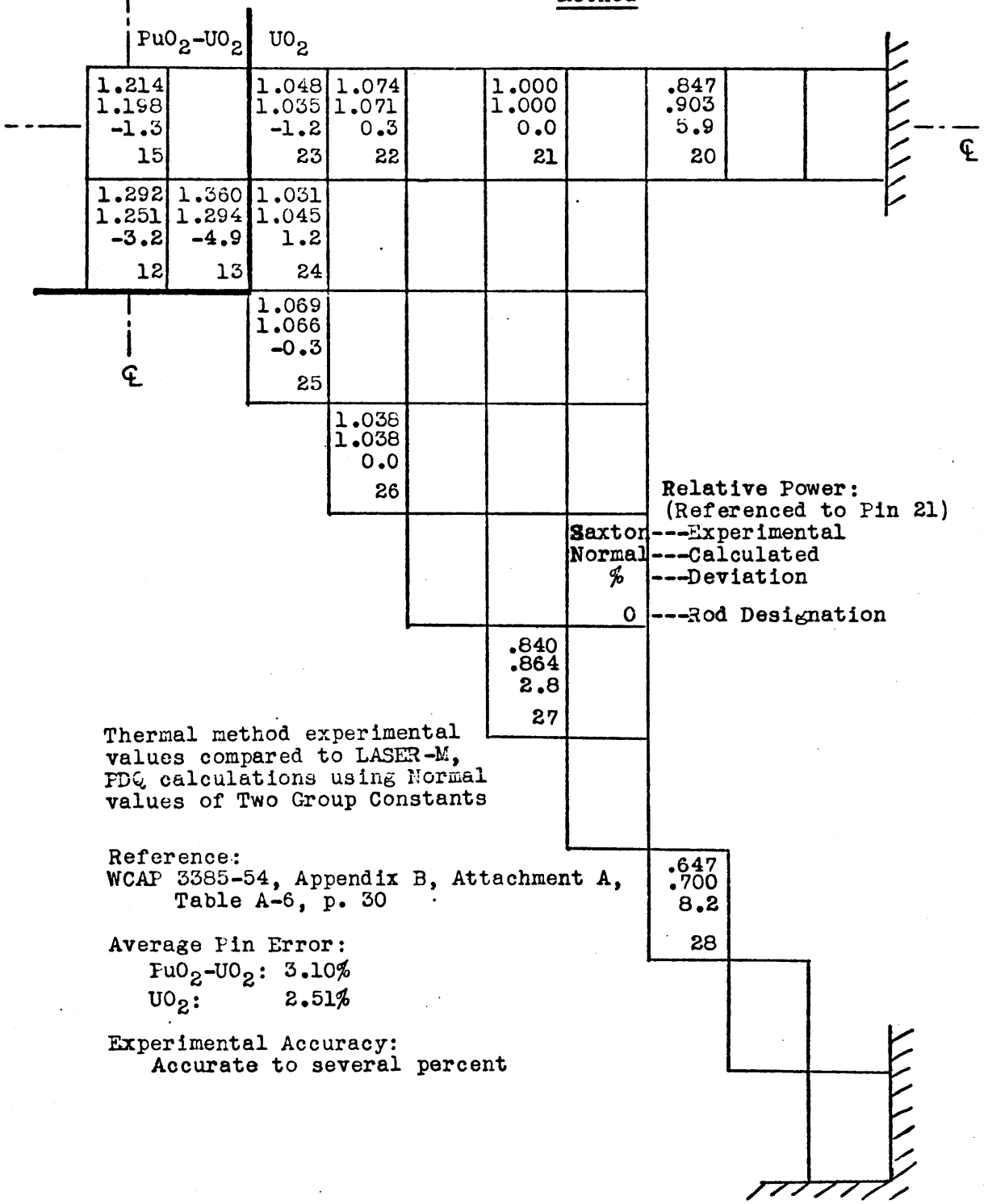

Thermal method experimental values compared to LASER-M, PDQ calculations using Normal values of Two Group Constants

Reference:
WCAP 3385-54, Appendix B, Attachment A, Table A-6, p. 30

Average Pin Error:
PuO_2-UO_2: 3.10%
UO_2: 2.51%

Experimental Accuracy:
Accurate to several percent

Figure 6.28 Saxton CRX Multiregion (3 x 3 Inner) Core Relative Power Distribution Comparison-GMND C/S, Thermal Method

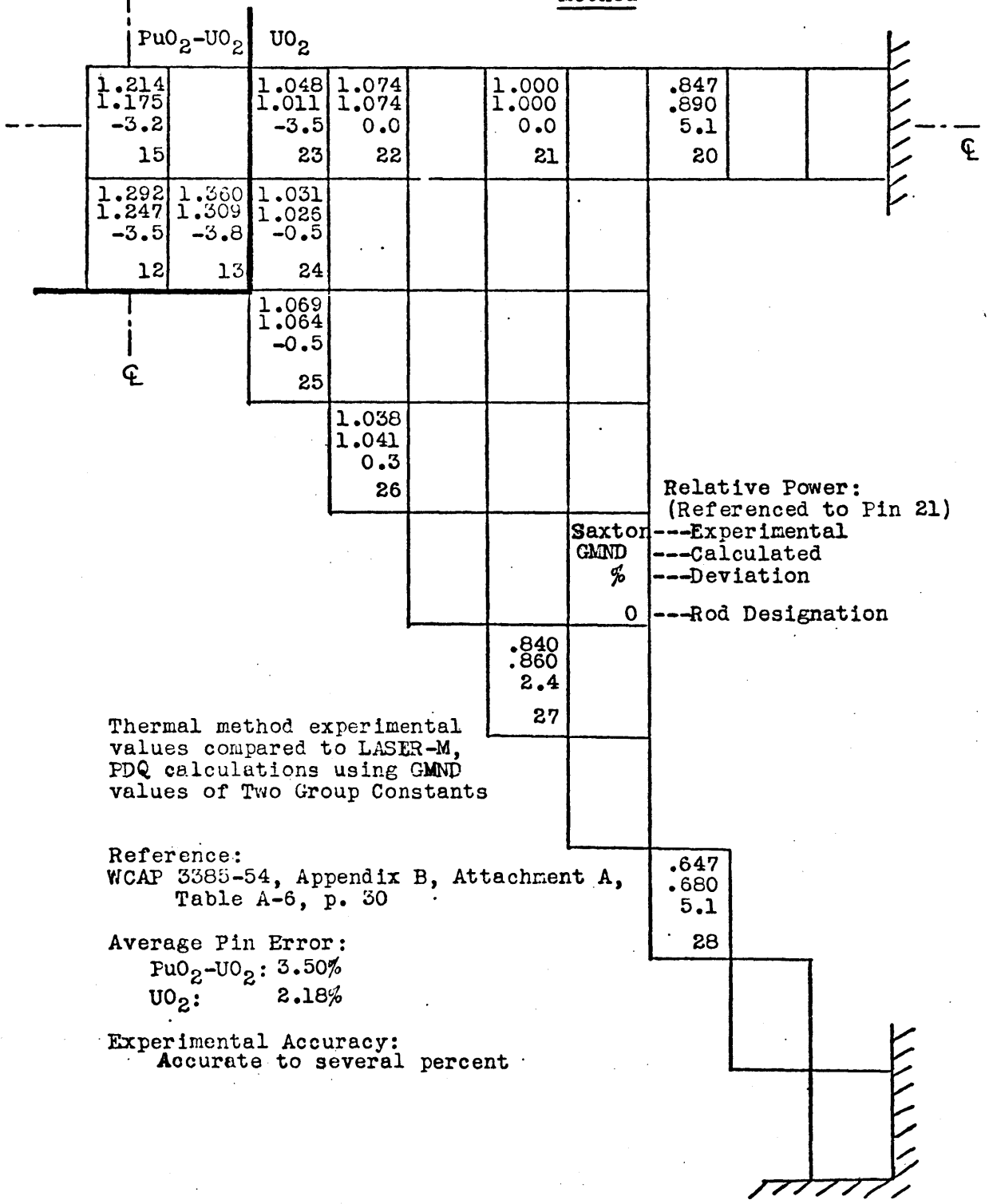

Thermal method experimental values compared to LASER-M, PDQ calculations using GMND values of Two Group Constants

Reference:
WCAP 3385-54, Appendix B, Attachment A, Table A-6, p. 30

Average Pin Error:
PuO_2-UO_2: 3.50%
UO_2: 2.18%

Experimental Accuracy:
Accurate to several percent

Figure 6.29 Saxton CRX Multiregion (3 x 3 Inner) Core Relative Power Distribution Comparison- TCL C/S , Thermal Method

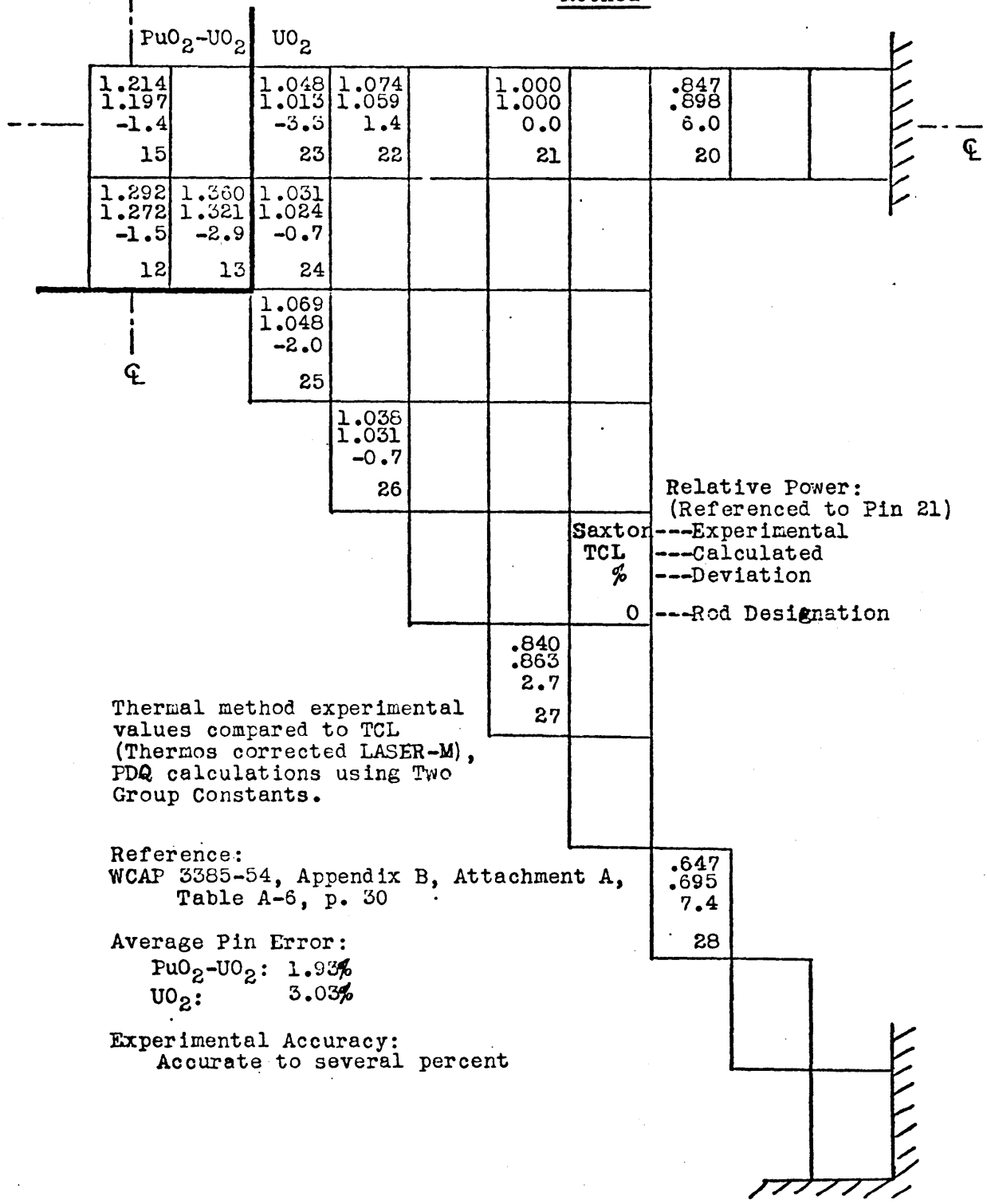

region boundary pin peaking, towards greater correspondence with the results of the thermal method experimental analysis. From the consideration of pin peaking at the mixed oxide boundary, the TCL method may be termed the most conservative (greatest peaking) for design purposes.

6.5.3 Comparison with Similar Calculations

The Saxton CRX program, as mentioned at the beginning of the chapter, was undertaken to verify the Westinghouse analytical methods for the Saxton Partial Plutonium Core. Extensive calculation to experiment comparisons are presented in WCAP 3385-51[17].

The Westinghouse results are contrasted to those obtained by the analyses presented in this chapter. The methods of spectrum calculation are significantly different (LEOPARD is the basic Westinghouse model) and the Westinghouse modifications are extensive (Figure 4.19). The purpose of the comparisons presented with experimental data and these calculations is to develop as much confidence as possible in the predictive abilities of the methods developed, in addition to noting the trends of deviations.

A summary of the results of the Saxton CRX calculations undertaken in Section 6.5.2 is given in Table 6.5. In summary, the GMND water slot peaking prediction was very good, the TCL good and the Normal unacceptable (underpredicting the peaking effect). All the mixed oxide boundary peaking predictions were good, in correspondence with the foil experimental results. The

Table 6.5

Saxton CRX Relative Power Distribution

Comparison- Summary

I. Central Cell Rows	Pin Deviation (%) Normal	GMND	TCL
Reference UO_2			
Average Deviation:	2.88	2.32	2.82
Reference PuO_2-UO_2			
Average Deviation:	1.72	1.45	1.53
Water Slot, UO_2			
Average Deviation:	2.60	0.95	2.20
Slot Pin:	-6.7	0.8	-2.6
Adjacent Pin:	0.3	1.0	2.0
Water Slot, PuO_2-UO_2			
Average Deviation:	2.12	0.94	1.00
Slot Pin:	-6.6	-1.2	-2.3
Adjacent Pin:	-1.2	-1.4	-0.1

II. Quarter Cores	Average Pin Deviation (%) Normal	GMND	TCL
Reference PuO_2-UO_2	2.11	1.88	2.21
Water Slot, PuO_2-UO_2	3.27	1.70	1.87
Multiregion (11x11)			
Thermal method/Foil method			
PuO_2-UO_2 inner pins:	0.71	0.82	1.05
UO_2 outer pins:	8.47/4.77 (high)	8.47/2.34 (high)	5.96/3.00 (high)
Multiregion (3 x 3)			
Thermal method/Foil method			
PuO_2-UO_2 inner pins:	3.10/2.07 (low)(hi)	3.50/2.18 (low)(hi)	1.93/3.63 (low)(hi)
UO_2 outer pins:	2.51	1.67	3.03

Experimental Errors:		
	Single Region (Cell rows and cores)	± 1.4%
	Multiregion	
	Thermal method	± several %
	Foil method	± 2.5%

trend of upward mixed oxide region power and boundary peaking was witnessed in the change of analysis method from Normal, to GMND, to TCL, so much so that the correspondence of the TCL and thermal experimental results was acceptable.

The Westinghouse analysis is based on modified LEOPARD calculations with PDQ. Figure 4.19 summarizes some of the methods' characteristics, although the methods themselves are proprietary. Note that MND constants are used in the Westinghouse analysis of these core configurations.

The water slot power peaking results of the Westinghouse analysis, as well as those presented in Section 6.5.2, are given for each core type in Tables 6.6 and 6.7. The Westinghouse LEOPARD calculations are described as "Soft Spectrum" and "Extra Region", the latter yielding acceptable results. The terms are explained in Figure 6.30. It should be realized that the Westinghouse PDQ calculations make use of an extra mesh point representation at the slot boundary. This complication, while a benefit in terms of results, was not used in the LASER-M calculations, as explained in Section 6.5.1.

Notice that the LEOPARD calculations overpredict the slot pin power, while underpredicting the power in the pin adjacent to it (two pins from the slot) for both core types. The LASER-M methods generally underpredict the slot pin power, and overpredict and underpredict the adjacent pin powers for the uranium and mixed oxide cores, respectively. The LASER-M GMND and TCL predictions are better or as good as those of the LEOPARD "Extra Region". The TCL results, however, in deviation direction,

Table 6.6

Saxton CRX Water Slot Power Peaking and

Reactivity Comparison- Experiment vs. Calculation

UO_2 Core

Method of obtaining two group constants	Deviation from Experimental Power(%)		Slot Worth (% Δk/k) and Deviation from Experimental
	Slot Pin	Adjacent Pin	
LEOPARD(1)			
Soft Spectrum	5.6	-	0.32 (0.06)
Extra Region	2.6	-0.9	0.23 (0.03)
LASER-M(2)			
Normal	-6.7	0.3	0.22 (-0.04)
GMND	0.8	1.0	0.36 (0.10)
TCL	-2.6	2.0	0.37 (0.11)

Experimental Slot Worth---------- 0.26

(1) LEOPARD calculations using MND cross sections. PDQ calculations use 2 mesh points per cell, 4 per cell at core boundary and water slot cells.

(2) LASER-M calculations with PDQ using 2 mesh points per cell, all cells. Group independent value of axial buckling used based on equivalent experimental buckling for single region core, namely 0.00113 cm(-2) (WCAP 3385-54, Appendix A, Table III, p. 5)

(Experimental and calculated power referenced to Pin 5 from core boundary)

Reference: WCAP 3385-51, Table 5.16, p. 5-31
Figure 5.3, p. 5-32

Table 6.7

Saxton CRX Water Slot Power Peaking and
Reactivity Comparison- Experiment vs. Calculation
PuO_2-UO_2 Core

Method of obtaining two group constants	Deviation from Experimental Power (%)		Slot Worth (% Δk/k) and Deviation from Experimental
	Slot Pin	Adjacent Pin	
LEOPARD[1]			
Soft Spectrum	7.5	-	0.60 (0.11)
Extra Region	4.4	-5.0	-
LASER-M[2]			
Normal	-6.8	-1.3	0.28 (-0.21)
GMND	-1.0	-1.2	0.39 (-0.10)
TCL	-2.1	0.1	0.54 (0.05)
Experimental Slot Worth			0.49

[1],[2] comments from previous table applicable

Experimental and calculated power referenced to Pin 6 from core boundary

Reference:
WCAP 3385-51, Table 5.17, p. 5-34
Figure 5.4, p. 5-35

Figure 6.30

WCAP LEOPARD Cross Sections used for

Water Slot Power Peaking Calculations

Two Group Constants	Description
Soft Spectrum	● Group constants obtained from the materials composition of the water slot alone
Extra Region	● Unit cell defined by the fuel rods surrounding the water slot ● Extra region composed of materials in the water slot ● Group constants for the water slot determined from the obtained group averaged microscopic cross sections and the number densities of water slot material

are not conservative for design purposes, as are the Westinghouse results.

The water slot core calculations are also compared on a slot reactivity worth prediction basis. The slot worth is determined experimentally from the known differential water height worth of the core water level. The slot worth is expressed as $\% \Delta k/k$, which is

$$\left(\% \ \Delta k/k \right)_{slot} = \frac{k_{eff}^{\text{slot core}} - k_{eff}^{\text{full core}}}{k_{eff}^{\text{full core}}} \times 100 \qquad (6.5)$$

The deviation of the calculated results from the experimental is simply

$$\text{Deviation from Experimental of } \% \Delta k/k = (\% \Delta k/k)_{calc} - (\% \Delta k/k)_{exp} \qquad (6.6)$$

The slot worth predictions generally follow the slot peaking predictions in relative direction. All of the calculated values are relatively poor predictions, owing to the core analysis problems mentioned in Section 6.5.1. The buckling representation in these cores is closely linked to k_{eff}, and its assumed group and region independent nature in these calculations is inadequate. The results, however, are given for comparison and completeness.

The multiregion core (11 x 11 and 3 x 3) power distribution experimental results (both foil and thermal method) and the LASER-M GMND, TCL and Westinghouse LEOPARD MND calculational results are given graphically in Figures 6.31 to 6.38. The pin values plotted represent core flat traverses

Figure 6.31

Saxton CRX Multiregion Core (11x11 PuO_2-UO_2 Inner Array)
Relative Power Distribution Comparison-
Leopard MND and LASER-M GMND, Flat Core Traverse

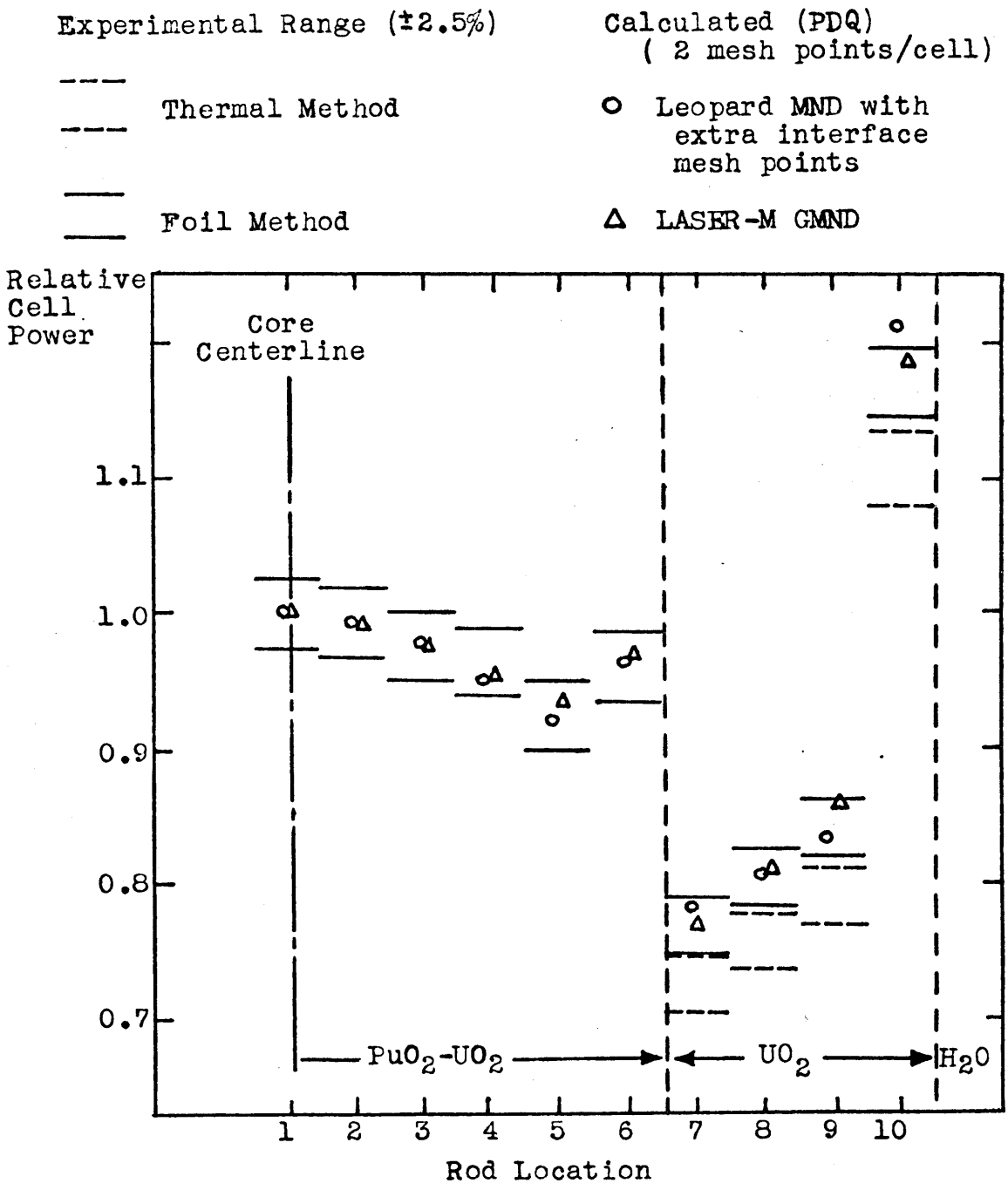

Reference: WCAP 3385-51, Figure 5.6, p. 5-41

Figure 6.32

Saxton CRX Multiregion Core (11x11 PuO_2-UO_2 Inner Array)
Relative Power Distribution Comparison-
Leopard MND and LASER-M GMND, Diagonal Core Traverse

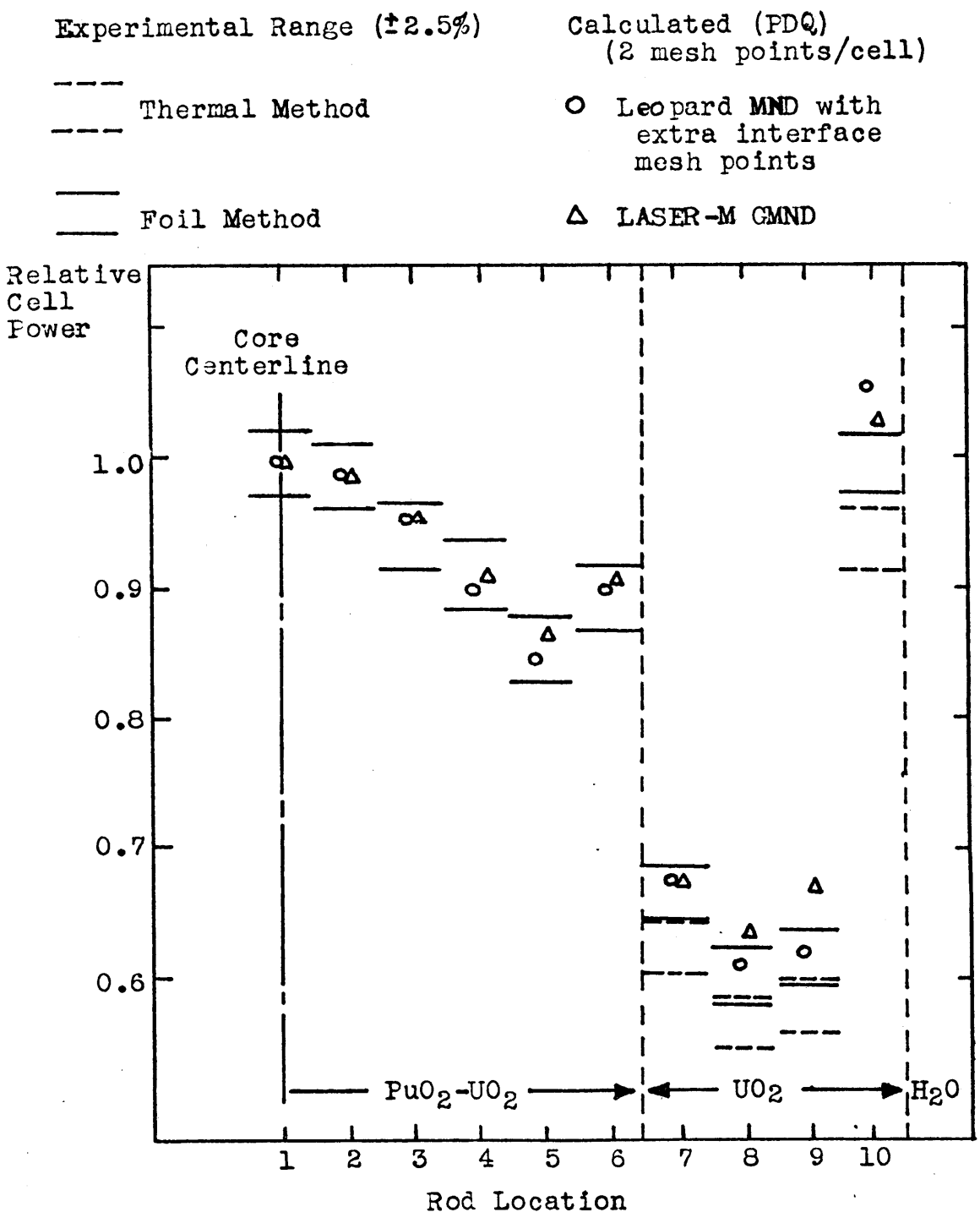

Reference: WCAP 3385-51, Figure 5.6, p. 5-41

Figure 6.33

Saxton CRX Multiregion Core (11x11 PuO_2-UO_2 Inner Array)
Relative Power Distribution Comparison-
Leopard MND and TCL C/S, Flat Core Traverse

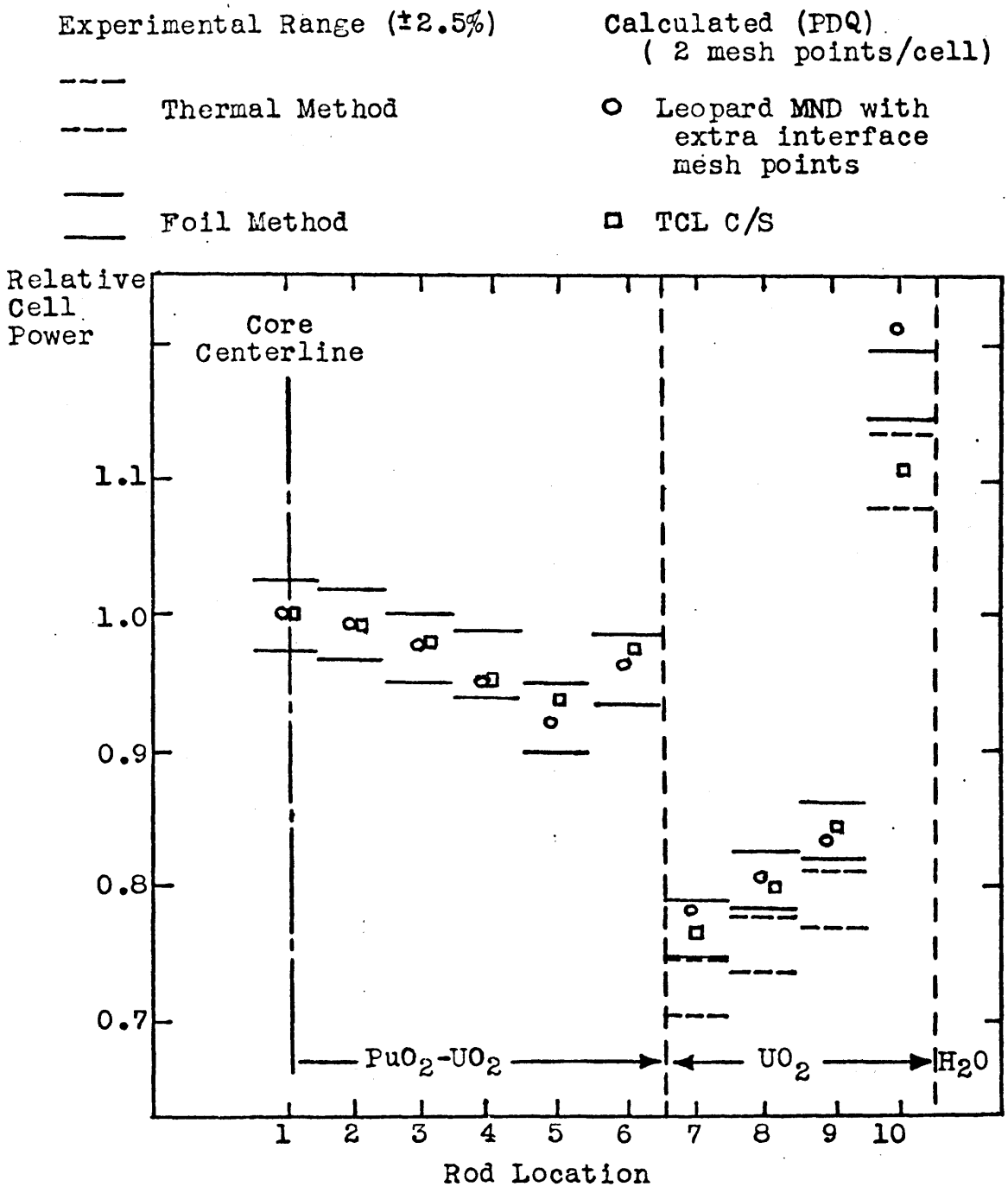

Reference: WCAP 3385-51, Figure 5.6, p. 5-41

Figure 6.34

Saxton Multiregion Core (11x11 PuO_2-UO_2 Inner Array)
Relative Power Distribution Comparison-
Leopard MND and TCL C/S, Diagonal Core Traverse

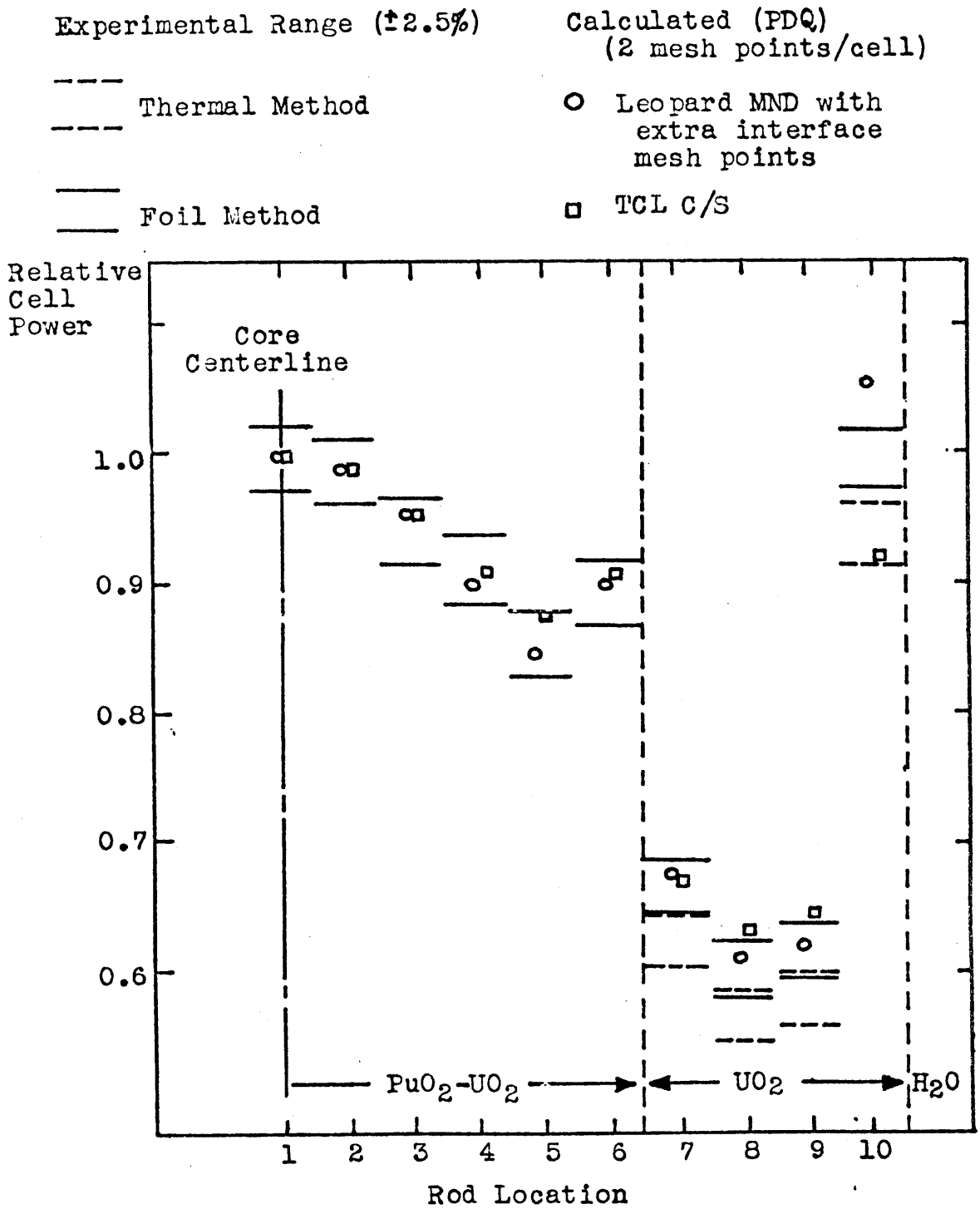

Reference: WCAP 3385-51, Figure 5.6, p. 5-41

Figure 6.35
Saxton CRX Multiregion Core (3x3 PuO_2-UO_2 Inner Array)
Relative Power Distribution Comparison-
Leopard MND and LASER-M GMND, Flat Core Traverse

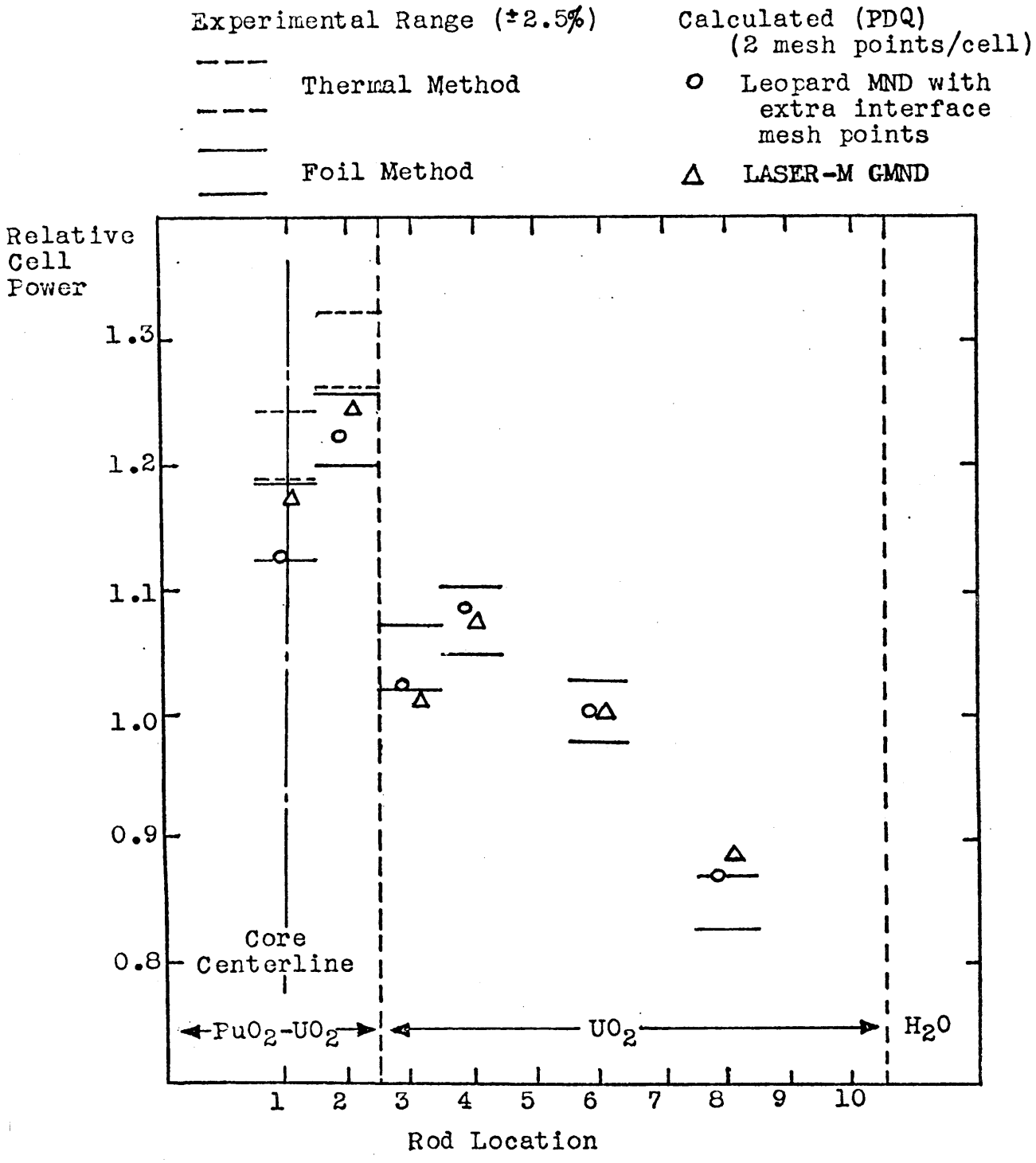

Reference: WCAP 3385-51, Figure 5.12, p. 5-47

Figure 6.36

Saxton CRX Multiregion Core (3x3 PuO_2-UO_2 Inner Array)
Relative Power Distribution Comparison-
Leopard MND and LASER-M GMND, Diagonal Core Traverse

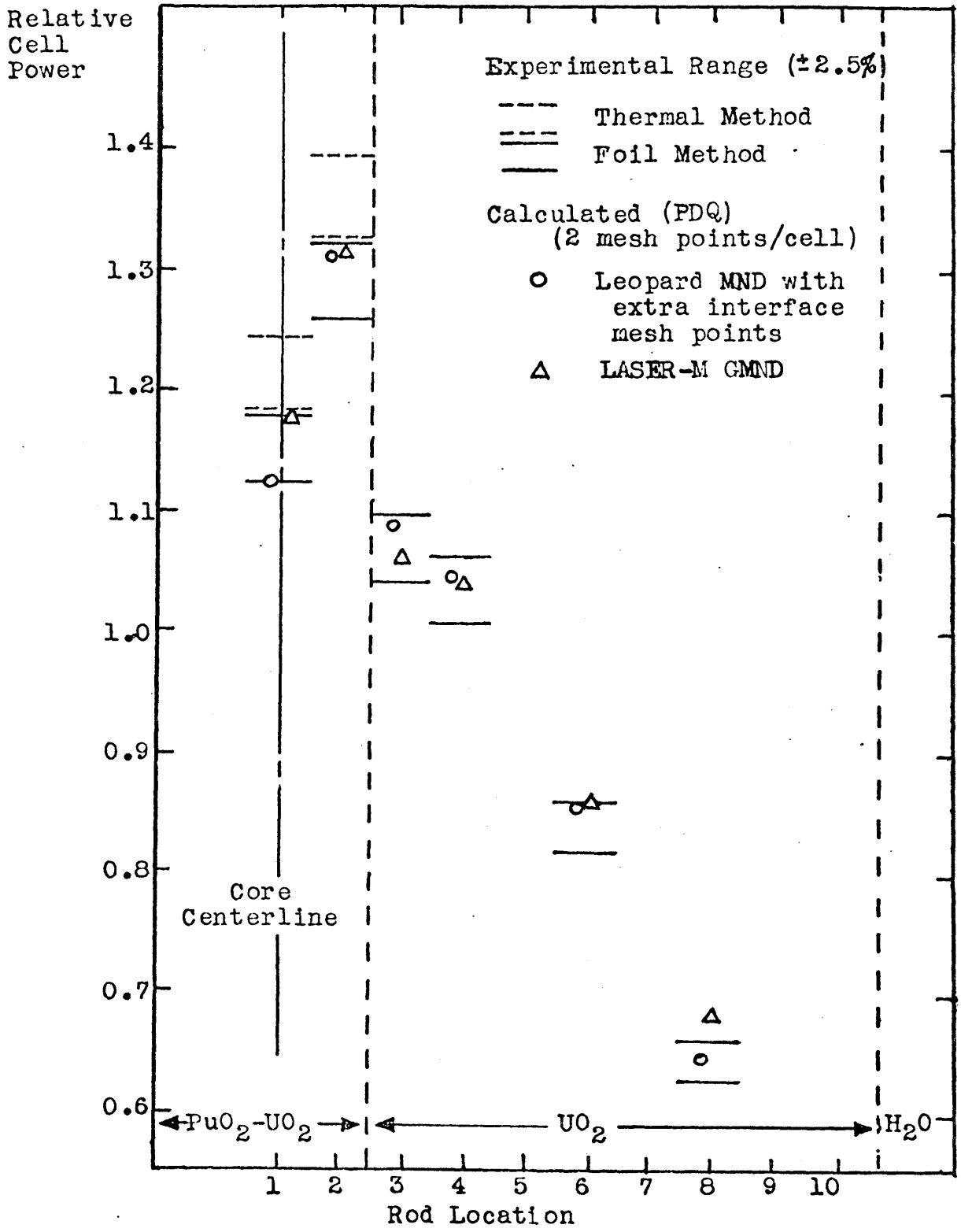

Reference: WCAP 3385-51, Figure 5.12, p. 5-47

Figure 6.37
Saxton CRX Multiregion Core (3x3 PuO_2-UO_2 Inner Array)
Relative Power Distribution Comparison-
Leopard MND and TCL C/S Flat Core Traverse

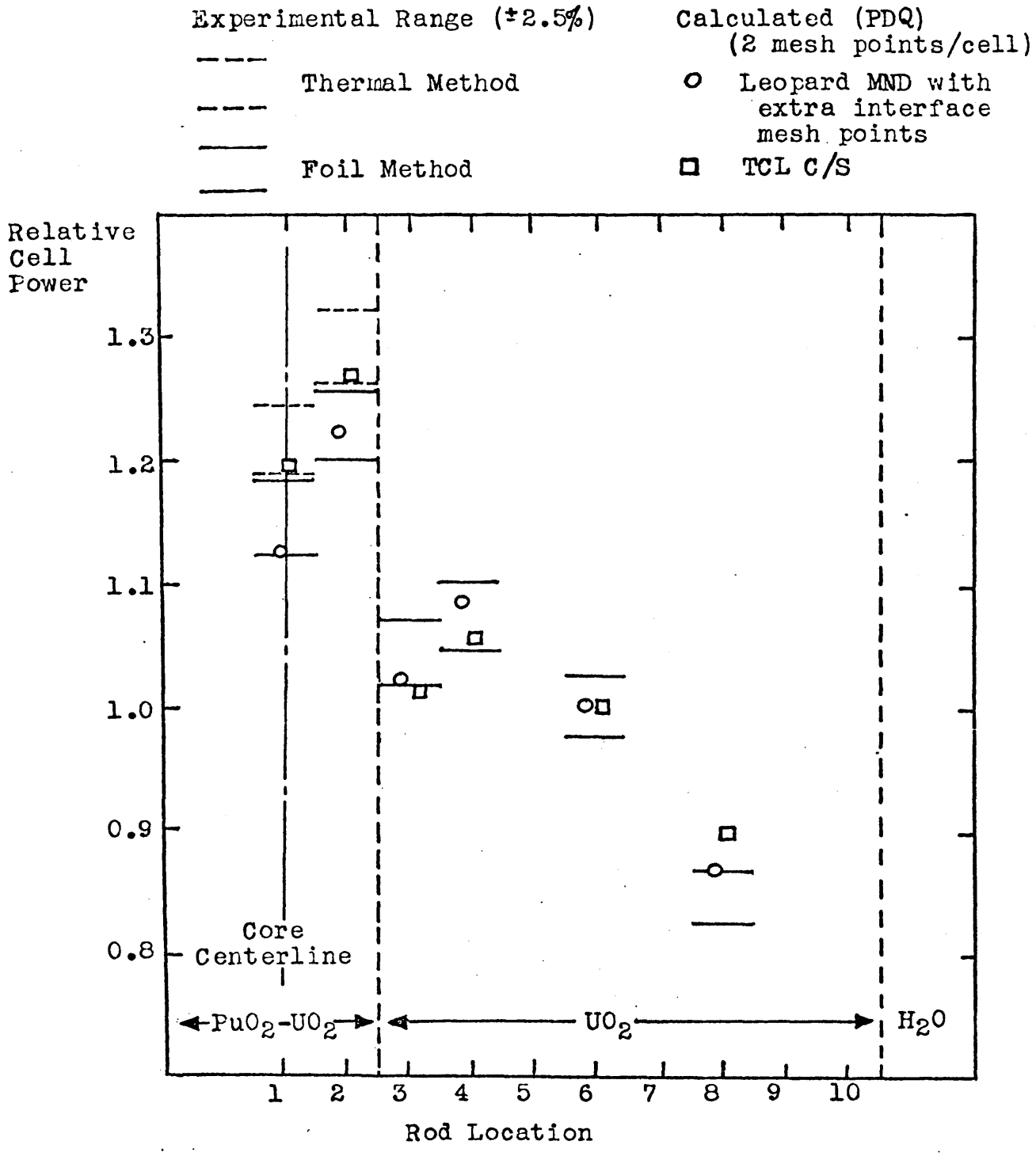

Reference: WCAP 3385-51, Figure 5.12, p. 5-47

Figure 6.38

Saxton CRX Multiregion Core (3x3 PuO_2-UO_2 Inner Array)
Relative Power Distribution Comparison-
Leopard MND and TCL C/S Diagonal Core Traverse

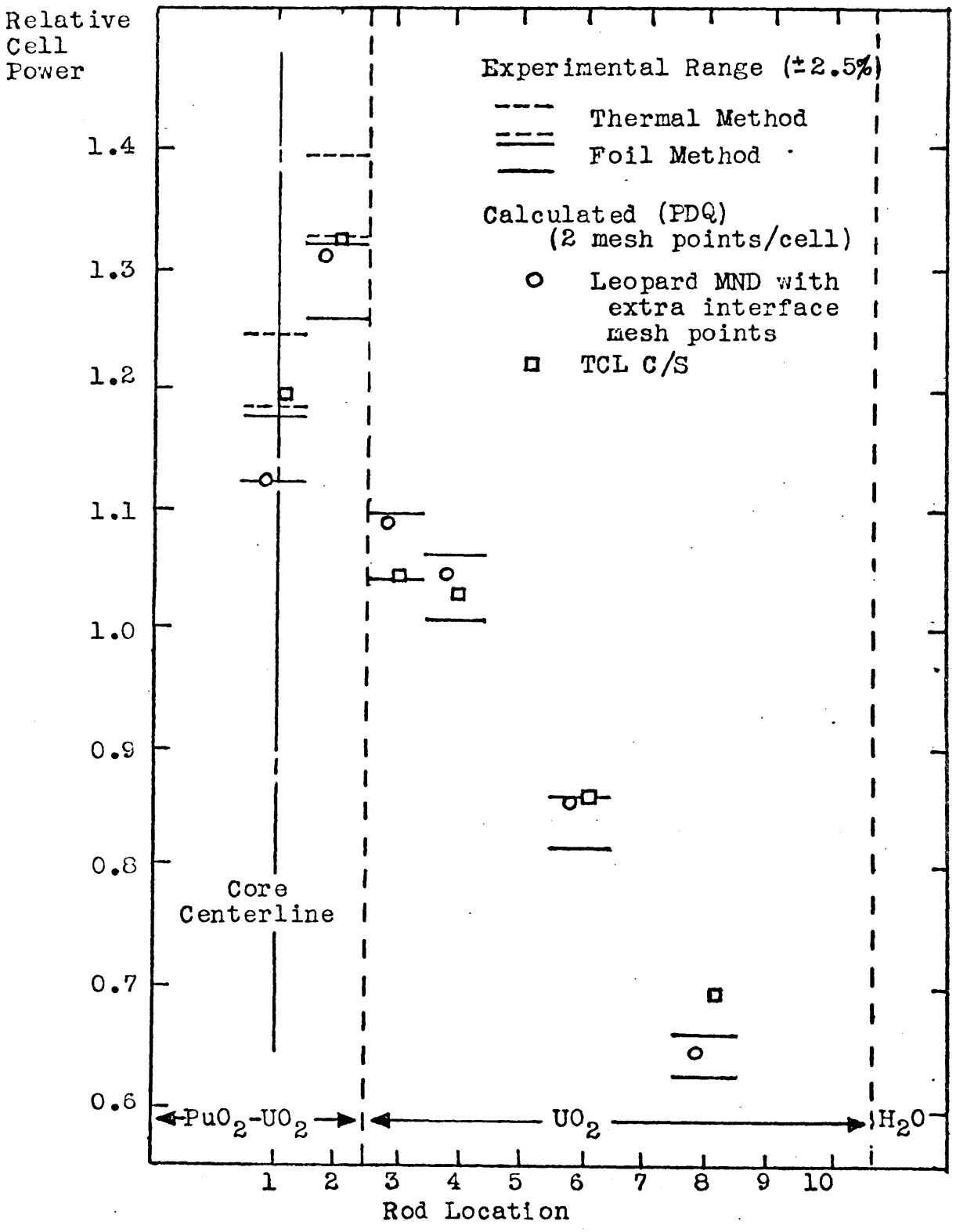

Reference: WCAP 3385-51, Figure 5.12, p. 5-47

(central cell rows) and core diagonal traverses. The experimental values are given as a region of ± 2.5% about the actual value. It is recalled from Section 6.2.1 that this is the expected experimental error of the foil method at shifted spectrum regions. The thermal method accuracy is given as several percent, so that the same percent value in error is assumed for these data points.

The Westinghouse PDQ calculations use an extra mesh point representation at both the mixed oxide boundary and the core boundary, similar to the water slot case. This is an obvious spatial detail advantage. Similarly, the use of LASER is a spectral detail advantage, and the TCL representation attempts to combine the advantages of both approaches.

The 11 x 11 inner region case (Figures 6.31 to 6.34) shows that all three methods yield very acceptable results, with correspondence of results to the foil method data. For the mixed oxide pins at the region boundary, the TCL prediction is slightly greater (power peaking more conservatively predicted) than the GMND, which in turn is slightly greater than the Westinghouse LEOPARD prediction. The core boundary calculational problems at the corner of the core (diagonal traverse) are more acute for the GMND and TCL cases which do not benefit from the greater spatial detail.

Similarly, the 3 x 3 inner region cases are given in Figures 6.35 to 6.38. Notice that the GMND and Westinghouse LEOPARD results indicate good correspondence with the foil method results. The TCL results, however, tend towards thermal

experimental values (higher mixed oxide pin powers). The peaking of the mixed oxide boundary pin is more conservatively predicted by the TCL and GMND group constants compared to those of the Westinghouse LEOPARD. It is true that the LEOPARD core power shape prediction is better, The core leakage representation in the Westinghouse calculations is not known and is a major determinant in the core flux shape prediction for this core size range.

A further comparison of calculational methods is obtained by viewing the progression of core configurations (from full uranium, to 3x3 mixed oxide, to 11 x 11 mixed oxide, to full mixed oxide) as a fuel substitution experiment. The change in k_{eff}, $\% \Delta k/k$, defined in a manner analogous to Eq. (6.5), is obtainable experimentally from the core water height worth values and the changes in water height necessary to maintain criticality. The calculations also provide this value. The comparison is specifically made on the basis of a change in k_{eff}, since the values themselves are quite sensitive to the core buckling and the buckling representation is not precise.

The fuel substitution results and comparison is given in Table 6.8. The results are not good for any method of analysis, resulting primarily from the core type with the leakage assumptions used. GMND and Normal LASER-M results, on a cumulative difference-from-experiment basis, supply a better prediction than do the LEOPARD results. Contrary to the power distribution results, the Normal LASER-M prediction is better than the GMND, as has been noted for calculations of k_{eff} in other

Table 6.8 Saxton CRX Fuel Substitution Criticality Comparison- Experiment vs Calculation

Core Configuration	PDQ Calculated k_{eff} Values			Experimental %Δk/k Relative to Uranium Core	PDQ Calculated %Δk/k and Difference from Exp.		
	Leopard (extra mesh)	LASER-M Normal	LASER-M GMND		Leopard (extra mesh)	LASER-M Normal	LASER-M GMND
1. UO_2	1.00379	0.99749	1.00757	-	-	-	-
					-	-	-
2. 3x3 Inner Region PuO_2-UO_2	1.00405	0.99767	1.00758	-0.03	0.03	0.02	0.001
					(-0.06)	(-0.05)	(-0.03)
3. 11x11 Inner Region PuO_2-UO_2	1.00312	1.00032	1.00898	-0.40	-0.07	-0.28	-0.14
					(-0.33)	(-0.12)	(-0.26)
4. PuO_2-UO_2	1.00892	1.00315	1.01283	0.06	0.51	0.57	0.52
					(-0.45)	(-0.51)	(-0.46)
Total Difference from Experimental for 3 Cores, %Δk/k					-0.84	-0.68	-0.75

LASER-M, PDQ calculations made using as input to PDQ a group independent axial buckling of 0.00113 cm^{-2} based on equivalent experimental bucklings for the single region cores as given in WCAP 3385-54, Appendix A, Table III, p. 5

Reference: WCAP 3385-51, Table 5.21, p. 5-71

Table 6.8 Saxton CRX Fuel Substitution Criticality Comparison- Experiment vs Calculation (Continued)

Core Configuration	PDQ Calculated k_{eff}		Experimental %Δk/k	PDQ Calculated %Δk/k and difference from experimental	
	Leopard (extra mesh)	TCL	Relative to Uranium Core	Leopard (extra mesh)	TCL
1. UO_2	1.00379	0.99988	-	-	-
				-	-
2. 3x3 Inner Region PuO_2-UO_2	1.00405	0.99985	-0.03	0.03	-0.003
				(-0.06)	(-0.03)
3. 11x11 Inner Region PuO_2-UO_2	1.00312	1.00294	-0.40	-0.07	0.31
				(-0.33)	(-0.71)
4. PuO_2-UO_2	1.00892	1.00740	0.06	0.51	0.75
				(-0.45)	(-0.69)
Total difference from Experimental for 3 Cores, % Δ k/k				-0.84	-1.43

TCL, PDQ calculations made using as input to PDQ a group independent axial buckling of 0.00113 cm^{-2} based on equivalent experimental bucklings for the single region cores as given in WCAP 3385-54, Appendix A, Table III, p. 5

Reference: WCAP 3385-51, Table 5.21, p. 5-71

cases[31]. The TCL results are least acceptable.

In conclusion, from the comparison with the Westinghouse calculations, the GMND and TCL methods yield as good calculational prediction of power distributions as do the proprietary methods for the spectrum discontinuities presented. The reactivity predictions, in all cases, are generally poor, although this is related more to the core arrangement than to any shortcoming in the models as applied to power reactor cases.

6.6 Conclusions

The GMND and TCL LASER-M based spectrum methods, used in conjunction with a PDQ spatial diffusion theory calculation, provide acceptable pinwise relative power prediction for the core analysis problems found in proposed LWR plutonium recycle assemblies and cores, namely water slot areas and mixed oxide (uranium- plutonium pin type) boundaries. It is to be noted that the problems studied in the Saxton CRX arrangements in this chapter are isolated spectrum discontinuities placed in the asymptotic region of a uniform lattice.

Concerning the Saxton CRX calculations,

(1) Water Slot Power Peaking Predictions

The Normal LASER-M unit cell constants grossly underpredict the power increases in the water slot area. The GMND results show excellent prediction of the peaking effect at the slot pin. The TCL results show good prediction of the slot pin peaking (a slight underprediction). The GMND and TCL results are acceptable, the former more conservative (for design purposes) in the case of the peak pin at the water slot. The GMND

and TCL results, in comparison with those of the Westinghouse LEOPARD MND (with extra mesh PDQ representation), are superior in prediction of the slot pin and adjacent pin powers for both core types, but not as conservative at the slot pin due to the Westinghouse LEOPARD overprediction.

(2) Mixed Oxide- Uranium Oxide Boundary Power Peaking

The LASER-M Normal, GMND and TCL results compare favorably with the foil method experimental results for relative power between mixed oxide and uranium oxide pins and power peaking of the mixed oxide boundary pin. This is similar to the Westinghouse LEOPARD MND results. The trend of increasing mixed oxide region power and increased peaking is evident in the change from Normal to GMND, and in turn to TCL, analysis methods, while remaining within the experimental accuracy of the foil method results. The GMND and TCL predictions are more conservative in this sense than are the Westinghouse predictions.

The thermal experimental method results show higher (about 5%) average mixed oxide pin power than do the foil experimental method results. The TCL analysis results are closest to these, the correspondence fair. For design purposes, the TCL results are the most conservative, although the discrepancy between experimental methods requires consideration in establishing power peaking limits with the use of mixed oxide fuels.

(3) Reactivity Predictions

The high leakage condition of the Saxton CRX core leads to inconclusive results of k_{eff} change prediction by the analysis methods.

CHAPTER 7

MODEL VERIFICATION AND APPLICATION: PLUTONIUM ISLAND DESIGN RECYCLE ASSEMBLY

7.1 Introduction

As mentioned in Section 1.4.4, the methods discussed and developed are applied to a plutonium recycle assembly design (Figure 1.1) proposed for use in a pressurized water reactor by Combustion Engineering. The following calculations of assembly pinwise relative power have been performed in a manner similar to those of the experimental cases (Chapter 6) using LASER-M Normal, LASER-M GMND or TCL two group spectrum averaged constants as input to the spatial (PDQ) calculation.

The comparison of the results with published calculations serves as a means of verification of the methods with respect to their ability to represent the relative power production characteristics of the pins of such an assembly. Note that this is not a comparison of the individual isotopic reaction rates in the cells. Such a comparison, making use of higher order calculations, is desireable but not within the scope of this study.

The verification in this chapter is supplemental to the Saxton CRX experimental power distribution comparisons of Chapter 6 in that the same two calculational problems, namely large water regions and mixed oxide- uranium oxide pin type boundaries, are present. The island design problem is quite different, however, as is evident from the quarter assembly diagram, Figure 7.1. Notice that the two spectrum discontinuity

Figure 7.1 Maine Yankee Assembly Design-
Plutonium Island Concept
Quarter Assembly Relative Power Edit Region

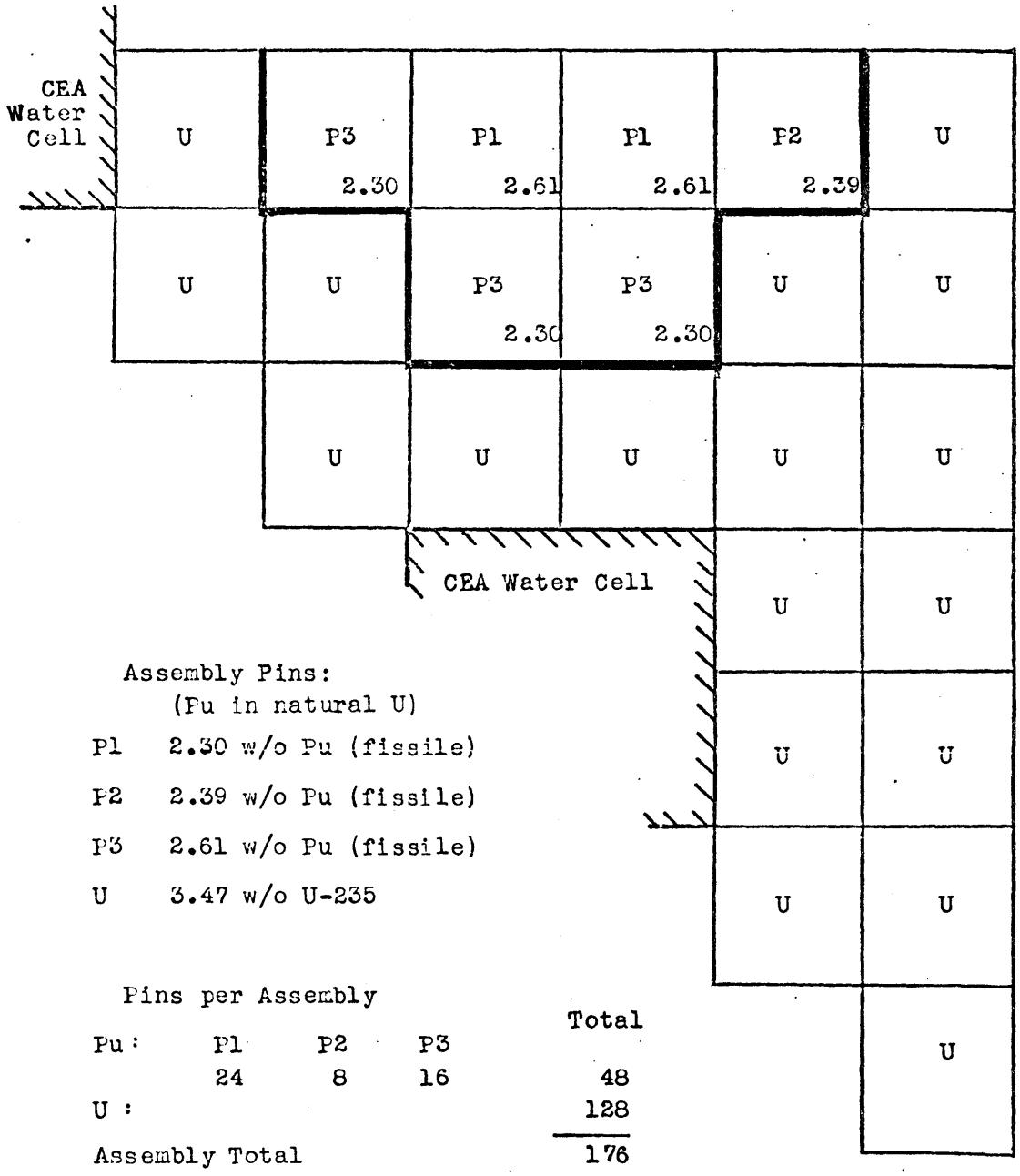

Assembly Pins:
(Fu in natural U)

P1	2.30 w/o Pu (fissile)
P2	2.39 w/o Pu (fissile)
P3	2.61 w/o Pu (fissile)
U	3.47 w/o U-235

Pins per Assembly

Pu:	P1	P2	P3	Total
	24	8	16	48
U :				128
Assembly Total				176

problems are not isolated, but in fact adjacent to each other. That is, the water region is adjacent to the mixed oxide-uranium oxide pin type boundary. The result is a more pronounced adjacent-area spectrum influence on the relative reaction rates in the individual pins. This aspect of the design assembly distinguishes its calculational difficulties from those present in Chapter 6.

7.2 Core and Assembly Characteristics (Maine Yankee PWR)

The design of a plutonium recycle assembly for light water reactor compatibility in a uranium core, as discussed in Section 1.2, begins with those core and assembly characteristics fixed by the as-built reactor design. For the purposes of this study, reactor parameters typical of a Combustion Engineering PWR are obtained from the Maine Yankee Reactor[18]. Table 7.1 lists the values applicable to the assembly relative power distribution calculation.

The most distinguishing characteristic of the normal assembly design, as seen in Figure 1.1, is the incorporation of a control rod scheme which creates five (5) areas in the assembly, each four (4) unit cells in area, for rod insertion. These large areas, under operational conditions with the rods primarily removed, are regions of excess thermalization resulting in power peaking for the neighboring fuel pins. This assembly characteristic makes the "island" approach a feasible design choice to accomodate good plutonium utilization within the power peaking constraints of the assembly, as discussed in the next section.

Table 7.1

Reference Core and Fuel Assembly Design Parameters (Maine Yankee PWR)

Core Thermal Performance	
Linear heat rating (kw/ft)	5.74
Average temperatures (°F)	
Fuel	1190
Clad	620
Moderator	565.4
System pressure (psia)	2250
Fuel Assemblies and Dimensions	
Fuel rods per assembly	176
Active core height (in.)	136.7
Assembly gap (in.)	0.060
Number of spacers in active core	7
Fuel rod pitch (in.)	0.580
Control rod guide tubes/assembly	5
Outer diameter (in.)	1.115
Thickness (in.)	0.040
Clad thickness (in.)	0.026
Active core structural material	Zr-4

Maine Yankee Type A Assembly Calculation

Fuel pellet diameter (in.)	0.3795
Enrichment (w/o U-235)	2.01
Weight U per assembly (kg)	394.8
Moderator natural boron (wppm)	400

Plutonium Island Design Assembly Calculation

Fuel pellet diameter (in.)	0.382
Fissile content(w/o)	
Assembly average Pu	2.42
Assembly average U	2.72
Pin Groups	
P1 (excluding natural U)	2.61
P2 (" " ")	2.39
P3 (" " ")	2.30
U	3.47
Loading (based on 150"active core region)	
kg fissile Pu/tonne Pu,U	6.6
kg fissile Pu/assembly	2.89
Moderator natural boron (wppm)	820
Plutonium isotopic distribution (w/o)	
Pu-239	58.0
Pu-240	23.6
Pu-241	13.7
Pu-242	4.7

7.3 Plutonium Island Design Recycle Assembly

The rationale employed in the island design plutonium recycle assembly is dictated by the following objective, which are achieved in the following ways:

(1) Regional (Mixed Oxide or Uranium) Power Matching

Optimum plutonium utilization in a recycle mode with the gradual introduction of assemblies into a uranium core entails reasonable regionwise (i.e., pin type) power equality for a given plutonium loading. This is accomplished by establishing areas of high plutonium content sufficiently far from water areas to reduce effective plutonium reaction rates to a level comparable to those of the surrounding pins.

(2) Power Peak Reduction

The high thermal reaction rates of plutonium plus the assembly design characteristic of large water areas requires separation of the plutonium pins from these water areas. Use of uranium pins around the water holes enables a shift of the peak pin power to the mixed oxide region. Here the peak value is reduced by plutonium content variation with pin position, known as plutonium region zoning. Alternate methods of power peak reduction (not incorporated in the present design) include use of burnable poison (gadolinium or boron carbide) and uranium region zoning.

(3) Rod Worth Maintenance

Increased reactivity control requirements for a plutonium bearing core (Section 2.1) are effectively offset by control rod

placement in high importance areas, namely areas of higher than average thermal flux. This is accomplished by having control rod areas that are composed primarily of uranium pins, as in the case of the island design.

The particular island design assembly chosen for analysis and given in Figure 7.1 employs plutonium islands consisting of twelve (12) pins each of three (3) different plutonium content pins- 2.61, 2.39 and 2.30 w/o Pu(fissile) in natural UO_2. The remaining pins in the assembly are 3.47 w/o U-235.

The characteristics of the standard uranium (Maine Yankee Type A) assembly and those of the island design assembly are given in Table 7.1 [4]. Notice that the plutonium isotopic content is only 58 w/o Pu-239, much less than that of the plutonium in the Saxton CRX program pins (Chapter 6). The large Pu-240 content (about 24 w/o of the plutonium) means that significant spectrum self shielding effects are present in the plutonium island regions. This plutonium isotopic content is characteristic of "first generation" plutonium, derived from initially all-uranium assemblies after their exposure lifetime in a typical PWR spectrum. Further plutonium exposure results in further buildup of the heavier plutonium isotopes relative to Pu-239.

The plutonium loading in the island design assembly is representative of a "self generated recycle" scheme. This is to say that the reactor loads only that amount of plutonium generated in a previous cycle. Both plutonium loadings and isotopic content change with cycle number and duration. An

eventual "equilibrium" condition is postulated after a given number of cycles, characterized by a saturation in the plutonium fissile content discharged.

The following sections deal with the analysis of the plutonium island design assembly, beginning with a spectrum analysis (LASER-M) of the pin types under infinite lattice assumptions, handling of extended spectrum effects(by THERMOS calculations with the TCL method) and finally a calculation of the relative power distributions. The procedure is parallel to that followed for the Saxton CRX experiment analysis in Chapter 6.

7.4 Spectrum Analysis: LASER-M Infinite Lattice Group Constants

The unit cell constants for each pin type under assumed infinite lattice conditions are calculated by the spectrum code LASER-M. LASER-M Normal constants correspond to cell spectrum averaged effective values, while LASER-M GMND constants are modified according to the theory presented in Section 2.2.4 and its application in Section 3.2.4.

7.4.1 Input Description

The LASER-M cell calculations for the unit cell types of the plutonium island design assembly were made using the basic data of Table 7.1. The computer input listings for the calculations are given in Appendix A. Specific input details include the following:

(1) The pin, clad and fuel dimensions were taken as cold, thermal expansion not being considered. Gap and clad homogenization was performed, as necessitated by LASER-M. The normal

unit cell included the amount of moderator in a square pitch around the fuel pin.

(2) The primary core structural meterial in a fuel pin region was grid spacers (seven (7) axially in the active core region of Maine Yankee). This structure was accomodated in the LASER-M model in the following way:

(A) The total volume per unit length of the seven (7) axial grid spacers in the assembly is divided by the 196 (or 14 x 14) unit cell regions in the assembly. This fraction of volume per unit length is the area by which the unit cell moderator region is reduced due to the excluded moderator volume. (Represents a reduction of 1.2% in the unit cell moderator volume.)

(B) The absorption which this structural material (Zr-4) provides is accounted for by the addition of an equivalent amount of boron to the moderator region. The equivalent value is obtained by a ratio of 2200 m/sec cross section values of Zr-4 (weighted by its constituent atom fractions) and B-10. As a result, natural boron concentration in the moderator increases about 3.3 wppm above the nominal moderator value of 820 wppm.

(3) Fuel region number densities were calculated based on the average assembly loadings as given and the known fuel height stack and pellet radius. The temperature used to Doppler broaden the U-238 resonances (resonance effective temperature) and the Pu-240 resonances was taken as the average fuel temperature.

The LASER-M options included the following. The materials

buckling was searched. The Nelkin kernel for scattering was used, as recommended in Section 2.2.3. The U-238 L factor was searched, with the remaining L factors for the isotopes set equal to 1.0. The epithermal U-238 spatial capture distribution was again obtained from Poncelet[36]. The standard THERMOS iteration technique was used without extrapolation.

LASER-M group constants for the water region were obtained from a small (less than 0.1 cm in radius) fuel region calculation, as discussed in Section 6.3.1. The LASER-M clad region in this calculation represented the structural material in the water region (i.e., four (4) unit cells in area), which consisted of the spacer material plus a control rod guide tube. The guide tube (Zr-4, 1.115 inch OD, 1.035 inch ID) area is about 10% of the water region area, which is quite significant.

In addition to what may be termed "normal" unit cells about the fuel pins, namely those representing a square pitch in area around the pin, calculations were also performed to determine the effect of moderator region size on the group constants themselves. Definitions of unit cells containing "extended" water regions are given as:

(1) Assembly Average Cells

These unit cells contain an amount of moderator determined by dividing the entire assembly transverse moderator area (that around each pin, plus the water region areas and the interassembly gap) by the number of fuel pins in the assembly. (These unit cells contain 119% of the moderator area of a normal unit cell for this assembly design.)

(2) Water Slot Cells

These unit cells contain an added amount of moderator determined by division of the water region (or slot) area moderator among those pins boardering on it. In the plutonium island design, eight (8) boardering pins share four (4) square pitch areas of water region, resulting in an addition to one normal unit cell moderator region an area of one- half ($\frac{1}{2}$) square pitch of moderator (half a unit cell area). (These unit cells contain 182% of the moderator area of a normal unit cell for this assembly design.)

The group constants generated by these cell type definitions were not used in the power distribution calculations in this study. An assembly average cell would be applicable to a depletion calculation in which the unit cell would represent the entire assembly, in a reaction rate sense. Water slot cell constants would be used to introduce some water slot spectral influence into the slot adjacent pins. The changes in the group constants, relative to the normal cell constants, due to these different calculational models are interesting to compare with those resulting from the TCL method (Section 7.5).

7.4.2 Unit Cell Comparison

The effective macroscopic two group constants of the normal unit cell LASER-M calculations for the four (4) fuel pin types and the water regions in the plutonium island design assembly are presented in Table 7.2. These constants are de-

Table 7.2

Macroscopic Group Constants
from LASER-M

Plutonium Island Design

Pin Type	Energy Group	Group Parameters: Diffusion (cm)	Absorption $(cm)^{-1}$	Removal $(cm)^{-1}$	NuFission $(cm)^{-1}$	KFission $(w\text{-}sec/cm) \times 10^{12}$	Thermal Average Velocity (units of 2200 meters/sec): $\bar{v}$ cell	$\bar{v}$ gradient
2.61 w/o Pu(f)	Fast+ Epi	1.4365	0.011811	0.014683	0.0095492	0.11130	2.4872	1.9341
	Thermal·Nor	0.40292	0.18311	-	0.25663	3.0366		
	·GMND	0.77931	0.45542	-	0.63829	7.5527		
2.39 w/o Pu(f)	Fast + Epi	1.4354	0.011553	0.014869	0.0090890	0.10603	2.4525	1.9129
	Thermal·Nor	0.40368	0.17519	-	0.24516	2.9038		
	·GMND	0.77219	0.42966	-	0.60126	7.1215		
2.30 w/o Pu(f)	Fast + Epi	1.4350	0.011445	0.014947	0.0088985	0.10385	2.4376	1.9047
	Thermal·Nor	0.40397	0.17182	-	0.24025	2.8468		
	·GMND	0.76944	0.41883	-	0.58563	6.9394		
3.47 w/o U-235	Fast + Epi	1.4210	0.010183	0.015444	0.0071179	0.090415	2.1917	1.4318
	Thermal·Nor	0.42511	0.086976	-	0.13926	1.8636		
	·GMND	0.80865	0.19063	-	0.30521	4.0846		
Water 820 wppm B	Fast + Epi	1.7044	0.00086690	0.048082	-	-	1.6793	6.6358
	Thermal·Nor	0.29163	0.022713	-	-	-		
	·GMND	1.9352	0.038141	-	-	-		

Values are w/o Pu(fissile) in natural uranium

fined by Eq. (6.1) in terms of the microscopic effective constants of Eq. (2.5). Similar to the Saxton CRX group constants of Section 6.3.2, both Normal and GMND constants are given, as are values of $\bar{v}_{cell}$ and $\bar{v}_{grad}$.

Notice that, for these infinite lattice calculations, the thermal absorption and fission constants for the mixed oxide pins are practically twice those of the uranium pin. This is evidence of the larger plutonium thermal cross section values, despite the increased hardness of the plutonium pin thermal spectrum (as seen by the difference in $\bar{v}_{cell}$). One should remember, too, that the plutonium pins are of smaller fissile content. Note that the sensitivity of the plutonium pin constants to change in fissile content is small.

The difference in the thermal constants between pin type is magnified in the GMND representation by $\bar{v}_{cell}$, which is at least 10% greater for the mixed oxide pin relative to the uranium one. Water region absorption is depressed in a similar way. As discussed in Section 6.3.2, the calculation of $\bar{v}_{grad}$ for the water region is unstable. In a practical sense, this is not significant in that the leakage term in the water region influences the reaction rates in neighboring pins to a smaller extent than does the change in the actual cell absorptions. The influence of the leakage terms, however, requires further investigation.

The macroscopic constants form the basis of the relative power distribution calculations to be discussed in Section 7.6 (LASER-M Normal and GMND results with PDQ-7). In addition, the LASER-M Normal constants are those modified to created TCL

constants (Section 7.5), also for power distribution calculation.

A comparison of the LASER-M Normal microscopic effective thermal group constants for two different pin types, the 3.47 w/o U-235 and the 2.61 w/o Pu(fissile) pins, is given in Table 7.3. Values are given (in barns) for the normal (or basic) unit cells. Percent changes from the basic unit cell values are listed for the assembly average and water slot cells defined in Section 7.4.1. The changes are expressed for the assembly average values (and similarly for the water slot values) as

$$\begin{pmatrix}\text{Percent change (\%) between a Normal and Assembly Average Cell value of } \bar{\sigma}_\alpha^{\,j}\end{pmatrix} = \frac{\bar{\sigma}_{\alpha,\,\text{Assembly Av}}^{\,j} - \bar{\sigma}_{\alpha,\,\text{Normal}}^{\,j}}{\bar{\sigma}_{\alpha,\,\text{Normal}}^{\,j}} \times 100 \qquad (7.1)$$

where $\bar{\sigma}_\alpha^{\,j}$ is the microscopic effective thermal group values from Eq. (2.5).

The table provides some interesting comparisons between the two unit cell fuel types (basic unit cells). A good indication of the difference in spectrum hardness between the uranium and mixed oxide unit cells is evident from the larger magnitude of the uranium pin thermal constants. This is vividly demonstrated by noting the large worth of the plutonium isotopes in the uranium pin spectrum (obtained by introducing plutonium into the uranium pin by a small depletion time step).

Addition of moderator volume to the unit cell by use of an assembly averaged cell calculation shows a significant change (generally an increase) in the constants. Most important is the decrease of the Pu-240 constants due to the reson-

Table 7.3

Plutonium Island Design

Comparison of LASER-M Thermal Microscopic Constants

Thermal Cutoff 1.855 ev.		Pin Description and Unit Cell Type				
		3.47w/o U-235			2.61w/o Pu(fissile)	
Microscopic Effective Thermal C/S (barns)[1]	Absorption	Basic Unit Cell C/S	Assembly Averaged (%)	Water Slot (%)	Basic Unit Cell C/S	Assembly Averaged (%)
	U-235	249.87	(2.83)	(8.22)	187.80	(4.39)
	U-238	1.1239	(2.34)	(6.70)	0.88845	(3.13)
	Pu-239	973.32*	-	-	628.72	(2.26)
	Pu-240	1431.7*	-	-	516.96	(-7.02)
	Pu-241	795.36*	-	-	539.74	(4.44)
	Pu-242	139.01*	-	-	11.877	(0.94)
	B-10	1861.1	(2.99)	(9.62)	1728.1	(3.85)
	Fission					
	U-235	211.74	(2.86)	(8.34)	159.86	(4.37)
	Pu-239	627.36*	-	-	410.26	(2.45)
	Pu-240	0.27324*	-	-	0.098662	(-7.02)
	Pu-241	587.96*	-	-	401.68	(4.52)
Region Averaged Thermal Velocity (units of 2200 m/sec) ($\bar{v}$)	Fuel	2.2685	(-3.00)	(-9.05)	2.5542	(-4.47)
	Moderator	2.1479	(-3.01)	(-9.28)	2.4540	(-4.36)
	Cell	2.1917	(-3.23)	(-9.84)	2.4872	(-4.52)
	Gradient	1.4318	(-3.76)	(-4.04)	1.9341	(-4.14)

[1] $\left(\text{Cell averaged number density}\right)_j \times \left(\text{Microscopic thermal effective C/S for} \propto\right)_j \times \left(\text{Cell averaged thermal flux}\right) = \left(\text{Thermal cell reaction rate for} \propto\right)_j$

-Unit Cell includes moderator within one lattice pitch
-Assembly Averaged Cell includes additional moderator from interassembly gap and control rod water cells (20 unit cells in area) averaged among 176 fuel rods
-Water Slot Cell includes additional moderator of $\frac{1}{8}$ unit cell area

* Values obtained from 100 hour depletion of uranium cell

ance absorption decrease around 1.0 ev as a result of the increased thermalization of the spectrum. This leads to two important observations:

(1) The plutonium pin's fractional isotopic thermal absorption characteristics are generally more spectrum sensitive than those of the uranium pin (namely, larger percent changes in the microscopic thermal constants).

(2) The overall macroscopic thermal absorption of the plutonium pin, however, is less spectrum sensitive. The Pu-240 decrease offsets the general increase in the constants. This is, of course, a function of the Pu-240 concentration which, for the cases studied, was appreciable at beginning of life and increased with burnup.

The relative moderator increase represented by the water slot cell calculation naturally increased the thermal microscopic constants of the uranium cell to an even greater degree.

The results of these calculational comparisons and the sensitivities of the thermal constants to changes in spectrum conditions induced through moderator volume or pin type changes enable us to conclude that:

(1) Serious consideration be given to representing adjacent cell spectrum effects in the pin spectrum calculations (as the TCL method attempts to do) of the plutonium island design assembly.

(2) Accounting for such effects can have a sizeable influence on design decisions. Thus, the methods applied to calculations of this type require careful evaluation through

comparison studies with higher order calculations. The calculation and comparison presented in this study are a small part of those necessary to develop confidence in a method of analysis for such a problem type.

7.5 Extended Spectrum Effects: TCL Thermal Group Constants

The discussion of TCL thermal group constants is parallel to that given in Section 6.4 in application of the theory (Chapter 5) to the Saxton CRX power distribution calculations. Necessary elements of the theory are the definitions of individual cell slabs and cell row multislabs as the THERMOS model slab representations of unit cells and cell rows, respectively. Their definitions are based on a spectrum equivalence concept and their use is calculation of correction factors which are applied, in this study, to the infinite lattice LASER-M Normal thermal group constants given in the previous section. The following sections follow the procedure of obtaining the TCL constants for application to the plutonium island assembly power distribution calculation.

7.5.1 Input Description

The TCL method makes use of a cell row representation by THERMOS slab calculations to obtain correction factors to account for adjacent pin spectrum effects. Figure 7.2 shows the plutonium island design quarter assembly with five (5) cell row types designated. These cell row types are those in the assembly which are used for THERMOS cell row multislab calculations

Figure 7.2 Plutonium Island Assembly
One Dimensional THERMOS Multislabs
with Quasi- Zero Current Boundaries

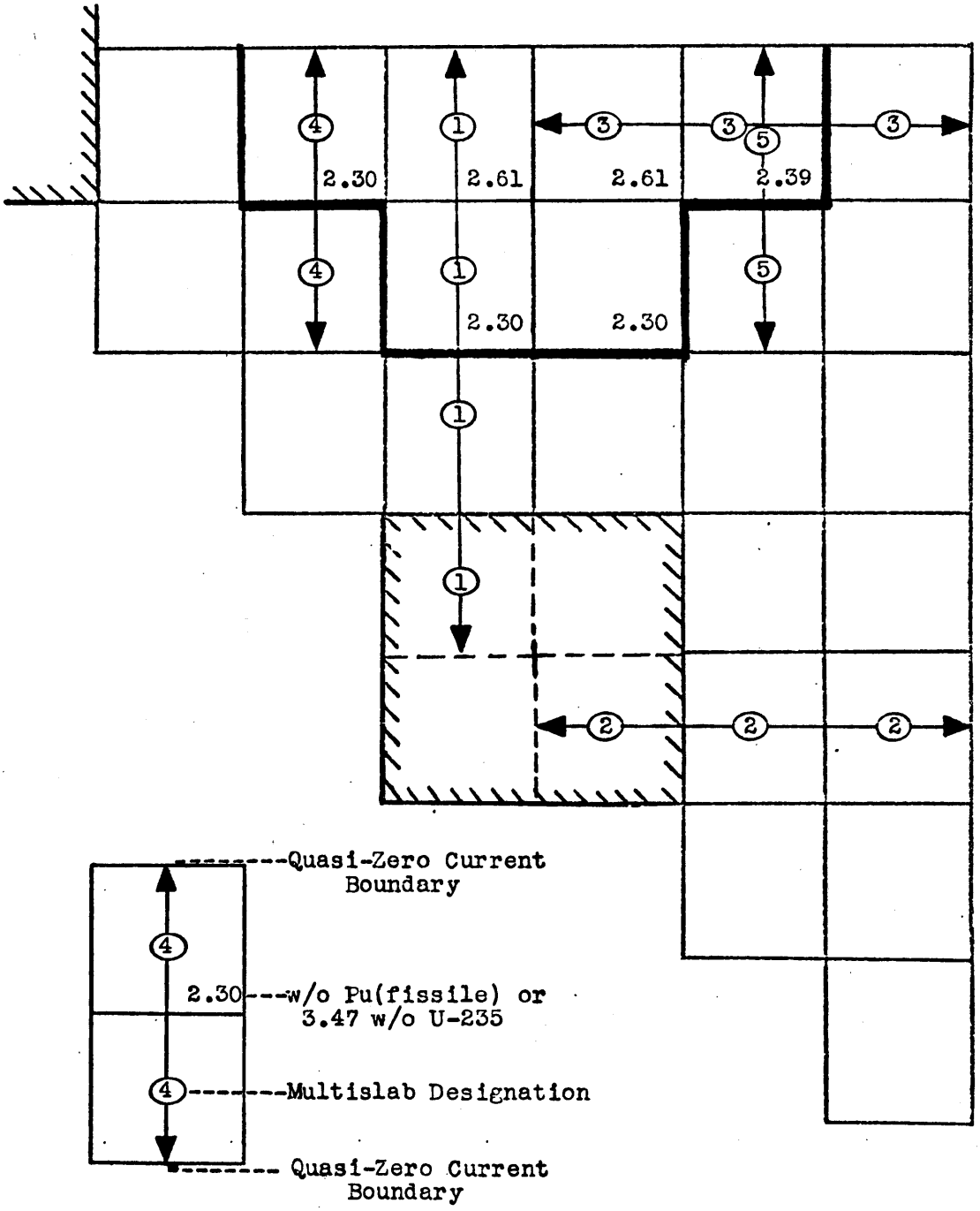

since:

(1) They include the spectrum overlap areas of the assembly as a result of pin type and water slot boundaries.

(2) Their calculation spectrally as a cell row with zero current boundary conditions is a good representation. That is, cell row multislabs ①, ② and ③ are zero-current slab groups (neglecting the interassembly gap) while ④ and ⑤ are quasi- zero current (that is, reflection for at least one unit cell in extent). The entire assembly itself has assumed zero current boundary conditions.

As in Section 6.4.1, a fuel pin slab region, either in the individual cell slab or cell row multislab calculation with THERMOS, is represented by a fuel slab surrounded by moderator slabs (Figure 5.1). The geometric parameters t, the fuel slab half thickness and T, the moderator slab thickness, are again determined by the equivalences to the cylindrical unit cell given by Eqs. (5.1) and (5.2). The following sections give the results of the procedure. The detailed THERMOS code input listing is given in Appendix A for each of the cases.

The similarity of these THERMOS calculations to those in Section 6.4.1 consist of:

(1) Fuel-clad-gap homogenization in the fuel slab

(2) The source terms ($\bar{\Sigma}_r$ of Table 7.2) for the moderator regions are a volume average of those of the fuel pins present in the particular cell row. Water slot region sources are explicitly input as separate source regions.

(3) An epithermal flux (source) dependence of 1/E is used.

(4) THERMOS iteration without extrapolation is used in the solution procedure,

7.5.2 Individual Cell Slabs

Individual cell slab calculations for each of the fuel pin types in the design assembly are necessary for comparison with cell row multislab calculations to obtain the slab environment deviations, $(\%\ \bar{\Sigma}_\alpha)_x$, similar to Eq. (5.3). These form the basis of the TCL group constants (Eqs. (5.4) and (5.5)).

The linear interpolation procedure discussed in Section 6.4.2 is used here to obtain representative values of t and T for the individual cell slab representation. The resulting t is most easily expressed as an "Equivalent t/R_{f+c}", where R_{f+c} is the actual fuel pin radius. Table 7.4 gives the equivalent slab dimensions for representation of each unit cell type by interpolation between calculations with arbitrary values (t_1 and t_2) of fuel slab half thickness.

Notice that the "Equivalent t/R_{f+c}" values for the mixed oxide pins are essentially equal, owing to the small sensitivity to plutonium content of the self-shielding, which variation in t produces. The value for the uranium cell slab is less, or the thickness required to represent the shielding in that pin is less.

The manner of equivalence of the individual cell slab to the cylindrical unit cell is discussed in Sections 5.2 and 5.3. Table 7.5 shows the individual cell slabs as spectral equi-

Table 7.4 Determination of THERMOS Individual Slab Fuel and Clad Thickness (t)

Equivalent to LASER-M Cylindrical Cell- Pu Island Design

(t/T)=(fuel plus clad thickness/moderator thickness)= 0.45491 (preserve water to metal ratio)

(t/R_{f+c})=(fuel plus clad thickness/pin outer radius) will be taken as that ratio at which the fuel plus clad to total cell thermal flux ratio is equal to that of the LASER-M cylindrical unit cell. (linear interpolation used)

Pin Type	Fuel plus clad thermal flux/ Total cell thermal flux			Equivalent
	LASER-M	(t_1/R_{f+c})=0.407	(t_2/R_{f+c})=0.868	(t/R_{f+c})
2.61w/o Pu	0.8746	0.8942	0.7837	0.489
2.30w/o Pu	0.8842	0.9022	0.7984	0.487
3.47w/o U-235	0.9495	0.9550	0.8985	0.454

The values of (t/R_{f+c}) will be those used in the THERMOS multislab for determination of deviation of thermal constants from the THERMOS individual slabs to account for the spectral effect of the cell row by use of TCL (THERMOS corrected LASER-M) constants.

Table 7.5 Comparison of Fractional Isotopic Thermal Absorption- LASER-M Normal C/S versus THERMOS Individual Slab C/S for Various Values of Fuel plus Clad Thickness (t)- Plutonium Island Design

Pin Type	Isotope	Percent of Cell Total Thermal Absorption				Difference (%)
		$(t_1/R_{f+c})=0.407$	$(t_2/R_{f+c})=0.868$	Interpolated (t/R_{f+c})	LASER-M	
2.61w/o Pu(fissile)	U-235	5.6	6.0	5.7	5.7	0.0
	U-238	3.6	3.9	3.7	3.6	0.1
	Pu-239	55.6	56.4	55.7	55.4	0.3
	Pu-240	19.8	17.3	19.4	18.4	1.0
	Pu-241	10.8	11.6	10.9	11.1	-0.2
	Pu-242	0.08	0.09	0.08	0.08	0.0
	etc.	4.5	4.7	4.5	5.8	-1.3
3.47w/o U-235	U-235	79.0	78.9	79.0	77.4	1.6
	U-238	10.0	10.0	10.0	9.6	0.4
	etc.	10.9	11.0	10.9	13.1	-2.8

valents of the LASER-M unit cells with respect to fractional isotopic thermal absorption. The good agreement between the "Interpolated t/R_{f+c}" column values and those of the LASER-M unit cell is noteworthy. The values of the slab thicknesses used for interpolation are also given to indicate the sensitivity to fuel slab thickness. The agreement is justification of the equivalence criteria (Eqs. (5.1) and (5.2)) as those upon which to model equivalent slabs spectrally.

7.5.3 Cell Row Multislabs

Cell row multislab calculations for each of the designated cell rows in Figure 7.2 were performed for the fuel slab half thickness values t_1 and t_2 of Table 7.4. From the comparison of the effective microscopic constants for the unit cell equivalent regions, values of $(\%\overline{\Sigma}_a)_x$ and $(\%\overline{\nu\Sigma}_f)_x$ are obtainable for each thickness value.

The linear interpolation procedure of Section 6.4.2 is again used to obtain the values of these slab environment thermal group constant deviations for use similar to that in Eqs.(5,4) and (5.5) to obtain TCL macroscopic thermal group constants.

The values of $(\%\overline{\Sigma}_a)_x$, the percent change in the effective macroscopic thermal absorption for a given unit cell position in a cell row, are given in Figures 7.3 and 7.4 for each fuel slab thickness t_1 and t_2. The value of the parameter at the "Equivalent t/R_{f+c}" , namely at the LASER-M equivalent thermal flux ratio (given by Eq. (5.2)), is indicated. This is the value used in establishing the TCL correction term (Eq. (5.5)).

Figure 7.3 Variation of THERMOS Multislab Thermal C/S as a Function of Slab Thickness Plutonium Island Design

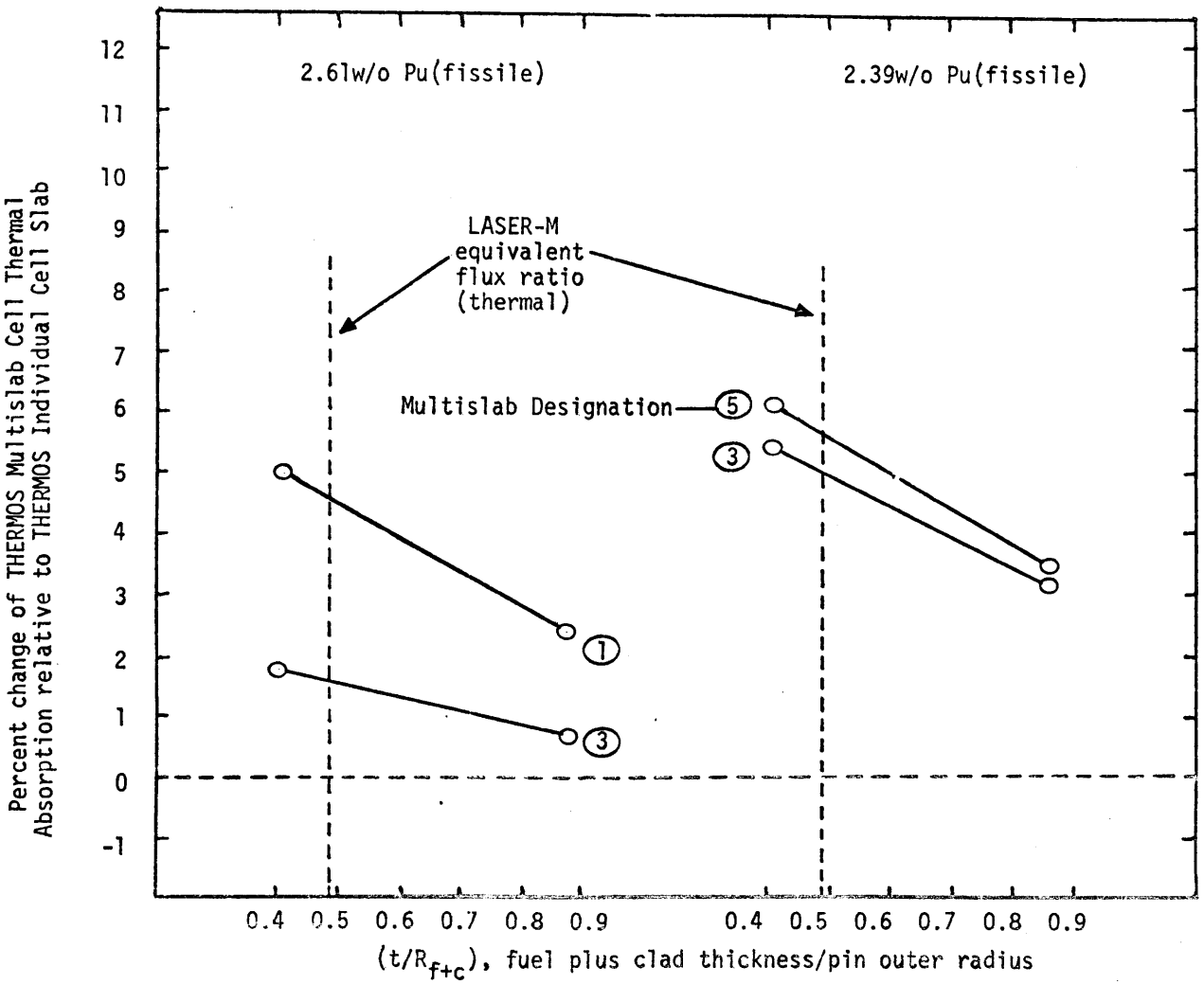

Figure 7.4 Variation of THERMOS Multislab Thermal C/S as a Function of Slab Thickness Plutonium Island Design

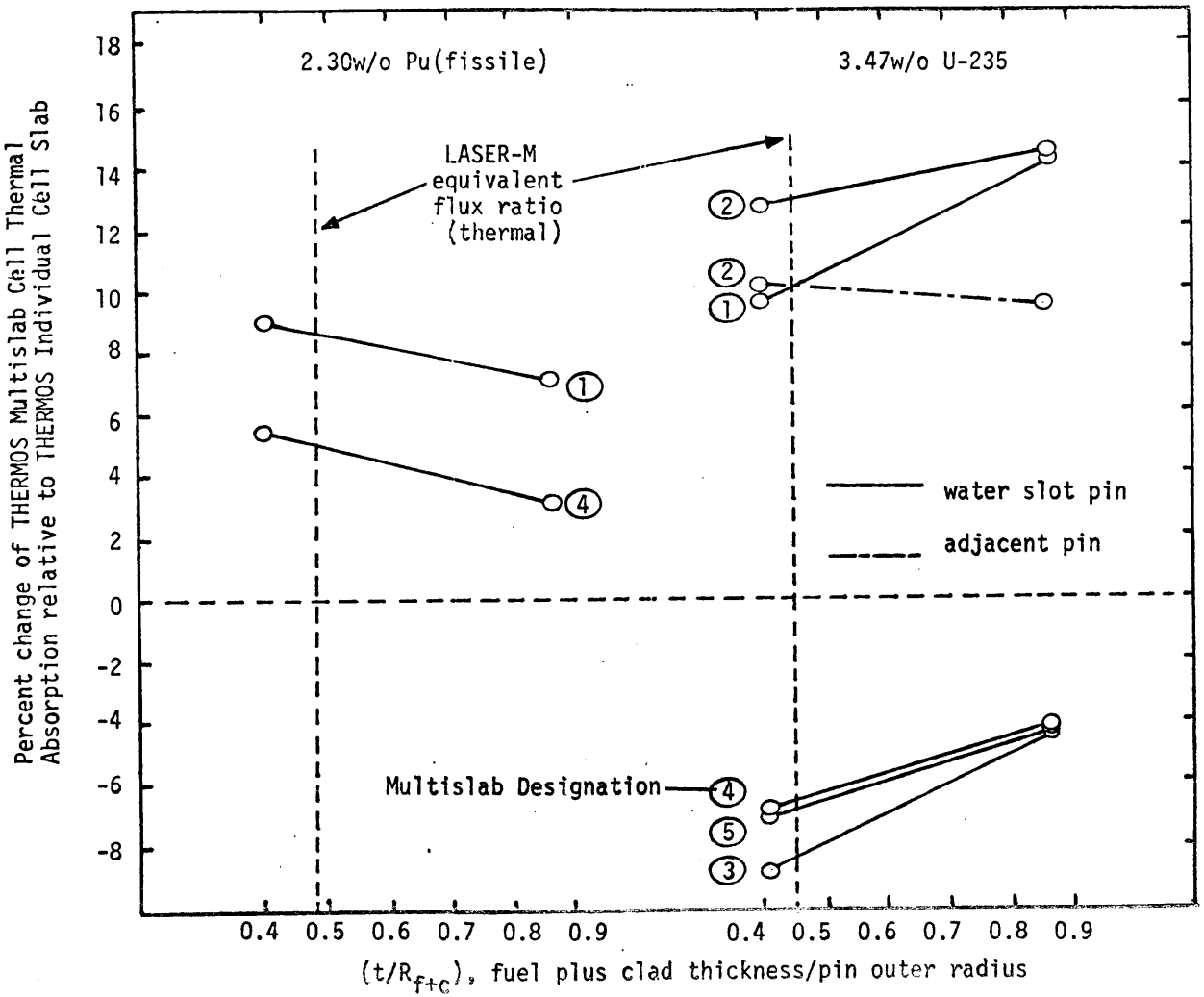

The TCL correction factors for the given unit cell region in the given multislab environment are shown in Figure 7.5 for $(\%\overline{\Sigma}_a)_x$ and $(\%\overline{\nu\Sigma}_f)_x$. The cell row designation "I" refers to the infinite medium calculation, or a zero current boundary condition for the individual cell slab. Such cell row correction factors are zero.

An appreciable increase in the group constants for the 2.30 w/o Pu(fissile) pin cell in Cell Row ① (Figure 7.5-(A)) is due partly to the softer spectrum uranium cell on the cell's right (as in Cell Row ④), but moreso to the spectrum influence of the water region. Certainly the changes are significant. A similar (but smaller) effect is evident in Figure 7.5-(B) for the 2.61 w/o Pu(fissile) pin cell, the greatest influence resulting from the water region inclusion in the cell row. Figure 7.5-(C) shows the changes for the 2.39 w/o Pu(fissile) pin cell. All of the changes are anticipated to have a marked effect on the assembly power distribution, as calculated with the TCL constants, particularly in the direction of increased mixed oxide pin powers.

The effects on the 3.47 w/o U-235 pin cell are demonstrated in Figure 7.5-(D). The water region has a significant positive effect on the values, as expected. A reduction in the group constants results from spectrum calculation in conjunction with an adjacent hard spectrum mixed oxide pin cell, as anticipated.

7.5.4 TCL Thermal Group Constants

The correction terms of Figure 7.5, as one dimensional

Figure 7.5 Variation of THERMOS Cell Row Thermal Constants-
Plutonium Island Assembly Design

Legend:

THERMOS Slab (1D) Calculation

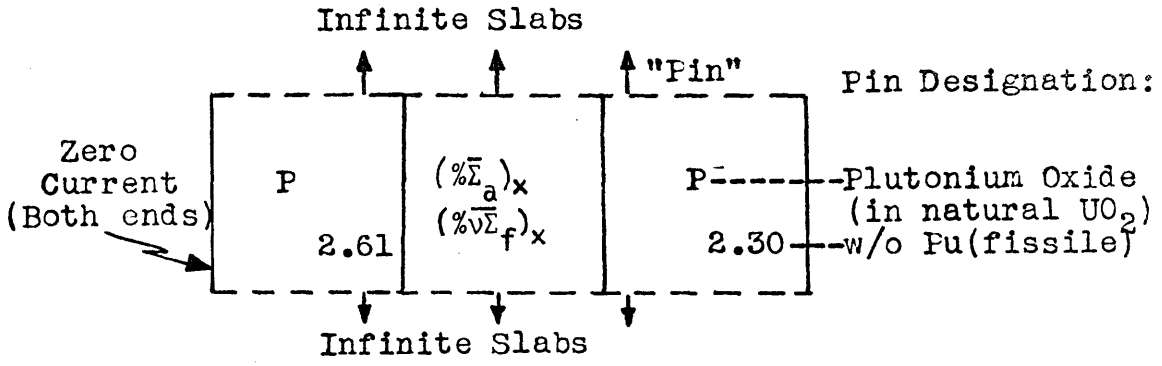

Each "Pin" represented by three slabs (moderator-fuel-moderator)
with space points in each slab(2 - 4 - 2)

Cell Row Designation refers to rows in Figure 7.2

(A) 2.30 w/o Pu(fissile)

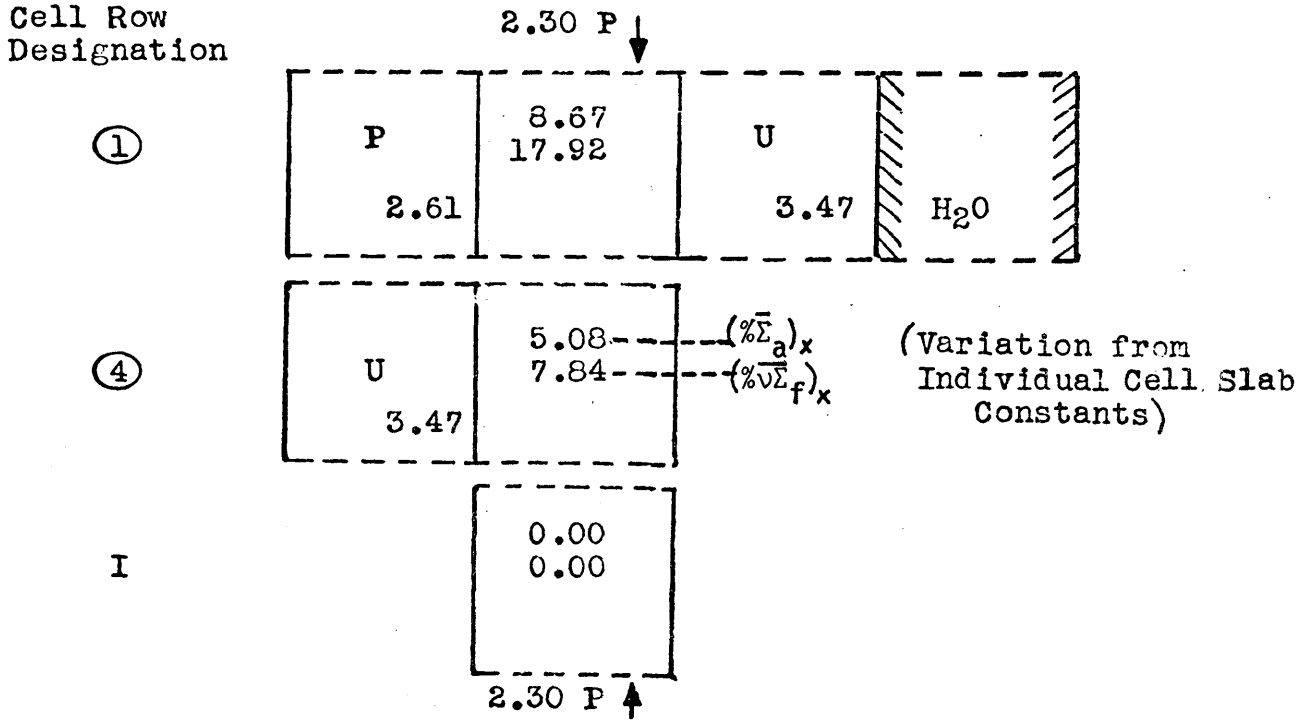

Figure 7.5 Variation of THERMOS Cell Row Thermal Constants-Plutonium Island Assembly Design (Continued)

(B) 2.61 w/o Pu(fissile)

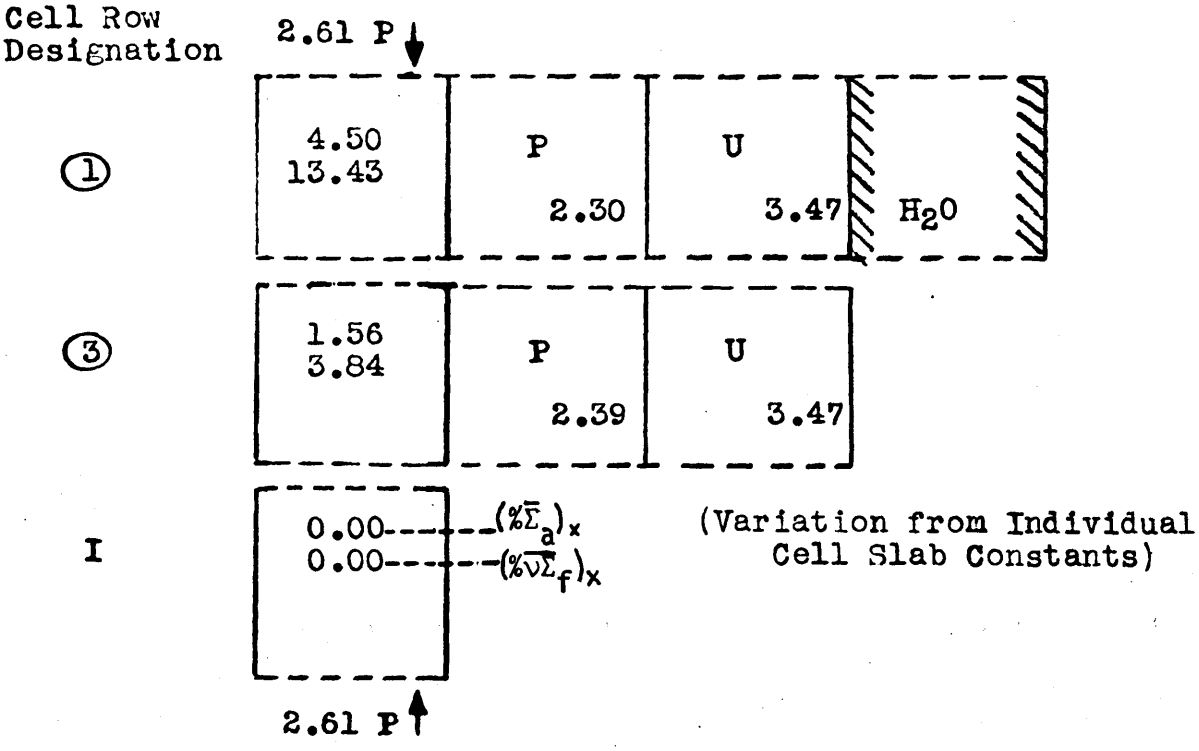

(C) 2.39 w/o Pu(fissile)

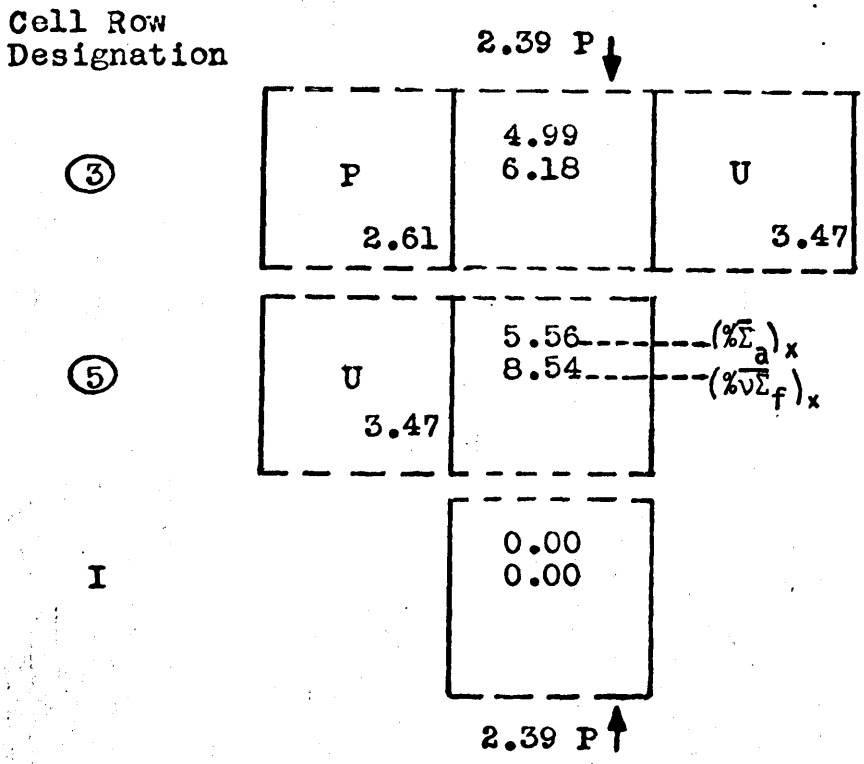

Figure 7.5 Variation of THERMOS Cell Row Thermal Constants-Plutonium Island Assembly Design (Continued)

(D) 3.47 w/o U-235

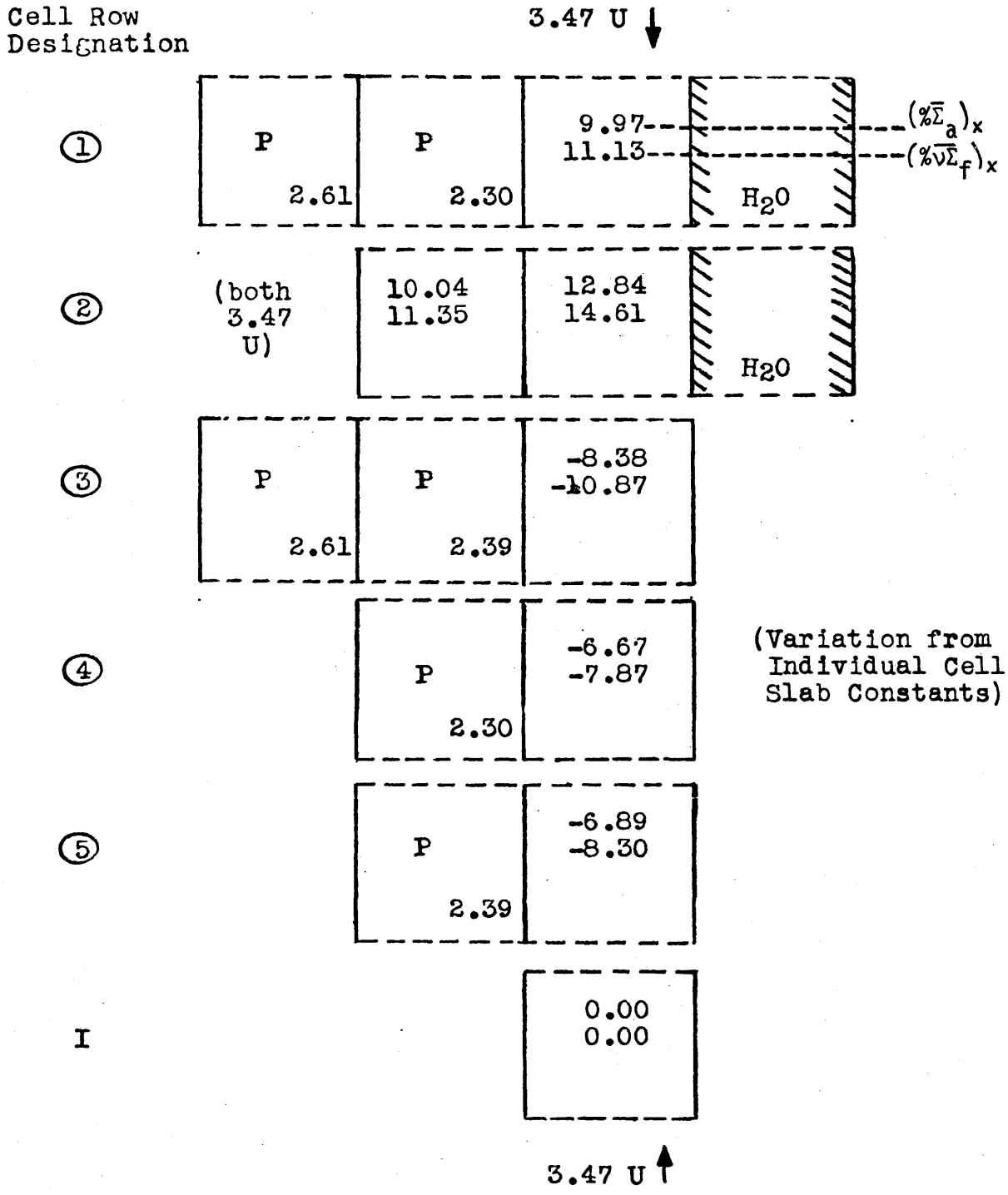

(x direction) cell row environment factors, are combined to form TCL thermal constants for each unit cell region in the assembly, as discussed in Section 5.5. The TCL macroscopic correction factor for each individual unit cell region is given as

$$C = 1 + 1/2 \left(\frac{(\%\bar{\Sigma}_\alpha)_x + (\%\bar{\Sigma}_\alpha)_y}{100} \right) \qquad (7.2)$$

in order to define a TCL macroscopic thermal group constant as

$$\bar{\Sigma}_\alpha^{TCL} = C \quad \bar{\Sigma}_\alpha^{LASER\text{-}M} \qquad (7.3)$$

where $\bar{\Sigma}_\alpha^{LASER\text{-}M}$ is chosen to be the LASER-M Normal macroscopic thermal group constant for reaction α, as discussed in Section 6.4.4.

The value (C - 1) is therefore an average of the two multislab correction terms (due to the x and y directions) which model the influences in each direction from the given unit cell region. From a similar point of view, it is also an average of the correction terms resultant from each of the four unit cells adjacent ot the given unit cell. This view, which gives the same result, is demonstrated in Figure 7.6, each unit cell correction factor composed of four equally weighted terms. (The cell row designations are again from Figure 7.2.) An "I" indicates an infinite medium (i.e., similar) adjacent cell, meaning a correction term of zero. This way of interpretation is helpful for cells at quasi-zero current boundaries, as with Cell Rows ④ and ⑤. From the figure, TCL thermal constants

Figure 7.6 Plutonium Island Assembly

Determination of Deviations of Unit Cell LASER-M Thermal C/S using THERMOS Multi-slabs and Individual Slabs

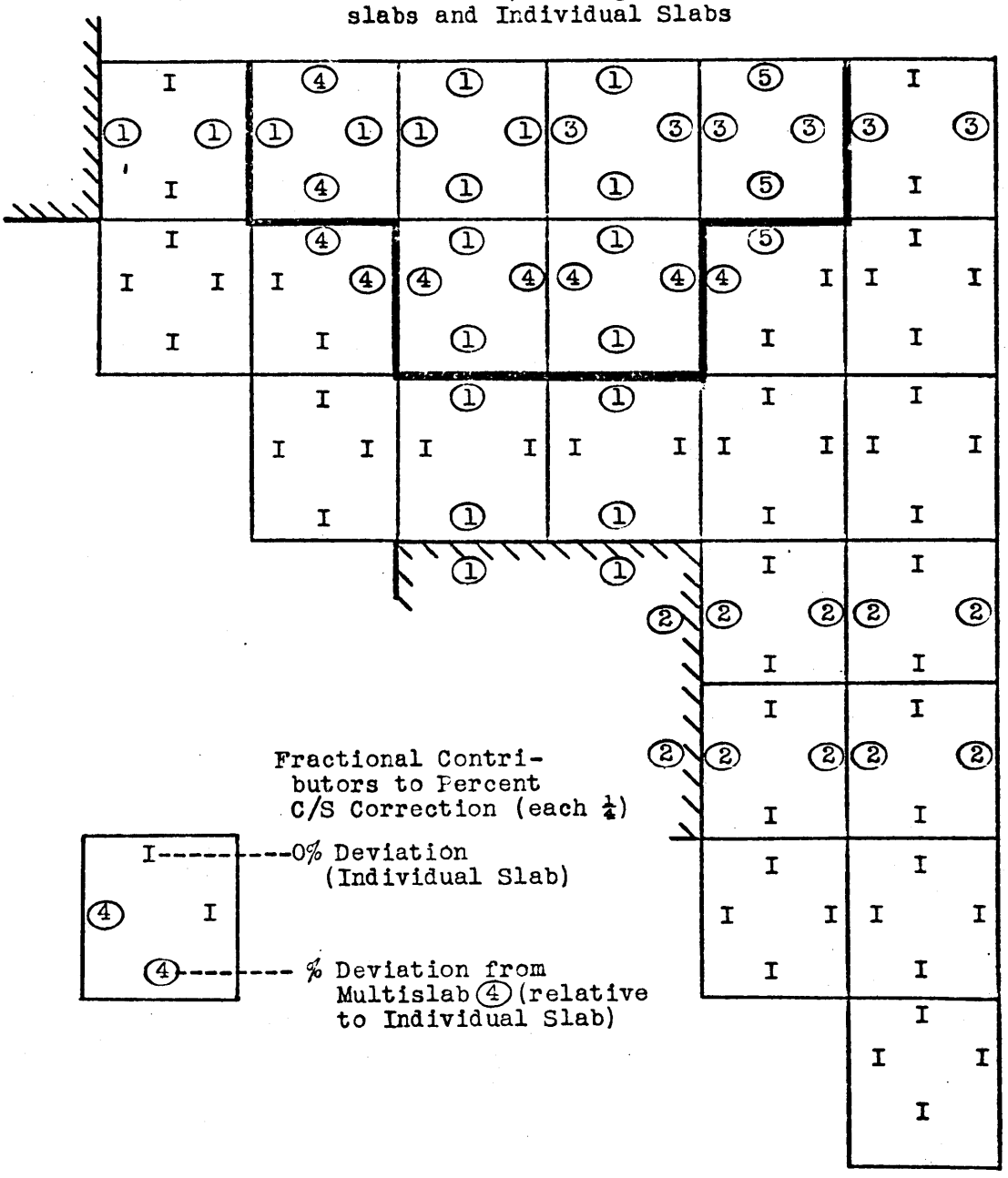

are easily obtained using the data of Figure 7.5 and the LASER-M normal thermal constants of Table 7.2.

TCL thermal values of $\overline{\Sigma}_a$, $\overline{\nu\Sigma}_f$, and $\overline{\kappa\Sigma}_f$ of the appropriate cell regions in the assembly configuration are used in the power distribution calculations for the plutonium island assembly. Soft spectrum constants (namely LASER-M Normal thermal group values) are used in the water regions. This is to say that the region is characterized as highly thermalized, which is conservative for water slot pin peaking. Arguments for correcting the water region constants in a manner similar to the TCL constants is worthy of consideration. The values of $\overline{D}$, the spectrum averaged diffusion coefficient, are taken equal to the LASER-M Normal values for each region, as discussed in Section 6.4.4.

The fast constants are the LASER-M Normal values, as they are in the GMND representation. They are of secondary importance in the power distribution calculations and are quite similar for each pin type in these calculations.

7.6 Spatial Analysis by Few Group Diffusion Theory: PDQ Relative Power Distribution Calculations

The Maine Yankee assembly configuration, for calculation of a standard uranium assembly and the plutonium island design assembly power distributions, is modeled with the spatial diffusion theory code PDQ-7. The code (discussed in Section 3.1.3) accepts the effective few group constants generated for the unit cell regions.

The standard Maine Yankee "Type A" uranium assembly power distribution has been calculated by using LASER-M Normal and GMND group constants with PDQ-7. This serves as a check of the methods by comparison with Yankee calculations and a demonstration of the effect of the different group constant models.

The plutonium island assembly power distribution calculations are performed with LASER-M Normal, LASER-M GMND and TCL two group constants with PDQ-7. In addition, a sensitivity analysis is performed on a number of significant parameters to the power distribution results. Comparison is made between these calculations and a published calculation.

7.6.1 Input Description

Two dimensional relative power distribution calculations were performed for the quarter assembly region of zero current boundary condition. The input listings for the PDQ calculations are given in Appendix A. The following points summarize the significant input modeling details:

(1) Macroscopic effective two group constants were used.

(2) A unit cell region was modeled as a 2 x 2 meshpoint region. The rationale behind the decision not to use an extra mesh point representation is given in Section 6.5.1.

(3) The interassembly gap was explicitly modeled as a moderator region.

(4) The group and region independent axial buckling term was input as the simple sinusoidal flux shape value.

The effect on the relative power distribution to changes in this term for such a large core is extremely small.

7.6.2 Maine Yankee Uranium Assembly Calculation

The Maine Yankee Type A (2.01 w/o U-235) assembly relative power distribution calculational results using LASER-M Normal and LASER-M GMND group constants are given in Figure 7.7. The percent deviation of the pinwise values from the reference calculation (in this case, the GMND calculation) is given for each pin as

$$\% \text{ Deviation} = \frac{\text{Normal} - \text{GMND}}{\text{GMND}} \times 100 \qquad (7.4)$$

Notice in the figure that the GMND calculation accentuates the power peaking around the water slot, as was evidenced in the Saxton CRX water slot results of Chapter 6. These GMND pinwise results matched Yankee MND calculations[59], with the worst pin having less than a 1% difference in power. This provides an acceptable check of our calculational methods.

7.6.3 Recycle Assembly Calculations

The plutonium island recycle assembly calculations were performed with PDQ using LASER-M Normal, LASER-M GMND and TCL macroscopic group constants. The results are expressed as pinwise relative power values.

A study of the sensitivity of the power distribution

Figure 7.7 Assembly Relative Power Distribution
Comparison of GMND and Normal LASER-M 2 Group Constants

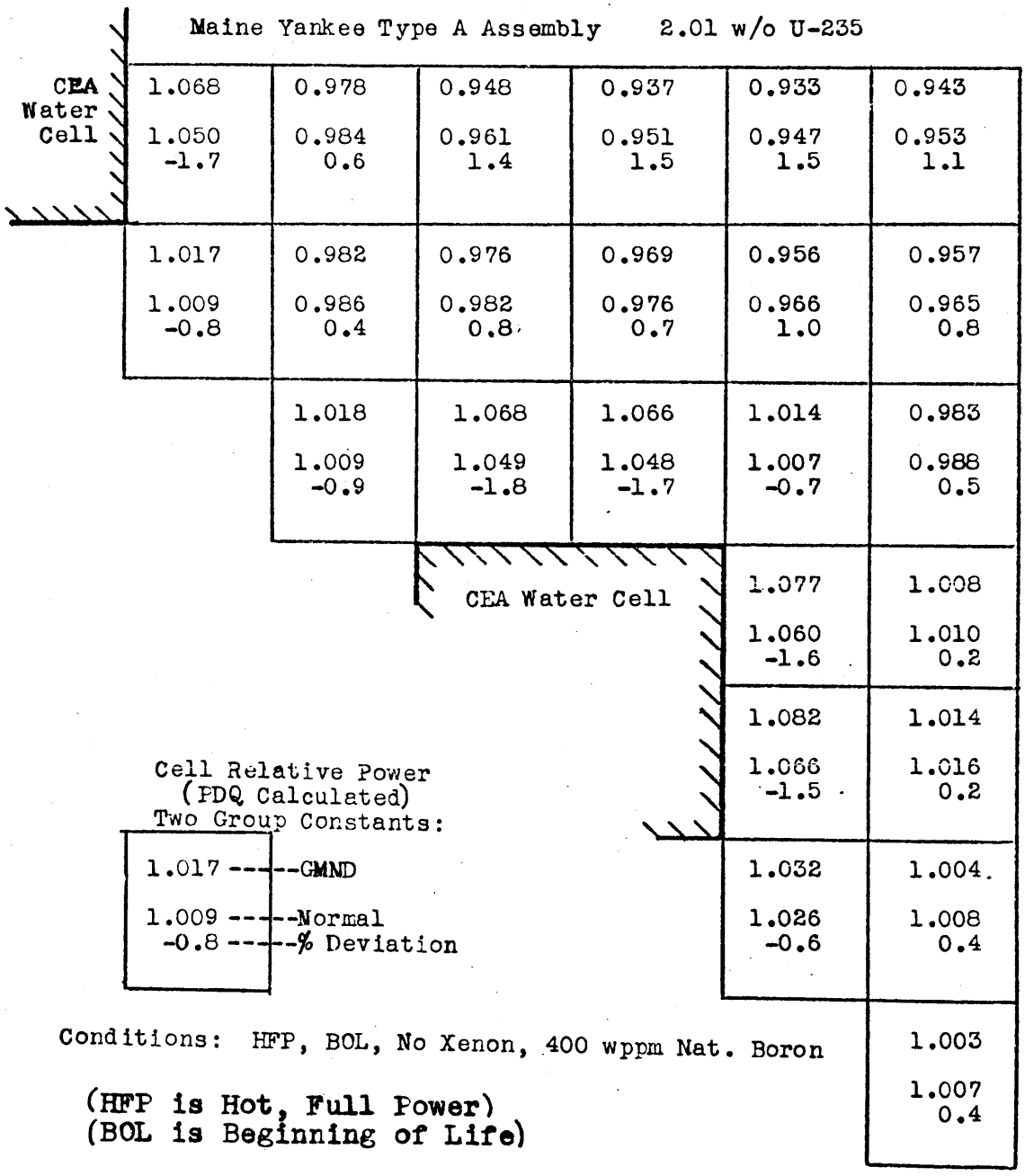

characteristics to changes in the group constants based on changes in the modeling assumptions is presented in Section 7.6.3.2.

7.6.3.1 LASER-M Infinite Lattice Normal and GMND Group Constants Results

The results of the power distribution calculations of the island design assembly with LASER-M Normal or LASER-M GMND group constants are given in Figure 7.8. The values of percent deviation for each pin are given using Eq. (7.4). The region average relative power value is an average of the pin powers in a given region (i.e., pin type) for all such pins in the entire assembly (i.e., the diagonal pins are weighted half that of the rest).

Comparison shows that the GMND calculations predict greater values in power for the pins around the water region, just as in the uranium assembly case. The peak pin (one of the 2.30 w/o Pu(fissile) pins) power also increases when the GMND values are used, but only slightly. Notice that the region average power values are essentially equivalent for the two types of group constants.

Further comparisons are made in Section 7.6.4.

7.6.3.2 Sensitivity of the Power Distribution to Changes in the Group Constants

It is of interest to investigate the sensitivity of the power distribution calculation to changes in the two group parameters for the plutonium island assembly. The two cal-

Figure 7.8 Plutonium Island Assembly Relative Power Distribution- Comparison of GMND and Normal LASER-M Two Group Cell Constants

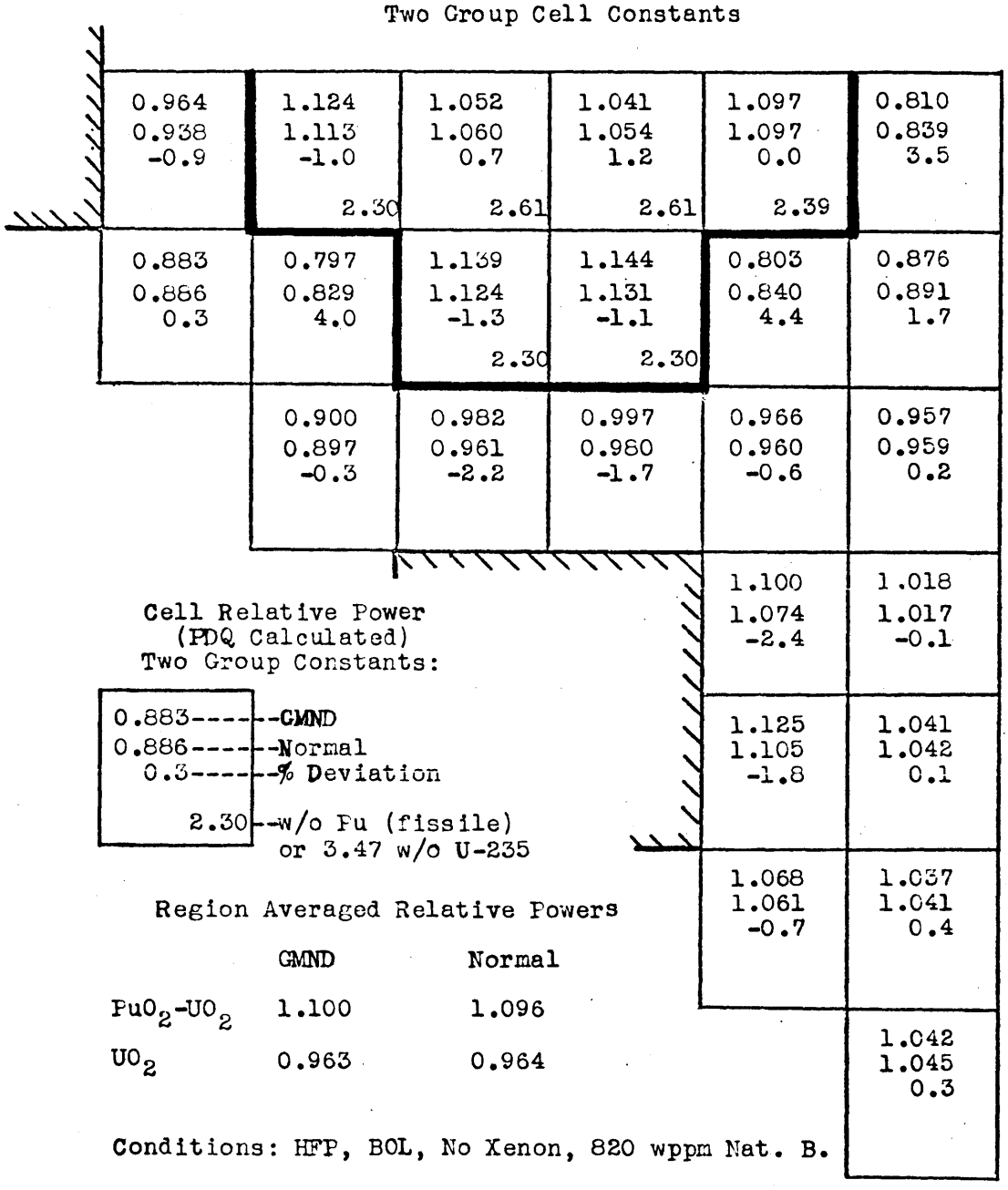

Region Averaged Relative Powers

	GMND	Normal
PuO_2-UO_2	1.100	1.096
UO_2	0.963	0.964

Conditions: HFP, BOL, No Xenon, 820 wppm Nat. B.

culations (Normal and GMND) of Section 7.6.3.1 were taken as base calculations from which to obtain the changes in significant assembly power distribution characteristics (region average and peak pin powers). The results are given in Table 7.6, and the model-imposed group constant changes and their influences are discussed, in the format of the table, below:

Normal C/S

1.2) Assembly Average Removal

The removal terms for each fueled region unit cell were changed to an assembly average value. Notice the lack of significant effect on the power distribution.

1.3) Adjacent Pin Averaged Micros

The spectrum interference of adjacent pins is modeled by use of thermal effective microscopic constants which are averages of the given pin cell micros and those of the four pins surrounding it. Notice the increased peak pin values and the mixed oxide region average value resulting from the plutonium spectrum softening and the water slot pin spectrum softening.

1.4) Uranium Pin Spectrum Micros

A large plutonium region power increase is obtained by use of a uranium pin thermal spectrum assumption for all pins. This is evidence of the vast spectrum difference.

1.5) Regional Bucklings

The PDQ group independent buckling is made region dependent. The buckling values for the mixed oxide pins are

Table 7.6

Plutonium Island Assembly
Relative Power Distribution Sensitivities

Base Cases: PDQ Calculations

Normal C/S: Normal LASER-M C/S, Normal Unit Cells, Geometric Input Buckling, 820 wppm natural Boron, BOL, HFP

GMND C/S: GMND LASER-M C/S, Normal Unit Cells, Geometric Input Buckling, 820 wppm natural Boron, BOL, HFP

Case No. and Description of Change		Relative Power			
		Peak Pu Pin	Peak U Pin	Average Pu	Average U
Normal C/S					
1.1	Base	1.131	1.105	1.096	0.964
1.2	Assembly Average Removal	1.135	1.100	1.103	0.961
1.3	Adjacent Pin Averaged Micros	1.183	1.141	1.121	0.955
1.4	Uranium Pin Spectrum Micros	1.251	1.130	1.174	0.935
1.5	Regional Bucklings	1.135	1.095	1.102	0.962
GMND C/S					
2.1	Base	1.144	1.125	1.100	0.963
2.2	Adjacent Pin Extended GMND	1.136	1.094	1.109	0.959
2.3	2830 wppm Boron	1.153	1.094	1.119	0.955
2.4	100 hrs.-Xenon	1.146	1.123	1.102	0.962
2.5	Adjacent 2.01w/o U Assemblies	1.109	1.140	1.083	0.969
2.6	Regional Bucklings	1.147	1.116	1.106	0.960

arbitrarily decreased according to the ratio of the LASER-M searched materials bucklings for the cell types (i.e., $B^2_{Pu}/B^2_U = 0.61$). The effect on the power distribution is small.

GMND C/S

2.2) Adjacent Pin Extended GMND

The evaluation of $\bar{v}_{grad}$ (Section 2.2.5) by Eq. (2.17) is performed as an average of the gradients from the given pin cell moderator region to the adjacent pin cell moderator regions. This is essentially a variation of the $\bar{D}^{GMND}$ values to include adjacent pin effects. The effect on the power distribution is not large.

2.3) 2830 wppm Boron

Increase of the pin cell moderator boron (nominal value 820 wppm) to a value at which k_{eff} of the assembly is about 1.0 results in a slight power distribution change due to the greater uranium pin power depression (i.e., different boron worth pin the different pin types).

2.4) 100 hrs.- Xenon

A burnup step to model Xe buildup results in a slight power distribution change due to the greater Xe worth in the uranium pins.

2.5) Adjacent 2.01 w/o U-235 Assemblies

A four assembly calculation (one the recycle assembly) vastly changes the power distribution so that peaking results along the recycle assembly edges boardering on the soft spectrum, low enrichment assemblies. Notice

that the peak pin is now a uranium pin (corner pin in the recycle assembly). To avoid this situation, recycle assemblies are not placed near fresh uranium assemblies in suggested recycle schemes.

2.6) Regional Bucklings

(similar to 1.5)

These studies give excellent order-of-magnitude indications of the sensitivities of the power distribution characteristics of this assembly design. Certainly items (1.3) and (1.4) are indications that the spectrum interference effect can have significant power peaking and region average power consequences, as taken into account by the TCL calculation in the next section.

7.6.3.3 TCL Thermal Group Constants Results

The TCL thermal group constants calculated for the plutonium island assembly (Section 7.5) are used in the PDQ calculation of relative power distribution of Figure 7.9. Comparison is made with the LASER-M GMND results, with the TCL values the reference values and the percents deviation again defined similar to Eq. (7.4).

The significant difference between the TCL and GMND results is the increase in both peak pin power (4.3%) and mixed oxide region averaged power (3.9%) for the TCL case. The power change is significant for each pin in the mixed oxide region. This is clearly a result of the inclusion of spectrum interference effects in the TCL method. As an indication of the magnitude

Figure 7.9 Plutonium Island Assembly Relative Power Distribution Comparison- TCL (THERMOS Corrected LASER-M) and LASER-M GMND Thermal Group Constants

(Fast Constants from LASER-M)

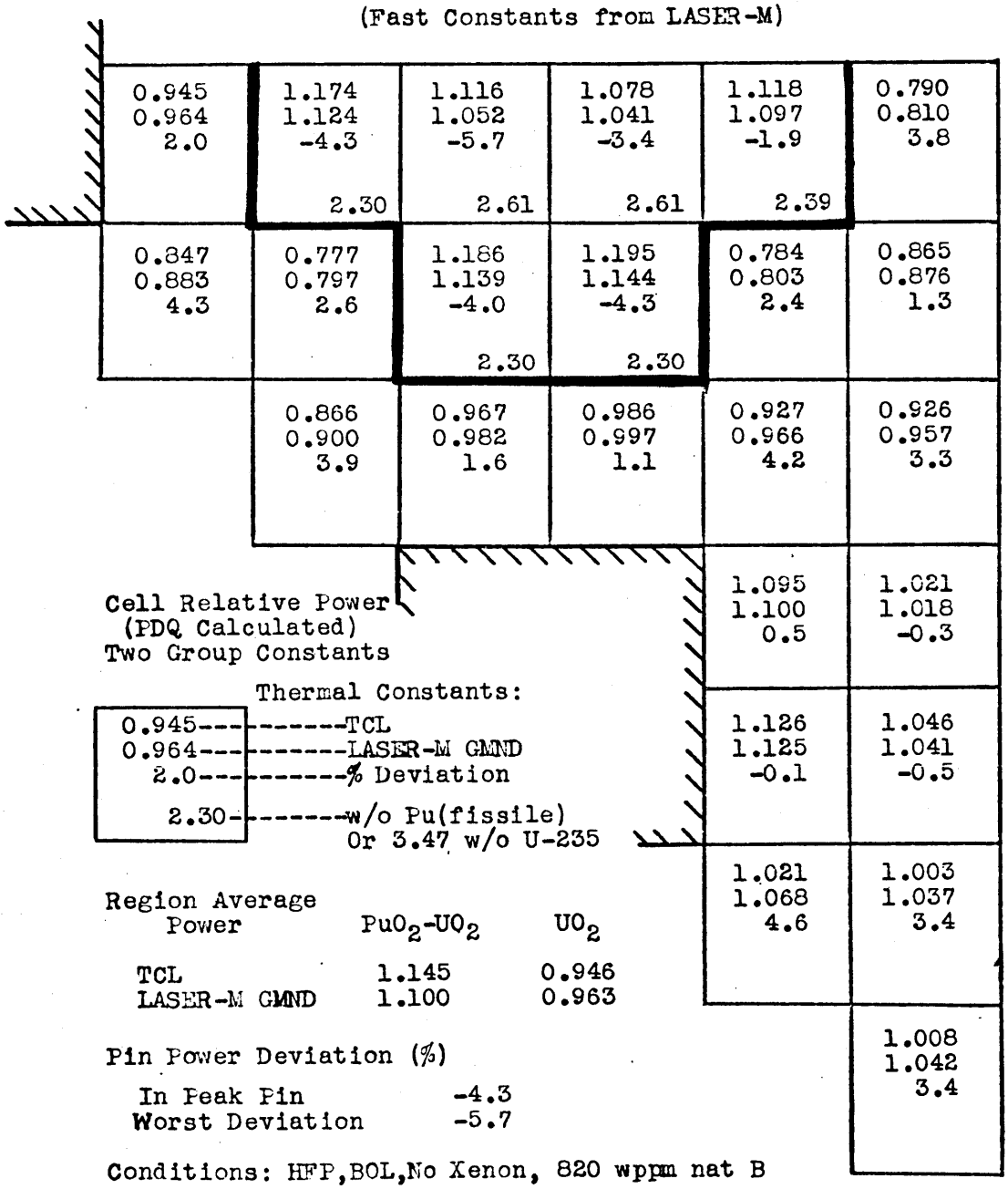

of these effects, note that these power increases are greater than those brought about by the "Adjacent Pin Averaged" microscopic thermal group constants (item (1.3)) of Section 7.6.3.8.

The Saxton CRX calculations of Chapter 6 showed that for isolated spectrum disturbances, namely single discontinuities in an asymptotic core region, the GMND and TCL results were both quite acceptable and essentially equivalent. For the more complicated spectrum overlap case presented here, this is no longer the case. The increased plutonium region power is indication of the presence of the water region, as was evident from the changes in group constants brought about by the TCL corrections from the cell row multislab calculations (Figure 7.5).

7.6.4 Comparison of Recycle Assembly Power Distribution Results with Similar Calculations

The primary fuel assembly power distribution characteristics, as calulcated by the LASER-M Normal, LASER-M GMND and TCL spectrum methods with PDQ are compared in Table 7.7 with the published Combustion Engineering calculated results[4].

Examination indicates that there is essentially good agreement between the TCL and CE results. This is to say that the TCL higher (than GMND) calculated mixed oxide pin power values are in greater correspondence with the reference calculation, which is presumably of higher order.

Concerning the TCL- CE comparison, notice that the peak plutonium pin values are essentially equal. The peak uranium pin is higher in the TCL results due to the extra power peak-

Table 7.7 Plutonium Island Design Assembly

Summary of Power Distribution Calculations

48 Pu pins per assembly 27% of fuel pins Zoned Pu content

Relative Power	Calculational method LASER-M Normal	LASER-M GMND	TCL	CE Calculations
Peak Pu pin	1.131	1.144	1.195	1.20
Peak U pin	1.105	1.125	1.126	1.08
Average Pu	1.096	1.100	1.145	1.17
Average U	0.964	0.963	0.946	0.94

ing around the water slot. This peak would not be as great were it not for the "soft spectrum" water region assumption of Section 7.5.4. A discrepancy in this direction is not verified by the experimental calculations (Chapter 6) in which the TCL prediction of the water slot peak was a slight underprediction. Nevertheless, the average region power values compare favorably, despite the effect which the excess peaking has on their magnitudes.

The mixed oxide region results for the TCL and CE calculations are presented graphically on Figure 7.10. The figure is more instructive, however, of how the island design power distribution changes with plutonium island region size. Notice the plutonium peak pin power decreases with increased region size until about 33% of the assembly is plutonium pin loaded. Further increases shift the peak to a uranium pin. Notice in particular that plutonium island zoning (different plutonium pin types) can effectively reduce this peak. The second part of the figure shows that the average plutonium region power decreases with a greater number of loaded plutonium pins, with no sensitivity to plutonium zoning.

In general, the optimum assembly power design considerations are minimum peak pin power and reasonable regional (pin type) power equality. Compatibility with adjoining assemblies may make desireable a slightly higher plutonium region power (i.e., lower uranium power pins along the assembly boundary). Each of these decisions is necessarily influenced by the economics of the reactor system and the fabrication penalty associated with mixed oxide fuels.

Figure 7.10 Peak and Regional Average Power Ratios for Plutonium Island Design
Zoned and Unzoned Plutonium Region
Calculations

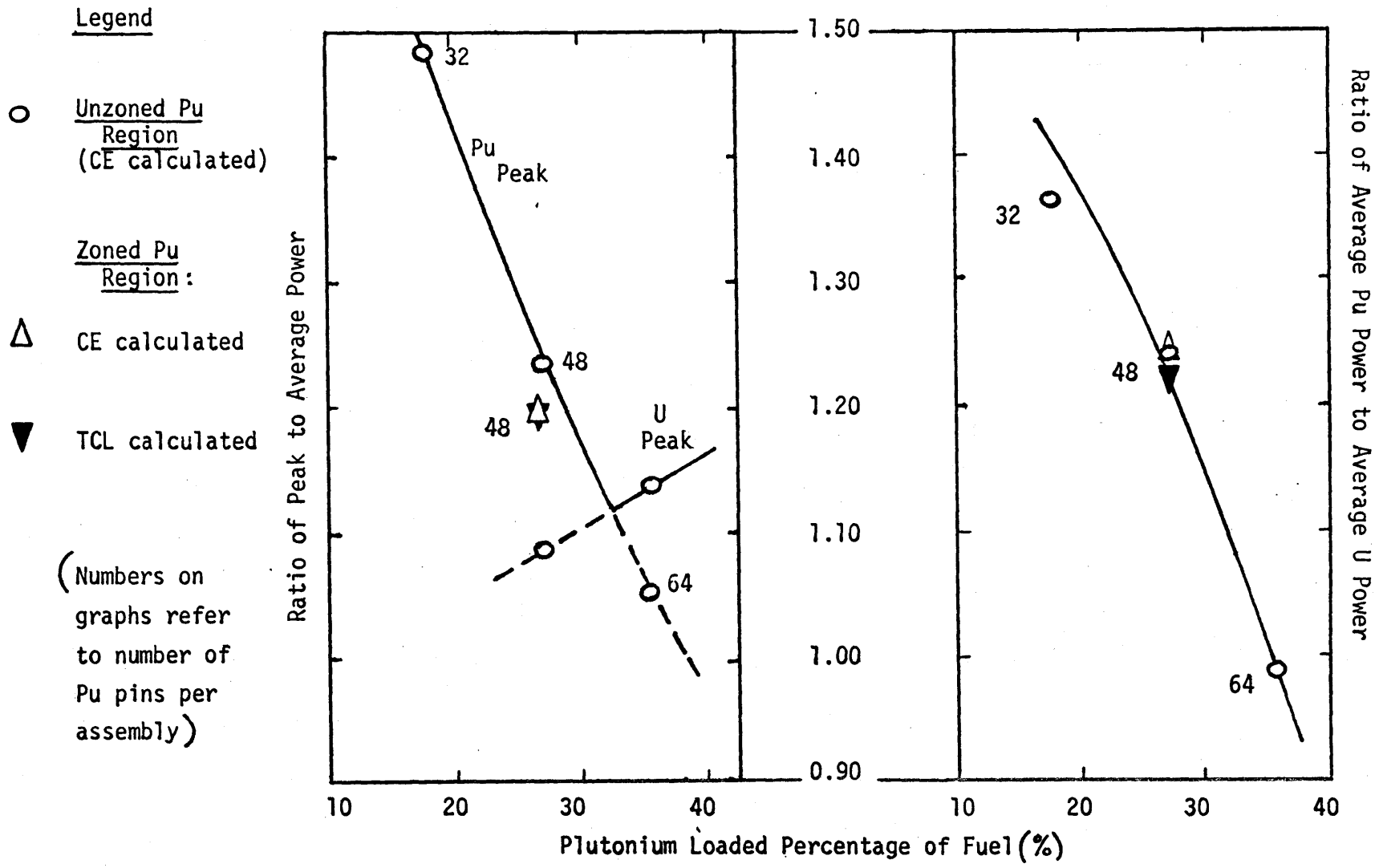

This comparison with CE results indicates that the TCL method can provide a relatively inexpensive means of providing basic data for the design decisions necessary for a plutonium island assembly design type. Further investigations are necessary to verify the procedures used in the TCL method by comparisons with higher order calculations.

7.7 Conclusions

The power distribution calculations for the plutonium island design assembly indicate a significant increase in plutonium region pin power with the TCL method calculation relative to those using the LASER-M infinite lattice methods. This is due primarily to the explicit assembly water region inclusion in the spectrum calculations. The TCL results generally agree with those of a published calculation.

CHAPTER 8

CONCLUSIONS AND RECOMMENDATIONS

The areas of experimental modeling analysis undertaken lead to the following conclusions concerning the LASER-M unit cell model (Section 3.2) as a tool for calculation of few group spectrum averaged cell parameters for mixed oxide fuels:

(1) Critical Experiment Analysis (Section 4.1)

The primary comparison between critical experiment results and the calculations made by using LASER-M were performed by Momsen[9]. These comparisons indicate that the inclusion of ENDF/B-II thermal plutonium cross sections in the original LASER version results in better criticality predictions (smaller spread in k_{eff} with lattice pitch and smaller deviations).

The additional comparisons given in Section 4.1.4 comparing the LASER versions are inconclusive, but the results are dependent upon Pu-240 content in the fuel. The Pu-240 absorption difference between the original LASER and LASER-M is significant.

The calculational results, overall, agree with those of Celnik, et.al.[26] as to the superiority of the LASER model for plutonium analysis, in contrast to LEOPARD.

(2) Isotopic Analysis Comparisons (Sections 4.2 and 4.3)

The Yankee Core I depletion (3.4 w/o U-235) to 40,000 MWD/MT was modeled by LASER-M and resulted in good main chain isotopic predictions on a pin averaged basis with burnup. Predictions

were as accurate as Yankee calculations, in general.

The Saxton Core II depletion (UO_2- 6.6 w/o PuO_2) to 20,000 MWD/MT was modeled with LASER-M, yielding good main chain isotopics predictions, both on a pin averaged basis and radially within the pin with burnup. Predictions were generally as accurate as those of Westinghouse.

Based on these results, the LASER-M unit cell model is deemed an adequate tool for asymptotic region cell depletion and spectrum analysis.

The LASER-M group constants (Normal or GMND (Section 2.2.5)), representative of "infinite lattice" unit cells, were used for power distribution calculations for mixed oxide lattices, to be compared with either experimental (Saxton CRX facility, Chapter 6) or calculational (Plutonium Island Design Assembly, Chapter 7) results.

In response to the spectral interference of closely spaced but quite dissimilar regions, a third set of group constants, called THERMOS Corrected LASER-M (TCL) constants, were developed (Chapter 5). The results of the application of the LASER-M Normal, LASER-M GMND and TCL group constants (with PDQ) to the calculation of power distributions for the cases of spectral discontinuity were:

(1) Saxton CRX Cores (Comparison with experimental results and Westinghouse calculations- Isolated Spectrum Discontinuities - Chapter 6)

(A) Water Slot Power Peaking

Normal constants grossly underpredicted the experimental peaking. The GMND prediction was excellent, while that

of the TCL constants was good (a slight underprediction of the peak pin power). The GMND and TCL predictions were better than those of the Westinghouse calculations.

(B) Mixed Oxide- Uranium Oxide Boundary Power Peaking

All models yielded good prediction. The GMND peaking prediction was slightly greater than that of the Normal constants, and slightly less than that of the TCL constants. The predictions were as good as those of Westinghouse.

(2) Plutonium Island Assembly (Comparison with published calculations- Complex Spectrum Overlapping- Chapter 7)

The GMND and Normal constants results were similar with respect to mixed oxide pin powers and power peaking. The GMND method gave slightly more water region power peaking. The TCL method predicted a significant increase in mixed oxide pin powers relative to the other two calculational methods. This is a result of the explicit inclusion of adjacent,dissimilar spectral areas in the spectrum calculation. The TCL results were analogous to those of published calculations.

The basic understanding gained from the power distribution calculations is recognition of the need for allowance in the spectrum calculation, in certain cases, of adjacent region effects, as provided by the TCL method. The infinite lattice GMND group constants, nevertheless, were quite acceptable for representing the power peaking effects near normal, isolated

(i.e., asymptotic region) discontinuities.

The following recommendations are given for future work in the designated areas:

Plutonium Calculational Methods- General

(1) Modifications to the unit cell code LEOPARD for more accurate representation of plutonium fueled systems are recommended. Work in this area was initiated by Spierling[28] at MIT.

(2) Development of the Advanced Recycle Methodology Program[8] (ARM) should be followed and its capabilities evaluated by the performance of benchmark calculations.

(3) Adequate capability to perform higher order calculations (Monte Carlo and 2D Transport Theory) for plutonium thermal lattices is necessary to evaluate various models, such as TCL, which attempt to account for complex spectral effects.

(4) More experimental data on water slot power peaking, regional power sharing and control rod worths would be beneficial, especially for larger, smaller leakage cores at standard LWR operating conditions.

LASER-M Unit Cell Model

(1) Cross section developments should be followed and modifications made to the cross section set based on published evaluations and applicability of the cross sections to thermal reactors.

(2) Further experiment- calculation comparisons should be performed as data is available. Comparisons with hot lattices are especially needed.

(3) Modification to the LASER input/output format is necessary for its practical use as a production model (like LEOPARD). Deficiencies include:

  (A) No thermal expansion of the cell structure

  (B) No options for the input of fuel loading values

  (C) No "extra region" capability

  (D) No flexibility in the burnup step duration

(4) Possible input and model modifications are given at the end of Section 4.3.4.

Lattice Power Distribution Calculational Methods

(1) The TCL method requires further evaluation as to its adequacy to represent spectral interferences between unit cells, especially on an isotopic reaction rate basis. Comparison with higher order calculations would be beneficial.

(2) The following modifications to the TCL model should be investigated. These areas are mentioned in Section 6.4.4.

  (A) Application of a combined TCL-GMND approach

  (B) Better representation of the diffusion coefficient by THERMOS calculation or modification

  (C) Better water region spectrum representation

(3) Similar calculations should be performed using a THERMOS cylindrical model for unit cell spectrum effects treatment.

REFERENCES

1. F.G. Dawson, "Thermal Reactor Plutonium Fuel Irradiation Programs in the United States," Proceedings of the Panel on Plutonium Recycling in Thermal Reactors, IAEA, Vienna, Austria (1971).

2. "The Generic Environmental Statement on the Use of Recycle Plutonium in Mixed Oxide Fuel in LWR's"(GESMO), Draft Report, WASH 1327, USAEC, August 1974.

3. "Technical Report on the Effects of Plutonium Utilization on the Performance of LWR's," WASH 1303, AEC Regulatory Staff, April 1974.

4. R.L. Hellens, "Problems in the Recycle of Plutonium in Pressurized Water Reactors,"Paper presented at the ANS Winter Meeting, Miami, Florida, October 1971.

5. E.A. Eschbach, S. Goldsmith, "Using Plutonium in Thermal Reactors," Nucleonics, 21, 48 (1963).

6. "E.E.I.- Westinghouse Plutonium Recycle Demonstration Program Progress Report for the Period Ending December 1970," WCAP 4167-2, Westinghouse Electric Corporation (1971).

7. R.C. Liikala, V.O. Uotinen, U.P. Jenquin, "Lattices of Plutonium Enriched Rods in Light Water- Part II: Theoretical Analysis of Plutonium- Fueled Systems," Nucl.Tech., 15, 272 (1972).

8. B.A. Zolotar, W.J. Eich, "Advanced Recycle Methodology Program: Preliminary Specifications for a New Nuclear Computational Capability," EPRI SR-2, July 1974.

9. B.F. Momsen, "An Analysis of Plutonium Recycle Fuel Elements in San Onofre-I," Department of Nuclear Engineering, Massachusetts Institute of Technology, MITNE- 161, June 1974.

10. C.G. Poncelet, "LASER- A Depletion Program for Lattice Calculations based on MUFT and THERMOS," WCAP 6073, Westinghouse Electric Corporation (1966).

11. V.O. Uotinen, et.al. "Lattices of Plutonium Enriched Rods in Light Water- Part I: Experimental Results," Nucl.Tech., 15, 257 (1972).

12. R.J. Nodvik, "Evaluation of Mass Spectrometric and Radiochemical Analyses of Yankee Core I and Core II Spent Fuels," WCAP 6086, Westinghouse Electric Corporation (1965).

13. P. G. Lacey, R. E. Radcliffe, "Diffusion Theory Depletion Analysis of the Yankee Core," WCAP 6077, Westinghouse Electric Corporation (1966).

14. "Saxton Plutonium Program Semiannual Progress Report for the Period Ending June 30, 1967," WCAP 3385-12, Westinghouse Electric Corporation (1967).

15. R.J. Nodvik, et.al. "Saxton Core II Fuel Performance Evaluation of Mass Spectrometric and Radiochemical Analyses of Irradiated Saxton Plutonium Fuel," WCAP 3385-56(Pt. 2), Westinghouse Electric Corporation (1970).

16. E. G. Taylor, "Saxton Plutonium Program- Critical Experiments for the Saxton Partial Plutonium Core," WCAP 3385-54, Westinghouse Electric Corporation (1965).

17. W. L. Orr, et.al. "Saxton Plutonium Program- Nuclear Design of the Saxton Partial Plutonium Core," WCAP 3385-51, Westinghouse Electric Corporation (1965).

18. R. J. Breen, "A One-Group Model for Thermal Activation Calculations," Nucl.Sci.Engr., 9, 91 (1961).

19. H. C. Honeck, "THERMOS- A Thermal Transport Theory Code for Reactor Lattice Calculations," BNL 5826, Battelle Northwest Laboratories (1961).

20. B.J. Toppel, I. Baksys, "The Argonne-Revised THERMOS Code," ANL-7023, Argonne National Laboratories (1965).

21. R. F. Barry, "LEOPARD- A Spectrum Dependent, Non-Spatial Depletion Code for the IBM-7094," WCAP 3269-26, Westinghouse Electric Corporation (1973).

22. H. Bohr, Jr., et.al. "MUFT-4 Fast Neutron Spectrum Code for the IBM-704," WAPD-TM-72 (1957).

23. H. Amster, R. Suarez, "The Calculation of Thermal Constants Averaged over a Wigner-Wilkins Flux Spectrum: Description of the SOFOCATE Code," WAPD-TM-39 (1957).

24. A. Amouyal, P. Benoist, J. Horowitz, "New Method of Determining the Thermal Utilization Factor in a Unit Cell," J. Nuclear Energy, 6, 79 (1957).

25. P. G. Mertens, "Analysis of Conventional and Recycle Unit Assemblies for the Yankee (Rowe) PWR," MIT-134 (Draft Report), Department of Nuclear Engineering, Massachusetts Institute of Technology (1971).

26. J. Celnik, et.al. "Evaluation of Plutonium Recycle Nuclear Calculational Methods by Comparison with Experimental Data," Topical Report on Development of Plutonium Recycle in Thermal Reactors, UNC 5168, United Nuclear Corporation (1967).

27. M. Nelkin, "Scattering of Slow Neutrons by Water," Phys. Rev., 119, 741 (1960).

28. H. Spierling, "The Value of Recycle Plutonium in Pressurized Water Reactors," Doctoral Thesis, Department of Nuclear Engineering, Massachusetts Institute of Technology (1972).

29. A. Radkowsky (ed.), Naval Reactor Physics Handbook: Vol.I Selected Basic Techniques, USAEC (1964).

30. W. R. Cadwell, "PDQ-7 Reference Manual," USAEC Report WAPD-TM- 678, Bettis Atomic Power Laboratory (1967).

31. B. F. Momsen, Personal Communication, Yankee Atomic Electric Company, January 1975.

32. H. C. Honeck, "ENDF/B- Specifications for an Evaluated Nuclear Data File for Reactor Applications," BNL-50066, USAEC (1966).

33. H. C. Honeck, "The Calculation of Thermal Utilization and Disadvantage Factors in Uranium Water Lattices," Nucl.Sci.Engr., 18, 48 (1964).

34. L. E. Strawbridge, R. F. Barry, "Criticality Calculations for Uranium Water-Moderated Lattices," Nucl.Sci.Engr., 23, 58 (1965).

35. E. Hellestrand, "Measurements of the Effective Resonance Integral in Uranium Metal and Oxide in Different Geometries," J.Appl.Phys., 28, 1493 (1957).

36. C. G. Poncelet, "Burnup Physics of Heterogeneous Reactor Lattices," WCAP 6069, Westinghouse Electric Corporation (1965).

37. L. A. Hageman, C. J. Pfeifer, "The Utilization of the Neutron Diffusion Program PDQ-5," WAPD-TM-395, Bettis Atomic Power Laboratory, Westinghouse Electric Corporation (1965).

38. A. W. Brown, J.A. McClure, R.J. Wagner, "Summary of PDQ-7 (IBM 360-370 Version) Input Data Requirements and Operating Procedures," ANCR 1061, Aerojet Nuclear Corporation (1972).

39. R. Breen, O.J. Marlowe, C.J. Pfeifer, "HARMONY- System for Nuclear Reactor Depletion Computation," USAEC Report WAPD-TM-478, Bettis Atomic Power Laboratory (1965).

40. C. S. Rim, "Neutronic and Thermal Analysis of Nuclear Fuels," Sc.D. Thesis, Department of Nuclear Engineering, Massachusetts Institute of Technology (1969)

41. R. Sher, J. Felberbaum, "Least Squares Analysis of the 2200 m/sec Parameters of U-233, U-235 and Pu-230," BNL-918 (1965).

42. V. O. Uotinen, B.R. Leonard, R.C. Liikala, "The Neutronics of Plutonium Recycling," Nucl.Tech., 18, 115 (1973).

43. R. L. Hellens, "Problems in Recycle of Plutonium in Pressurized Water Reactors," Trans. Am. Nucl. Soc., 14, 820 (1971).

44. L. C. Schmidt, R.C. Liikala, W.P. Stinson, J.R. Worden, "Critical Masses and Bucklings of PuO_2-UO_2-H_2O Systems," J. of Am. Nucl. Soc., 7, 216 (1964).

45. N. R. Nelson, "Saxton Plutonium Program-Quarterly Progress Report for the Period Ending June 30, 1965," WCAP 3385-4, Westinghouse Electric Corporation (1965).

46. N. R. Nelson, "Saxton Plutonium Program Quarterly Progress Report for the Period Ending December 31, 1964," WCAP 3385-2, Westinghouse Electric Corporation (1965).

47. B. F. Momsen, Personal Communication, Yankee Atomic Electric Company, May 1975.

48. R. C. Liikala, W. P. Stinson, "Experimental and Analytical Results for PuO_2-UO_2-H_2O Lattices," Trans. Am. Nucl. Soc., 9, 127 (1966).

49. K. B. Stewart, "BNW Master Library," BNWL-CC-325, Pacific Northwest Laboratories, September 1965 (and subsequent revisions).

50. R. P. Matsen, "An Analysis of Yankee Rowe Burnup Data," BNWL-1122, Pacific Northwest Laboratories (1969).

51. R. J. Cacciapouti, "Evaluation of the Yankee Method for Calculating Uranium Depletion and Plutonium Production in Exposed Fuel," YAEC-1060, Yankee Atomic Electric Company (1972).

52. R.J. Cacciapouti, R.R. McCoy, "A Comparison of Measured Yankee Isotopic Data to the Results of the LOCALUX Computer Program," YAEC 1053, Yankee Atomic Electric Company (1971).

53. T.R. England, "CINDER- A One-Point Depletion and Fission Product Program," WAPD-TM-334, August 1972.

54. "Large Closed Cycle Water Reactor Research and Development Program, Progress Report, October 1- December 31, 1963," WCAP 3750, Westinghouse Electric Corporation (1964).

55. J.M. Friscella, "LOCALUX-2 Program Description- Revision 3 of Phys/Math 5201," NED 725, July 1970.

56. "Saxton Plutonium Program Semiannual Progress Report for the Period Ending June 30, 1967," WCAP 3385-12, Westinghouse Electric Corporation (1967).

57. R.J. Nodvik, et.al.,"Supplemental Report on Evaluation of Mass Spectrometric and Radiochemical Analyses of Yankee Core I Spent Fuel, Including Isotopes of Elements Thorium through Curium," WCAP 6086, Westinghouse Electric Corporation (1969).

58. Maine Yankee Atomic Power Station- Final Safety Analysis Report (FSAR), AEC Docket 50309 (Volume I).

59. D. Denver, Personal Communication, Yankee Atomic Electric Company, May 1974.

60. A. Addae, "The Reactor Physics of the MITR Redesign," Doctoral Thesis, Massachusetts Institute of Technology, August 1970.

61. W. H. Reed, "An Extension of the THERMOS code to Two-Dimensional Geometries," Course 22.25 Project, Massachusetts Institute of Technology, January 1968.

APPENDIX A

COMPUTER INPUT LISTINGS

LASER-M Input Listings: Hanford UO_2-2 w/o PuO_2 Criticals

```
 PU CRITICALS 2 W/O PUO2 ( 8 A/O PU 240) HEX PITCH=0.80 IN TEMP=22 C          2
  014     0     0                                                            3
14 5 4 1 3 1 1 1 1 0 1 0 1 1 1 1                                             4
    144.  0.00937   295.16                                                8 .80 5
    1.        1.        .7        1.        1.        1.        1.            6
11111233333344                                                               7
    1     5 .64135                                                           8
    2     1 .07620                                                           9
    3     6 .34941                                                        .80   10
    4     2 .11647                                                        .80   11
.14831E-03          .20711E-01.38836E-03.32446E-04.29716E-05.13141E-06   8     12
                              .42567E-01.33372E-01.43749E-01                 8     13
 1 295.16                                                                   8     14
```

```
 PU CRITICALS 2 W/O PUO2 ( 8 A/O PU 240) HEX PITCH=0.93 IN TEMP=22 C          2
  015     0     0                                                            3
14 5 4 1 3 1 1 1 1 0 1 0 1 1 1 1                                             4
    144.  0.01033   295.16                                                8 .93 5
    1.        1.        .7        1.        1.        1.        1.            6
11111233333344                                                               7
    1     5 .64135                                                           8
    2     1 .07620                                                           9
    3     6 .52259                                                        .93   10
    4     2 .17420                                                        .93   11
.14831E-03          .20711E-01.38836E-03.32446E-04.29716E-05.13141E-06   8     12
                              .42567E-01.33372E-01.43749E-01                 8     13
 1 295.16                                                                   8     14
```

```
 PU CRITICALS 2 W/O PUO2 ( 8 A/O PU 240) HEX PITCH=1.05 IN TEMP=22 C          2
  016     0     0                                                            3
14 5 4 1 3 1 1 1 1 0 1 0 1 1 1 1                                             4
    144.  0.01013   295.16                                                8 1.055
    1.        1.        .7        1.        1.        1.        1.            6
11111233333344                                                               7
    1     5 .64135                                                           8
    2     1 .07620                                                           9
    3     6 .68268                                                       1.05   10
    4     2 .22756                                                       1.05   11
.14831E-03          .20711E-01.38836E-03.32446E-04.29716E-05.13141E-06   8     12
                              .42567E-01.33372E-01.43749E-01                 8     13
 1 295.16                                                                   8     14
```

```
 PU CRITICALS 2 W/O PUO2 (24 A/O PU 240) HEX PITCH=0.80 IN TEMP=24 C          2
  017    0    0                                                              3
14 5 4 1 3 1 1 1 1 0 1 0 1 1 1 1                                             4
    144.  0.00631   297.16                                                24 .80 5
    1.        1.       .7         1.        1.        1.        1.           6
11111233333344                                                               7
    1    5 .64135                                                            8
    2    1 .07620                                                            9
    3    6 .34941                                                          .80  10
    4    2 .11647                                                          .80  11
.14831E-03          .20711E-01.30392E-03.99528E-04.17280E-04.27952E-05    24   12
                          .42566E-01.33372E-01.43749E-01                   24   13
 1 297.16                                                                  24   14
```

```
 PU CRITICALS 2 W/O PUO2 (24 A/O PU 240) HEX PITCH=0.93 IN TEMP=24 C          2
  018    0    0                                                              3
14 5 4 1 3 1 1 1 1 0 1 0 1 1 1 1                                             4
    144.  0.00794   297.16                                                24 .93 5
    1.        1.       .7         1.        1.        1.        1.           6
11111233333344                                                               7
    1    5 .64135                                                            8
    2    1 .07620                                                            9
    3    6 .52259                                                          .93  10
    4    2 .17420                                                          .93  11
.14831E-03          .20711E-01.30392E-03.99528E-04.17280E-04.27952E-05    24   12
                          .42566E-01.33372E-01.43749E-01                   24   13
 1 297.16                                                                  24   14
```

```
 PU CRITICALS 2 W/O PUO2 (24 A/O PU 240) HEX PITCH=1.05 IN TEMP=24 C          2
  019    0    0                                                              3
14 5 4 1 3 1 1 1 1 0 1 0 1 1 1 1                                             4
    144.  0.00776   297.16                                                24 1.055
    1.        1.       .7         1.        1.        1.        1.           6
11111233333344                                                               7
    1    5 .64135                                                            8
    2    1 .07620                                                            9
    3    6 .68268                                                        1.05   10
    4    2 .22756                                                        1.05   11
.14831E-03          .20711E-01.30392E-03.99528E-04.17280E-04.27952E-05    24   12
                          .42566E-01.33372E-01.43749E-01                   24   13
 1 297.16                                                                  24   14
```

LASER-M Depletions

LASER-M Yankee 3.4 w/o U-235 Depletion Input Listing

```
YANKEE CORE 1 3.40 W/O DEPLETION 100,500 ,2500,4500,ETC HRS                    3  3
 023    0    3                                                                 4  4
14 5 4 1 1 1 4 3 3 0 1 0                                                       5  5
 73.305   0.0007    980.38                                                     6  6
    1.0      1.0     0.872       1.0         1.0         1.0         1.0       7  7
11111233333344                                                          HOT    8  8
    1    5 .3750                                                        HOT    8  9
    2    1 .0587                                                        RH     8 10
    3    6 .1863                                                        RH     8 11
    4    2 .0621                                                              9 12
.77110E-03.43200E-05.21625E-01                                                 9 13
                          .44968E-01.26059E-01.76941E-01.58870E-05             14 14
 0 980.38                                                                      17 15
 0.72000E+07.36000E+06.14400E+07.39120E-05                                     18 16
.0135     .0140     .0150     .0180     .0299                           U     19 17
148.64    -.0060009 .26701E-06-.4922E-11                                    U  19 18
18.815    .77706E-03-.7100E-07.15416E-11
0
```

LASER-M Saxton Core II 6.6w/o PuO_2 Depletion Input Listing

```
 SAXTON 6.6 W/O PUO2 DEPLETION,0.58 IN PITCH,50,250,1250,2250 ETC HRS
    1    0   12                                                              I  3  3
14 5 4 1 3 1 6 3 3 0 1 0 1 1 0 1 0 0 0                                       I  4  4
4.5886E+070.00498   828.72                                                  I  5  5
1.0       1.0       0.74436   1.0       1.0       1.0       1.0           I  6  6
11111233333344                                                              I  7  7
    1   50.428498                                                           I  8  8
    2   10.068072                                                           I  8  9
    3   60.3345942                                                          I  8 10
    4   20.1115                                                             I  8 11
.15614E-03          .21273E-01.13296E-02.12636E-03.12870E-04.65946E-06      I  9 12
                          .45798E-01.25691E-01.37895E-01                    I  9 13
 0 828.72                                                                   I 14 15
 0.36000E+07.18000E+06.07200E+071.0                                         I 17 16
.0135     .0140     .0150     .0180     .0299                              I 18 17
273.7     -.013414  .50359E-06-.9694E-11                                   I 19 18
19.026    .0014903  -.1163E-06.25236E-11                                    I 19 19
0
```

LASER-M Input Listings: Saxton CRX Power Distribution
Unit Cells: 6.6w/o PuO_2
5.742w/o U^{-235}
Water Cell

```
SAXTON 6.6 W/O PUO2 UNIT CELL,NO BORON,COLD                                    ITEM 2
    1    1    0                                                               ITEM 3
14 5 4 1 3 1 1 1 1 0 1 0 1 1 0 1                                               ITEM 4
1.0        0.01215   289.0                                                     ITEM 5
1.0        1.0       0.7       1.0       1.0       1.0       1.0             ITEM 6
11111233333344                                                                 ITEM 7
    1    50.428498                                                             ITEM 8 P
    2    10.068072                                                             ITEM 8 P
    3    60.3059336                                                            ITEM 8 P
    4    20.102                                                                ITEM 8 P
.15313E-03          .21085E-01.13529E-02.12762E-03.13189E-04.60336E-06         ITEM 9 P
                              .45465E-01.33390E-01.38324E-01                   ITEM 9 P
 5 0.001                                                                       ITEM 13
 0 289.0                                                                       ITEM 14
                                                                               ITEM 1
SAXTON 5.742 W/O UO2 UNIT CELL,NO BORON,COLD                                   ITEM 2
    2    1    0                                                               ITEM 3
14 5 4 1 1 1 1 1 1 0 1 0 1 1 0 1                                               ITEM 4
1.0        0.01215   289.0                                                     ITEM 5
1.0        1.0       0.7       1.0       1.0       1.0       1.0             ITEM 6
11111233333344                                                                 ITEM 7
    1    50.45339                                                              ITEM 8 U
    2    10.04318                                                              ITEM 8 U
    3    60.3059336                                                            ITEM 8 U
    4    20.102                                                                ITEM 8 U
.13054E-02          .21159E-01                                                 ITEM 9 U
                              .44928E-01.33390E-01.78124E-01                   ITEM 9 U
 5 0.001                                                                       ITEM 13
 0 289.0                                                                       ITEM 14
```

```
SAXTON  WATER CELL,NO BORON,COLD                                               ITEM 2
    3    0    0                                                               ITEM 3
14 5 4 1 3 1 1 1 1 0 0 0 1 1 0 1                                               ITEM 4
1.0        0.01281   289.0                                                     ITEM 5
1.0        1.0       0.65245   1.0       1.0       1.0       1.0             ITEM 6
11111233333344                                                                 ITEM 7
    1    50.0002                                                               ITEM 8 W
    2    10.0002                                                               ITEM 8 W
    3    60.8021036                                                            ITEM 8 W
    4    20.2672                                                               ITEM 8 W
0.00001             0.001                                                      ITEM 9 W
                              0.002     0.03339   0.038324                     ITEM 9 W
0                                                                              ITEM 1
```

THERMOS Individual Cell Slabs Input Listings:
Saxton CRX Core

```
 SAXTON QUARTER CORE: PU 6.6 W/O         0.56 IN PITCH  COLD              CARD 1
    1     0 2 0 0 2 0 0 12130 0 0 0 0 0 0 0 0 0                           CARD 2
    4    30     2     9     4     0     0     0     0                     CARD 3
2211                                                                      CARD 4
1110200001.00011402    0.0                                               CARD 5
1110300001.015700      0.0                                               CARD 5
1110400001.0010074     0.0                                               CARD 5
1110500001.000095028   0.0                                               CARD 5
0110600001.000009820A 0.0                                                CARD 5
0105500001.000000449270.0                                                CARD 5
0101300001.033853      .033390                                           CARD 5
0040200001.0097872     0.0                                               CARD 5
11001001000.0          .066780                                           CARD 5
11102000021.0                                                            CARD 6
11104000021.0                                                            CARD 6
11105000021.0                                                            CARD 6
0110600002 1.0                                                           CARD 6
    1     12.0                                                           CARD 10
1.0         1.0        0.0        0.0                                    CARD 11
    21.0          .023685                                                CARD 12
    1     2                                                              CARD 13
    1     2 .69065                                                       CARD 14
    1     2 .42850                                                       CARD 14
1.00005     1.0        0.05       40.0       1.0          200    10    20   200  CARD 15
    1    30                                                              CARD 16
                                                                         CARD 17
.00284.00280.00279.00278.00277.00276.04167.00731-1.0                     CARD 18A
                                                                         CARD 18B
                                                                         CARD 19
```

```
 SAXTON QUARTER CORE:  U 5.742 W/O       0.56 IN PITCH  COLD              CARD 1
    1     0 2 0 0 2 0 0 12130 0 0 0 0 0 0 0 0 0                           CARD 2
    4    30     2     5     1     0     0     0     0                     CARD 3
2211                                                                      CARD 4
1110200001.0010883     0.0                                               CARD 5
1110300001.017693      0.0                                               CARD 5
1101300001.037454      .033390                                           CARD 5
1030400001.012996      0.0                                               CARD 5
01001001000.0          .066780                                           CARD 5
01102000021.0                                                            CARD 6
    1     12.0                                                           CARD 10
1.0         1.0        0.0        0.0                                    CARD 11
    21.0          .024687                                                CARD 12
    1     2                                                              CARD 13
    1     2 .69065                                                       CARD 14
    2     2 .42850                                                       CARD 14
0.00005     1.0        0.05       40.0       1.0          200    10    20   200  CARD 15
    1    30                                                              CARD 16
                                                                         CARD 17
.00284.00280.04167.01220-1.0                                             CARD 18A
                                                                         CARD 18B
                                                                         CARD 19
```

THERMOS Multislabs Input Listings:

Saxton CRX Core

```
 SAXTON QUARTER CORE: 1-1/2 5.742 U,1-1/2 6.6 PU  0.56 IN PITCH SLAB     CARD 1
    1    0 2 0 0 1 0 0 12130 0 0 0 0 0 0 0 0                             CARD 2
   24   30    3   10    4    0    0    0    0                            CARD 3
33222233332222111222211                                                 CARD 4
1110200001.00011402   0.0          .0010883                             CARD 5
1110300001.015700     0.0          .017693                              CARD 5
1110400001.0010074    0.0          0.0                                  CARD 5
1110500001.000095028  0.0          0.0                                  CARD 5
0110600001.0000098208 0.0          0.0                                  CARD 5
0105500001.000000449270.0           0.0                                 CARD 5
0101300001.033853     .033390      .037454                              CARD 5
0040200001.0097872    0.0          0.0                                  CARD 5
10304000010.0         0.0          .012996                              CARD 5
11001001000.0         .066780      0.0                                  CARD 5
11102000021.0                                                           CARD 6
11104000021.0                                                           CARD 6
01105000021.0                                                           CARD 6
01106000021.0                                                           CARD 6
    1    12.0                                                          CARD 10
0.0       0.0       1.0       1.0       1.0       1.0       0.0        CARD 11
1.0       0.0       0.0       1.0       1.0       1.0       1.0        CARD 11
1.0       0.0       0.0       0.0       1.0       1.0       1.0        CARD 11
1.0       0.0       0.0                                               CARD 11
   21.0        .024186                                                 CARD 12
    1   10                                                            CARD 13
    2    2 .69065                                                     CARD 14
    3    2 .69065                                                     CARD 14
    4    4 .85700                                                     CARD 14
    5    2 .69065                                                     CARD 14
    6    2 .69065                                                     CARD 14
    7    4 .85700                                                     CARD 14
    8    2 .69065                                                     CARD 14
    9    2 .69065                                                     CARD 14
   10    2 .42850                                                     CARD 14
0.00005   1.0       0.05      40.0      1.0         200   10   20  200 CARD 15
    1   30                                                            CARD 16
                                                                      CARD 17
.00284.00280.00279.00278.00277.00276.04167.00731.01220-1.0            CARD 18A
                                                                      CARD 18B
                                                                      CARD 19
```

```
 SAXTON QUARTER CORE: 2 5.742 U. H20 PINS  0.56 IN PITCH  SLAB          CARD 1
    1    0 2 0 0 2 0 0 12130 0 0 0 0 0 0 0 0                           CARD 2
   20   30    3    5    1    0    0    0    0                          CARD 3
22111122221111223333                                                  CARD 4
0110200001.0010883     0.0          0.0                               CARD 5
0110300001.017693      0.0          0.0                               CARD 5
0101300001.037454      .033390      .033390                           CARD 5
0030400001.012996      0.0          0.0                               CARD 5
01001001000.0          .066780      .066780                           CARD 5
01102000021.0                                                         CARD 6
    2    12.0                                                         CARD 10
1.0        1.0        0.0        0.0        0.0        0.0        1.0  CARD 11
1.0        1.0        1.0        0.0        0.0        0.0        0.0  CARD 11
1.0        1.0        1.0        1.0        1.0        1.0             CARD 11
    21.0        .024687                                               CARD 12
    31.0        .048688                                               CARD 12
    1    7                                                            CARD 13
    1    2 .69065                                                     CARD 14
    2    4 .85700                                                     CARD 14
    3    2 .69065                                                     CARD 14
    4    2 .69065                                                     CARD 14
    5    4 .85700                                                     CARD 14
    6    2 .69065                                                     CARD 14
    7    4 1.1192                                                     CARD 14
0.00005   1.0        0.05       40.0       1.0          200   10   20  200 CARD 15
    1   30                                                            CARD 16
                                                                      CARD 17
.00284.00280.04167.01220-1.0                                          CARD 18A
```

```
 SAXTON QUARTER CORE: 2 6.6 PU . H20 PINS  0.56 IN PITCH  SLAB          CARD 1
    1    0 2 0 0 2 0 0 12130 0 0 0 0 0 0 0 0                           CARD 2
   20   30    3    9    4    0    0    0    0                          CARD 3
22111122221111223333                                                  CARD 4
0110200001.00011402    0.0          0.0                               CARD 5
0110300001.015700      0.0          0.0                               CARD 5
0110400001.0010074     0.0          0.0                               CARD 5
0110500001.000095028   0.0          0.0                               CARD 5
0110600001.0000098208  0.0          0.0                               CARD 5
0105500001.000000449270.0           0.0                               CARD 5
0101300001.033853      .033390      .033390                           CARD 5
0040200001.0097872     0.0          0.0                               CARD 5
01001001000.0          .066780      .066780                           CARD 5
01102000021.0                                                         CARD 6
01104000021.0                                                         CARD 6
01105000021.0                                                         CARD 6
01106000021.0                                                         CARD 6
    2    12.0                                                         CARD 10
1.0        1.0        0.0        0.0        0.0        0.0        1.0  CARD 11
1.0        1.0        1.0        0.0        0.0        0.0        0.0  CARD 11
1.0        1.0        1.0        1.0        1.0        1.0             CARD 11
    21.0        .023685                                               CARD 12
    31.0        .048688                                               CARD 12
    1    7                                                            CARD 13
    1    2 .69065                                                     CARD 14
    2    4 .85700                                                     CARD 14
    3    2 .69065                                                     CARD 14
    4    2 .69065                                                     CARD 14
    5    4 .85700                                                     CARD 14
    6    2 .69065                                                     CARD 14
    7    4 1.1192                                                     CARD 14
0.00005   1.0        0.05       40.0       1.0          200   10   20  200 CARD 15
    1   30                                                            CARD 16
                                                                      CARD 17
.00284.00280.00279.00278.00277.00276.04167.00731-1.0                  CARD 18A
                                                                      CARD 18B
0                                                                     CARD 19
```

Saxton CRX Single Region Core: PDQ Input Listing

```
=SAXTON U CORE,THERMOS MULTISLAB C/S
010001,2,0,2,1,2,1,1,65,4,2,26,26,1,0,1
010002,1,0,1,0,1,1
010003,100+1,100-3
010004,100+1,0+0
010005,0,26,0,26,0,1,1,1
010006,0,26,0,26,0,1,1,1
010009,0,1,1,1
030001,65,1,65,1,2,37,45,2,52,55,2,60
030002,38,2,41,53,2,53,61,2,61,63,2,63
030003,42,4,44
030004,62,4,62
030005,64,4,64
030006,54,4,54
050101,28+0,23,112+1,24,28+1,25,56+1,26
801000,26,26,01,0,01
801001,65,0,26,0,26,64,17,19,3,17,63,15,17,5,15
801002,62,1,17,17,19,61,1,15,15,17,60,1,13,13,15
801003,1,0,1,0,1,2,0,1,1,3,3,1,3,0,1,4,1,3,1,3
801004,5,3,5,0,1,6,3,5,1,3,7,3,5,3,5,8,5,7,0,1
801005,9,5,7,1,3,10,5,7,3,5,11,5,7,5,7,12,7,9,0,1
801006,13,7,9,1,3,14,7,9,3,5,15,7,9,5,7,16,7,9,7,9
801007,17,9,11,0,1,18,9,11,1,3,19,9,11,3,5,20,9,11,5,7
801008,21,9,11,7,9,22,9,11,9,11,23,11,13,0,1,24,11,13,1,3
801009,25,11,13,3,5,26,11,13,5,7,27,11,13,7,9
801010,28,11,13,9,11,29,11,13,11,13,30,13,15,0,1
801011,31,13,15,1,3,32,13,15,3,5,33,13,15,5,7
801012,34,13,15,7,9,35,13,15,9,11,36,13,15,11,13
801013,37,13,15,13,15,38,15,17,0,1,39,15,17,1,3
801014,40,15,17,3,5,41,15,17,15,17,42,17,19,0,1
801015,43,17,19,1,3,44,17,19,17,19,45,1,3,3,5
801016,46,3,5,9,11,47,0,1,3,5,48,0,1,5,7
801017,49,0,1,7,9,50,0,1,9,11,51,0,1,11,13
801018,52,0,1,13,15,53,0,1,15,17,54,0,1,17,19
801019,55,1,5,5,7,56,1,7,7,9,57,1,3,9,11
801020,58,5,9,9,11,59,1,11,11,13
170001,01,010,0,0,0,0
013001,1,0,1,-54
110001,1,1,2,2,3,3,4,4
080001,113-2,4
*   D,SIGA,SIGR,NUSIGF,KAPSIGF
```

Macroscopic C/S Input Cards

Saxton CRX Multiregion Cores: PDQ Input Listings

```
=SAXTON MULTIREGION CORE,11X11 P INNER
010001,2,0,2,1,2,1,1,65,9,2,26,26,1,0,1
010002,1,0,1,0,1,1
010003,100+1,100-3
010004,100+1,0+0
010005,0,26,0,26,0,1,1,1
010006,0,26,0,26,0,1,1,1
010009,0,1,1,1
030001,65,1,65
030002,42,4,44,54,4,54,62,4,62,64,4,64
030003,38,3,41,53,3,53,61,3,61,63,3,63
030004,1,2,11,45,2,45,47,2,48,55,2,55
030005,30,5,37,52,5,52,60,5,60
030006,23,6,29,51,6,51,59,6,59
030007,12,7,16,49,7,49,56,7,56
030008,17,8,22,46,8,46,50,8,50,57,8,58
050101,28+0,23,112+1,24,28+1,25,56+1,26
801000,26,26,01,0,01
801001,65,0,26,0,26,64,17,19,3,17,63,15,17,5,15
801002,62,1,17,17,19,61,1,15,15,17,60,1,13,13,15
801003,1,0,1,0,1,2,0,1,1,3,3,1,3,0,1,4,1,3,1,3
801004,5,3,5,0,1,6,3,5,1,3,7,3,5,3,5,8,5,7,0,1
801005,9,5,7,1,3,10,5,7,3,5,11,5,7,5,7,12,7,9,0,1
801006,13,7,9,1,3,14,7,9,3,5,15,7,9,5,7,16,7,9,7,9
801007,17,9,11,0,1,18,9,11,1,3,19,9,11,3,5,20,9,11,5,7
801008,21,9,11,7,9,22,9,11,9,11,23,11,13,0,1,24,11,13,1,3
801009,25,11,13,3,5,26,11,13,5,7,27,11,13,7,9
801010,28,11,13,9,11,29,11,13,11,13,30,13,15,0,1
801011,31,13,15,1,3,32,13,15,3,5,33,13,15,5,7
801012,34,13,15,7,9,35,13,15,9,11,36,13,15,11,13
801013,37,13,15,13,15,38,15,17,0,1,39,15,17,1,3
801014,40,15,17,3,5,41,15,17,15,17,42,17,19,0,1
801015,43,17,19,1,3,44,17,19,17,19,45,1,3,3,5
801016,46,3,5,9,11,47,0,1,3,5,48,0,1,5,7
801017,49,0,1,7,9,50,0,1,9,11,51,0,1,11,13
801018,52,0,1,13,15,53,0,1,15,17,54,0,1,17,19
801019,55,1,5,5,7,56,1,7,7,9,57,1,3,9,11
801020,58,5,9,9,11,59,1,11,11,13
013001,1,0,1,-54
170001,01,010,0,0,0,0
110001,1,1,2,2,3,3,4,4,5,5,6,6,7,7,8,8
080001,113-2,8
*    D,SIGA,SIGR,NUSIGF,KAPSIGF
```

```
    Macroscopic C/S Input Cards
```

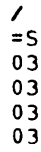

```
/
=SAXTON MULTIREGION CORE,3X3 P INNER
030004,12,2,37,46,2,46,49,2,52,56,2,60
030005,8,5,11,48,5,48,55,5,55
030006,5,6,7,45,6,45,47,6,47
030007,1,7,1
030008,2,8,4
*    D,SIGA,SIGR,NUSIGF,KAPSIGF
```

```
    Macroscopic C/S Input Cards
```

LASER-M Input Listings: Pu Island Design

```
 BOL.2.61 W/OF PU(1ST GEN).NORMAL.HFP.820 PPM.COLD DIM                          2  2
  020     0    1                                                               3  3
14 5 4 1 3 1 9 3 3 0 0 0 1 1 0 1                                               4  4
  188.32   .002465  916.5                                                     5  5
       1.0       1.0   .82561        1.0       1.0       1.0       1.0      6  6
11111233333344                                                                 7  7
    1    5.48514                                                               8  8
    2    1.07366                                                               8  9
    3    6.269704                                                         N    8 10
    4    2.089901                                                         N    8 11
.16117E-03          .21378E-01.47024E-03.19054E-03.11011E-03.37633E-04  P1   9 12
                          .44695E-01.24253E-01.39510E-01.33246E-04  P1N  9 13
 0 916.5
```

```
 BOL.2.39 W/OF PU(1ST GEN).NORMAL.HFP.820 PPM.COLD DIM                          2  2
  002     0    0                                                               3  3
14 5 4 1 3 1 9 3 3 0 1 0 1 1 0 1                                               4  4
  188.32  0.002465   916.5                                                     5  5
       1.0       1.0       .85        1.0       1.0       1.0       1.0      6  6
11111233333344                                                                 7  7
    1    5.48514                                                               8  8
    2    1.07366                                                               8  9
    3    6.269704                                                         N    8 10
    4    2.089901                                                         N    8 11
.16117E-03          .21446E-01.43060E-03.17448E-03.10083E-03.34461E-04  P2   9 12
                          .44696E-01.24253E-01.39510E-01.33246E-04  P2N  9 13
 0 916.5                                                                      14 15
```

```
 BOL.2.30 W/OF PU(1ST GEN).NORMAL.HFP.820 PPM.COLD DIM                          2  2
  021     0    1                                                               3  3
14 5 4 1 3 1 9 3 3 0 0 0 1 1 0 1                                               4  4
  188.32  0.002465   916.5                                                     5  5
       1.0       1.0   .82530        1.0       1.0       1.0       1.0      6  6
11111233333344                                                                 7  7
    1    5.48514                                                               8  8
    2    1.07366                                                               8  9
    3    6.269704                                                         N    8 10
    4    2.089901                                                         N    8 11
.16117E-03          .21474E-01.41439E-03.16791E-03.97031E-04.33163E-04  P3   9 12
                          .44696E-01.24253E-01.39510E-01.33246E-04  P3N  9 13
 0 916.5
```

```
 BOL,3.47 W/O U235,NORMAL,HFP,820 PPM,COLD DIM                                  2  2
  022     0     1                                                               3  3
14 5 4 1 3 1 9 3 3 0 0 0 1 1 0 1                                                 4  4
  188.32    .004040  916.5                                                     5  5
       1.0         1.0    .82536         1.0         1.0         1.0         1.0    6  6
11111233333344                                                                  7  7
    1     5.48514                                                               8  8
    2     1.07366                                                               8  9
    3     6.269704                                                          N   8 10
    4     2.089901                                                          N   8 11
.78546E-03            .21575E-01                                            U   9 12
                                 .44721E-01.24253E-01.39510E-01.33246E-04   UN   9 13
 0 916.5
```

Pu Island Design: 3.47w/o U-235 Fuel Pin with Adjacent Water Cell Water

```
 BOL,3.47 W/O U235,WATER CELL,HFP,820 PPM,COLD DIM                              2  2
  005     0     0                                                               3  3
14 5 4 1 3 1 9 3 3 0 1 0 1 1 0 1                                                 4  4
  188.32  0.00404    916.5                                                     5  5
       1.0         1.0         .85         1.0         1.0         1.0         1.0    6  6
11111233333344                                                                  7  7
    1     5.48514                                                               8  8
    2     1.07366                                                               8  9
    3     6.43867                                                           W   8 10
    4     2.14622                                                           W   8 11
.78546E-03            .21575E-01                                            U   9 12
                                 .44721E-01.24253E-01.39510E-01.33246E-04   UW   9 13
 0 916.5                                                                        14 15
```

Pu Island Design: Water Region

```
 WATER CELL,NORMAL,820 PPM, COLD DIM 0.01 CM RADIUS FUEL,FULL EDIT              2  2
  013     0     0                                                               3  3
14 5 4 1 3 1 9 3 3 0 0 0                                                         4  4
   .1      0.00404    916.5                                                     5  5
       1.0         1.0         .85         1.0         1.0         1.0         1.0    6  6
11111233333344                                                                  7  7
    1     5.01                                                                  8  8
    2     1.2535                                                                8  9
    3     6.5651                                                                8 10
    4     2.1550                                                                8 11
.00001                                                                      W   9 12
                                       .24253E-01.43749E-01.33246E-04       W   9 13
```

THERMOS Individual Cell Slabs Input Listing:

Pu Island Design

```
 MAINE YANKEE SINGLE PIN AS SLAB: 2.61 PU                                    CARD 1
    1    0 2 0 0 2 0 0 12130 0 0 0 0 0 0 0 0                                 CARD 2
    4   30    2   11    4    0    0    0    0                                CARD 3
1122                                                                         CARD 4
 1102    10.0          .00012148                                             CARD 5
 1103    10.0          .016113                                               CARD 5
 1104    10.0          .00035443                                             CARD 5
 1105    10.0          .00014362                                             CARD 5
 1106    10.0          .000082993                                            CARD 5
 1055    10.0          .000028365                                            CARD 5
 1013    5.024253      0.0                                                   CARD 5
 1013   110.0          .033688                                               CARD 5
 1009    1.6582700E-050.0                                                    CARD 5
  402    10.0          .0097301                                              CARD 5
 1001  550.048506      0.0                                                   CARD 5
 1102    21.0                                                                CARD 6
 1104    21.0                                                                CARD 6
 1105    21.0                                                                CARD 6
 1106    21.0                                                                CARD 6
    1    12.0                                                                CARD 10
1.0       1.0        0.0        0.0                                         CARD 11
   11.01       .014680   1.0        1.91                                    CARD 12
    1    3                                                                   CARD 13
    1    2 .58131                                                            CARD 14
    2    2 .48514                                                            CARD 14
0.00005   1.0        0.05       40.0       1.0          200   10   20  200  CARD 15
    1   30                                                                   CARD 16
                                                                             CARD 17
.00284.00280.00279.00278.00277.00276.04167.04167.06667.00731-1.0             CARD 18A
                                                                             CARD 18B
0                                                                            CARD 19
```

```
 MAINE YANKEE SINGLE PIN AS SLAB: 2.30 PU                                  CARD 1
    1    0 2 0 0 2 0 0 12130 0 0 0 0 0 0 0 0                               CARD 2
    4   30    2   11    4    0    0    0    0                              CARD 3
1122                                                                       CARD 4
 1102    10.0          .00012148                                           CARD 5
 1103    10.0          .016186                                             CARD 5
 1104    10.0          .00031234                                           CARD 5
 1105    10.0          .00012656                                           CARD 5
 1106    10.0          .000073137                                          CARD 5
 1055    10.0          .000024996                                          CARD 5
 1013    5.024253      0.0                                                 CARD 5
 1013   110.0          .033688                                             CARD 5
 1009    1.6582700E-050.0                                                  CARD 5
  402    10.0          .0097301                                            CARD 5
 1001  550.048506      0.0                                                 CARD 5
 1102    21.0                                                              CARD 6
 1104    21.0                                                              CARD 6
 1105    21.0                                                              CARD 6
 1106    21.0                                                              CARD 6
    1    12.0                                                              CARD 10
1.0       1.0        0.0        0.0                                        CARD 11
    11.01       .014947   1.0        1.91                                  CARD 12
    1    3                                                                 CARD 13
    1    2 .58131                                                          CARD 14
    2    2 .48514                                                          CARD 14
0.00005   1.0        0.05       40.0       1.0          200   10   20  200 CARD 15
    1   30                                                                 CARD 16
                                                                           CARD 17
.00284.00280.00279.00278.00277.00276.04167.04167.06667.00731-1.0           CARD 18A
                                                                           CARD 18B
0                                                                          CARD 19
```

```
 MAINE YANKEE SINGLE PIN AS SLAB: 3.47U                                    CARD 1
    1    0 2 0 0 2 0 0 12130 0 0 0 0 0 0 0 0                               CARD 2
    4   30    2    7    1    0    0    0    0                              CARD 3
1122                                                                       CARD 4
 1102    10.0          .00059203                                           CARD 5
 1103    10.0          .016262                                             CARD 5
 1013    5.024253      0.0                                                 CARD 5
 1013   110.0          .033708                                             CARD 5
 1009    1.6582700E-050.0                                                  CARD 5
  402    10.0          .0097301                                            CARD 5
 1001  550.048506      0.0                                                 CARD 5
 1102    21.0                                                              CARD 6
    1    12.0                                                              CARD 10
1.0       1.0        0.0        0.0                                        CARD 11
    11.01       .015444   1.0        1.91                                  CARD 12
    1    3                                                                 CARD 13
    1    2 .58131                                                          CARD 14
    2    2 .48514                                                          CARD 14
0.00005   1.0        0.05       40.0       1.0          200   10   20  200 CARD 15
    1   30                                                                 CARD 16
                                                                           CARD 17
.00284.00280.04167.04167.06667.00731-1.0                                   CARD 18A
                                                                           CARD 18B
0                                                                          CARD 19
```

THERMOS Multislabs Input Listings:

Pu Island Design

```
 M YANKEE QUARTER PU ASSY: 2.61P,2.30P,3.47U PINS,H2O CELL  SLAB          CARD 1
    1     0 2 0 0 2 0 0 12130 0 0 0 0 0 0 0 0 0                          CARD 2
   25    30     6    11     4     0     0     0     0                    CARD 3
2255552222444422221111223                                               CARD 4
0110200001.00059203    0.0          0.0          .00012148    .00012148  CARD 5
          0.0                                                           CARD5111
0110300001.016262      0.0          0.0          .016186      .016113    CARD 5
          0.0                                                           CARD5111
01104000010.0          0.0          0.0          .00031234    .00035443  CARD 5
          0.0                                                           CARD5111
01105000010.0          0.0          0.0          .00012656    .00014362  CARD 5
          0.0                                                           CARD5111
01106000010.0          0.0          0.0          .000073137   .000082993 CARD 5
          0.0                                                           CARD5111
01055000010.0          0.0          0.0          .000024996   .000028365 CARD 5
          0.0                                                           CARD5111
01013000050.0          .024253      .024253      0.0          0.0        CARD 5
          0.0                                                           CARD5111
0101300011.033708      0.0          0.0          .033688      .033688    CARD 5
          0.0                                                           CARD5111
01009000010.0          .6582700E-05.6685400E-050.0          0.0        CARD 5
          0.0                                                           CARD5111
0040200001.0097301     0.0          0.0          .0097301     .0097301   CARD 5
          0.0                                                           CARD5111
01001005500.0          .048506      .048506      0.0          0.0        CARD 5
          0.0                                                           CARD5111
01102000021.0                                                           CARD 6
01104000021.0                                                           CARD 6
01105000021.0                                                           CARD 6
01106000021.0                                                           CARD 6
    2    12.0                                                           CARD 10
1.0         1.0         0.0         0.0         0.0         0.0         1.0        CARD 11
1.0         1.0         1.0         0.0         0.0         0.0         0.0        CARD 11
1.0         1.0         1.0         1.0         0.0         0.0         0.0        CARD 11
0.0         1.0         1.0         1.0                                            CARD 11
    21.0         .015282    1.0         1.91                                      CARD 12
    31.0         .032542    1.0         1.91                                      CARD 12
    1   10                                                                       CARD 13
    1    2 .58131                                                                CARD 14
    2    4 .97028                                                                CARD 14
    3    2 .58131                                                                CARD 14
    4    2 .58131                                                                CARD 14
    5    4 .97028                                                                CARD 14
    6    2 .58131                                                                CARD 14
    7    2 .58131                                                                CARD 14
    8    4 .97028                                                                CARD 14
    9    2 .58131                                                                CARD 14
   10    1 2.1329                                                                CARD 14
0.00005    1.0         0.05        40.0         1.0          200    10   20  200 CARD 15
    1   30                                                                       CARD 16
                                                                                 CARD 17
.00284.00280.00279.00278.00277.00276.04167.04167.06667.00731-1.0                 CARD 18A
                                                                                 CARD 18B
0                                                                                CARD 19
```

```
 MAINE YANKEE 3 PINS AS SLABS: 2.61 PU,2.39 PU,3.47 U                              CARD 1
    1     0 2 0 0 2 0 0 12130 0 0 0 0 0 0 0 0                                      CARD 2
   24    30     6    11     4     0     0     0     0                              CARD 3
225555222266662222111122                                                          CARD 4
0110200001.00059203    0.0          0.0          .00012148    .00012148    CARD 5
          .00012148                                                          CARD 5
0110300001.016262      0.0          0.0          .016186      .016113      CARD 5
          .016165                                                            CARD 5
01104000010.0          0.0          0.0          .00031234    .00035443    CARD 5
          .00032456                                                          CARD 5
01105000010.0          0.0          0.0          .00012656    .00014362    CARD 5
          .00013377                                                          CARD 5
01106000010.0          0.0          0.0          .000073137   .000082993   CARD 5
          .000075999                                                         CARD 5
01055000010.0          0.0          0.0          .000024996   .000028365   CARD 5
          .000025947                                                         CARD 5
01013000050.0          .024253      .024253      0.0          0.0          CARD 5
          0.0                                                                CARD 5
0101300011.033708      0.0          0.0          .033688      .033688      CARD 5
          .033688                                                            CARD 5
01009000010.0          .6582700E-05.6685400E-050.0          0.0          CARD 5
          0.0                                                                CARD 5
0040200001.0097301     0.0          0.0          .0097301     .0097301     CARD 5
          .0097301                                                           CARD 5
01001005500.0          .048506      .048506      0.0          0.0          CARD 5
          0.0                                                                CARD 5
01102000021.0                                                                CARD 6
01104000021.0                                                                CARD 6
01105000021.0                                                                CARD 6
01106000021.0                                                                CARD 6
    1     12.0                                                               CARD 10
1.0        1.0        0.0        0.0        0.0        0.0        1.0        CARD 11
1.0        1.0        1.0        0.0        0.0        0.0        0.0        CARD 11
1.0        1.0        1.0        1.0        0.0        0.0        0.0        CARD 11
0.0        1.0        1.0                                                    CARD 11
    21.0        .015282   1.0        1.91                                    CARD 12
    1     9                                                                  CARD 13
    1     2 .58131                                                           CARD 14
    2     4 .97028                                                           CARD 14
    3     2 .58131                                                           CARD 14
    4     2 .58131                                                           CARD 14
    5     4 .97028                                                           CARD 14
    6     2 .58131                                                           CARD 14
    7     2 .58131                                                           CARD 14
    8     4 .97028                                                           CARD 14
    9     2 .58131                                                           CARD 14
0.00005    1.0        0.05       40.0       1.0          200    10    20   200   CARD 15
    1    30                                                                  CARD 16
                                                                             CARD 17
.00284.00280.00279.00278.00277.00276.04167.04167.06667.00731-1.0           CARD 18A
                                                                             CARD 18B
0                                                                            CARD 19
```

```
 MAINE YANKEE 2 PINS AS SLABS: 2.30 PU,3.47 U                                    CARD 1
    1    0 2 0 0 2 0 0 12130 0 0 0 0 0 0 0 0                                     CARD 2
   16   30    6   11    4    0    0    0    0                                    CARD 3
224444222111122                                                                 CARD 4
0110200001.00059203   0.0          0.0          .00012148    .00012148          CARD 5
          .00012148                                                             CARD 5
0110300001.016262     0.0          0.0          .016186      .016113            CARD 5
          .016165                                                               CARD 5
01104000010.0         0.0          0.0          .00031234    .00035443          CARD 5
          .00032456                                                             CARD 5
01105000010.0         0.0          0.0          .00012656    .00014362          CARD 5
          .00013377                                                             CARD 5
01106000010.0         0.0          0.0          .000073137   .000082993         CARD 5
          .000075999                                                            CARD 5
01055000010.0         0.0          0.0          .000024996   .000028365         CARD 5
          .000025947                                                            CARD 5
01013000050.0         .024253      .024253      0.0          0.0                CARD 5
          0.0                                                                   CARD 5
0101300011.033708     0.0          0.0          .033688      .033688            CARD 5
          .033688                                                               CARD 5
01009000010.0         .6582700E-05.6685400E-050.0           0.0                CARD 5
          0.0                                                                   CARD 5
0040200001.0097301    0.0          0.0          .0097301     .0097301           CARD 5
          .0097301                                                              CARD 5
01001005500.0         .048506      .048506      0.0          0.0                CARD 5
          0.0                                                                   CARD 5
01102000021.0                                                                   CARD 6
01104000021.0                                                                   CARD 6
01105000021.0                                                                   CARD 6
01106000021.0                                                                   CARD 6
    1    12.0                                                                   CARD 10
1.0       1.0       0.0       0.0       0.0       0.0       1.0                CARD 11
1.0       1.0       1.0       0.0       0.0       0.0       0.0                CARD 11
1.0       1.0                                                                   CARD 11
    21.0        .015282   1.0       1.91                                      CARD 12
    1    6                                                                      CARD 13
    1    2 .58131                                                               CARD 14
    2    4 .97028                                                               CARD 14
    3    2 .58131                                                               CARD 14
    4    2 .58131                                                               CARD 14
    5    4 .97028                                                               CARD 14
    6    2 .58131                                                               CARD 14
0.00005   1.0       0.05      40.0      1.0         200   10   20   200        CARD 15
    1   30                                                                      CARD 16
                                                                                CARD 17
.00284.00280.00279.00278.00277.00276.04167.04167.06667.00731-1.0                CARD 18A
                                                                                CARD 18B
0                                                                               CARD 19
```

Pu Island Design: IDC Input Listing

```
=MY PU ASSY-LASER C/S, THERMOS MULTISLAB CORRECTED
010001,2,0,2,1,2,1,01,50,12,2,15,15,1,0,1
010002,1,1,1,1,1,1
010003,100+1,1000-3
010004,100+1,0+0
010005,0,15,0,15,0,1,1,1
010006,0,15,0,15,0,1,1,1
010009,0,1,1,1
030001,1,11,50,1,12,1,25,12,26,32,12,33
030002,50,12,50,10,10,10,16,10,16,7,8,7
030003,43,8,43,2,5,2,8,5,8,37,9,37
030004,13,9,13,18,5,19,39,6,40,46,7,47
030005,24,5,24,31,5,31,28,7,28,35,7,35
030006,27,6,27,34,6,34,5,2,5,22,1,22
030007,29,2,29,4,1,4,35,4,36,6,4,6
030008,3,3,3,11,3,12,15,3,15,23,3,23,30,3,30
050101,290+0,14,300-1,15
801000,15,15,01,0,01
801001,1,0,2,0,2,2,0,2,2,4,3,0,2,4,6,4,0,2,6,8
801002,5,0,2,8,10,6,0,2,10,12,7,0,2,12,14
801003,8,2,4,0,2,9,2,4,2,4,10,2,4,4,6,11,2,4,6,8
801004,12,2,4,8,10,13,2,4,10,12,14,2,4,12,14
801005,15,4,6,0,2,16,4,6,2,4,17,4,6,4,6,18,4,6,6,8
801006,19,4,6,8,10,20,4,6,10,12,21,4,6,12,14
801007,22,6,8,0,2,23,6,8,2,4,24,6,8,4,6,25,6,8,6,8
801008,26,6,8,8,10,27,6,8,10,12,28,6,8,12,14
801009,29,8,10,0,2,30,8,10,2,4,31,8,10,4,6,32,8,10,6,8
801010,33,8,10,8,10,34,8,10,10,12,35,8,10,12,14
801011,36,10,12,0,2,37,10,12,2,4,38,10,12,4,6,39,10,12,6,8
801012,40,10,12,8,10,41,10,12,10,12,42,10,12,12,14
801013,43,12,14,0,2,44,12,14,2,4,45,12,14,4,6,46,12,14,6,8
801014,47,12,14,8,10,48,12,14,10,12,49,12,14,12,14
801015,50,14,15,0,15,50,0,15,14,15
170001,01,010,0,0,0,0
013001,1,0,8,9,15,-17,22,-24,29,-31,36,-41,43,-49
110001,1,1,2,2,3,3,4,4,5,5,6,6,7,7,8,8
110002,9,9,10,10,11,11,12,12
080001,82-4,12
*   LASER THERMAL C/S,THERMOS MULTISLAB CORRECTED
*            FAST C/S FROM LASER
*     D,SIGA,SIGR,NUSIGF,KSIGF
401000,1
401001,COMP 1: 2.61P TYPE1
401100,14365+1,11811-1,14683-1,95492-2,11130-12
401200,40292+0,19135+0,0+0,29110+0,34444-11
402000,2
402001,COMP 2: 2.61P TYPE2
402100,14365+1,11811-1,14683-1,95492-2,11130-12
402200,40292+0,18866+0,0+0,27880+0,32990-11
403000,3
403001,COMP 3: 2.30P
403100,14350+1,11445-1,14947-1,88985-2,10385-12
403200,40397+0,18364+0,0+0,27119+0,32135-11
404000,4
404001,COMP 4: 2.39P
404100,14354+1,11553-1,14869-1,90890-2,10603-12
404200,40368+0,18444+0,0+0,26385+0,31175-11
```

```
405000,5
405001,COMP 5: 3.47U  P-W
405100,14210+1,10183-1,15444-1,71179-2,90415-13
405200,42511+0,91307-1,0+0,14700+0,19672-11
406000,6
406001,COMP 6: 3.47U  J-W
406100,14210+1,10183-1,15444-1,71179-2,90415-13
406200,42511+0,92560-1,0+0,14943+0,19996-11
407000,7
407001,COMP 7: 3.47U  JU-W
407100,14210+1,10183-1,15444-1,71179-2,90415-13
407200,42511+0,91342-1,0+0,14717+0,19695-11
408000,8
408001,COMP 8: 3.47U  P-U
408100,14210+1,10183-1,15444-1,71179-2,90415-13
408200,42511+0,83984-1,0+0,13348+0,17863-11
409000,9
409001,COMP 9: 3.47U  PP-JU
409100,14210+1,10183-1,15444-1,71179-2,90415-13
409200,42511+0,84028-1,0+0,13280+0,17771-11
410000,10
410001,COMP10: 3.47U  PP-UU
410100,14210+1,10183-1,15444-1,71179-2,90415-13
410200,42511+0,84080-1,0+0,13377+0,17902-11
411000,11
411001,COMP11: 3.47U  NORMAL
411100,14210+1,10183-1,15444-1,71179-2,90415-13
411200,42511+0,86976-1,0+0,13926+0,18636-11
412000,12
412001,COMP12: H2O
412100,17044+1,86690-3,32542-1,0+0,0+0
412200,29163+0,22713-1,0+0,0+0,0+0
.
```

APPENDIX B

NOTES ON THERMOS AT MIT

The version of THERMOS used in this study, as described in Section 3.1.1, was made available by the Yankee Atomic Electric Company. The computer runs were made at the Control Data facilities of Technology Square, near MIT.

The THERMOS versions available at MIT are not in an operable state for use on the IBM 360/370 system. As noted by Addae[60], the source terms output by the code, Q_{ki}, which indicate convergence of the solution, are not sufficiently close to 1.0 after performance of the iteration scheme. The problem arose following the modifications made to the program version available, which is operable on the CDC machine. The modifications included format statement changes and restructuring of the subroutine formats.

The most probable cause of this condition is the difference in decimal point precision between the IBM and CDC systems. Changing the variables to double precision might correct the problem.

The THERMOS versions at MIT are:

(1) Original, untouched Argonne version (CDC operable) on cards and source tape form

(2) MITR (Research Reactor) modified version of Addae[60]

(3) THERMOS- CLUCOP MITR version of Reed[61]

(4) 35 Energy Group THERMOS, modified by the author to comply with the ENDF/B-II thermal cross section set of LASER-M, as described by Momsen[9] . The modifications included those

of Addae concerning "do" loops. The modified program is in card form, in addition to the load module contained on

Diskpack 234019 PV.M11534.12618.THERM35.LOD2

at the MIT information processing center. The Nuclear Engineering code library contains necessary information.

A 35-group library for use with this version was created by a version of the code LIBP, called LIBP35, using the ENDF/B-II cross section set. Only one temperature was used for scattering in its creation (i.e., only one scattering matrix). The library may be expanded, using LIBP35 and the ENDF/B-II cross section set cards contained in the Nuclear Engineering code library. The library is on disk under

Diskpack 234019 PV.M11534.12618.THERM35.LIBR

APPENDIX C

SAXTON CORE II DEPLETION

CORRECTION TO PU-241 ISOTOPIC CONTENT RESULTING FROM DECAY TO AM-241

The Saxton Core II isotopics comparison with LASER-M calculations is presented in Section 4.3. This appendix is an explanation of the correction made to the Pu-241 atom percent (a/o) content with burnup, given in Table 4.7 and Figures 4.17 and 4.25.

The LASER-M code depletion format is deficient in comparison to that in a production-type code since the depletion time steps must be of equal magnitude (neglecting initial time steps for Xe and Sm). In addition to time steps, changes in parameters such as linear power rating or temperature, as witnessed under reactor operating conditions, must be explicitly handled by program termination, modification of parameters from a code-punched continuation deck, and resumption of execution.

These deficiencies were overcome by depletion at an average value of linear power, obtained by knowledge of the cumulative hours of non-zero power operation and the cumulative burnup (Table 4.6). As a result, a correction must be applied for the zero power hours. The significant change of interest occurs in the loss of Pu-241 by decay to Am-241, with a half life (taken from the LASER code) of 13.2 years ($\lambda = 0.1665 \times 10^{-8}$/sec). A correction for such decay must also be made for the time period between core end of life (EOL) and

the date of isotopic analysis. Since the isotopic data is an average of the data from five (5) samples, an average effective date of isotopic analysis is used for the end of life decay period calculation.

Table C.1 contains the uncorrected and corrected LASER-M values of Pu-241 isotopic content with burnup. The reference report for core operating data is WCAP 3385-56(2)[15] (The time history is given in Appendix G, Table G-1, p. G-2 of the report). The following steps were taken in calculation of a corrected Pu-241 value at a given zero power time step (refer to Table C.1).

(1) The percent decay during the zero power time step was calculated by knowing its duration and assuming exponential decay.

(2) The uncorrected LASER-M Pu-241 a/o value at a given point in time was obtained by linear interpolation between calculated LASER-M time step Pu-241 a/o values using the accumulated non-zero power time of the reactor.

(3) Two changes in Pu-241 content were made from one corrected value of Pu-241 atom percent to the next, namely

- A value representing the production of Pu-241 during the non-zero power interval was added (this also includes decay during the non-zero power interval). This was taken as the difference between successive values of uncorrected LASER-M Pu-241 atom percents.

A value representing the destruction due to decay of Pu-241 during the zero power time step was subtracted. This was taken as a product of the fraction decayed during the zero power time step and the previous value of corrected Pu-241 content.

A similar procedure was used for the time period from core EOL to the date of isotopic analysis. The following dates were used to arrive at the length of this period. References are to WCAP 3385-56(2).

(1) Core End of Life 10/18/68 (Appendix H, p. H-4)

(2) Isotopic Analysis Dates (Appendix A)

Rod Number	Zone	Date
1. RI	4	11/10/69
2. RI	6	9/ 3/69
3. RI	8	11/10/69
4. JF	7	8/20/69
5. MY	6	9/20/69

Average Effective Date: 10/ 1/69

Note that the final result of the correction is that, at 20,000 MWD/MT (approximately) and the date of isotopic analysis, Pu-241 content is about 8.8% less than would be calculated neglecting zero power and EOL decay.

The primary assumption made in this calculational correction is that the spectrum change due to the excess Pu-241 present, whose zero power decay was not accounted for during the LASER-M calculation, is negligible. This is reasonable due to the fact that the Pu-241 total and resonance absorption in

Table C.1 Saxton Core II Depletion - Correction of Pu-241 Isotopic Content due to Zero Power Time Period Decay

Zero Power Step	Start of Zero Power Time Step (hrs)	Accumulated Non-Zero Power Time (hrs)	Zero Power Time Step (hrs)	Percent Decayed during Zero Power Time Step (%)	Uncorrected LASER-M Pu-241 (a/o)	----Pu-241 Changes------- Production during Non-Zero Power Interval(a/o)	Destruction during Zero Power Time Step(a/o)	Corrected Value of Pu-241 (a/o)
1	1344	1344	72	0.04	1.534	-	0.001	1.533
2	2280	2208	576	0.34	1.977	0.443	0.005	1.971
3	4344	3696	120	0.07	2.774	0.797	0.001	2.767
4	4992	4224	744	0.44	3.064	0.290	0.012	3.045
5	7008	5496	1152	0.69	3.782	0.718	0.021	3.742
6	9624	6960	4868	2.88	4.633	0.851	0.108	4.485
7	14876	7344	936	0.56	4.860	0.227	0.025	4.687
8	16508	8040	984	0.59	5.276	0.416	0.026	5.077
9	17828	8376	1008	0.60	5.477	0.201	0.030	5.248
10	19676	9216	1440	0.59	5.986	0.509	0.031	5.726
11	21692	9792	744	0.44	6.339	0.353	0.025	6.054
	Core EOL	10468	0	0.0	6.905	0.566	0.0	6.620
12	23112	10468	8358	4.89	6.905	0.0	0.323	6.297

the thermal range is small relative to Pu-239 and Pu-240, due to the difference in number density and the size of the respective resonances (According to LASER-M core EOL values, Pu-241 absorptions are 3% of the cell total, Pu-239 and Pu-240 absorptions are 66%). Another assumption is the neglect of the spectrum effect associated with the Am-241 buildup, in addition to the reduced Pu-242 production. Both are of secondary importance.